ON SOME WAVE STRUCTURE INTERACTION PROBLEMS IN THE LINEARISED THEORY OF WATER WAVES

Thesis
Submitted for the Degree of
Doctor of Philosophy
in Science

By

Gour Das

Department of Mathematics
Jadavpur University
Kolkata - 700032

July 2024

যাদবপুর বিশ্ববিদ্যালয়

FACULTY OF SCIENCE
DEPARTMENT OF MATHEMATICS

JADAVPUR UNIVERSITY
Kolkata - 700 032, India
Telephone : 91 (33) 2457 2269

CERTIFICATE FROM THE SUPERVISOR

This is to certify that the thesis entitled " **On Some Wave Structure Interaction Problems In The Linearised Theory Of Water Waves** " submitted by **Gour Das**, who got his name registered on 08.08.2019 for the award of Ph.D. (Science) degree of Jadavpur University, is absolutely based upon his own work under the supervision of Prof. Sudeshna Banerjea, Department of Mathematics, Jadavpur University and Dr Rumpa Chakraborty, Department of Mathematics, Diamond Harbour Women's University, West Bengal and that neither this thesis nor any part of it has been submitted for any degree/diploma or any other academic award anywhere before.

Sudeshna Banerjea.

(Sudeshna Banerjea)
Department of Mathematics
Jadavpur University
Kolkata-700032
India.

Professor
DEPARTMENT OF MATHEMATICS
Jadavpur University
Kolkata - 700 032, West Bengal

Rumpa Chakraborty

(Rumpa Chakraborty)
Department of Mathematics
Diamond Harbour Women's University
Diamond Harbour, Sarisha, South 24 Pargana
Pin 743368, West Bengal, India.

Dr. RUMPA CHAKRABORTY
Assistant Professor
Department of Mathematics
Diamond Harbour Women's Univers
South 24 Parganas, West Bengal

Dedicated to my mother ***Mrs. Shibani Das***

and my father ***Mr. Asis Das***

Acknowledgement

First and foremost, I want to convey my heartfelt gratitude to Prof. Sudeshna Banerjea, my Ph.D. supervisor in the Department of Mathematics at Jadavpur University. Her unwavering support throughout my doctoral studies and research, along with her patience, encouragement, passion and profound expertise, played an integral role in assisting me throughout the entire research and thesis-writing process.

I also want to express my gratitude to Dr. Rumpa Chakraborty, my co-supervisor at Diamond Harbour Women's University, for her guidance, encouragement and collaboration throughout my research journey. Additionally, I extend my thanks to Prof. B. N. Mandal, a retired professor from the Physics and Applied Mathematics Unit at the Indian Statistical Institute in Kolkata, for his motivation and insightful feedback.

I would like to acknowledge the valuable contributions of my Research Advisory Committee (RAC) member, Prof. Abhijit Lahiri, Jadavpur University, for his guidance, support and constructive input on my research topics.

My sincere gratitude goes to the current and former Heads of the Department of Mathematics at Jadavpur University for providing the essential infrastructure required for my work. I also appreciate the assistance and cooperation of all the department's administrative staff members.

The research work presented in the thesis is financially supported first by the SVMCM, Government of West Bengal and later by the State Government Departmental Fellowship Scheme.

I extend my heartfelt thanks and deep appreciation to all the fellow research scholars in the Department of Mathematics at Jadavpur University, with special mention to Piyali Kundu, Anushree Samanta, Shreya Banerjee, and my senior Dibakar Mondal.

Lastly, but certainly not least, my profound gratitude is reserved for my family for their unflagging love and support throughout my life. I am grateful to my father Shri Asis Das and mother Smt. Shibani Das for their considerate care and love. I would also like to thank my younger brother Nitai Das for his patience, love and belief in me.

July, 2024 **Gour Das**

CONTENTS

ABSTRACT 1

PART I GENERAL INTRODUCTION 3

1 INTRODUCTION 4

1.1 PREAMBLE 4

1.2 BRIEF DESCRIPTION OF PREVIOUS RELATED WORK 8

1.3 OUTLINE OF THE THESIS 13

2 MATHEMATICAL PRELIMINARIES 17

2.1 BASIC EQUATIONS 17

2.1.1 WATER WITH A FREE SURFACE 17

2.1.2 BASIC EQUATIONS TAKING INTO ACCOUNT THE EFFECT OF SURFACE TENSION 21

2.1.3 WATER WITH AN ICE-COVER 23

2.2 HAVELOCK'S EXPANSION 25

2.2.1 HAVELOCK'S EXPANSION THEOREM 25

2.2.2 HAVELOCK'S EXPANSION OF WATER WITH A FREE SURFACE(TWO DIMENSIONAL CASE) 26

2.2.3 HAVELOCK'S EXPANSION OF WATER WITH ICE COVER SURFACE 27

2.2.4 HAVELOCK'S EXPANSION OF WATER WITH SURFACE TENSION . . . 29
2.3 TWO-DIMENSIONAL SOURCE POTENTIAL . . . 30
2.3.1 WATER WITH A FREE SURFACE . . . 30
2.3.2 WATER WITH ICE-COVER . . . 32
2.3.2.1 SOURCE POTENTIAL FOR DEEP WATER . . . 33
2.3.2.2 SOURCE POTENTIAL FOR FINITE DEPTH WATER . . . 34
2.4 GREEN'S THEOREMS . . . 35
2.5 GALERKIN METHOD . . . 35
2.6 INTEGRAL EQUATION WITH STRONGLY SINGULAR KERNEL . . . 38
2.6.1 SOLUTION OF SINGULAR INTEGRAL EQUATION OF FIRST KIND WITH CAUCHY KERNEL . . . 38
2.6.2 HYPERSINGULAR INTEGRAL EQUATION . . . 42
2.7 BOUNDARY ELEMENT METHOD TO SOLVE HYPERSINGULAR INTEGRAL EQUATION . . . 44

PART II **46**

3 PROPAGATION OF SURFACE GRAVITY WAVES BY A SUBMERGED THIN ELASTIC PLATE BENEATH AN ICE COVER **47**
3.1 INTRODUCTION . . . 47
3.2 FORMULATION OF THE BOUNDARY VALUE PROBLEM . . . 51
3.3 METHOD OF SOLUTION . . . 54
3.4 NUMERICAL RESULTS AND DISCUSSIONS . . . 60
3.5 CONCLUSIONS . . . 69

4 SCATTERING OF WATER WAVES BY A VERTICAL POROUS BARRIER OVER A RECTANGULAR TRENCH **70**
4.1 INTRODUCTION . . . 70
4.2 FORMULATION OF THE PROBLEM . . . 73
4.3 METHOD OF SOLUTION . . . 77
4.4 NUMERICAL RESULTS . . . 92
4.5 CONCLUSIONS . . . 103

5 SCATTERING OF WATER WAVES BY RECTANGULAR THICK BARRIERS IN PRESENCE OF SURFACE TENSION 104

5.1 INTRODUCTION 104

5.2 FORMULATION OF THE PROBLEM 106

5.3 METHOD OF SOLUTION 108

5.4 NUMERICAL RESULTS AND DISCUSSIONS 130

5.5 CONCLUSIONS 136

6 WATER WAVE SCATTERING BY THICK RECTANGULAR SLOTTED BARRIERS IN PRESENCE OF ICE COVER 142

6.1 INTRODUCTION 142

6.2 FORMULATION OF THE PROBLEM 145

6.3 METHOD OF SOLUTION 148

6.4 NUMERICAL DISCUSSION 158

6.5 CONCLUSIONS 166

7 EFFECT OF NONUNIFORM POROSITY IN CURVED BREAKWATER ON WATER WAVES 174

7.1 INTRODUCTION 174

7.2 PROBLEM FORMULATION 178

7.3 METHOD OF SOLUTION 180

7.4 NUMERICAL RESULTS 188

7.5 CONCLUSIONS 199

8 WATER WAVE INTERACTION WITH A VERTICAL WALL WITH A GAP SUBMERGED IN DEEP WATER 201

8.1 INTRODUCTION 201

8.2 FORMULATION OF THE PROBLEM 203

8.3 NUMERICAL RESULTS 209

8.4 CONCLUSIONS 209

FUTURE SCOPE OF WORK 211

BIBLIOGRAPHY 213

ABSTRACT

The present thesis focuses on investigating water wave propagation problems in water under the assumption of linearised theory and associated mathematical methods. Among the important classes of water wave propagation problems, one of the most significant is the scattering of waves by obstacles with diverse geometric shapes. When a series of surface waves, originating from a considerable distance, encounters an obstacle within a fluid, it undergoes partial reflection off the obstacle and partial transmission either beneath or over it. In the context of the linearized theory of water waves, the determination of reflection and transmission coefficients constitutes a wave scattering problem. Here in the present thesis we have worked on the following scattering problems.

1. Propagation of surface gravity waves by a submerged thin elastic plate beneath an ice cover.
2. Effect of porosity on wave scattering by a vertical porous barrier over a rectangular trench.
3. Scattering of water waves by rectangular thick barriers in presence of surface tension.
4. Water wave scattering by thick rectangular slotted barriers in presence of ice cover.
5. Wave propagation in presence of a curved barrier with variable permeability.
6. Water wave interaction with a vertical wall with a gap submerged in deep water.

In the problem 1, a theoretical analysis involving surface gravity waves propagation by oblique incidence wave due to a thin elastic plate submerged in finite depth water with ice cover is studied. Applying Greens function technique, the boundary value problem is reduced to integral equations whose solutions are then utilised to find the reflection and transmission coefficients.

The interaction of surface wave with a vertical porous barrier over a rectangular trench is studied in problem 2 under the assumption of linearized theory of water waves. For the solution, the fluid region is divided into four subregions depending on the position of

the barrier and the trench. Using the eigen function expansion of water wave potential in different regions along with suitable matching conditions at the interface of different regions, the problem is formulated in terms of three integral equations. Considering the edge conditions at the submerged end of the barrier and at the edges of the trench, these integral equations are solved using multi-term Galerkin approximation technique taking orthogonal Chebyshevs polynomials and ultraspherical Gegenbauer polynomial as its basis function. Using the solutions of the integral equations, the reflection coefficient, transmission coefficient, energy dissipation coefficient and horizontal wave force are determined.

The influence of surface tension on an obliquely incident waves in presence of thick rectangular barriers present in water of uniform finite depth is discussed in problem 3. The three different configurations of the thick barrier, viz., bottom-standing submerged barrier, fully submerged rectangular block and fully submerged block extending down to the bottom with a finite gap are considered. An appropriate multi-term Galerkin approximation technique involving ultraspherical Gegenbauer polynomial is employed for solving the integral equations arising in the mathematical analysis. The reflection and transmission coefficients are evaluated by utilizing the solution of the integral equations.

The problem 4 is concerned with scattering of surface water waves by a thick vertical slotted barrier of rectangular cross section with an arbitrary number of slots of unequal lengths present in water of finite depth with ice cover surface. The problem is formulated in terms of an integral equation in disjoint intervals, by suitable matching of eigen function expansion of water wave potential. Galerkin approximations involving ultraspherical Gegenbauer polynomials are utilised in the mathematical analysis for solving the integral equations to obtain a very accurate numerical estimates for the reflection coefficient.

The phenomena of scattering of waves by a circular arc shaped barrier with nonuniform porosity is studied in problem 5. The water region is considered to be infinitely deep or of finite depth. Based on judicious application of Greens integral theorem, the corresponding boundary value problem is reduced to a hypersingular integral equation of second kind. The boundary element method and the collocation method are adopted to solve the hypersingular integral equation and a good matching of the solutions obtained by two methods are ensured. The reflection coefficient and energy dissipation are evaluated by using the solution of the integral equation which are then studied graphically.

The problem of water wave scattering by a thin vertical wall with a gap submerged in deep water is studied using singular integral equation formulation. The corresponding boundary value problem is reduced to a Cauchy type singular integral equation of first kind in two disjoint intervals where the unknown function satisfying the integral equation has square root zero at the end points of the two intervals. In this case the solution exists if the forcing function satisfies two solvability conditions. The reflection coefficient is determined here using the solvability conditions without solving the integral equation and also the boundary value problem.

PART I

GENERAL INTRODUCTION

CHAPTER 1

INTRODUCTION

1.1 PREAMBLE

A wave is a disturbance that propagates through a medium with a definite velocity, transferring energy from one part of the medium to another without causing any permanent displacement of the particles within the medium. The type of wave motion, which most people are familiar with, is the waves that occur on the free surface of water. When we stand on the beach, we observe that water is moving towards shore rolling in and out. These are the water waves. Waves are encountered in nearly all branches of mathematical physics which includes continuum mechanics, quantum mechanics, acoustics, the theory of electromagnetism, etc. Throughout the study of waves, water waves have consistently served as models for wave theory in general to the scientists primarily because they can be observed with the naked eye. In the theory of water waves, the restoring force is gravity and therefore these waves are known as surface gravity waves. The subject of surface gravity waves is diverse and captivating, which involves a study of general aspects of wave motion or the study of behavior of waves in the presence of obstacles with various geometric configurations. This area of study is particularly relevant to ship designers and oceanographers. However, even the simplest problem appears to be difficult to tackle mathematically unless some assumptions are

made about the medium as well as the wave motion. Consequently water is assumed to be incompressible, inviscid and homogeneous fluid. Thus if one assumes that the motion in water to be irrotational, then the problems concerning propagation of water waves reduce to a boundary value problem consisting of Laplace equation together with appropriate boundary conditions. Again the boundary conditions including the free surface condition are nonlinear in nature. Thus further assumptions are required regarding the wave motion to simplify the boundary conditions so as to handle the boundary value problem mathematically. The nature of assumptions provides a natural way to classify the theory of water waves. Consequently two approximate theories, *viz*, the linearised theory and the shallow water theory are developed from the basic hydrodynamic theory. The linear water wave theory is based on the assumption that the amplitude of waves is much less than the wave length. In the shallow water theory, one assumes that the depth of the fluid region is significantly smaller than the wavelength of the waves.
The present thesis is concerned with a study of wave propagation under the assumption of linear theory. The basic assumptions of the linearised theory implies that the velocity components of a fluid element and the free surface elevation (or depression) very small so that the powers and products of these quantities are neglected. The fundamental equations in the linearized theory of water waves are derived from the equation of continuity and Euler's equation of motion. If the motion is time-harmonic, irrotational then the equation of continuity leads to Laplaces equation and the Eulers equation of motion together with the kinematical condition on the free surface after linearisation produce the linearised free surface boundary condition.

The linearized theory of water waves play a very crucial role in offshore, polar and other ocean related industrial problems. This theory finds extensive applications in physical problems, such as the study of waves on sloping beaches, the diffraction of waves around a breakwater, wave impact on a very large floating structures, waves in a running stream, the motion of ships as floating rigid bodies in a seaway, the generation of waves due to instantaneous disturbances at the ocean surface caused by storms in the atmosphere or at the sea floor created by earthquakes, among other scenarios. Furthermore, the validity of employing the linearized theory in water wave problems has been substantiated multiple times in the existing literature. For instance, Ursell,

Dean and Yu (1960) conducted experiments on the height of water waves generated by a flat vertical piston wavemaker. The obtained results demonstrated a high level of agreement with theoretical results derived under the assumptions of the linearized theory for small amplitude gravity waves. Dean and Ursell (1959), Yu and Ursell (1961) also experimented with a circular cylinder in deep water as well as in finite depth water. In both experiments, they observed that wave amplitudes from the experiments closely align with the theoretical results obtained using linear theory. These experimental evidences confirm and establish the validity of the linearized theory of water waves. To investigate water wave problems, a diverse range of mathematical techniques, both analytical and computational, are employed. These include integral transforms, integral equations, asymptotic evaluation of integrals and the solution of partial differential equations, theory of complex variable, function theoretic method etc.

In the present thesis, our focus is on the study of wave propagation in presence of obstacles with various configurations under the assumption of linearized theory. This class of problems are called scattering problems. When a train of surface water waves travelling from a large distance is incident on an obstacle, it experiences partial reflection and partial transmission. The ratio of the amplitude of the reflected wave to the amplitude of the incident wave is termed the reflection coefficient, while the ratio of the amplitude of the transmitted wave to the amplitude of the incident wave is referred to as the transmission coefficient. The reflection and transmission coefficients are immensely significant quantities in the mathematical study of scattering problems. Understanding the reflection and transmission coefficients provides crucial insights into the amount of wave energy that is either reflected or transmitted by an obstacle. This knowledge is essential for the design and construction of offshore and marine structures, including breakwaters.

Recently, with the growing scientific activities in polar oceans, which are often modeled as water with an ice cover, researchers have found water wave problems in the presence of an ice cover to be increasingly attractive. Ice is one of the most common material on Earth, yet it is very different from all other known materials. Depending on its morphology and microstructure, it may behave as an elastic plate or as a brittle structure or as an viscoelastic material or even as a quasi-liquid material. Moreover, ice is present on earth in different forms, notably the fresh water ice that occurs in

ice caps, glaciers, icebergs, frozen rivers and lakes and many varieties of sea ice that form in the polar and subpolar oceans. A mathematical model for treating the ice sheet as floating thin elastic plate is well known and a significant research has been carried out using this model to study the problems related to ocean wave interaction with sea ice (cf. Fox and Squire (1994); Squire (2007); Chung and Fox (2002); Linton and Chung (2003); Chakrabarti (2000); Gayen *et al.*(2005)). The study of ocean wave interactions with a very large thin, floating elastic plate has gained immense importance since last decade as it can be used to model a wide range of physical systems. One of its important applications consists in modelling a very large floating structure (VLFS) that is used in ocean space utilization for the construction of megafloats such as floating airports, offshore runways, floating restaurant etc. It is a technology that allows these megafloats, which are considered to be artificial lands to float on rising sea level and has a minimal effect on marine habitat, natural and tidal current flow (cf. Wang *et al.* 2010; Wadhams 1978). Owing to the large surface area and relatively small depth, VLFS behaves elastically under wave action (cf. Wang *et al.* 2010). In the polar region, surface gravity waves propagate from the open ocean into ice-covered seas. Understanding the modus operandi of formation of sea ice and its distribution is imperative to explain the geophysical phenomena occurring in the polar regions and in the marginal ice zone. A precinct between ocean and atmosphere, the sea ice arrests the escape of heat from the ocean to the air above. Consequently it plays a crucial role in conservation of marine life. An uninterrupted expanse of unbroken ice over a vast stretch in the polar region often encounters waves propagating at free surface. It is well known that waves may weaken and rupture the continuous sea ice causing fissures which may lead to melting of sea ice. This phenomena is an indicator of global climatic change. The amplitude of the waves travelling beneath the ice needs to be studied as it causes the ice-cover to bend. The bending of ice-cover is attributed to its elastic property. In order to minimize the impact of wave action on a VLFS or ice sheet, various anti motion structures and devices such as breakwaters, submerged plates, oscillating water column breakwater, air cushion, curtain pile breakwater are designed (cf. Wang *et al.* (2010); Tari *et al.* (2000)). Also, a number of experiments measuring wave propagation through marginal ice zone have been reported of which first measurement was carried out by a ship borne wave recorder (cf. Kohout and Meylan (2008)). Later, measurements were carried out by a echo sounder from a submerged hovering

submarine, acoustic Doppler Current Profiler mounted on an autonomous under water vehicle (cf. Kohout and Meylan (2008), Wadhams (1978)). Thus the study of the waves in presence of thin plate under ice cover or VLFS is important. Mathematically, the boundary value problem (BVP) related to study of water waves in ocean with ice-cover is interesting as it involves fifth order derivative of the potential function in the boundary condition on ice cover whereas the governing partial differential equation is of second order. In this thesis, we have focused on studying wave scattering problems involving barriers of various geometric shapes, considering both free surface water and ice-covered surface water.

With this Preamble we now give a brief literature review related to the problems given in the thesis.

1.2 BRIEF DESCRIPTION OF PREVIOUS RELATED WORK

The subject of surface gravity waves is varied and fascinating. From mathematical point of view the theory of water waves has been a source of intriguing and often difficult mathematical problem. Virtually every classical mathematical technique appears somewhere within its confine. The founding fathers of this subject are Euler, Lagrange, Cauchy, Poisson. Further contributions in the theory of water waves have been made by Stokes, Lord Kelvin, Kirchhoff and Lamb who constructed a number of explicit solutions. In the twentieth century Havelock, Kochin, Sretensky, Stoker, John and others applied Fredholm theory of boundary integral equations to the field of water waves. A general exposition of the classical theory is given in the books of Lamb (1932), Stoker (1957), Wehausen and Laitone (1960), Sretensky (1977), Lighthill (1978), Whitham (1979), Crapper (1984), Mandal and Chakrabarti (2000) & Kuznetsov *et al.* (2001). Various aspects of linear theory of water waves have been discussed in the works of Havelock (1963) and Ursell (1994). Applications and mathematical methods associated with the theory of water waves have been discussed in Wehausen (1971), Newman

(1977), Mei (1983), Linton and McIver (2001).

Problems of water wave scattering involving obstacles of various geometrical shapes have been studied extensively in the literature from mid-twentieth century. Dean(1945) obtained the explicit solution for the water wave scattering problem involving a submerged thin vertical rigid barrier extending infinitely downwards in deep water. Ursell (1947) utilized Havelock's expansion (cf. Havelock (1929)) of water wave potential to derive explicit solutions for the scattering problem involving a surface-piercing thin vertical rigid barrier and also the submerged vertical barrier considered by Dean (1945). Subsequently, several mathematical techniques were developed to investigate the boundary value problem associated with the scattering of waves by rigid vertical thin barriers, as mentioned in the works of Levine and Rodemich (1958), Williams (1966), Evans (1970), Porter (1953), Porter (1972) and Evans and Morris (1972). It may be noted here that an exact solution to the aforesaid boundary value problem exists when the barrier is in the form of a vertical plate in deep ocean conditions and for normal incidence of the incoming wave train. However, in all other cases, only approximate analytical or numerical methods are employed to obtain an approximate solution. Levine and Rodemich (1958) solved the problem involving a partially immersed barrier by utilizing Greens integral theorem to formulate the velocity potential function that describes the motion in the fluid. Applying the reduction method, Williams (1966) reexamined the problem of a submerged barrier, while Evans (1970), employing complex variable theory, solved the scattering problem involving a thin plate of finite height submerged in deep water. Porter employed two methods to solve the problem of wave scattering by a semi-infinite thin vertical rigid barrier extending downwards from the free surface and contained a gap of arbitrary width at the same depth. One method was based on a reduction procedure and the other was based on an integral equation formulation. A comprehensive explanation of this technique can be found in the monograph by Mandal and Chakrabarti (2000). Goswami (1983) utilized the Greens function technique to solve the scattering problem involving a vertical rigid plate submerged in water of uniform finite depth. Mandal and Dolai (1994) later reinvestigated the problem involving thin vertical rigid barrier present in uniform finite depth water by utilizing Galerkin approximation method. Additionally, scattering problems involving nearly vertical barriers have been studied by Shaw (1985), Mandal and Chakrabarti

(1989), Mandal and Banerjea (1992) and Mandal and Banerjea (1993).

The water wave propagation in the presence of a circular arc-shaped rigid breakwater submerged in water has been studied by numerous researchers (cf. Parsons and Martin (1994), McIver and Urka (1995), Kanoria and Mandal (2002), Mondal *et al.* (2017), Liu and Li (2012, 2013)) employing various mathematical tools. In 1994, Parsons and Martin investigated the scattering problem involving a circular arc-shaped barrier symmetric about the vertical axis. They utilized a first-kind hypersingular integral equation formulation based on a judicious application of Green's Integral theorem. McIver and Urka (1995) studied the problem of wave interaction with a symmetric circular arc-shaped plate submerged in deep water by using matched series expansion and Schwinger variational principal method. Subsequently, Kanoria and Mandal (2002) employed a hypersingular integral equation formulation to investigate the wave propagation problem involving a circular arc-shaped barrier that is not symmetric about the vertical axis and is present in deep water.

The water wave scattering problems involving a thick vertical barrier with a rectangular cross-section, situated in water of uniform finite depth and subjected to normal incidence wave trains, have been previously studied by Mei and Black (1969) and Kanoria *et al.* (1999). Mei and Black (1969) considered surface piercing and bottom standing thick vertical barriers, employing variational formulations as the basis for numerical computations of the reflection and the transmission coefficients. Kanoria *et al.* (1999) and Mandal and Kanoria (2000) investigated the problems of normal and oblique wave scattering by thick barriers, wherein the barriers have four types of configurations such as surface-piercing or bottom standing thick barrier or a submerged block or a thick wall with a gap. They used the multi-term Galerkin approximation method involving ultraspherical Gegenbauer polynomials for solving first kind integral equations arising in the mathematical analysis to obtain very accurate numerical estimates for the reflection coefficient.

In the aforesaid problems, the plates or barriers are assumed to be rigid. However one can take into account that the effect of elasticity of the plate. Meylan (1995), Meylan and Peter (2009) and Peter and Meylan (2010) extended the problem of the

surface-piercing thin vertical rigid plate, initially studied by Ursell (1947), to include a thin vertical elastic plate. Chakrabarti (2000) examined the scattering problem involving a semi-infinite elastic plate floating on infinitely deep water by reducing it to the solution of a singular integral equation of Carleman type. Sahoo *et al.* (2001) explored a similar problem for finite-depth water using the eigenfunction expansion method. Gayen and Mandal (2009) also investigated the problem of water wave scattering by a thin elastic plate of arbitrary width floating in deep water, reducing the problem to a singular integral equation of Carleman type.

During the later half of twentieth century, study of wave interaction with porous coastal structures like rubble mound breakwaters became important in coastal engineering as the structural voids in the porous breakwaters can dissipate wave energy efficiently. Also in coastal engineering, porous breakwaters drawn special attention to the scientist and researchers because of the rigid breakwaters were collapsed due to huge load, which were mainly constructed to protect harbours and coastal villages. Porous structures in the form of thin permeable barriers have been used to dissipate and reflect incoming wave energy from sea. The mathematical modeling of porous structures as thin porous vertical wavemakers was pioneered by Chwang in 1983, while Solitt and Cross (1972) had previously studied the problem of wave propagation through porous media. Based on the model of Solitt and Cross (1972), many researchers studied the problem of scattering of water waves by porous breakwater. Yu (1995) specifically investigated the scattering problem involving a semi-infinite porous breakwater using an approximate method. Later McIver (1999) used the Wiener-Hopf technique to show that the problem of Yu (1995) has an exact solution for all angles of incidence. Lee and Chwang (2000) employed eigenfunction expansion in conjunction with dual series relations to investigate the scattering problem by thin porous vertical plates. Liu and Li (2012, 2013) utilized the multipole expansion method to study the problem of wave interaction with a perforated semicircular barrier. In a recent study, Gayen and Mondal (2014) employed a second-kind hypersingular integral equation formulation to investigate the problem of wave scattering by a submerged porous plate in the ocean with a free surface. Mondal *et al.* (2017) studied the scattering problem involving permeable circular arc shaped barrier not symmetric about the vertical axis present in water of finite depth with ice cover. Also many researchers used sophisticated mathematical

techniques to study scattering problems involving porous barrier mainly in any form of straight orientation.

Due to considerable interest increase in different types of scientific and industrial activities in polar regions and arctic oceans towards the later half of the last century, study of wave propagation problems in polar oceans covered by floating ice has become very attractive to many researchers. The floating ice cover is modelled as a thin elastic plate. A floating thin elastic plate can also be regarded as a practical model for the frozen ocean or for a large floating structure such as a floating airport or Quite a number of models for the ice-cover have been proposed for the purpose of mathematical investigation of wave propagation problems [cf. Maiti *et al.* (2015), Mondal and Banerjea (2016a)]. Interaction of ocean waves with shore fast sea ice modelled as a thin elastic plate was first considered by Fox and Squire (1990, 1994). Scattering of an oblique wave caused by a narrow crack in ice sheets floating on water of finite depth were studied by Evans and Porter (2003). Vaughan and Squire (2006) studied the propagation of waves under an ice sheet of variable thickness, which was interpolated by using low-order piecewise polynomials. The topics in the general area of ocean wave or sea ice interactions, especially in relation to mathematical modeling, were described in the review paper of Squire (2007). Later, Sturova (2011) considered steady oscillations of a horizontal cylinder submerged in a linearly stratified fluid layer with an ice cover using the Boussinesq approximation. Bhattacharjee and Soares (2012) investigated the behavior of flexural gravity waves propagating over a semi-infinite floating ice sheet under the assumptions of the small-amplitude linear wave theory. The problems involving wave interaction with floating ice present in upper surface of water become more accepted among engineers and researchers due to their effective scientific activities in Arctic and cold ocean regions.

The scattering of normally incident monochromatic plane progressive wave by rectangular submarine trench of constant depth containing two fluids of constant but different densities was studied by Lassiter (1972). Lee and Ayer (1981) investigated the effect of a symmetric rectangular trench by dividing the fluid domain into subregions. Miles (1982) used a conformal mapping to solve the trench problem for normal incidence of wave train. The diffraction of obliquely incident surface waves by an asymmet-

ric trench was investigated using linearized potential theory by Kirby and Dalrymple (1983). They solved a set of integral equations derived by matching eigen function expansions of the velocity potentials. Later, Kirby *et al.* (1987) developed the theory of wave diffraction over a rectangular trench where currents flowing parallel to the trench boundary. The normal and oblique incidence by the two-dimensional wave scattering by a rectangular submarine trench was considered by Chakraborty and Mandal (2014, 2015) reducing the problem to solving appropriate integral equation which is solved by multi-term Galerkin approximation involving ultraspherical Gegenbauer polynomials. Later, Roy *et al.* (2017) considered the problem of water wave scattering by an asymmetric rectangular trench using an approach similar to Chakraborty and Mandal (2014, 2015).

1.3 OUTLINE OF THE THESIS

The contents of the proposed thesis is divided into two parts, namely I and II. Part I is the general introductory part consisting two chapters. Chapter 1 is concerned with an introduction which contains a brief description of the different problems of this thesis and previous related work with them. Chapter 2 deals with some mathematical preliminaries relevant to the various problems presented in the thesis. This chapter comprises several sections that address fundamental equations related to a free surface, the inclusion of surface tension, scenarios involving an ice-covered surface and methodologies such as the Galerkin method and the boundary element method.

Part II consists of six chapters, namely chapter 3, chapter 4, chapter 5, chapter 6, chapter 7 and chapter 8. In chapter 3, a theoretical analysis involving surface gravity waves propagation by oblique incidence wave due to a thin elastic plate submerged in finite depth water in presence of ice cover has been studied extensively employing Greens function technique. Employing Green's function technique, the boundary condition satisfied on the elastic plate is transformed into an integral involving the difference in velocity potentials (unknown) across the plate multiplied by an appropriate Green's function. Utilizing Green's integral theorem, the reflection and transmission energy coefficients are explained in terms of integrals involving combinations of the

unknown velocity potential on the two sides of the plate. These combinations satisfy three simultaneous integral equations, which are solved numerically.

In chapter 4, the effect of porosity on surface wave scattering by a vertical porous barrier over a rectangular trench is studied. The fluid region is subdivided into four subregions based on the positions of the barrier and the trench. Utilizing Havelock's expansion of water wave potential in different regions and implementing suitable matching conditions at the interfaces of these regions, the problem is expressed through three integral equations. Taking into account the edge conditions at the submerged end of the barrier and at the edges of the trench, these integral equations are solved using a multi-term Galerkin approximation technique. The approximation technique employs orthogonal Chebyshev polynomials, ultra-spherical Gegenbauer polynomials and simple polynomials as its basis functions. By utilizing the solutions obtained from the integral equations, the reflection coefficient, transmission coefficient, energy dissipation coefficient and horizontal wave force are determined and presented graphically.

In chapter 5, the impact of surface tension on obliquely incident waves in the presence of thick rectangular barriers in water of uniform finite depth is discussed. Three distinct structures are considered: a bottom-standing submerged barrier, a submerged rectangular block that does not extend to the bottom and a fully submerged block that extends down to the bottom with a finite gap. A suitable multi-term Galerkin approximation technique involving ultraspherical Gegenbauer polynomials is employed to solve the integral equations that arise. The reflection and transmission coefficients for two-dimensional time-harmonic motion are determined using linearized potential theory.

In chapter 6, the scattering of surface water waves by a thick vertical slotted barrier of rectangular cross section with an arbitrary number of slots of unequal lengths along the vertical direction and present in finite depth with ice cover surface is discussed. Two distinct geometrical configurations of the slotted barrier are considered here. The barriers can either be bottom-standing and submerged or take the form of a submerged slotted thick block that does not extend down to the bottom. In the mathematical analysis, Galerkin approximations involving ultraspherical Gegenbauer polynomials as

basis functions are employed to solve first-kind integral equations valid in the union of several disjoint intervals.

In chapter 7, the study of water wave propagation in presence of a thin porous curved barrier with variable porosity of present in water of finite and infinite depth is studied. The problem is expressed as a second-kind hypersingular integral equation concerning the discontinuity in the potential across the plate. This integral equation is subsequently solved using two methods: the boundary element method and the collocation method using Chebychev's polynomial as basis functions.

In chapter 8, the problem of water wave scattering by a thin vertical wall with a gap submerged in deep water is studied using singular integral equation formulation. The corresponding boundary value problem is reduced to a Cauchy type singular integral equation of first kind in two disjoint intervals where the unknown function satisfying the integral equation has square root zero at the end points of the two intervals. In this case the solution exists if the forcing function satisfies two solvability conditions. The reflection coefficient is determined here using the solvability conditions without solving the integral equation and also the boundary value problem.

This completes the description of the contents of the present thesis.

The work reported in the present thesis is mainly based on the following papers:

1. Rumpa Chakraborty and Gour Das, Propagation of surface gravity waves by a submerged thin elastic plate beneath an ice cover, *Archive of Applied Mechanics*, 93 (2023), pp. 1507-1524.

2. Gour Das and Rumpa Chakraborty, Effect of porosity on wave scattering by a vertical porous barrier over a rectangular trench, *Journal of Marine Science and Application*, 74 (2023), pp. 491-505.

3. Gour Das and Rumpa Chakraborty, Scattering of water waves by rectangular thick barriers in presence of surface tension, *Journal of University of Shanghai for Science and Technology*, 23(11) (2021), pp. 30-55.

4. Gour Das and Rumpa Chakraborty, Water wave scattering by thick rectangular slotted barriers in presence of ice cover,(Communicated).

5. Dibakar Mondal, Anushree Samanta, Gour Das and Sudeshna Banerjea, Effect of nonuniform porosity in curved breakwater on water waves, (communicated after revision).

6. Gour Das, Sudeshna Banerjea and B.N.Mandal, A water wave scattering problem: Revisited,(Communicated).

CHAPTER 2

MATHEMATICAL PRELIMINARIES

Some mathematical preliminaries used in the problems of the present thesis are briefly studied in the chapter.

2.1 BASIC EQUATIONS

2.1.1 WATER WITH A FREE SURFACE

We consider an irrotational motion in water which is assumed to be incompressible, inviscid and homogeneous fluid having a constant volume density ρ. A rectangular cartesian coordinate system is chosen with y-axis vertically downwards into the water and the horizontal xz-plane is the undisturbed free surface. The only external force acting is the force of gravity. Basic equations in the theory of water waves are derived from two natural laws, viz, the conservation of mass and the conservation of momentum.

The law of conservation of mass gives the equation of continuity as

$$\nabla.\vec{q} = 0. \tag{2.1}$$

The law of conservation of momentum gives Euler's equation of motion as

$$\frac{\partial \vec{q}}{\partial t} + (\vec{q}.\nabla)\vec{q} = \nabla(-\frac{p}{\rho} + gy), \tag{2.2}$$

where $\vec{q} = (u, v, w)$ is the fluid velocity, p is the fluid pressure and ρ is volume density.

Since the motion starts from rest it is irrotational and can be described by velocity potential $\Phi(x, y, z, t)$ such that

$$\vec{q} = \vec{\nabla}\Phi. \tag{2.3}$$

Using this in (2.1), we get

$$\nabla^2\Phi = 0 \text{ in the fluid region.} \tag{2.4}$$

Substituting (2.3) in (2.2) and then integrating, we have Bernoulli's equation as

$$\frac{\partial \Phi}{\partial t} + \frac{1}{2}|\vec{q}|^2 + \frac{p}{\rho} - gy = c(t). \tag{2.5}$$

Here $c(t)$ is a constant depending on time only which can be absorbed in Φ by redefining Φ.
For small motion, the term $\frac{1}{2}|\vec{q}|^2$ can be neglected so that Bernoulli's equation (2.5) reduces to

$$\frac{\partial \Phi}{\partial t} = gy - \frac{p}{\rho}, \tag{2.6}$$

in the fluid region.
Let y=$\eta(x, z, t)$ denotes the free surface depression below the mean free surface $y = 0$. Now the pressure on the free surface is the atmospheric pressure which is a constant. This constant can be taken to be equal to zero by a suitable choice of scale. Hence (2.6) gives

$$\frac{\partial \Phi}{\partial t} = g\eta \text{ on } y = \eta(x, z, t). \tag{2.7}$$

Expanding $\frac{\partial \Phi}{\partial t}(x, y, z, t)$ by Taylor's series about $y = 0$ and neglecting terms of

higher order of smallness we get the linearised dynamical boundary condition as

$$\frac{\partial \Phi}{\partial t} = g\eta \quad \text{on } y = 0. \tag{2.8}$$

Let us consider the equation of free surface as

$$F(x, y, z, t) = \eta(x, z, t) - y = 0. \tag{2.9}$$

Since $F = 0$ is a boundary of the fluid, so we must have

$$\frac{\partial F}{\partial t} + u\frac{\partial F}{\partial x} + v\frac{\partial F}{\partial y} + w\frac{\partial F}{\partial z} = 0 \quad \text{on } y = \eta.$$

Noting (2.9), the above condition becomes

$$\frac{\partial F}{\partial t} + u\frac{\partial F}{\partial x} + v + w\frac{\partial F}{\partial z} = 0 \quad \text{on } y = \eta. \tag{2.10}$$

Since the velocity components and the free surface depression together with their partial derivatives are small quantities, so their squares, products and higher powers can be neglected.
Thus the equation (2.10) gives

$$\frac{\partial \eta}{\partial t} = \frac{\partial \Phi}{\partial y} \quad \text{on } y = \eta.$$

Expanding $\frac{\partial \Phi}{\partial y}(x, y, z, t)$ by Taylor's series and neglecting the terms of higher order of smallness, we obtain the kinematic boundary condition as

$$\frac{\partial \eta}{\partial t} = \frac{\partial \Phi}{\partial y} \quad \text{on } y = 0. \tag{2.11}$$

This condition states that the fluid particles on the free surface and the free surface itself has the same velocity along the normal to the free surface.

Eliminating η between (2.8) and (2.11) we get the linearised free surface condition

as

$$\frac{\partial^2 \Phi}{\partial t^2} = g\frac{\partial \Phi}{\partial y} \quad \text{on } y = 0. \tag{2.12}$$

The condition of no motion at the bottom gives

$$\nabla \Phi \to 0 \quad \text{as} \quad y \to \infty, \tag{2.13}$$

when the fluid is of infinite depth, and

$$\frac{\partial \Phi}{\partial y} = 0 \quad \text{on } y = h, \tag{2.14}$$

when the fluid is of constant finite depth h.

For a time harmonic motion, the velocity potential Φ may be expressed as

$$\Phi(x, y, z, t) = Re\{\phi(x, y, z)e^{-i\sigma t}\}, \tag{2.15}$$

where σ is the angular frequency.

Substituting Φ from (2.15) into (2.12), (2.13) and (2.14) we find $\phi(x, y, z)$ satisfies

$$\nabla^2 \phi = 0 \quad \text{in the fluid region.} \tag{2.16}$$

The free surface condition is

$$K\phi + \frac{\partial \phi}{\partial y} = 0, \quad \text{where} \quad K = \frac{\sigma^2}{g}. \tag{2.17}$$

The condition of no motion at bottom gives

$$\nabla \phi \to 0 \quad \text{as} \quad y \to \infty \text{ for deep water,} \tag{2.18}$$

and

$$\frac{\partial \phi}{\partial y} = 0 \quad \text{on} \quad y = h \text{ for finite depth } h. \tag{2.19}$$

Eqns (2.16)-(2.19) give the basic equations in the theory of water waves.

2.1.2 BASIC EQUATIONS TAKING INTO ACCOUNT THE EFFECT OF SURFACE TENSION

In this section we take into consideration the effect of surface tension of water at the free surface so that the free surface condition gets modified.

Due to the effect of the surface tension, the surface of the fluid is curved so that the pressure on both sides of the fluid are different and they differ by an amount depending upon the curvature of the surface.

Consider the pressure at the inner side and outer side of the water surface as p_1 and p_2 respectively, so that,

$$p_1 - p_2 = \frac{T}{R}, \quad \text{on } y = \eta, \tag{2.20}$$

where R = radius of curvature, T = coefficient of surface tension.

Now,

$$\frac{1}{R} = \frac{\eta_{xx}}{\sqrt{(1+\eta_x^2)^3}} + \frac{\eta_{zz}}{\sqrt{(1+\eta_z^2)^3}}$$

Since, under the assumption of linearised theory, η_x, η_z are small so their squares can be neglected. Hence we have,

$$\frac{1}{R} \simeq \eta_{xx} + \eta_{zz}.$$

Thus equation (2.20) takes the form

$$p_1 - p_2 = T(\eta_{xx} + \eta_{zz}), \text{ on } y = \eta. \tag{2.21}$$

From Bernoulli's equation (2.6), the pressure p_1 can be expressed as

$$\frac{p_1}{\rho} = g\eta - \frac{\partial \Phi}{\partial t}$$

so that from equation (2.21) we obtain

$$\frac{p_2}{\rho} = g\eta - \Phi_t - \frac{T}{\rho}(\eta_{xx} + \eta_{zz}), \text{ on } y = \eta, \tag{2.22}$$

where p_2 is the atmospheric pressure on the free surface (outer surface) of the water which is a constant. Differentiating equation (2.22) partially with respect to t, we get

$$0 = g\eta_t - \phi_{tt} - \frac{T}{\rho}(\eta_{xxt} + \eta_{zzt}).$$

Noting the kinematic condition on the free surace given by $\eta_t = \Phi_y$, on $y = \eta$ we have

$$0 = g\Phi_y - \Phi_{tt} - \frac{T}{\rho}\frac{\partial}{\partial y}(\Phi_{xx} + \Phi_{zz}).$$

Since Φ satisfies Laplace's equation, so,

$$\begin{aligned} & g\Phi_y - \Phi_{tt} + \frac{T}{\rho}\Phi_{yyy} = 0 \\ \implies & \Phi_y - \frac{1}{g}\Phi_{tt} + M\Phi_{yyy} = 0, \text{ on } y = \eta, \end{aligned}$$

where $M = \frac{T}{\rho g}$.

Using Taylor's expansion about $y = 0$ and linearising the above equation, we get

$$\Phi_y - \frac{1}{g}\Phi_{tt} + M\Phi_{yyy} = 0 \qquad \text{on } \ y = 0. \tag{2.23}$$

This is the free surface condition in presence of surface tension.

For time harmonic motion, $\Phi(x, y, z, t) = Re[\phi(x, y, z)e^{-i\sigma t}]$ and the linearised free

surface condition (2.23)

$$\phi_y + K\phi + M\phi_{yyy} = 0 \tag{2.24}$$

where $K = \frac{\sigma^2}{g}$ and $M = \frac{T}{\rho g}$.

Thus basic equations of water waves in presence of surface tension effect are

$$\begin{aligned} \nabla^2\phi &= 0, \\ K\phi + \phi_y + M\phi_{yyy} &= 0, \\ \nabla\phi \to 0 \quad &\text{as} \quad y \to \infty \text{ for deep water}, \\ \frac{\partial\phi}{\partial y} &= 0 \quad \text{on} \quad y = h, \end{aligned}$$

when the water region is of finite depth h.

2.1.3 WATER WITH AN ICE-COVER

Here we derive the basic equations when the water surface is covered by a thin sheet of ice which is modelled as a thin elastic plate of uniform surface density $\delta\rho$, Young's modulus E and Poisson ratio ν. The density of water is ρ and δ is a constant having dimension of length.

We choose a rectangular cartesian coordinate system in which y-axis is directed vertically downwards into the water region so that water occupies the region $y \geq 0$. The x-axis is along the thin ice cover at rest.

We assume the motion to start from rest so that it is irrotational and can be described by a velocity potential $\Phi(x, y, z, t)$.

The equation of continuity gives

$$\nabla^2\Phi = 0 \tag{2.25}$$

in the fluid region.

The linearised Bernoulli's equation gives

$$\frac{\partial \Phi}{\partial t} = gy - \frac{p}{\rho}. \tag{2.26}$$

Let us consider the depression of the ice covered surface below the horizontal level as $y = \zeta(x, z, t)$.
Then Newton's equation of motion gives

$$m\frac{\partial^2 \zeta}{\partial t^2} = mg + \Pi - p - L\nabla^4_{x,z}\zeta \qquad \text{on } y = \zeta. \tag{2.27}$$

Here $m = \rho\delta = h_i\rho_i$, Π is the atmospheric pressure and $L = \frac{Eh_i^3}{12(1-\nu^2)}$, with h_i as the thickness of ice, which is small and ρ_i as density of ice, $\nabla^4_{x,z}$ represents the two-dimensional biharmonic operator.
Using (2.26) in (2.27), we get after simplification and linearisation

$$m\frac{\partial^2 \zeta}{\partial t^2} = mg + \Pi - \rho\left(g\zeta - \frac{\partial \Phi}{\partial t}\right) - L\nabla^4_{x,z}\zeta \qquad \text{on } y = 0. \tag{2.28}$$

Also the kinematic condition gives

$$\frac{\partial \zeta}{\partial t} = \frac{\partial \Phi}{\partial y} \qquad \text{on } \; y = 0. \tag{2.29}$$

Eliminating ζ between (2.28) and (2.29), we obtain

$$\frac{\partial^2}{\partial t^2}\left[\Phi - \delta\Phi_y\right] = g\left[1 + D\nabla^4_{x,z}\right]\Phi_y \qquad \text{on } y = 0, \tag{2.30}$$

where $D = \frac{L}{\rho g}$.

The bottom condition for Φ is

$$\nabla\Phi \to 0 \qquad \text{as } y \to \infty, \tag{2.31}$$

for deep water and

$$\frac{\partial \Phi}{\partial y} = 0 \quad \text{on } \; y = h, \tag{2.32}$$

when the water region is of uniform finite depth h.

Now let us consider two-dimensional time harmonic motion with angular frequency σ so that $\Phi = Re\{\phi(x,y)e^{-i\sigma t}\}$.
Then ϕ satisfies

$$\nabla^2\phi = 0 \quad \text{in} \quad y > 0. \tag{2.33}$$

The ice cover condition (2.28) becomes

$$K\phi + \left(1 - \delta K + D\partial^4_{xxxx}\right)\phi_y = 0 \quad \text{on } y = 0. \tag{2.34}$$

The bottom condition becomes

$$\nabla\phi \to 0 \quad \text{as} \quad y \to \infty, \tag{2.35}$$

for deep water and

$$\frac{\partial\phi}{\partial y} = 0 \quad \text{on} \quad y = h, \tag{2.36}$$

when the water is of uniform finite depth h.
Thus eqs (2.33)-(2.36) give the basic equations when the water surface is covered with ice.

2.2 HAVELOCK'S EXPANSION

2.2.1 HAVELOCK'S EXPANSION THEOREM

Let $f(x)$ be a function which satisfies the conditions of Fourier integral theorem. Then Havelock's expansion for $f(x)$ in $(0,\infty)$ is given by

$$f(x) = Ae^{-Kx} + \int_0^\infty g(y)\,(y\cos xy - K\sin xy)\,dy, \tag{2.37}$$

where K is a non negative parameter,

$$A = 2K \int_0^\infty f(x) e^{-Kx} dx, \tag{2.38}$$

and

$$g(y) = \frac{2}{\pi} \frac{1}{y^2 + K^2} \int_0^\infty f(x)(y \cos xy - K \sin xy) dx. \tag{2.39}$$

Expansion (2.37) combined with the relations (2.38) and (2.39) is regarded as Havelock's expansion theorem in the water wave theorem. This is in fact a generalisation of Fourier cosine transform. This is clear if we put K=0 in these relations.

This gives

$$f(x) = \int_0^\infty y g(y) \cos xy dy, \tag{2.40}$$

and

$$y g(y) = \frac{2}{\pi} \int_0^\infty f(x) \cos xy dx. \tag{2.41}$$

This transform was first used by Havelock in 1929 in connection with a plane vertical wave maker problem. A generalisation of this theorem can be done when the surface tension effect at the free surface is taken into account and when the water region has ice cover surface. In these cases the special care has to be taken regarding the orthogonality of the eigen functions. A detailed discussion is given in Manam *et al.* (2006).

2.2.2 HAVELOCK'S EXPANSION OF WATER WITH A FREE SURFACE(TWO DIMENSIONAL CASE)

In the problems concerning two dimensional motion, the velocity potential is described by $\mathrm{Re}\{\phi(x, y)e^{-i\sigma t}\}$ where ϕ satisfies Laplace's equation together with free surface condition and bottom condition.

For two dimensional motion, using the method of separation of variables, the progressive wave solution and local solutions of Laplace's equation satisfying the free surface condition and bottom condition in water of infinite depth are $e^{-Ky \pm iKx}$ and

$(k\cos ky - K\sin ky)e^{\pm kx}$,
$k > 0$. These form a basis for expansion of $\phi(x,y)$ which is given by

$$\begin{aligned}\phi(x,y) &= Ae^{-Ky+iKx} + Be^{-Ky-iKx} \\ &+ \begin{cases} \int_0^\infty C(k)(k\cos ky - K\sin ky)e^{-kx}dk & x > 0, \\ \int_0^\infty D(k)(k\cos ky - K\sin ky)e^{kx}dk & x < 0, \end{cases}\end{aligned} \tag{2.42}$$

where A, B are unknown constants and $C(k)$ and $D(k)$ are unknown functions of k. This is known as Havelock's expansion of water wave potential $\phi(x,y)$.

For water of finite depth h, the basis functions are $\cosh k_0(h-y)e^{\pm ik_0x}$ and $\cos k_n(h-y)e^{\pm k_nx}$, where $\pm k_0$, $\pm ik_n(k_0, k_n$ are real) are roots of the transcendental equation

$$k\tanh kh = K.$$

Thus Havelock's expansion of water wave potential for water of finite depth h is given by

$$\begin{aligned}\phi(x,y) &= A_0\frac{\cosh k_0(h-y)}{\cosh k_0h}e^{ik_0x} + B_0\frac{\cosh k_0(h-y)}{\cosh k_0h}e^{-ik_0x} \\ &+ \begin{cases} \sum_{n=1}^\infty C_ne^{-k_nx}\frac{\cos k_n(h-y)}{\cos k_nh} & x > 0, \\ \sum_{n=1}^\infty D_ne^{k_nx}\frac{\cos k_n(h-y)}{\cos k_nh} & x < 0, \end{cases}\end{aligned} \tag{2.43}$$

where A_0, B_0, C_n and D_n are unknowns.

2.2.3 HAVELOCK'S EXPANSION OF WATER WITH ICE COVER SURFACE

We consider irrotational two dimensional motion in water with ice cover described by the velocity potential $\mathrm{Re}\{\phi(x,y)e^{-i\sigma t}\}$ for deep water where ϕ satisfies the Laplace's

equation, ice cover condition and the bottom condition given by (2.33)-(2.35).
The method of separation of variables, the progressive wave solutions and the local solutions of Laplace's equation with the ice cover condition for two dimensional harmonic motion in deep water are $e^{-\lambda_0 y \pm i\lambda_0 x}$, $e^{-\lambda_1 y \pm i\lambda_1 x}$, $e^{-\bar{\lambda}_1 y \pm i\bar{\lambda}_1 x}$ and $\{(Dk^4 + 1 - \delta k)k\cos ky - K\sin ky\}\, e^{-k|x|}$, where λ_0 is the unique real positive root of the equation

$$Dk^4 + (1 - \delta K)k - K = 0. \tag{2.44}$$

The other two pairs of complex conjugate zeros of (2.44) are $(\lambda_1, \bar{\lambda}_1)$ and $(\lambda_2, \bar{\lambda}_2)$ with Re $\lambda_1 > 0$, Im $\lambda_1 > 0$, Re $\lambda_2 < 0$ and Im $\lambda_2 > 0$ (Chakrabarti (2000)).

Hence for the irrotational motion in water with ice cover, the expansion for wave potential $\phi(x, y)$ is given as

$$\begin{aligned}\phi(x,y) &= P_1 e^{-\lambda_0 y + i\lambda_0 x} + P_2 e^{-\lambda_0 y - i\lambda_0 x} \\ &+ \begin{cases} P_3 e^{-\lambda_1 y + i\lambda_1 x} + P_4 e^{-\bar{\lambda}_1 y - i\bar{\lambda}_1 x} \\ + \int_0^\infty Q(\xi)\left\{\xi(D\xi^4 + 1 - \delta K)\cos\xi y - K\sin\xi y\right\} e^{-\xi x} d\xi & x > 0, \\ P_5 e^{-\lambda_1 y - i\lambda_1 x} + P_6 e^{-\bar{\lambda}_1 y + i\bar{\lambda}_1 x} \\ \int_0^\infty R(\xi)\{\xi(D\xi^4 + 1 - \delta K)\cos\xi y - K\sin\xi y\} e^{\xi x} d\xi & x < 0. \end{cases}\end{aligned} \tag{2.45}$$

Here $P_1, P_2, ..., P_6$ and $Q(\xi), R(\xi)$ are unknowns.

Again for water of uniform finite depth h, the method of separation of variables of Laplace's equation for two dimensional motion produces the progressive and local solutions, satisfying the ice cover condition and bottom condition given by (2.34) and (2.36) respectively as $\frac{\cosh\mu_0(h-y)}{\cosh\mu_0 h} e^{\pm i\mu_0 x}$, $\frac{\cosh\mu_1(h-y)}{\cosh\mu_1 h} e^{\pm i\mu_1 x}$, $\frac{\cosh\bar{\mu}_1(h-y)}{\cosh\bar{\mu}_1 h} e^{\pm i\bar{\mu}_1 x}$ and $\frac{\cos\mu_n(h-y)}{\cos\mu_n h} e^{\pm\mu_n x}$, where μ_0 is the unique positive real root of the equation

$$k(Dk^4 + 1 - \delta K)\sinh kh - K\cosh kh = 0, \tag{2.46}$$

and $\pm\mu_1$ and $\pm\bar{\mu}_1$ with Re(μ_1) <Im(μ_1), Re$(\mu_1) > 0$ and Im$(\mu_1) > 0$ are its four complex conjugate roots and $\pm i\mu_n^*$ are infinite number of purely imaginary zeros

($\mu_n^* > 0$ and real, n=1,2,....) of (2.46) with $h\mu_n^* \to n\pi$ as $n \to \infty$ (Chung and Fox (2002)).

Hence the Havelock's expansion of $\phi(x, y)$ for finite depth h of water is given by

$$\phi(x,y) = G_1 \frac{\cosh \mu_0(h-y)}{\cosh \mu_0 h} e^{i\mu_0 x} + G_2 \frac{\cosh \mu_0(h-y)}{\cosh \mu_0 h} e^{-i\mu_0 x} + \begin{cases} G_3 \frac{\cosh \mu_1(h-y)}{\cosh \mu_1 h} e^{i\mu_1 x} + G_4 \frac{\cosh \bar{\mu}_1(h-y)}{\cosh \bar{\mu}_1 h} e^{-i\bar{\mu}_1 x} + \sum_{n=1}^{\infty} S_n \frac{\cos \mu_n^*(h-y)}{\cos \mu_n^* h} e^{-\mu_n^* x} & \\ & x > 0, \\ G_5 \frac{\cosh \mu_1(h-y)}{\cosh \mu_1 h} e^{-i\mu_1 x} + G_6 \frac{\cosh \bar{\mu}_1(h-y)}{\cosh \bar{\mu}_1 h} e^{i\bar{\mu}_1 x} + \sum_{n=1}^{\infty} T_n \frac{\cos \mu_n^*(h-y)}{\cos \mu_n^* h} e^{\mu_n^* x} & \\ & x < 0, \end{cases} \tag{2.47}$$

where $G_1, G_2, ..., G_6, S_n$ and T_n are unknowns.

2.2.4 HAVELOCK'S EXPANSION OF WATER WITH SURFACE TENSION

For deep water, the eigen function expansion is given by

$$\phi(x,y) = A_0 e^{-k_1 y + ik_1 x} + B_0 e^{-k_1 y - ik_1 x} + \begin{cases} \int_0^\infty C_0(k)(k(1-Mk^2)\cos ky - K \sin ky) e^{-kx} dk & x > 0, \\ \int_0^\infty D_0(k)(k(1-Mk^2)\cos ky - K \sin ky) e^{kx} dk & x < 0, \end{cases} \tag{2.48}$$

where k_1 is the real positive root of $K - k(1 + Mk^2) = 0$ and $A_0,\ B_0,\ C_0(k),\ D_0(k)$ are unknowns (cf. Rhodes Robinson (1971)).

For water of finite depth $'h'$, the eigen function expansion is given by

$$\phi(x,y) = \frac{\cosh\gamma_0(h-y)}{\cosh\gamma_0 h}\{C_1 e^{-i\gamma_0 x} + D_1 e^{i\gamma_0 x}\} + \sum_{n=1}^{\infty} \mathcal{B}_n \frac{\cos\gamma_n(h-y)}{\cos\gamma_n h} e^{\gamma_n(x-b)}, x < 0, + \sum_{n=1}^{\infty} \mathcal{A}_n \frac{\cos\gamma_n(h-y)}{\cos\gamma_n h} e^{-s_n(x-b)}, x > 0, \quad (2.49)$$

where $\gamma_0,\ \pm i\gamma_n$ satisfy the equation $K = \gamma(1+M\gamma^2)\tanh\gamma h$ and $C_1,\ D_1,\ \mathcal{A}_n,\ \mathcal{B}_n$ are unknowns (cf. Rhodes Robinson (1971)).

2.3 TWO-DIMENSIONAL SOURCE POTENTIAL

Velocity potentials due to the presence of different types of singularities in an incompressible, inviscid fluid, assuming irrotational motion of small amplitude play a significant role in the study of the problem of scattering or radiation of waves due to the presence of obstacles in fluid medium. When a body or a number of bodies present in fluid undergoes some oscillations, the resulting motion in fluid can be described by a series of singularities placed on the bodies. These singularities are characterised by their giving rise to velocity potentials which are typical singular solutions of Laplace's equation in the neighbourhood of singularities.

For two-dimensional problems these singularities are logarithmic type or multipole type and for three dimensional problems these are point source or point multipoles.

In the present section we shall consider only the logarithmic singularity.

2.3.1 WATER WITH A FREE SURFACE

Under two dimensional motion of an ideal fluid under gravity g, the potential function $G(x,y;\xi,\eta)$ describing a time harmonic motion due to a submerged line source at (ξ,η)

satisfies

$$\nabla^2 G = 0 \qquad \text{except at} \quad (\xi, \eta), \tag{2.50}$$

$$KG + G_y = 0 \qquad \text{on} \quad y = 0, \tag{2.51}$$

$$G \sim \ln \rho \qquad \text{as} \quad \rho \to 0, \tag{2.52}$$

$$\rho = \{(x-\xi)^2 + (y-\eta)^2\}^{\frac{1}{2}}, \tag{2.53}$$

$$\nabla G \to 0 \quad \text{as} \quad y \to \infty \quad \text{for deep water,} \tag{2.54}$$

and

$$G_y = 0 \quad \text{on } y = h \quad \text{for finite depth } h. \tag{2.55}$$

Here G behaves as outgoing waves as $|x - \xi| \to \infty$.

The solution for G satisfying the conditions (2.50)-(2.54) is given by

$$G(x, y; \xi, \eta) = \ln \frac{\rho}{\rho'} - 2 \int_0^\infty \frac{e^{-k(y+\eta)}}{k - K} \cos k(x - \xi) dk, \tag{2.56}$$

where $\rho' = \{(x-\xi)^2 + (y+\eta)^2\}^{\frac{1}{2}}$ and the path of integration is along the real k-axis from $(0, \infty)$ with a small indentation below the pole at $k = K$.

An alternative representation of $G(x, y; \xi, \eta)$ is given by

$$G(x, y; \xi, \eta) = -2\pi i e^{-K(y+\eta)+iK|x-\xi|} - 2 \int_0^\infty \frac{e^{-k|x-\xi|}}{k(k^2 + K^2)} L(k, y) L(k, \eta) dk. \tag{2.57}$$

Also a suitable representation of G satisfying (2.50)-(2.53) and (2.55) is given by

$$G(x,y;\xi,\eta) = \ln\frac{\rho}{\rho'} - 2\int_{c_1}\frac{e^{-k(y+\eta)}}{k-K}\cos k(x-\xi)dk$$
$$-2\int_{c_2}\frac{L(k,y)L(k,\eta)e^{-kh}\cos k(x-\xi)}{k(k-K)(k\sinh kh - K\cosh kh)}dk, \tag{2.58}$$

where the paths of integration $c_1,\ c_2$ are along the positive real axis in the complex k-plane indented below the pole at $k=K$ for c_1 and $k=K,\ k_0$ for c_2, where k_0 is real positive zero of

$$k\sinh kh - K\cosh kh = 0.$$

An alternative representation of $G(x,y;\xi,\eta)$ is given by

$$G(x,y;\xi,\eta) = -4\pi i\frac{\cosh k_0(h-\eta)\cosh k_0(h-y)}{2k_0h+\sinh 2k_0h}e^{ik_0|x-\xi|}$$
$$-4\pi\sum_{n=1}^{\infty}\frac{\cos k_n(h-\eta)\cos k_n(h-y)}{2k_nh+\sin 2k_nh}e^{-k_n|x-\xi|}. \tag{2.59}$$

Here $\pm k_0$ and $\pm ik_n$ (n=1,2,....) are the roots of

$$k\tanh kh = K.$$

The detailed calculation for the derivation of (2.56) and (2.59) are given by Thorne (1953) and Mandal (1987).

2.3.2 WATER WITH ICE-COVER

Assuming linear theory and irrotational motion, the velocity potential due to a time harmonic line source submerged in water at (ξ,η) is denoted by $\mathrm{Re}\{\phi(x,y)e^{-i\sigma t}\}$, where ϕ satisfies

$$\nabla^2\phi = 0 \text{ in the fluid region except at } (\xi,\eta),$$

the ice cover condition

$$K\phi + (D\partial^4_{xxxx} - \delta K + 1)\phi_y = 0 \quad \text{on} \quad y = 0. \tag{2.60}$$

Here $D = \frac{Eh_0^3}{12(1-\nu^2)\rho g}$, $K = \frac{\sigma^2}{g}$, g being the gravity, $\delta = \frac{\rho_i}{\rho}h_i$, E being the Young's modulus, ν being Poisson ratio of the material of ice cover, ρ being the density of water, ρ_i is the density of ice and h_i is the thickness of ice cover.

Also,

$$\phi \text{ behaves as } \ln\rho \text{ as } \rho = \{(x-\xi)^2 + (y-\eta)^2\}^{\frac{1}{2}} \to 0, \tag{2.61}$$

$$\nabla\phi \to 0 \text{ as } y \to \infty \text{ for deep water,} \tag{2.62}$$

$$\frac{\partial\phi}{\partial y} = 0 \text{ on } y = h \text{ when the water region is of depth } h \tag{2.63}$$

and

$$\phi \text{ behaves as outgoing wave as } |x-\xi| \to \infty. \tag{2.64}$$

2.3.2.1 SOURCE POTENTIAL FOR DEEP WATER

Source potential due to a logarithmic singularity in water with ice cover surface for deep water is given as

$$\phi(x,y) = -2\int_0^\infty \frac{\{k(1-\delta K + Dk^4)\cosh ky_< - K\sinh ky_<\}}{k\{k(1-\delta K + Dk^4) - K\}} e^{-ky_>}\cos k(x-\xi)dk, \tag{2.65}$$

where the path of integration is over a line on the real axis in the k-plane with an indentation below the real positive zero of $k(1-\delta K + Dk^4) - K$ and $y_<$ and $y_>$ respectively denote the lesser and greater of y and η.

Alternately, ϕ can be simplified as

$$\begin{aligned}\phi(x,y) = -2\int_0^\infty \frac{L(k,y)L(k,\eta)}{k\{k^2(1-\delta K+Dk^4)+K^2\}}e^{-k|x-\xi|}dk \\ -2\pi i\frac{1}{\lambda(1-\delta K+5DK^4\lambda^4)}e^{-K\lambda(y+\eta)+iK\lambda|x-\xi|} \\ -2\pi i[\frac{1}{\lambda_1(1-\delta K+5DK^4\lambda_1^4)}e^{-K\lambda_1(y+\eta)+iK\lambda_1|x-\xi|} \\ -\frac{1}{\bar{\lambda}_1(1-\delta K+5DK^4\bar{\lambda}_1^4)}e^{-K\bar{\lambda}_1(y+\eta)-iK\bar{\lambda}_1|x-\xi|}]\end{aligned} \tag{2.66}$$

where

$$L(k,y) = k(1-\delta K+Dk^4)\cos ky - K\sin ky$$

and real positive root $K\lambda$ and two pairs of complex conjugate zeros $K\lambda_1,\ K\bar{\lambda}_1$ and $K\lambda_2,\ K\bar{\lambda}_2$ with Re $(\lambda_1) > 0$, Re $(\lambda_2) < 0$, Im $(\lambda_1, \lambda_2) > 0$ are the roots of the equation

$$\Delta(k) = (1-\delta K+Dk^4)k - K = 0. \tag{2.67}$$

2.3.2.2 SOURCE POTENTIAL FOR FINITE DEPTH WATER

Source potential for finite depth water with ice cover surface is given as

$$\phi(x,y) = -2\int_0^\infty \frac{\{k(1-\delta K+Dk^4)\cosh ky_< - K\sinh ky_<\}}{k\Delta_0(k)}\cosh k(h-y_>)\cos k(x-\xi)dk, \tag{2.68}$$

where the path of integration is over a line on the real axis in the k-plane with an indentation below the real positive zero of $\Delta_0(k)$. Alternately

$$\begin{aligned}\phi(x,y) = -4\pi\sum_{n=1}^{\infty} f(\alpha_n;y,\eta)e^{-K\alpha_n|x-\xi|} - 4\pi i g(\mu;y,\eta)e^{iK\mu|x-\xi|} \\ -4\pi i g(\mu_1;y,\eta)e^{iK\mu_1|x-\xi|} + 4\pi i g(\bar{\mu}_1;y,\eta)e^{-iK\bar{\mu}_1|x-\xi|},\end{aligned} \tag{2.69}$$

where

$$f(\alpha; y, \eta) = \frac{(1 - \delta K + DK^4\alpha^4)\cos K\alpha(h-\eta)\cos K\alpha(h-y)}{2K\alpha h(1 - \delta K + DK^4\alpha^4) + (1 - \delta K + 5DK^4\alpha^4)\sin 2K\alpha h}, \tag{2.70}$$

and

$$g(\alpha; y, \eta) = if(i\alpha; y, \eta). \tag{2.71}$$

Here, the two real roots $\pm K\mu(\mu > 0)$, two pairs of complex conjugate zeros $K\mu_1$, $K\bar{\mu}_1$ and $-K\mu_1$, $-K\bar{\mu}_1$ with Re ($\mu_1 0$ <Im (μ_1), and an infinite number of purely imaginary zeros $\pm iK\alpha_n$ ($\alpha_n > 0$ and real, n=1,2,...) are the roots of the transcendental equation

$$\Delta_0(k) = k(1 - \delta K + Dk^4)\sinh kh - K\cosh kh = 0. \tag{2.72}$$

A detailed derivation of (2.65), (2.66), (2.68) and (2.69) is given by Gayen (2004).

2.4 GREEN'S THEOREMS

Green's theorem is stated as follows:

$$\int_R (u\nabla^2 v - v\nabla^2 u)dV = \int_S \left(u\frac{\partial v}{\partial n} - v\frac{\partial u}{\partial n}\right)dS \tag{2.73}$$

where S is boundary of the region R, n is unit normal outward to S. The functions u and v have partial derivatives of the second order and are continuous in the bounded region R.

2.5 GALERKIN METHOD

One of the most important weighted residual method is Galerkin approximation method. To describe the method, we need some idea regarding the inner product.

Definition : In a vector space V of real functions whose domain is an closed interval $A = [a, b]$, an inner product of two real functions $f(x)$ and $g(x)$ is defined as

$$\langle f(x), g(x) \rangle = \int_a^b f(x)g(x)dx. \tag{2.74}$$

GALERKIN APPROXIMATION :

Let us consider an operator equation as

$$(Ly)(x) = f(x), \quad x \in A \tag{2.75}$$

where L is a linear operator in a certain inner product space S to itself, A is a domain in S and $f(x) \in S$ represents the forcing function.

In some problems of physical interest, it is desired to evaluate an inner product $\langle y, f \rangle$, where

$$\langle y, f \rangle = \int_{x \in A} y(x)f(x)dx. \tag{2.76}$$

A real valued function $y(x)$ is said to solve the operator equation (2.75) if and only if

$$\langle Ly, \lambda \rangle = \langle \lambda, Ly \rangle = \langle \lambda, f \rangle \text{ for all } \lambda \in S. \tag{2.77}$$

Now using (2.74) and (2.77) the function $y(x)$ can be evaluated at least approximately. Here we replace $y(x)$ by $F(x)$, where F is the approximate solution of equation (2.75), so that

$$\langle \lambda, LF \rangle = \langle \lambda, f \rangle \text{ for all } \lambda \in S \tag{2.78}$$

whenever the approximation relation as in equation (2.78) holds good, then we can consider F as the approximate solution of the operator equation (2.75). The determination of such approximate solutions of the equation (2.75) involving the function F

in the form of a truncated series as given by

$$F(x) = \sum_{j=1}^{n} a_j \phi_j(x) \tag{2.79}$$

is known as Galerkin approximation method, $\{\phi_j\}_{j=1}^{n}$ (n is finite) being the set of basic functions.

Applying the linear operator L on both side of the equation (2.79) and taking inner product with $\lambda \in S$ on both sides and then using the approximate identity equation (2.78) , we get

$$\sum_{j=1}^{n} a_j \big\langle L\phi_j(x), \lambda(x) \big\rangle \approx \big\langle f(x), \lambda(x) \big\rangle \quad \text{for } \lambda \in S. \tag{2.80}$$

Single-term Galerkin approximation :

If we take $n = 1$ in equation (2.80), and choose $\lambda(x) = \phi_1(x)$, then we get $a_1 = \frac{\langle f, \phi_1 \rangle}{\langle L\phi_1, \phi_1 \rangle}$ producing the approximate solution for $y(x)$ as

$$F(x) = a_1 \phi_1(x). \tag{2.81}$$

The approximate evaluation of the quantity $\langle y, f \rangle$ in (2.76), can be completed by using the approximate relation $\langle y, f \rangle \approx \langle F, f \rangle$, which takes up the value $a_1 \langle \phi_1, f \rangle$, if only the single-term Galerkin approximation is used.

Multi-term Galerkin approximation :

Let us choose $\lambda(x) = \phi_k(x)$ for some fixed positive integer k, such that $1 \leq k \leq n$, then we obtain from (2.80), that

$$\sum_{j=1}^{n} a_j \big\langle L\phi_j(x), \phi_k(x) \big\rangle = \big\langle f(x), \phi_k(x) \big\rangle, \quad k = 1, 2, ..., n. \tag{2.82}$$

Thus here we obtain exactly n linear equations for the determination of the n unknown constants and these constants can be easily determined by appropriate choice of the set of functions $\{\phi_j(x)\}_{j=1}^{n}$. The approximation of y by F, where F is given

by the n-term truncated series (given in (2.81)), is termed as multi-term Galerkin approximations. Once the n constants $a_1, a_2, ..., a_n$ are determined by solving the linear system (2.80), $\langle y, f \rangle$, the quantity of our physical interest, is approximately evaluated as

$$\langle y, f \rangle \approx \sum_{j=1}^{n} a_j \langle \phi_j, f \rangle. \tag{2.83}$$

The inner product $\langle \phi_j, f \rangle$ is defined by an integral defined as in equation (2.76), and is evaluated by using appropriate numerical quadrature formula.

The choice of the basis functions $\{\phi_j\}_{j=1}^{n}$ are chosen suitably by keeping in mind the regarding boundary conditions of the physical problems. A detailed discussion is given in Mandal and Chakrabarty (2000).

2.6 INTEGRAL EQUATION WITH STRONGLY SINGULAR KERNEL

2.6.1 SOLUTION OF SINGULAR INTEGRAL EQUATION OF FIRST KIND WITH CAUCHY KERNEL

Singular integral equation of first kind with Cauchy kernel is considered as an important tool in applied mathematics. Solutions of many problems in continuum mechanics depend on the solution of a singular integral equation of first kind with Cauchy type kernel of the form

$$\frac{1}{\pi} \int_G \frac{\phi(t)}{t - x} \, dt = \psi(x), \quad x \in G, \tag{2.84}$$

where the integral is defined in the sense of Cauchy principal value. The functions $\phi(x)$ and $\psi(x)$ are Holder continuous functions and G consists of either a single interval or disjoint multiple intervals.

In this section the solution of the above singular integral equation is obtained by

using the function-theoretic method where

(i) G consists of a single finite interval,

(ii) G consists of two finite disjoint intervals.

Solution of the integral equation (2.84) for $G = (a, b)$:

The solution of

$$\frac{1}{\pi} \int_a^b \frac{\phi(t)}{t-x}\, dt = \psi(x), \quad x \in (a, b), \tag{2.85}$$

is given in Gakhov (1966), Mandal and Chakrabarti (2016). Here the solution can be obtained when $\phi(t)$ has any one of the three following behaviours at the end points $t = a, b$ are given

$$\begin{aligned} (I) \quad \phi(t) &= O(|t-a|^{-\frac{1}{2}}), \quad \text{as} \quad t \to a, \\ \phi(t) &= O(|t-b|^{-\frac{1}{2}}), \quad \text{as} \quad t \to b; \end{aligned}$$

In this case the solution is given by

$$\phi(t) = -\frac{1}{\pi} \frac{1}{\{(t-a)(b-t)\}^{\frac{1}{2}}} \left[\int_a^b \frac{\{(x-a)(b-x)\}^{\frac{1}{2}}}{t-x} \psi(x) dx + C \right], \quad a < t < b, \tag{2.86}$$

where C is an arbitrary constant.

$$\begin{aligned} (II) \quad \phi(t) &= O(|t-a|^{-\frac{1}{2}}), \quad \text{as} \quad t \to a, \\ \phi(t) &= O(|t-b|^{\frac{1}{2}}), \quad \text{as} \quad t \to b; \end{aligned}$$

Here the solution is given by

$$\phi(t) = -\frac{1}{\pi} \frac{(b-t)^{1/2}}{(t-a)^{1/2}} \int_a^b \frac{(x-a)^{1/2}}{(b-x)^{1/2}} \frac{\psi(x)}{t-x} dx, \quad a < t < b. \tag{2.87}$$

Similar result can be obtained when

$$\phi(t) = O(|t-a|^{\frac{1}{2}}), \quad \text{as} \quad t \to a,$$
$$\phi(t) = O(|t-b|^{-\frac{1}{2}}), \quad \text{as} \quad t \to b;$$

$$(III) \quad \phi(t) = O(|t-a|^{\frac{1}{2}}), \quad \text{as} \quad t \to a,$$
$$\phi(t) = O(|t-b|^{\frac{1}{2}}), \quad \text{as} \quad t \to b;$$

In this case the solution is given by

$$\phi(t) = -\frac{1}{\pi}\{(t-a)(b-t)\}^{1/2} \int_a^b \frac{1}{\{(x-a)(b-x)\}^{1/2}} \frac{\psi(x)}{t-x} dx, \quad a < t < b. \tag{2.88}$$

It may be noted that the forcing function $\psi(x)$ has to satisfy the following solvability condition in order that the solution in this case exists:

$$\int_a^b \frac{\psi(x)}{\{(x-a)(b-x)\}^{1/2}}\, dx = 0. \tag{2.89}$$

A detailed discussion is given by Mandal and Chakrabarty (2016).

Solution of the integral equation (2.84) for $G = (a,b) + (c,d)$:

Here we solve the Cauchy type integral equation (2.84) where G consists of two disjoint finite intervals. This type of integral equation arises in the aerofoil theory, wave guide theory (cf. Tricomi (1951), Lewin (1975)). In this case the integral equation is

$$\frac{1}{\pi} \int_G \frac{\phi(t)}{t-x}\, dt = \psi(x), \quad x \in G, \tag{2.90}$$

where G consists of two disjoint intervals $(a,b)\cup(c,d)$, and

$$\phi(t)\sim\begin{cases}O(|t-a|^{-\frac{1}{2}}), & t\to a,\\ O(|t-b|^{-\frac{1}{2}}), & t\to b,\\ O(|t-c|^{-\frac{1}{2}}), & t\to c,\\ O(|t-d|^{-\frac{1}{2}}), & t\to d.\end{cases}\tag{2.91}$$

The solution in this case is given by (cf. Tricomi (1951), Gakhov (1966), Lewin (1975))

$$\phi(t)=-\frac{1}{\pi}|(t-a)(b-t)(t-c)(d-t)|^{-\frac{1}{2}}m(t)\tag{2.92}$$

$$\left(\int_a^b-\int_c^d\right)|(x-a)(b-x)(x-c)(d-x)|^{\frac{1}{2}}\frac{\psi(x)}{t-x}dx\tag{2.93}$$

$$+\frac{Dt+D_1}{|(t-a)(b-t)(t-c)(d-t)|^{\frac{1}{2}}}m(t),t\in G\tag{2.94}$$

where

$$m(t)=\begin{cases}-1,\ \text{when } t\in(a,b),\\ 1,\ \text{when } t\in(c,d),\end{cases}\tag{2.95}$$

and D and D_1 are constants.

If $\phi(t)$ has the following behaviour at the end points $t=a,b,c,d$

$$\phi(t)\sim\begin{cases}O(|t-a|^{\frac{1}{2}}), & t\to a,\\ O(|t-b|^{\frac{1}{2}}), & t\to b,\\ O(|t-c|^{\frac{1}{2}}), & t\to c,\\ O(|t-d|^{\frac{1}{2}}), & t\to d,\end{cases}\tag{2.96}$$

then the solution of (2.90) is given by (cf. Gakhov (1966), Lewin (1975))

$$\phi(t) = -\frac{1}{\pi}\sqrt{|(t-a)(b-t)(c-t)(d-t)|}\; m(t)$$
$$\left(\int_a^b - \int_c^d\right)\frac{\psi(x)}{t-x}\;\; \frac{dx}{\sqrt{|(x-a)(b-x)(c-x)(d-x)|}},\; t \in G, \tag{2.97}$$

where $m(t)$ is given by (2.95) and the solution exists if the forcing function $\psi(x)$ satisfies the following solvability conditions

$$\left(\int_a^b - \int_c^d\right)\frac{\psi(x)}{\sqrt{|(x-a)(b-x)(c-x)(d-x)|}}dx = 0 \tag{2.98}$$

and

$$\left(\int_a^b - \int_c^d\right)\frac{x\;\psi(x)}{\sqrt{|(x-a)(b-x)(c-x)(d-x)|}}dx = 0. \tag{2.99}$$

When the unknown function is bounded at some end points and unbounded at other end points, the solution of the integral equation is given in the book of Gakhov (1966).

2.6.2 HYPERSINGULAR INTEGRAL EQUATION

An equation of the form

$$\not\int_{-1}^{1}\;\left[\frac{1}{(x-t)^2} + K(x,t)\right]f(t)\;dt = \phi(x), \quad -1 \le x \le 1 \tag{2.100}$$

is a general first kind hypersingular integral equation with $f(\pm 1) = 0$ and $K(x,t)$ a regular function of x and t. $\phi(x)$, the forcing term belongs to a class of functions having Holder continuous first derivatives with exponent $\alpha, (0 < \alpha < 1)$ in the interval $(-1, 1)$. In the special case of $K(x,t) = 0$ we have the simple hypersingular integral equation. The part of the integral equation containing the singularity is understood as

the Hadamard finite part defined by,

$$\oint\!\!\!\!\!\!\diagup_{-1}^{1} \frac{f(t)}{(x-t)^2}dt = \lim_{\epsilon\to 0}\left[\int_{-1}^{x-\epsilon}\frac{f(t)}{(x-t)^2}dt + \int_{x+\epsilon}^{1}\frac{f(t)}{(x-t)^2}dt - \frac{f(x+\epsilon)+f(x-\epsilon)}{\epsilon}\right]. \tag{2.101}$$

Let

$$(Tf)(x) = \frac{1}{\pi}\oint_{-1}^{1}\frac{f(t)}{x-t}dt, \tag{2.102}$$

$$(Hf)(x) = \frac{1}{\pi}\oint\!\!\!\!\!\!\diagup_{-1}^{1}\frac{f(t)}{(x-t)^2}dt, \tag{2.103}$$

then, T is called Cauchy operator and H is called Hypersingular operator and $(Hf)(x)$ can be interpreted as

$$(Hf)(x) = -\frac{d}{dx}[(Tf)(x)]. \tag{2.104}$$

The integral equation

$$\frac{1}{\pi}\oint\!\!\!\!\!\!\diagup_{-1}^{1}\frac{f(t)}{(x-t)^2}dt = \phi(x), \quad -1 < x < 1 \tag{2.105}$$

with $f(\pm 1) = 0$, is generally referred to as simple hypersingular integral equation. It's solution can be obtained by a variety of methods [cf. Martin (1992), Chakrabarti and Mandal (1998)] and is given by

$$f(x) = \frac{1}{\pi}\int_{-1}^{1}\phi(t)\ \ln\frac{|x-t|}{1-xt+\{(1-x^2)(1-t^2)\}^{\frac{1}{2}}}dt. \tag{2.106}$$

2.7 BOUNDARY ELEMENT METHOD TO SOLVE HYPERSINGULAR INTEGRAL EQUATION

In this section we solve the equation

$$\int_{-1}^{1} \frac{f(t)}{(x-t)^2} dt = \phi(x). \tag{2.107}$$

by boundary element method. It is given that $f(\pm 1) = 0$. To solve (2.107), let

$$f(t) = \sqrt{1-t^2}\psi(t) \tag{2.108}$$

where $\psi(t)$ is an unknown function which is regular function in $[-1, 1]$.
Now substituting (2.108) in (2.107), we rewrite the hypersingular integral equation as

$$\int_{-1}^{1} \frac{\sqrt{1-t^2}\ \psi(t)}{(x-t)^2} \psi(t) dt = \phi(x). \tag{2.109}$$

Now we divide the range of integration $[-1, 1]$ into n number of line elements, i.e. $[-1, 1] = \bigcup_{j=1}^{n} [b_{j-1}, b_j]$, where b_{j-1} and b_j are the end points of jth line element and $b_0 = -1$, $b_n = 1$ and $b_j = b_0 + jr'$, $r' = \frac{b_n - b_0}{n}$.
Now we take $t = t_j$ where $t_j \in [b_{j-1}, b_j], j = 1, 2...., n$. So

$$t_j = (1-\tau)b_{j-1} + \tau b_j, \quad 0 \leq \tau \leq 1. \tag{2.110}$$

Also x belonging to line element joining b_{i-1} and b_i, we write $x = x_i = (1-\gamma)b_{i-1} + \gamma b_i,\ 0 \leq \gamma \leq 1\ ,\ i = 1, 2, ..., n$.
So, equation (2.109) can be rewritten as

$$\sum_{j=1}^{n} \int_0^1 \sqrt{1-t_j^2}\ \{\frac{\psi(t_j)}{(x_i - t_j)^2}\}\ \ r'\ d\tau = \phi(x_i)\ ,\ i = 1, 2, ..., n \tag{2.111}$$

Now in this Boundary Element Method, we assume that the unknown function

in the integral equation takes constant values in each small intervals, i.e. we take $\psi(t_j) = \psi_j$ as a constant for jth line element, $j = 1, 2, ..., n$. So, under this assumption Integral equation (2.111) is reduced to a system of linear equations which can be written as

$$\sum_{j=1}^{n} a_{ij}\psi_j = \phi_i \ , \ i = 1, 2, ..., n \tag{2.112}$$

where

$$a_{ij} = \int_0^1 \frac{\sqrt{1-t_j^2}}{(x_i - t_j)^2}\, r' \, d\tau \ , \ i = 1, 2, ..., n; \quad j = 1, 2, ..., n, \tag{2.113}$$

$$\phi_i = \phi(x_i) \ , \quad i = 1, 2, ..., n. \tag{2.114}$$

Now when $i = j$, the integral $\int_0^1 \frac{\sqrt{1-t_j^2}}{(x_i - t_j)^2}\ d\tau \ , \ x_i, t_i \ \in [b_{i-1}, b_i]$ becomes hypersingular integral. It is difficult to find any quadrature formula to evaluate this hypersingular integral. However this can be evaluated exactly by simple algebraic manipulation and is given by

$$\begin{aligned}\int \frac{A(t)}{(t-x)^2}\, dt \ = \ & \frac{x}{A(x)} \ \log\left|\frac{xt - (1 + A(t))(1 + A(x))}{xt - (1 - A(t))(1 + A(x))}\right| \\ & - \ 2A(x)\left(\frac{\frac{t}{(1+A(x))A(t)} - \frac{x}{A(x)}}{(\frac{xt}{1+A(t)} - 1)^2 - A(x)^2}\right) \ - \ \sin^{-1}(t)\end{aligned} \tag{2.115}$$

where $A(t) = \sqrt{1 - t^2}$.
Now choosing $x_i = \frac{b_i + b_{i-1}}{2}$, $i = 1, 2, ..., n$, the system of equation (2.112) is solved to obtain the unknown functions ψ_j, $j = 1, 2, ..n$ and hence $f(t_j)$ is approximated in each $[b_{j-1}, b_j]$. A detailed discussion is given in Samanta *et al.* (2021).

PART II

CHAPTER 3

PROPAGATION OF SURFACE GRAVITY WAVES BY A SUBMERGED THIN ELASTIC PLATE BENEATH AN ICE COVER

3.1 INTRODUCTION

The wave structure interaction problems involving fixed or floating obstacles of various geometrical shapes created considerable interest among the researchers since last century as this class of problems have immense application in construction of coastal structures like break waters. Various researchers have studied the wave propagation problems by thin vertical rigid barriers for its various configurations [cf. Evans (1970), Porter and Evans (1995), Goswami (1983), Mandal and Dolai (1994)]. Assuming linear theory and irrotational motion, the two-dimensional problem of water wave scattering

[0]† The content of this chapter is based on the paper " Propagation of surface gravity waves by a submerged thin elastic plate beneath an ice cover ", *Archive of Applied Mechanics*, 93 (2023), 1507-1524.

by a thin vertical rigid plate of finite length submerged in deep water was studied long back by Evans (1970) using a method based on the theory of complex variable. Porter and Evans (1995) considered oblique wave scattering by a thin vertical rigid barrier in water of uniform finite depth having four basic configurations namely, a surface piercing barrier, a bottom standing barrier, a barrier with a gap and a totally submerged barrier. For each configuration of the barrier, they used an approximate method based on the Galerkin approximation and numerical estimates for the reflection and transmission coefficients were obtained for different values of wave numbers. Also, earlier Goswami (1983) employed Greens function technique to reduce the scattering problem involving a fixed vertical rigid plate submerged in water of uniform finite depth and solved it approximately by using a perturbation method. Mandal and Dolai (1994) later obtained very accurate upper and lower bounds for the reflection and transmission coefficients for the problem of water wave scattering by a thin vertical rigid barrier present in uniform finite depth water by using the Galerkin approximation method. In all the aforementioned problems, the obstacle bodies are considered to be rigid. In recent past, breakwater with appreciable flexure, in form of elastic plate is an important area of research as the flexibility of the elastic structure provides the additional feature of wave attenuation through structural deflections.However, a limited literature exists in studying wave structure interaction phenomena involving elastic barriers.

The wave scattering problems involving elastic or viscoelastic structures as a floating breakwater is mentioned in Stoker (1957). Though the problem is considered for long waves in shallow water but explicit results to this problems were not given. Later, utilizing the linearized theory in deep water, Fox and Squire (1994) investigated the problem of water wave scattering by a floating ice-sheet modeled as an elastic plate. Later, Meylan and Squire (1994) used Green's function technique to study the scattering problem involving horizontal floating elastic plate. In recent past, the water wave propagation problems involving elastic plates of different geometrical shapes are studied by a number of authors. Sturova (2003) investigated the unsteady motion due to a circular elastic plate floating on shallow water under the action of an external load. A study of wave interaction with a floating rectangular elastic plate modeled a floating-airport is an important area of study, where one can determine the effects of periodic surface pressure on a rectangular floating elastic plate. Gayen and Mandal

(2009) used Carleman integral equation formulation to study water wave scattering problem by a thin elastic plate of arbitrary width, floating in deep water. All these problems involve horizontal elastic plates, floating or submerged in water of infinite or finite depth. A water wave problem involving a vertical thin elastic plate was studied by Meylan (1995) who considered the scattering problem by a surface piercing thin vertical elastic plate in finite depth water. The time-dependent version of this problem was solved by Peter and Meylan (2010) using a generalized eigenfunction expansion. Utilizing Green's function technique, Chakraborty and Mandal (2013, 2014) investigated the wave scattering problem by elastic plate fully submerged in infinitely deep water and finite depth water. They established the relevant energy balance relation and coefficient of energy dissipation occurred by elastic plate. Wave interaction with an elastic plate floating in finite depth water with clamped or free ends was studied by Chakraborty *et al.* (2016) by using hypersingular integral equation method.
During later half of the last century, there is a surge of different types of scientific and industrial activities in polar regions and arctic region. A study of wave propagation problems in polar oceans covered by floating ice has become very attractive to many researchers. The floating ice cover is modeled as a thin elastic plate. A floating thin elastic plate can also be regarded as a practical model for the frozen ocean or for a very large floating structure such as a floating airport, floating city etc (cf. Kashiwagi (2004)). Mathematical study of wave propagation problems in water with ice cover is interesting in the sense that under the assumption of linear theory and irrotational motion, the linearised ice-cover condition involves fifth-order partial derivative of the potential function while the governing differential equation is of second order.

Interaction of ocean waves with shore fast sea ice modeled as a thin elastic plate was first considered by Fox and Squire (1990, 1994). Scattering of an oblique wave caused by a narrow crack in ice sheets floating on water of finite depth were studied by Evans and Porter (2003). Vaughan and Squire (2006) studied the propagation of waves under an ice sheet of variable thickness. The topics in the general area of ocean wave or sea ice interactions, especially in relation to mathematical modeling, were described in the review paper of Squire (2007). Sturova (2011) considered steady oscillations of a horizontal cylinder submerged in a linearly stratified fluid layer with an ice cover using the Boussinesq approximation. Bhattacharjee and Soares (2012) investigated the behavior of flexural gravity waves propagating over a semi-infinite floating ice sheet

under the assumptions of the small-amplitude linear wave theory.

A study of the problems concerning wave interaction with vertical elastic plate is an important class of problems wherein a vertical elastic plate may serve as a model for a seawall, wave damper or a breakwater. Submerged plates are mainly used as the protectors of shoreward area of the breakwater from actions of rough sea by means of diminishing the effect of incoming waves. Such structures are useful as they allow the free exchange of water mass through them so that the pollution of water in the sheltered area is minimized. The submerged structures are also capable of absorbing some wave energy caused due to premature break up of waves and thus, they control the beach erosion.

Our main motivation in this chapter is to the study the composite effect of vertical elastic plate present in water of finite depth and ice cover of water surface, which is also considered to be elastic, on the ocean waves. The problem is formulated in terms of a boundary value problem for the velocity potential function where the boundary condition on the elastic plate is derived from the Bernoulli-Euler equation of motion. An appropriate application of Green's integral theorem in the fluid region determines the reflection and transmission coefficients in terms of integrals involving the unknown velocity potentials on either sides of the plate and a normal velocity of the elastic plate. By using the Greens function technique to solve Bernoulli-Euler equation of motion, a relation expressing the normal velocity of the elastic plate in terms of an integral involving the difference of velocity potentials (unknown) across the plate is derived. Two more relations in form of integral equations connecting the velocity potentials on either sides of the plate and the normal velocity of the elastic plate are obtained by a judicious application of Greens integral theorem in the fluid region. These three relations produce the velocity potentials on either sides of the plate and the normal velocity of the elastic plate which are then used to evaluate the reflection and transmission coefficient. These coefficients were computed numerically for various values of different non-dimensional parameters and presented graphically in a number of figures. Other physical quantities, viz, hydrodynamic force, plate deflection, shear force and shear strain are computed for the elastic plate and presented graphically for different values of rigidity coefficients of ice cover.

3.2 FORMULATION OF THE BOUNDARY VALUE PROBLEM

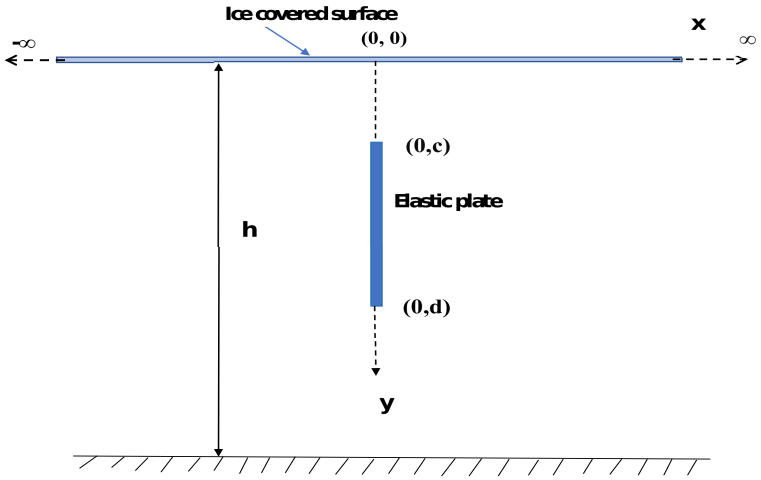

Figure 3.1: Schematic diagram of the problem

We consider two-dimensional, irrotational motion under the action of gravity in water which is an inviscid, incompressible and homogeneous fluid of density ρ_1. A rectangular Cartesian coordinate system (x, y) is chosen wherein the y-axis is taken vertically downwards into the fluid region and the plane $y = 0$ represents the undisturbed ice cover surface, so that water ocupies the region $0 < y < h$. The position of the submerged thin elastic vertical plate is given by $x = 0,\ c < y < d$ and is shown in the schematic diagram Figure (3.1). It is assumed that a monochromatic flexural gravity wave is obliquely incident from the negative x-direction on the elastic barrier with the angle of incidence θ with the horizontal axis and it is partially reflected by the plate and partially transmitted over or below the plate. The resulting time-harmonic motion with angular frequency σ is described by the velocity potential function $\Phi(x, y, t) = Re\{\phi(x, y)e^{-i\kappa z+i\sigma t}\}$, where $\kappa = \xi_0 \sin\theta$ and ξ_0 is the unique real positive root of

$$\xi(1 - \epsilon K + D\xi^4) \tanh \xi h = K. \tag{3.1}$$

The function $\phi(x, y)$ satisfies Laplace's equation

$$(\nabla^2 - \kappa^2)\phi = 0, \quad \text{in the fluid region,} \tag{3.2}$$

the boundary condition on ice covered upper surface [cf. Fox and Squire (1990) and Chapter (2.1.3)]

$$\left\{ D(\frac{\partial^2}{\partial x^2} - \kappa^2)^2 + 1 - \epsilon K \right\} \phi_y + K\phi = 0 \quad \text{on } y = 0, \tag{3.3}$$

where $K = \frac{\sigma^2}{g}$, σ being the circular frequency of incoming wave train, g being gravitational acceleration and $D = \frac{\mathcal{Y} h_0^3}{12(1-\nu^2)\rho_1 g}$, $\epsilon = \frac{\rho_0 h_0}{\rho_1}$, where ρ_0 is the density of ice, h_0 is the small thickness of the ice-cover and $\mathcal{Y}, \nu$ are respectively the Youngs modulus and Poisson's ratio of the ice which is considered as an elastic material. There is no flow at the rigid bottom boundary and the condition is

$$\frac{\partial \phi}{\partial y} = 0 \quad \text{on } y = h. \tag{3.4}$$

Suppose $\mathrm{W_E}(y, t)$ represents the deflection of the elastic plate from its mean vertical position $x = 0$, then Bernoulli-Euler equation of motion for the submerged thin vertical elastic plate can be written as [cf. Chakraborty and Mandal (2013)]

$$\frac{\partial^2 \mathrm{W_E}}{\partial t^2} + \upsilon^2 \frac{\partial^4 \mathrm{W_E}}{\partial y^4} = \frac{P_+ - P_-}{\rho' h'} \quad \text{on} \quad x = 0, \quad c < y < d, \tag{3.5}$$

where $\upsilon^2 = \frac{E' h'^2}{12\rho'(1-\nu'^2)}$, E' is the Youngs modulus and ν' is Poissons ratio of the material of the elastic plate, ρ' denotes the density of the elastic plate and h' is its small thickness,

$$P_{\mp} = P(\mp 0, y, t), \quad c < y < d, \tag{3.6}$$

$P(x, y, t)$ is the pressure at a point (x, y) of the fluid region at time t .

The pressure $P(x, y, t)$ is given by the Bernoullis equation:

$$\frac{\partial \Phi}{\partial t} = gy - \frac{P}{\rho_1}$$

so that

$$P_- - P_+ = -\rho_1(\frac{\partial \Phi_1}{\partial t} - \frac{\partial \Phi_2}{\partial t}) \tag{3.7}$$

where

$$\Phi_{1,2} = \Phi(\mp 0, y, t), \quad c < y < d. \tag{3.8}$$

Since

$$\frac{\partial W_E}{\partial t}(y,t) = \frac{\partial \Phi}{\partial x}(0,y,t), \quad c < y < d \tag{3.9}$$

so we find from equation (3.5), after using relations (3.7), (3.8) and (3.9), as

$$\frac{\partial^2 \Phi_x}{\partial t^2} + \mu^2 \frac{\partial^4 \Phi_x}{\partial y^4} = -\frac{\rho_1}{\rho' h'} \frac{\partial^2}{\partial t^2}(\Phi_1 - \Phi_2), \quad c < y < d. \tag{3.10}$$

The equation (3.10) can be rewritten in terms of ϕ after noting $\phi_x(y) = \frac{\partial \phi}{\partial x}(0,y)$ as

$$D' \frac{d^4 \phi_x}{dy^4} - \epsilon' K \phi_x = K[\phi](y) \quad \text{on} \quad x = 0, c < y < d, \tag{3.11}$$

where

$$[\phi](y) = \{\phi_1(y) - \phi_2(y)\}, \quad \text{and} \quad \phi_{1,2}(y) = \phi(\mp 0, y),$$

$$D' = \frac{E' h'^3}{12(1-\nu'^2)\rho_1 g}, \quad \epsilon' = \frac{\rho' h'}{\rho_1}.$$

We may note here that as $\phi(x,y)$ is continuous across the gap over and below the plate, so

$$\phi_1(\tau) = \phi_2(\tau), \quad \text{for} \quad 0 < y \leq c \text{ and } d \leq y < h. \tag{3.12}$$

If the two ends of the submerged elastic plate are assumed to be free, then the conditions at the two ends of the submerged plate can be obtained as [cf. Meylan and Squire (1994)]

$$\frac{d^2 \phi_x}{dy^2} = 0 = \frac{d^3 \phi_x}{dy^3} \quad \text{at } y = c, d. \tag{3.13}$$

In the vicinity of sharp submerged edges, velocity potential function satisfy [cf. Hassan *et al.* (2009)]

$$\nabla\phi \sim O(r^{-\frac{1}{2}}) \text{ as } r \to 0, \tag{3.14}$$

where r denotes the distance of any point in the fluid from either sharp edge of the elastic plate.

Now, if $\phi_0(x, y)$ represents incident velocity potential for a train of surface waves incident on the plate, then

$$\phi_0(x, y) = e^{i\omega x}\frac{\cosh \xi_0(h - y)}{\cosh \xi_0 h}, \tag{3.15}$$

where $\omega = \xi_0 \cos\theta$.

Also $\phi(x, y)$ satisfies the infinity requirements that

$$\phi(x, y) \sim \begin{cases} \phi_0(x, y) + R\phi_0(-x, y) & \text{as} \quad x \to -\infty, \\ T\phi_0(x, y) & \text{as} \quad x \to \infty. \end{cases} \tag{3.16}$$

Here R and T are the reflection and transmission coefficients respectively.

3.3 METHOD OF SOLUTION

In this section we shall evaluate $|R|$ and $|T|$ from the boundary value problem (3.2) to (3.16) satisfied by $\phi(x, y)$. Before proceeding to obtain $|R|$ and $|T|$, we need to solve (3.11) along with (3.13) to find $\phi_x(y)$.

The condition (3.11) on the plate $x = 0, c < y < d$ can be rewritten as

$$\frac{d^4\phi_x}{dy^4} - \beta^4\phi_x = \frac{K}{D'}[\phi], \quad \text{on } c < y < d, \tag{3.17}$$

where

$$\beta^4 = \frac{\epsilon' K}{D'}.$$

To solve for $\phi_x(y)$ from (3.17) and (3.13) we shall adopt Green's function technique [cf. Meylan (1995)]. Let $g1(\tau, y)$ be the Greens function which satisfies

$$\frac{d^4 g1}{d\tau^4} - \beta^4 g1 = \delta(\tau - y), \ c < \tau, y < d, \tag{3.18}$$

$$\frac{\partial^2 g1}{\partial \tau^2} = 0 = \frac{\partial^3 g1}{\partial \tau^3}, \quad \text{at} \quad \tau = c, d, \tag{3.19}$$

$$g1,\ g1_\tau,\ g1_{\tau\tau} \ \text{ to be continuous at } \tau = y,$$

$$g1_{\tau\tau\tau}(y+0, y) - g1_{\tau\tau\tau}(y-0, y) = -1 \tag{3.20}$$

so that

$$\phi_x(0, y) = \frac{K}{D'} \int_c^d g1(\tau, y)[\phi](\tau) d\tau, \quad c < y < d. \tag{3.21}$$

The general solution of (3.18) is given by

$$g1(\tau, y) = \begin{cases} P_1 e^{i\beta\tau} + Q_1 e^{-i\beta\tau} + R_1 e^{\beta\tau} + S_1 e^{-\beta\tau} & \text{as} \quad c < \tau < y < d, \\ P_2 e^{i\beta\tau} + Q_2 e^{-i\beta\tau} + R_2 e^{\beta\tau} + S_2 e^{-\beta\tau} & \text{as} \quad c < y < \tau < d, \end{cases} \tag{3.22}$$

where $P_1, Q_1, R_1, S_1; P_2, Q_2, R_2, S_2$ are functions of y only. Using the conditions (3.19) and (3.20), the unknowns P_1, Q_1, R_1 and S_1 are determined from the following linear system

$$\begin{bmatrix} -e^{i\beta c} & -e^{-i\beta c} & e^{\beta c} & e^{-\beta c} \\ -ie^{i\beta c} & ie^{-i\beta c} & e^{\beta c} & -e^{-\beta c} \\ -e^{i\beta d} & -e^{-i\beta d} & e^{\beta d} & e^{-\beta d} \\ -ie^{i\beta d} & ie^{-i\beta d} & e^{\beta d} & -e^{-\beta d} \end{bmatrix} \begin{bmatrix} P_1 \\ Q_1 \\ R_1 \\ S_1 \end{bmatrix} = \frac{1}{4\beta^3} \begin{bmatrix} 0 \\ 0 \\ -ie^{i\beta(d-y)} + ie^{-i\beta(d-y)} + e^{\beta(d-y)} - e^{-\beta(d-y)} \\ e^{i\beta(d-y)} + e^{-i\beta(d-y)} + e^{\beta(d-y)} + e^{-\beta(d-y)} \end{bmatrix}$$

. (3.23)

while P_2, Q_2, R_2 and S_2 are given by

$$P_2 = P_1 - \frac{i}{4\beta^3} e^{-i\beta y}; Q_2 = Q_1 + \frac{i}{4\beta^3} e^{i\beta y};$$

$$R_2 = R_1 - \frac{1}{4\beta^3}e^{-\beta y}; S_2 = S_1 + \frac{1}{4\beta^3}e^{\beta y}. \tag{3.24}$$

Thus knowing $g1$, the function $\phi_x(y)$ can be obtained from (3.21).

Next we shall proceed to evaluate $|R|$ and $|T|$. For this let, $G(\gamma, \tau; x, y)$ be the source potential which describes the motion in water with ice cover, due to the presence of a line source at (x, y). The representation of $G(\gamma, \tau; x, y)$ is given below [cf. Gayen (2004), Chapter 2.3.2.2].

$$G(\gamma,\tau;x,y) = -4\pi\sum_{n=1}^{\infty}\frac{\xi_n(D\xi_n^4+1-\epsilon K)\cos\xi_n(h-y)\cos\xi_n(h-\tau)}{2\xi_n h(D\xi_n^4+1-\epsilon K)+(5D\xi_n^4+1-\epsilon K)\sin 2\xi_n h}\frac{e^{-(\xi_n^2+\kappa^2)^{\frac{1}{2}}|x-\gamma|}}{(\xi_n^2+\kappa^2)^{\frac{1}{2}}}$$

$$-4\pi i\left[\frac{\xi_0(D\xi_0^4+1-\epsilon K)\cosh\xi_0(h-y)\cosh\xi_0(h-\tau)}{2\xi_0 h(D\xi_0^4+1-\epsilon K)+(5D\xi_0^4+1-\epsilon K)\sinh 2\xi_0 h}\frac{e^{i(\xi_0^2-\kappa^2)^{\frac{1}{2}}|x-\gamma|}}{(\xi_0^2-\kappa^2)^{\frac{1}{2}}}\right.$$

$$+\frac{\mu(D\mu^4+1-\epsilon K)\cosh\mu(h-y)\cosh\mu(h-\tau)}{2\mu h(D\mu^4+1-\epsilon K)+(5D\mu^4+1-\epsilon K)\sinh 2\mu h}\frac{e^{i(\mu^2-\kappa^2)^{\frac{1}{2}}|x-\gamma|}}{(\mu^2-\kappa^2)^{\frac{1}{2}}}$$

$$\left.+\frac{\bar{\mu}(D\bar{\mu}^4+1-\epsilon K)\cosh\bar{\mu}(h-y)\cosh\bar{\mu}(h-\tau)}{2\bar{\mu}h(D\bar{\mu}^4+1-\epsilon K)+(5D\bar{\mu}^4+1-\epsilon K)\sinh 2\bar{\mu}h}\frac{e^{-i\{(-\bar{\mu})^2-\kappa^2\}^{\frac{1}{2}}|x-\gamma|}}{\{(-\bar{\mu})^2-\kappa^2\}^{\frac{1}{2}}}\right]. \tag{3.25}$$

Here $\pm\xi_0$ are the real, $i\xi_n (n = 1, 2, ...)$ are the imaginary and $\pm\mu, \pm\bar{\mu}$ are the complex roots of the equation (3.1).
Now, the Greens integral theorem is applied to the functions $\psi(\gamma, \tau) = \phi(\gamma, \tau) - \phi_0(\gamma, \tau)$ and $G(\gamma, \tau; x, y)$ $(x < 0)$, in the regions bounded externally by the lines

$$\tau = 0,\ -X \le \gamma \le 0;\ \gamma = 0,\ 0 \le \tau \le h;\ \tau = h,\ -X \le \gamma \le 0;\ \gamma = -X,\ 0 \le \tau \le h$$

and internally by a circle with very small radius δ with center at (x, y). By making

$X \to \infty$ and $\delta \to 0$, we obtain

$$\phi(x,y) = e^{i\omega x}\frac{\cosh\xi_0(h-y)}{\cosh\xi_0 h} + \int_0^h \left[\frac{\partial G}{\partial \gamma}(0,\tau;x,y)\phi_1(\tau) - G(0,\tau;x,y)\phi_x(\tau)\right] d\tau,\ x<0. \tag{3.26}$$

It may be noted that G is symmetric in (γ, x) and (τ, y) and behaves as an outgoing wave as $|\gamma - x| \to \infty$. The equation (3.26) gives a representation of $\phi(x,y)$ for $x < 0$, and hence the reflection coefficient R is obtained by making $x \to -\infty$ in (3.26) and comparing with (3.16). This produces

$$R = 2\int_0^h (\xi_0\phi_1(\tau) - i\phi_x(\tau))\frac{(D\xi_0^4 + 1 - \epsilon K)\cosh\xi_0(h-\tau)\cosh\xi_0 h}{2\xi_0 h(D\xi_0^4+1-\epsilon K) + (5D\xi_0^4+1-\epsilon K)\sinh 2\xi_0 h}d\tau. \tag{3.27}$$

Again, to obtain $\phi_1(y) = \phi(-0, y)$, we apply Green's integral theorem to the functions $\psi(\gamma,\tau)$ and $G(\gamma,\tau;0-,y),\ c<y<d$, in the region bounded by the lines

$$\tau = 0,\ -X \le \gamma \le 0;\ \gamma = 0,\ 0 \le \tau \le h;\ \tau = h,\ -X \le \gamma \le 0;\ \gamma = -X,\ 0 \le \tau \le h$$

and by a semicircle with very small radius δ_1 with center at $(0-, y),\ c < y < d$. Thus making $\delta_1 \to 0$, we obtain an integral equation for $\phi_1(y)$ in $(0, h)$ as

$$\frac{1}{2}\phi_1(y) = \frac{\cosh\xi_0(h-y)}{\cosh\xi_0 h} + \frac{1}{2\pi}\int_0^h \left[\frac{\partial G}{\partial\gamma}(0,\tau;0,y)\phi_1(\tau) - G(0,\tau;0,y)\phi_x(\tau)\right] d\tau, 0<y<h. \tag{3.28}$$

Similarly, applying Greens integral theorem to the functions $\phi(\gamma,\tau)$ and $G(\gamma,\tau;x,y)$ $(x>0)$ in the regions bounded externally by the lines

$$\tau = 0,\ 0 \le \gamma \le X;\ \gamma = 0,\ 0 \le \tau \le h;\ \tau = h,\ 0 \le \gamma \le X;\ \gamma = X,\ 0 \le \tau \le h$$

and internally by a circle of very small radius δ_2 with center at (x, y) and ultimately making $X \to \infty$ and $\delta_2 \to 0$, we obtain

$$\phi(x,y) = -\int_0^h \left[\frac{\partial G}{\partial\gamma}(0,\tau;x,y)\phi_2(\tau) - G(0,\tau;x,y)\phi_x(\tau)\right] d\tau,\ \text{for } x>0. \tag{3.29}$$

The equation (3.29) gives a representation of $\phi(x,y)$ for $x>0$ and hence the transmission coefficient T is obtained by making $x\to\infty$ in equation (3.29) and comparing with equation (3.16), we find

$$T=2\int_0^h(\xi_0\phi_2(\tau)+i\phi_x(\tau))\frac{(D\xi_0^4+1-\epsilon K)\cosh\xi_0(h-\tau)\cosh\xi_0 h}{2\xi_0 h(D\xi_0^4+1-\epsilon K)+(5D\xi_0^4+1-\epsilon K)\sinh 2\xi_0 h}d\tau. \tag{3.30}$$

Again, to obtain $\phi_2(y)=\phi(0+,y)$, we apply Green's integral theorem to the functions $\phi(\gamma,\tau)$ and $G(\gamma,\tau;0+,y),\ c<y<d$, in the region bounded by the lines

$$\tau=0,\ 0\le\gamma\le X;\ \gamma=0,\ 0\le\tau\le h;\ \tau=h,\ 0\le\gamma\le X;\ \gamma=X,\ 0\le\tau\le h$$

and by a semicircle with very small radius δ_3 with center at $(0+,y),\ c<y<d$. Thus making $\delta_3\to 0$, we obtain an integral equation for $\phi_2(y)$ in $(0,h)$ as

$$\phi_2(y)=-\frac{1}{\pi}\int_0^h\left[\frac{\partial G}{\partial\gamma}(0,\tau;0,y)\phi_2(\tau)-G(0,\tau;0,y)\phi_x(\tau)\right]d\tau, 0<y<h. \tag{3.31}$$

Noting the relation (3.12), the equations (3.28), (3.31), (3.21) together, produce three simultaneous integral equations in terms of three unknowns $\phi_1(y),\ \phi_2(y)$ and $\phi_x(y)$ in $(0,h)$. By solving these integral equations numerically and utilizing the solutions in (3.27) and (3.30), produce reflection and transmission coefficients $|R|$ and $|T|$ numerically for various values of different parameters.

Dynamic force:

We determine the mathematical expression for dynamic wave force. From the linearised Bernoulli's equation, the dynamic pressure jump across the elastic barrier can be written in the following form

$$P_- - P_+ = -i\rho_1\sigma\left(\phi_1-\phi_2\right),\ \text{for } y\in[c,d]. \tag{3.32}$$

The magnitude of horizontal wave force per unit width acting on barrier is then obtained after integrating the dynamic pressure jump along the elastic barriers is given

by

$$\mathcal{F} = -i\rho_1\sigma \int_c^d (\phi_1 - \phi_2)\, dy. \tag{3.33}$$

The non dimensional form of the horizontal force coefficient on the elastic plate becomes

$$F1 = \frac{K|\mathcal{F}|}{\rho_1 g}. \tag{3.34}$$

The deflection of the plate:

It is aleady known from relation (3.9) that

$$\frac{\partial \mathrm{W_E(y,t)}}{\partial t} = \frac{\partial \Phi(0,y,t)}{\partial x} \text{ at } x = 0,\ c < y < d. \tag{3.35}$$

If $\mathrm{W_E(y,t)} = Re\{\mathrm{W_E(y)}e^{i\sigma t}\}$ [cf. Hassan *et al.* (2009)], then the non-dimensional form of the plate deflection is given by

$$|\mathrm{W1_E(y)}| = |\sigma \mathrm{W_E(y)}| = |\frac{\partial \phi}{\partial x}(0,y)|,\ c < y < d. \tag{3.36}$$

Shear force and shear strain:

The shear force along the elastic barrier in terms of horizontal displacement is given by the relation [cf. Kaligatla and Manam (2014)]

$$\zeta(y) = -\frac{D^{'}\rho_1 g}{K}\frac{\partial^3}{\partial y^3}\mathrm{W_E}(y),\ c \le y \le d. \tag{3.37}$$

Then the non dimensional form of shear force can be written as

$$|\zeta 1(y)| = |\frac{4K}{\epsilon_1\rho_1(d-c)g}\zeta(y)|,\ c \le y \le d. \tag{3.38}$$

The shear strain of the elastic plate is given by

$$\eta_{sh}(y) = -\frac{ih}{2\sigma}\frac{d^2\phi_x}{d^2y},\ c \le y \le d. \tag{3.39}$$

Then the magnitude of the shear strain becomes

$$|\eta 1(y)| = |-16\frac{i\beta K D^{'}}{(d-c)h}\eta_{sh}(y)|,\ c \le y \le d \tag{3.40}$$

3.4 NUMERICAL RESULTS AND DISCUSSIONS

The three integral equations (3.28), (3.31) and (3.21) together with (3.12), involving $\phi_1(y), \phi_2(y)$ and $\phi_x(y)$ have the finite range $(0, h)$. For numerical evaluation of the integrals in a finite interval, we employ the Gauss quadrature rule in the form

$$\int_A^B f(\eta)d\eta \equiv \frac{B-A}{2}\sum_{j=1}^{N} l_j f(\frac{B-A}{2}y_j + \frac{B+A}{2}) \tag{3.41}$$

in each of the integrals mentioned above, where $l_j, y_j (j = 1, 2, ..., N)$ are defined below.

For numerical calculations, we non-dimensionalize the variables y, τ and the other parameters with the help of h and $y_j (j = 1, 2, ..., N)$ in (3.41) are the zeros of Legendre-polynomial $P_N(y)$ of degree N and $l_j (j = 1, 2, ..., N)$ are the corresponding weight functions given by

$$l_j = \frac{2}{(1-y_j)^2(P'_N(y_j))^2}, \tag{3.42}$$

$P'_N(y)$ being the derivative of $P_N(y)$. There will be $3N$ unknowns $\phi_1(y_j), \phi_2(y_j)$ and $\phi_x(y_j) (j = 1, 2, ..., N)$ in the approximation of the three integral equations.

Substituting $y = y_k (k = 1, 2, ..., N)$ in each of the integral equations, we obtain $3N$ linear equations for determining $3N$ unknowns $\phi_1(y_j), \phi_2(y_j)$ and $\phi_x(y_j) (j = 1, 2, ..., N)$.

Using these values, we calculate the approximate form of R and T from the relations (3.27) and (3.30) respectively and the energy balance relation is verified.

In this section, we present numerical results for the reflection and the transmission coefficients $|R|$ and $|T|$, horizontal hydrodynamic force $F1$, shear force $\zeta 1$, shear strain $\eta 1$ of the thin elastic plate, taking some typical parameter sets. Here, we make different physical quantities dimensionless with respect to h.

Accuracy and validation of the result

To check the accuracy of the present result, it is compared with Chakraborty and Mandal's (2013) result by considering the ice cover parameters to be very small($\frac{D}{d^4} =$

$0.0005, \frac{\epsilon}{d} = 0.0001$) and $\theta = 0$. Chakraborty and Mandal (2013) considered the wave scattering problem involving thin elastic plate with free surface of water. In the paper, they have non dimensionalized the parameters by lower end depth of elastic plate from free surface. Now for accurate comparison, here also we consider the same parameter values $\frac{c}{d} = 0.05, \frac{D'}{d^4} = 1, \frac{\epsilon'}{d} = 0.01, \frac{h}{d} = 2$ as chosen by Chakraborty and Mandal (2013). These values of $|R|$ are tabulated in Table (3.1) and the data set almost matched with each other upto four figure accuracy. This provides a check on the validation of the present method.

Kd	Present Result ($\|R\|$)	Chakraborty and Mandal's result(2013)($\|R\|$)
0.1	0.00325571	0.00327487
1.2	0.82359812	0.82861321
2.2	0.09871319	0.09824339
3.5	0.0056131	0.00569314

Table 3.1: Comparison between present result, considering ice cover coefficient $\frac{D}{d^4} = 0.0005, \theta = 0$(very small value and Chakraborty and Mandal's (2013) result without ice cover with $\frac{c}{d} = 0.05, \frac{D'}{d^4} = 1, \frac{\epsilon'}{d} = 0.01, \frac{h}{d} = 2$)

Convergence analysis

The convergence of the numerical results depends on the values of N in Gauss quadrature formula given in (3.41). In the Table (3.2), $|R|$ is tabulated for different wave numbers $Kh(= 0.5, 1.0, 1.5, 2.0, 2.5$ and $3)$ with fixed values of $(d-c)/h = 0.2, D/h^4 = 0.5, D^{'}/h^4 = 0.1, \epsilon/\epsilon^{'} = 0.01$ and $\theta = 0$. Here different values of $N(= 5, 7, 10, 12$ and $14)$ are considered and it is observed that for $N = 10, 12$ and 14, the numerical values of $|R|$ coincide upto 4 decimal places. Also the present method is checked for all other values of the parameters and wave numbers and it almost converges upto 4 decimal places when $N = 10$.

Effect of variation of length of the elastic barrier on reflection and transmission coefficients

In the present study, we non-dimensionalize different parameters by constant water depth h. We consider $(d - c)/h$ as the length of the plate and the distance of the

Truncation number (N)	**Kh**=0.5	**Kh**=1	**Kh**=1.5	**Kh**=2	**Kh**=2.5	**Kh**=3
5	0.539225	0.375438	0.300753	0.261398	0.237335	0.221137
7	0.539361	0.375623	0.300948	0.261568	0.237514	0.221253
10	0.539574	0.375816	0.301087	0.261754	0.237668	0.221417
12	0.539574	0.375816	0.301087	0.261754	0.237668	0.221417
14	0.539574	0.375816	0.301087	0.261754	0.237668	0.221417

Table 3.2: Convergence of $|R|$ with N at $(d-c)/h = 0.2, D/h^4 = 0.5, D^{'}/h^4 = 0.1, \epsilon/\epsilon^{'} = 0.01, \theta = 0$.

plate from upper surface of water is fixed ($c/h = 0.1$). The effect of the length of elastic plate on reflection and transmission coefficients for fixed values of the parameters $\theta = \frac{\pi}{4}, D/h^4 = 0.5, D^{'}/h^4 = 0.1$ and $\epsilon/\epsilon^{'} = 0.01$ is shown in Figures 3.2 and 3.3 respectively. Here we consider different values of $(d-c)/h = 0.1, 0.5$ and 0.8. These figures reveal the fact that as the length of the thin elastic plate increases the reflection coefficient $|R|$ increases while the transmission coefficient decreases. This happens because longer plate enhances reflection. Also increasing length of the barrier decreases the amplitude of transmission coefficient which is also quite obvious physically.

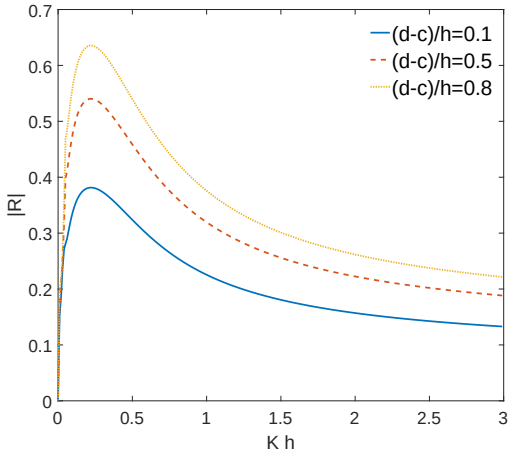

Figure 3.2: Reflection coefficient against Kh for different values of $(d-c)/h$ with $\theta = \pi/4, \epsilon/\epsilon^{'} = 0.01, D^{'}/h^4 = 0.1, D/h^4 = 0.5$.

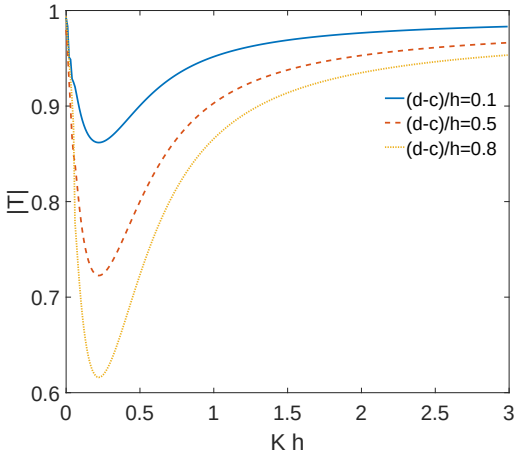

Figure 3.3: Transmission coefficient against Kh for different values of $(d-c)/h$ with $\theta = \pi/4, \epsilon/\epsilon^{'} = 0.01, D^{'}/h^4 = 0.1, D/h^4 = 0.5$.

Effect of variation of angle of incidence on reflection and transmission coefficients

In Figures 3.4 and 3.5, magnitudes of the reflection coefficient $|R|$ and the transmission coefficient $|T|$ are plotted against the dimensionless wave number Kh for three different values of the parameter $\theta(= \pi/4, \pi/6, \pi/10)$. Here we choose $(d-c)/h = 0.4, D/h^4 = 0.5, D^{'}/h^4 = 0.1$ and $\epsilon/\epsilon^{'} = 0.01$, where $\epsilon/h = 0.001, \epsilon^{'}/h = 0.1$. These figures reveal the fact that as the angle of incidence increases the amount of the reflection increases whereas the transmission decreases. For small wave number, more reflection occurs and it gradually decreases for large values of the wave number. The vice versa phenomena is occurred in transmission curve.

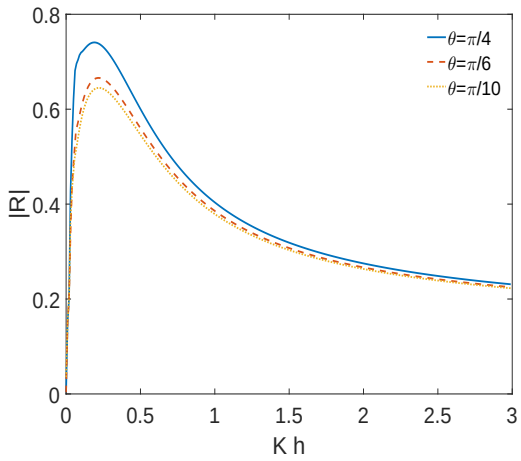

Figure 3.4: Reflection coefficient against Kh for different values of θ with $(d-c)/h = 0.4, \epsilon/\epsilon^{'} = 0.01, D^{'}/h^4 = 0.1, D/h^4 = 0.5$.

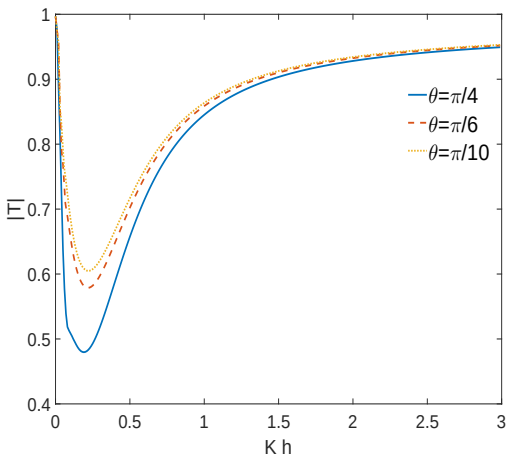

Figure 3.5: Transmission coefficient against Kh for different values of θ with $(d-c)/h = 0.4, \epsilon/\epsilon^{'} = 0.01, D^{'}/h^4 = 0.1, D/h^4 = 0.5$.

Effect of variation of elasticity of ice cover and elastic coefficient of the barrier on reflection coefficients

In Figure 3.6, the reflection coefficient $|R|$ is plotted against the dimensionless wave number Kh for different values of the parameter $D/h^4(= 0.01, 0.50, 2.00, 5.00)$. Here we take the fixed values of $(d-c)/h = 0.4, D^{'}/h^4 = 0.1, \epsilon/\epsilon^{'} = 0.01$ and $\theta = \pi/4$. In this figure we see that as D/h^4 increases, the reflection coefficient $|R|$ decreases. Thus

the elasticity of the ice cover decreases the amount of reflection.

In Figure 3.7, the reflection coefficient $|R|$ is plotted against the dimensionless wave number Kh for different values of the parameter $D^{'}/h^4(= 0.01, 0.50, 1.00)$. Here we take the fixed values of $(d-c)/h = 0.4, D/h^4 = 0.5, \epsilon/\epsilon^{'} = 0.01$ and $\theta = \pi/4$. Here also we see that for increasing values of the elastic coefficient of the barrier the amount of reflection decreases.

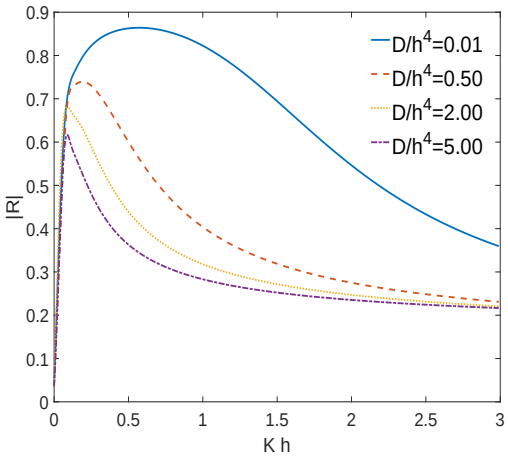

Figure 3.6: Reflection coefficient against Kh for different values of D/h^4 with $(d-c)/h = 0.4, \epsilon/\epsilon^{'} = 0.01, D^{'}/h^4 = 0.1, \theta = \pi/4$.

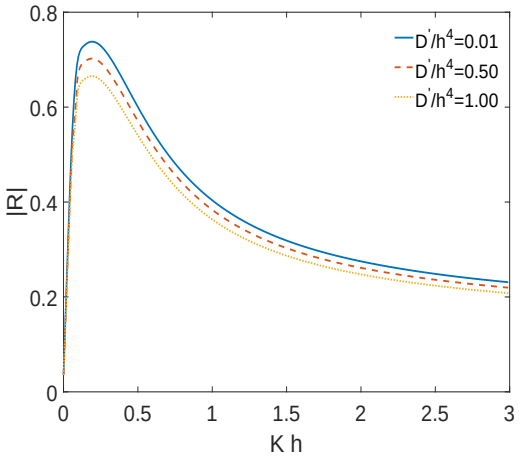

Figure 3.7: Reflection coefficient against Kh for different values of $D^{'}/h^4$ with $(d-c)/h = 0.4, D/h^4 = 0.5, \epsilon/\epsilon^{'} = 0.01,\ \theta = \pi/4$.

Effect of various parameters on a normally incident wave train

The following figures are drawn for normally incident wave train ($\theta = 0$).

Effect of variation of elasticity of ice cover on reflection and transmission coefficients

In Figures 3.8 and 3.9, the reflection coefficient $|R|$ and transmission coefficient $|T|$ are plotted against the dimensionless wave number Kh for four different values of the parameter $D/h^4(= 0.01, 0.5, 2.0, 5.0)$ respectively. Here we choose $(d-c)/h = 0.2, \theta = 0, D^{'}/h^4 = 0.1$ and $\epsilon/\epsilon^{'} = 0.01$, where $\epsilon/h = 0.001, \epsilon^{'}/h = 0.1, c/h = 0.2$. In all the following figures we consider the same values of c/h. The Figure 3.8 reveals the fact

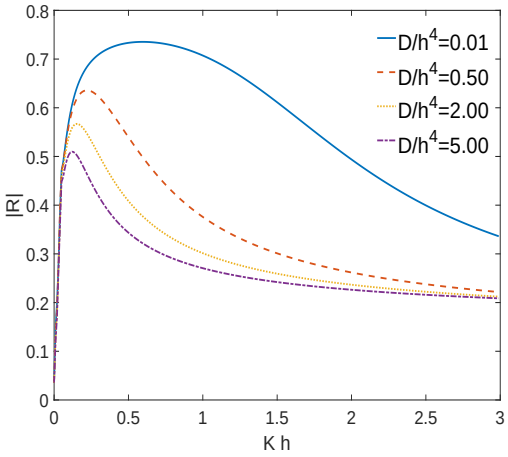

Figure 3.8: Reflection coefficient against Kh for different values of D/h^4 with $(d-c)/h = 0.2, \epsilon/\epsilon^{'} = 0.01, D^{'}/h^4 = 0.1, \theta = 0$.

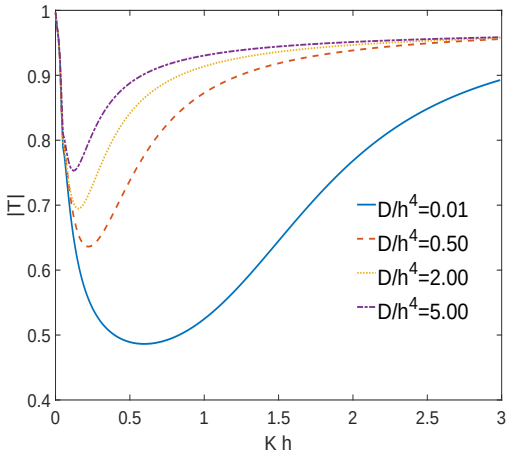

Figure 3.9: Transmission coefficient against Kh for different values of D/h^4 with $(d-c)/h = 0.2, \epsilon/\epsilon^{'} = 0.01, D^{'}/h^4 = 0.1, \theta = 0$.

that $|R|$ decreases as D/h^4 increases and Figure 3.9 shows $|T|$ increases with increasing values of D/h^4. Thus, the elasticity of the ice cover reduces the reflection and enhances the transmission of the incident wave energy.

Effect of variation of elastic coefficient of the barrier on reflection coefficients

The Figure (3.10) shows the behavior of $|R|$ for different values of $D'/h^4 = 0.01, 0.50$ and 1 and fixed values of $(d-c)/h = 0.3, \theta = 0, D/h^4 = 0.1$ and $\epsilon/\epsilon^{'} = 0.01$, where $\epsilon/h = 0.001, \epsilon^{'}/h = 0.1$. It is clearly visible from the figure that, as the elasticity of the barrier increases, the reflection of short surface waves increases while the reflection of waves with larger wavelength decreses. This phenomena is attributed to the interaction of waves with the elastic barrier.

Effect of change of density ratio between elastic plate and ice cover on reflection coefficient

In Figure (3.11), the reflection coefficient $|R|$ is plotted against the dimensionless wave number Kh for three different values of the parameter $\epsilon/\epsilon^{'}(= 0.01, 0.50, 1.00)$, where $\epsilon^{'}/h$ is taken as 0.1. Here we choose $(d-c)/h = 0.2, \theta = 0, D/h^4 = 0.5$ and $D^{'}/h^4 = 0.1$. This figure reveal the fact that $|R|$ decreases as $\epsilon/\epsilon^{'}$ increases.

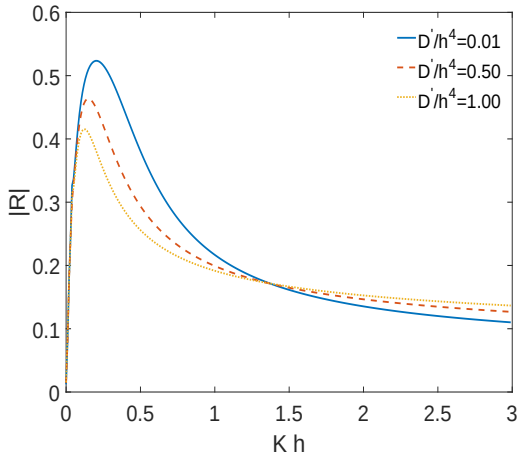

Figure 3.10: Reflection coefficient against Kh for different values of $D^{'}/h^4$ with $(d-c)/h = 0.3, D/h^4 = 0.1, \epsilon/\epsilon^{'} = 0.01, \theta = 0$.

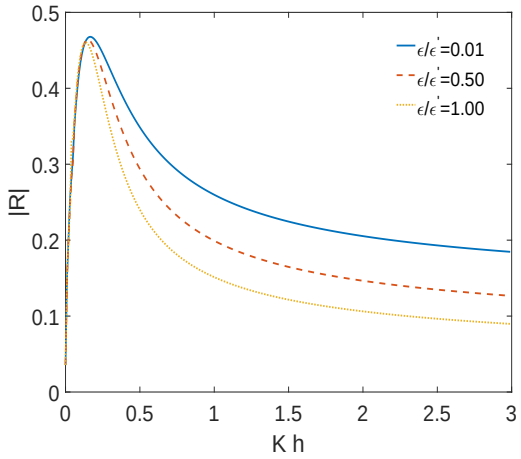

Figure 3.11: Reflection coefficient against Kh for different values of $\epsilon/\epsilon^{'}$ with $(d-c)/h = 0.2, D/h^4 = 0.5, D^{'}/h^4 = 0.1, \theta = 0$.

Effect of change of flexural rigidity of ice cover on horizontal force

The magnitude of the horizontal component of the hydrodynamic force acting on the elastic plate is evaluated from the relation (3.34) and is represented graphically in the Figure (3.12). In this figure, the graphs are plotted for four different values of $D/h^4 (= 0.1, 0.5, 1.0, 3.0)$. The horizontal component of the hydrodynamic force $F1$ acting on the elastic plate exhibits oscillatory behaviour when the flexural rigidity of the ice cover D/h^4 is small. However, as D/h^4 increases, $F1$ slowly increases with Kh.

Deflection of the elastic plate

The effect of flexural rigidity parameter of the elastic plate on the plate deflection is presented against y/d in Figure (3.13). Here we non-dimensionalize all the parameters with respect to d. In this figure, the graphs are plotted for three different values of $D^{'}/d^4 (= 0.1, 0.5, 1.0)$ and for fixed values of the parameters $c/d = 0.5, h/d = 1.5, D/d^4 = 2.5, Kh = 0.5, \frac{\epsilon}{d} = 0.15, \frac{\epsilon^{'}}{d} = 0.015, \theta = 0$. If $D^{'}/d^4$ increases, the deflection of the plate from its mean position decreases. With increasing $D^{'}/d^4$, the lower end of the plate is more deflected than the upper end.

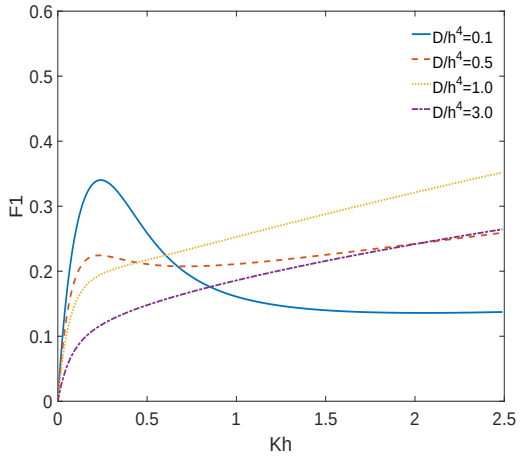

Figure 3.12: Hydrodynamic force against wave number for different values of D/h^4 and $D'/h^4 = 0.05, (d-c)/h = 0.1, \epsilon/h = 0.01, \theta = 0$.

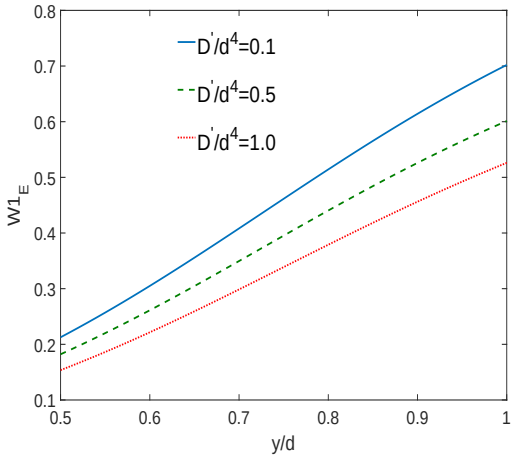

Figure 3.13: Magnitude of plate deflection of the elastic plate against y/d for different values of $D^{'}/d^4$ and fixed values of $c/d = 0.5, h/d = 1.5, D/d^4 = 2.5, Kh = 0.5, \frac{\epsilon}{d} = 0.15, \frac{\epsilon^{'}}{d} = 0.015, \theta = 0$.

Variation of shear force

The magnitude of the shear force of the plate as a function of y/h is presented in the Figure (3.14). The graphs are for the different values of the wave number $Kh(= 0.50, 1.00, 2.00)$, $\frac{\epsilon}{h} = 0.1, \frac{\epsilon^{'}}{h} = 0.01, D/h^4 = 0.5, D^{'}/h^4 = 0.1, c/h = 0.2, d/h = 0.6, \theta = 0$. When Kh is small, shear force $\zeta 1$ more or less remain constant throughout the length of the plate. This is beacause the longer waves which are near the bottom of the water region do not feel the presence of the barrier. However as Kh increases, the shear force first decreases and then increases towards the lower end of the barrier. In Figure (3.15), the shear force graphs taken against y/h for different values of elastic parameter, $\frac{D'}{h^4}(= 0.50, 1.00, 2.00)$ of the barrier and fixed values of $\frac{\epsilon}{h} = 0.1, \frac{\epsilon^{'}}{h} = 0.01, D/h^4 = 0.5, Kh = 0.01, c/h = 0.2, d/h = 0.6, \theta = 0$. For smaller values of flexural rigidity of elastic barrier, i.e., $D/h^4 = 0.5, 1.0$, the shear force slowly decreases towards the lower end of the barrier. However for larger value of $D/h^4 = 2.0$, the shear force is significant towards the two ends of the barrier and is very small at the centre of the barrier.

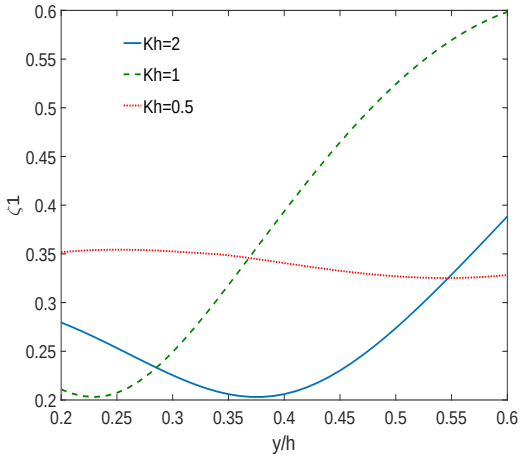

Figure 3.14: Magnitude of shear force for elastic plate $\frac{\epsilon}{h} = 0.1, \frac{\epsilon^{'}}{h} = 0.01, D/h^4 = 0.5, D^{'}/h^4 = 0.1, c/h = 0.2, d/h = 0.6, \theta = 0.$

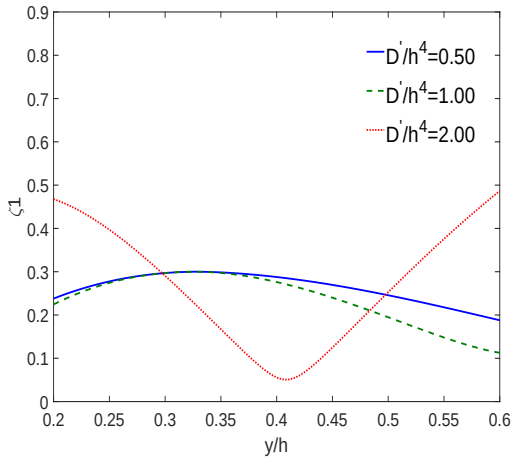

Figure 3.15: Magnitude of shear force for elastic plate $\frac{\epsilon}{h} = 0.1, \frac{\epsilon^{'}}{h} = 0.01, D/h^4 = 0.5, Kh = 0.01, c/h = 0.2, d/h = 0.6, \theta = 0$

Shear strain of the elastic plate

Figure (3.16) shows the variation of magnitude of the shear strain against y/h for an elastic plate submerged in finite depth water with $Kh = 0.05, 0.1, 1$ and 2, $\frac{\epsilon}{h} = 0.1, \frac{\epsilon^{'}}{h} = 0.01, D/h^4 = 0.5, D^{'}/h^4 = 0.1, c/h = 0.2, d/h = 0.6, \theta = 0$. From the figure it is seen that waves with longer wavelength which are towards the bottom of the water region are not affected by the barrier and consequently the shear strain $\eta 1$ remains almost constant throughout the length of the plate. However as the wave number increases, the shear strain decreases as we move down from the upper end of the barrier and then again increases slowly towards the lower end of the barrier. Figure (3.17) depicts the variation of shear strain against y/h for an elastic plate submerged in finite depth water with $\frac{D'}{h^4} = 0.01, 0.5, 2$ and 3, $\frac{\epsilon}{h} = 0.1, \frac{\epsilon^{'}}{h} = 0.01, D/h^4 = 0.5, Kh = 0.1, c/h = 0.2, d/h = 0.6, \theta = 0$. The figure shows that increasing flexural rigidity of the elastic plate increases the shear strain on the plate.

In most of the graphical results it is clear that the variation of different parameters affect the nature of reflection and transmission curves more for small wave numbers. Increasing values of wave number reduces the differences between the reflection curves drawn for different parametric values in same figure.

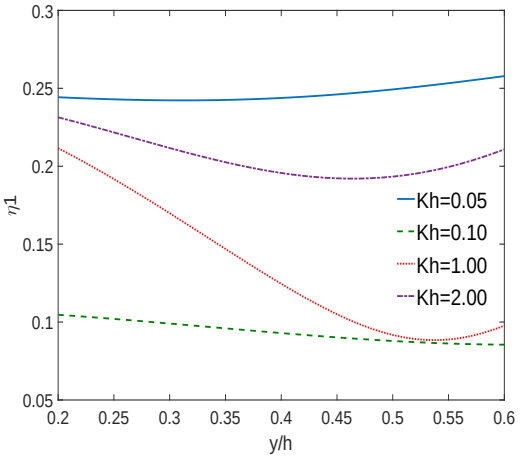

Figure 3.16: Magnitude of shear strain for elastic plate $\frac{\epsilon}{h} = 0.1, \frac{\epsilon^{'}}{h} = 0.01, D/h^4 = 0.5, D^{'}/h^4 = 0.1, c/h = 0.2, d/h = 0.6, \theta = 0.$

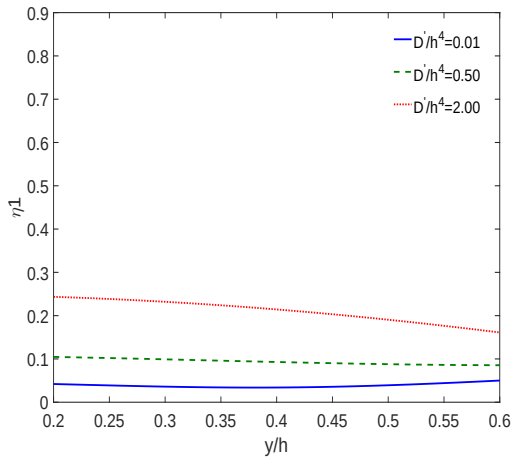

Figure 3.17: Magnitude of shear strain for elastic plate. $\frac{\epsilon}{h} = 0.1, \frac{\epsilon^{'}}{h} = 0.01, D/h^4 = 0.5, Kh = 0.1, c/h = 0.2, d/h = 0.6, \theta = 0.$

3.5 CONCLUSIONS

In this chapter, the interaction between obliquely incident waves with an elastic thin barrier submerged in ice covered ocean is investigated. The boundary conditions on the elastic plate and upper surface of water are derived from Bernoulli Euler Beam equation. The Green's function technique is used to solve the problem.

Some outcomes are summarized below:

Physical quantities such as reflection, transmission coefficients, horizontal hydrodynamic force, deflection of elastic plate, shear force and shear strain on the elastic plate are evaluated and plotted graphically against suitable parameters. The effect of elasticity of the barrier reduces the amplitude of reflection coefficient and hydrodynamic force . Longer barrier reflects more energy than the shorter one.

Due to increasing flexural rigidity of the plate, the lower end of the plate is more deflected than the upper end.

Increasing flexural rigidity of the elastic plate increases the shear strain on the plate.

CHAPTER 4

SCATTERING OF WATER WAVES BY A VERTICAL POROUS BARRIER OVER A RECTANGULAR TRENCH

4.1 INTRODUCTION

During the last few decades, the study of propagation of surface water waves over a rectangular trench was being considered by many researchers because of their possible applications in coastal and ocean engineering. It has a significant role in understanding the characteristics of wave in harbour and offshore regions. The scattering of normally incident monochromatic plane progressive wave by rectangular submarine trench of constant depth containing two fluids of constant but different densities was studied by Lassiter (1972). Lee and Ayer (1981) investigated the effect of a symmetric rectangular trench on the waves, by dividing the fluid domain into subregions and thereby matching the eigen function expansion of velocity potentials in the common boundary of two

[0]† The content of this chapter is based on the paper " Effect of porosity on wave scattering by a vertical porous barrier over a rectangular trench", *Journal of Marine Science and Application*, 74 (2023), 491-505.

subregions. Miles (1982) used a conformal mapping to solve the problrm of scattering of a normally incident wave train by a trench. The diffraction of obliquely incident surface waves by an asymmetric trench was investigated using linearized potential theory by Kirby and Dalrymple (1983). They divided the fluid domain into different regions and solved a set of integral equations derived by matching eigen function expansions of the velocity potentials in the common boundary of the regions. Later, Kirby *et al.* (1987) studied the problem of wave diffraction over a rectangular trench considering the effect of current flowing parallel to the trench boundary. A study of wave scattering of normally and obliquely incident wave train over a rectangular submarine trench was carried out by Chakraborty and Mandal (2014, 2015) by reducing the problem to solving appropriate integral equation. This integral equation was solved by multiterm Galerkin approximation involving ultraspherical Gegenbauer polynomials. Later, Roy *et al.* (2017) considered the problem of water wave scattering by an asymmetric rectangular trench using an approach similar to Chakraborty and Mandal (2014, 2015).

Interaction of water waves with a thin plate assuming the linear theory has been a subject of considerable interest as this phenomenon serves as a model for a wide range of physical situations which include wave interaction with breakwaters, very large floating structures. Breakwaters are coastal structures which are widely constructed to reduce the wave action in inshore water and thereby reduce the coastal erosion and protect a port or harbour from the effect of rough sea. Usually the breakwaters are mathematically modeled as rigid impermeable thin vertical plate either partially immersed or submerged in ocean. A number of researchers were engaged in solving the boundary value problem associated with the study of water wave scattering by a thin rigid vertical plate present in ocean with free surface and consequently many sophisticated mathematical concepts evolved. Dean (1945), Ursell (1947), Evans (1970) were pioneers with such types of studies. It may be noted here that exact solution of the aforesaid boundary value problem exists when the barrier is in the form of a rigid vertical plate present in the deep water and for normal incidence of the incoming wave train. In all other cases only approximate analytical or numerical methods are used to obtain approximate solution. The scattering problem involving a partially immersed and submerged rigid plate using first kind of hypersingular integral equation was studied by Parsons and Martin (1992, 1994). Based on application of Green's integral theorem,

they reduced the boundary value problem to a solution of first kind hypersingular integral equation where the unknown function is the difference of velocity potential across the plate. The hypersingular integral equation was then solved by using collocation method based on approximating the unknown function satisfying the integral equation by Chebyshev's polynomial. The problem of wave diffraction by rigid vertical barrier in finite depth water was considered by Goswami (1983). Goswami (1983) employed Green's function technique to reduce the scattering problem involving a fixed vertical rigid plate submerged in water of uniform finite depth, to an integral equation. The integral equation was then solved approximately by using a perturbation method and reflection and transmission coefficients were thereby obtained. Losada *et al.* (1992) obtained the reflection and transmission coefficients of the above mentioned problem by using an eigenfunction expansion method. Later on, Porter and Evans (1995) considered oblique wave scattering by a thin vertical rigid barrier in uniform finite depth water having four basic configurations namely, a surface piercing barrier, a bottom standing barrier, a barrier with a gap and a totally submerged barrier. For each case, they have used an approximate method based on the Galerkin approximation. Also, Mandal and Dolai (1994) considered oblique water wave scattering by thin vertical barrier in uniform finite depth water. They employed one-term Galerkin approximation to evaluate the upper and lower bounds for the transmission and reflection coefficients.

During the later half of twentieth century, study of wave interaction with porous coastal structures like rubble mound breakwaters became important in coastal engineering as the structural voids in the porous breakwaters can dissipate wave energy efficiently. Also in coastal engineering, porous breakwaters drew special attention of the scientist and researchers because the rigid breakwaters collapsed due to huge wave load. Also, a porous breakwaters are eco-friendly as water can pass through the holes which helps to protect marine environment. Mathematical modeling of porous structure as thin porous vertical wave maker was pioneered by Chwang (1983). Based on the model of Solitt and Cross (1972), Yu (1995) studied the problem of wave diffraction by a semi-infinite porous barriers. Li *et al.* (2015) studied the problem of water wave scattering by thin vertical porous barriers utilizing multi-term Galerkin approximation. Roy *et al.* (2016a, 2016b) analyzed water wave scattering by two unequal vertical barriers and two submerged plates by using Galerkin's approximation technique. More

recently, Ray *et al.* (2021) considered the wave scattering problem by thin rigid plate above the rectangular trench and Sarkar *et al.* (2022) analyzed oblique wave scattering by two thin rigid plate over an asymmetrical trench. The above mentioned problems were solved by applying multi-term Galerkin approximation technique using simple polynomial as basis functions.

In the present paper, water wave scattering by a rectangular submarine trench in presence of a thin vertical porous barrier are investigated. As mentioned earlier, the porosity of the barrier is effective in dissipating wave energy and it helps to reduce wave force on the barrier [cf. Manam and Sivanesan (2016)]. Here the porous barrier is positioned at a distance $'l'$ from the middle of the trench. The whole fluid region is divided into four subregions and in each subregion, a suitable eigen function expansion of water wave potential is written. Using Havelock's inversion formula in four subregions and matching conditions at the interfaces of these subregions we construct three Fredholm type integral equations. To solve these integral equations we use multi-term Galerkin approximation technique taking orthogonal Chebyshevs polynomials and ultraspherical Gegenbauer polynomial as its basis function. This choice is due to the edge conditions at the submerged end of the barrier and at the edges of the trench respectively. We have also consider simple polynomial as basis function to solve the integral equation as done in Ray *et al.* (2021). The reflection coefficient and the transmission coefficient are determined in terms of the solutions of the integral equations.

4.2 FORMULATION OF THE PROBLEM

We consider two dimensional, time harmonic, irrotational motion in water due to interaction of a wave train incident normally on a thin vertical porous barrier partially immersed in water region with a submarine trench at the bottom. We choose rectangular cartesian coordinate system where x-axis is along the mean free surface and y-axis is taken vertically downwards into the fluid region. A rectangular submarine trench symmetrical about y-axis, of width $2b$ and depth 'c' below the mean free surface is situated at the bottom of water region so that water occupies the region $(-\infty < x < -b,\ 0 < y < h) + (-b < x < b,\ 0 < y < c) + (b < x < \infty,\ 0 < y < h)$.

A porous thin vertical barrier is situated along a vertical line $x = l$, which is partially immersed upto a depth 'a' below the mean free surface so that configuration of the barrier is given by $x = l,\ 0 < y < a;\ l < b$. A train of time harmonic waves from negative infinity with angular frequency σ, represented by the velocity potential function $Re[\phi^{inc}(x, y)e^{-i\sigma t}]$, is incident normally on the barrier and is partially reflected and partially transmitted below the barrier so that R and T are the amplitudes of the reflected and transmitted waves respectively. A schematic diagram of the problem is shown in Figure (4.1).

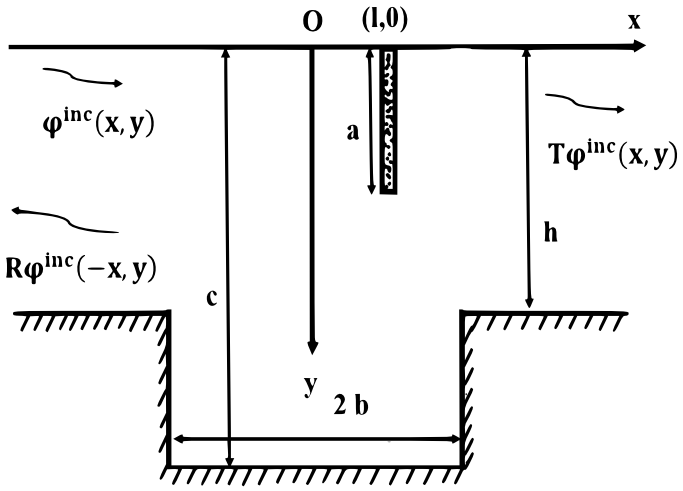

Figure 4.1: Schematic diagram

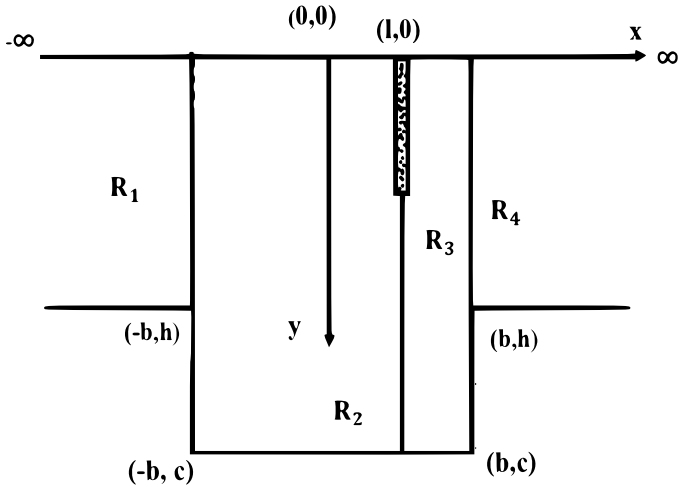

Figure 4.2: Subregions of the fluid domain

Here

$$\phi^{inc}(x,y) = \frac{\cosh \alpha_0(h-y)\ e^{i\alpha_0(x+b)}}{\cosh \alpha_0 h}, \tag{4.1}$$

where α_0 is the unique real positive root of dispersion relation

$$\alpha \tanh \alpha h = K, \tag{4.2}$$

$K = \frac{\sigma^2}{g}$, g is the acceleration due to gravity.

To study the problem under consideration, we divide the fluid region into four sub-regions, viz, $R_1,\ R_2,\ R_3,\ R_4$ [see Figure (4.2)] where
$R_1 \equiv (-\infty < x < -b, 0 < y < h)$;
$R_2 \equiv (-b < x < l, 0 < y < c)$;
$R_3 \equiv (l < x < b, 0 < y < c)$;
$R_4 \equiv (b < x < \infty, 0 < y < h)$.
Let the resulting motion in the fluid be described by the velocity potential $Re[\phi_j(x,y)e^{-i\sigma t}]$, then $\phi_j(x,y)$ satisfies

$$\nabla^2 \phi_j = 0 \ \text{ in the fluid region}, j = 1,2,3,4, \tag{4.3}$$

the linearized free surface condition

$$(\frac{\partial}{\partial y} + K)\phi_j = 0 \text{ on } y = 0\ , -\infty < x < \infty, \tag{4.4}$$

the bottom boundary condition

$$\phi_{jy} = 0 \quad \begin{cases} \text{on } y = c \ \ \text{j=2,3,} \\ \text{on } y = h \ \ \text{j=1,4,} \end{cases} \tag{4.5}$$

the conditions on the two sides of the trench

$$\phi_{jx} = 0 \text{ on } x = \pm b \ \ , j = 2,3, h < y < c, \tag{4.6}$$

the edge conditions

$$r_1^{\frac{1}{3}}\nabla\phi_1, \quad r_2^{\frac{1}{2}}\nabla\phi_2, r_3^{\frac{1}{3}}\nabla\phi_3 \text{ are bounded as } r_1, r_2, r_3 \to 0 \tag{4.7}$$

where r_1, r_2, r_3 are the distances from the submerged left edge of the trench, the submerged edge of the barrier and the submerged right edge of the trench respectively so that
$r_1^2 = (x+b)^2 + (y-h)^2, \quad r_2^2 = (x-l)^2 + (y-a)^2, \quad r_3^2 = (x-b)^2 + (y-h)^2.$

The condition on the porous barrier surface is given by

$$\frac{\partial\phi_2}{\partial x} = \frac{\partial\phi_3}{\partial x} = -i\alpha_0 G(\phi_3 - \phi_2) \text{ on } x = l, \ y \in (0, a). \tag{4.8}$$

Here $G = G^r + iG^i$ is the dimensionless porous parameter given by $G = \frac{\delta(f+iS)}{K\tau(f^2+S^2)}$ where δ is the porosity, f is the resistance force coefficient, S is the inertial force coefficient and τ is the thickness of the porous medium. Thus the real part G^r of G is related to the resistance force coefficient and the imaginary part G^i is related to the inertial force coefficient of the porous material. The quantity G^r resists passage of fluid through the pores while G^i allows the fluid through the pores of the porous material. When $G^i << G^r$, i.e., when the inertial force coefficient is much less than the resistance force coefficient then G is considered as real.

The continuity of normal velocity and pressure across the free-flowing interfaces yields

$$\begin{aligned}
\frac{\partial\phi_1}{\partial x} = \frac{\partial\phi_2}{\partial x} \text{ and } \phi_1 = \phi_2, \text{ for } x = -b, \ y \in (0, h),\\
\frac{\partial\phi_2}{\partial x} = \frac{\partial\phi_3}{\partial x} \text{ for } x = l, \ y \in (0, c),\\
\phi_2 = \phi_3, \text{ for } x = l, \ y \in (a, c),\\
\frac{\partial\phi_3}{\partial x} = \frac{\partial\phi_4}{\partial x} \text{ and } \phi_3 = \phi_4, \text{ for } x = b, \ y \in (0, h).
\end{aligned} \tag{4.9}$$

The far field behavior of the potential functions are described by

$$\phi_1(x,y) \sim \phi^{inc}(x,y) + R\phi^{inc}(-x,y) \quad \text{as} \quad x \to -\infty,$$
$$\phi_4(x,y) \sim T\phi^{inc}(x,y) \quad \text{as} \quad x \to \infty \tag{4.10}$$

where R and T are the unknown complex reflection and transmission coefficients respectively to be determined.

4.3 METHOD OF SOLUTION

By Havelock's expansion of water wave potential, the eigen function expansions of $\phi_j(x,y)$ satisfying (4.3) to (4.9) in the different regions $R_j,\ j = 1,2,3,4$ are given below.

$$\phi_1(x,y) = \left\{e^{i\alpha_0(x+b)} + Re^{-i\alpha_0(x+b)}\right\}\psi_0(y) + \sum_{n=1}^{\infty} A_n e^{\alpha_n(x+b)}\psi_n(y),$$
$$\phi_2(x,y) = \{B_0\cos\lambda_0 x + C_0\sin\lambda_0 x\}\,\chi_0(y) + \sum_{n=1}^{\infty}\{B_n\cosh\lambda_n x + C_n\sinh\lambda_n x\}\,\chi_n(y),$$
$$\phi_3(x,y) = \{D_0\cos\lambda_0 x + E_0\sin\lambda_0 x\}\,\chi_0(y) + \sum_{n=1}^{\infty}\{D_n\cosh\lambda_n x + E_n\sinh\lambda_n x\}\,\chi_n(y),$$
$$\phi_4(x,y) = Te^{i\alpha_0(x-b)}\psi_0(y) + \sum_{n=1}^{\infty} F_n e^{-\alpha_n(x-b)}\psi_n(y) \tag{4.11}$$

where $\{A_n\}_{n=1}^{\infty},\ \{B_n\}_{n=0}^{\infty},\ \{C_n\}_{n=0}^{\infty},\ \{D_n\}_{n=0}^{\infty},\ \{E_n\}_{n=0}^{\infty},\ \{F_n\}_{n=1}^{\infty},\ R,\ T$ are unknowns to be determined. Here

$$\psi_0(y) = \frac{\cosh\alpha_0(h-y)}{\cosh\alpha_0 h}, \psi_n(y) = \frac{\cos\alpha_n(h-y)}{\cos\alpha_n h}, n = 1,2,...,$$
$$\chi_0(y) = \frac{\cosh\lambda_0(c-y)}{\cosh\lambda_0 c}, \chi_n(y) = \frac{\cos\lambda_n(c-y)}{\cos\lambda_n c}, n = 1,2,.... \tag{4.12}$$

and $\alpha_0, \pm i\alpha_n$ are the roots of the equation (4.2) and $\lambda_0, \pm i\lambda_n$ are the roots of the

equation

$$\lambda \tanh \lambda c = K. \tag{4.13}$$

For determination of the unknowns $A'_n s,\ B'_n s,\ C'_n s,\ D'_n s, E'_n s, F'_n s, R$ and T, we proceed as follows. Let us define

$$\begin{aligned} f_j(y) &= \left[\frac{\partial \phi_j}{\partial x}\right]_{x=-b,l,b} = \left[\frac{\partial \phi_{j+1}}{\partial x}\right]_{x=-b,l,b}, \quad j = 1,2,3, \\ g_j(y) &= \left[\phi_{j+1} - \phi_j\right]_{x=-b,l,b}, \quad j = 1,2,3 \end{aligned} \tag{4.14}$$

where $y \in (0,h)$ for j=1,3 and $y \in (0,c)$ for j=2.
Using the representation (4.11) in the equation (4.14), we obtain

$$\begin{aligned} f_1(y) &= i\alpha_0 \{1-R\} \psi_0(y) + \sum_{n=1}^{\infty} \alpha_n A_n \psi_n(y) \\ &= \lambda_0 \{B_0 \sin \lambda_0 b + C_0 \cos \lambda_0 b\} \chi_0(y) + \sum_{n=1}^{\infty} \lambda_n \{-B_n \sinh \lambda_n b + C_n \cosh \lambda_n b\} \chi_n(y) \end{aligned}$$

$$\begin{aligned} g_1(y) = \{B_0 \cos \lambda_0 b - C_0 \sin \lambda_0 b\} \chi_0(y) &+ \sum_{n=1}^{\infty} \{B_n \cosh \lambda_n b - C_n \sinh \lambda_n b\} \chi_n(y) \\ &- \{1+R\} \psi_0(y) - \sum_{n=1}^{\infty} A_n \psi_n(y) \end{aligned}$$

$$\begin{aligned} f_2(y) &= \lambda_0 \{-B_0 \sin \lambda_0 l + C_0 \cos \lambda_0 l\} \chi_0(y) + \sum_{n=1}^{\infty} \lambda_n \{B_n \sinh \lambda_n l + C_n \cosh \lambda_n l\} \chi_n(y) \\ &= \lambda_0 \{-D_0 \sin \lambda_0 l + E_0 \cos \lambda_0 l\} \chi_0(y) + \sum_{n=1}^{\infty} \lambda_n \{D_n \sinh \lambda_n l + E_n \cosh \lambda_n l\} \chi_n(y) \end{aligned}$$

$$g_2(y) = \{D_0 \cos\lambda_0 l + E_0 \sin\lambda_0 l\}\,\chi_0(y) + \sum_{n=1}^{\infty} \{D_n \cosh\lambda_n l + E_n \sinh\lambda_n l\}\,\chi_n(y)$$
$$- \{B_0 \cos\lambda_0 l + C_0 \sin\lambda_0 l\}\,\chi_0(y) - \sum_{n=1}^{\infty} \{B_n \cosh\lambda_n l + C_n \sinh\lambda_n l\}\,\chi_n(y)$$

$$f_3(y) = \lambda_0 \{-D_0 \sin\lambda_0 b + E_0 \cos\lambda_0 b\}\,\chi_0(y) + \sum_{n=1}^{\infty} \lambda_n \{D_n \sinh\lambda_n b + E_n \cosh\lambda_n b\}\,\chi_n(y)$$
$$= i\alpha_0 T\psi_0(y) - \sum_{n=1}^{\infty} \alpha_n F_n \psi_n(y)$$
$$g_3(y) = T\psi_0(y) + \sum_{n=1}^{\infty} F_n \psi_n(y)$$
$$- \{D_0 \cos\lambda_0 b + E_0 \sin\lambda_0 b\}\,\chi_0(y) - \sum_{n=1}^{\infty} \{D_n \cosh\lambda_n b + E_n \sinh\lambda_n b\}\,\chi_n(y). \qquad (4.15)$$

Now applying the Havelock's inversion formula to equation (4.15), we obtain the unknown constants as,

$$1 - R = \frac{-4i\cosh\alpha_0 h}{\delta_0} \int_0^h f_1(u)\cosh\alpha_0(h-u)du, \qquad (4.16)$$

$$A_n = \frac{4\cos\alpha_n h}{\delta_n} \int_0^h f_1(u)\cos\alpha_n(h-u)du, \qquad (4.17)$$

$$B_0 = \frac{4\cosh\lambda_0 c}{\gamma_0 \sin\lambda_0(b+l)} \left[\cos\lambda_0 l \int_0^h f_1(u)\cosh\lambda_0(c-u)du \right.$$
$$\left. - \cos\lambda_0 b \int_0^c f_2(u)\cosh\lambda_0(c-u)du\right], \qquad (4.18)$$

$$B_n = \frac{4\cos\lambda_n c}{\gamma_n \sinh\lambda_n(b+l)}\left[\cosh\lambda_n b\int_0^c f_2(u)\cos\lambda_n(c-u)du - \cosh\lambda_n l\int_0^h f_1(u)\cos\lambda_n(c-u)du\right], \tag{4.19}$$

$$C_0 = \frac{4\cosh\lambda_0 c}{\gamma_0 \sin\lambda_0(b+l)}\left[\sin\lambda_0 l\int_0^h f_1(u)\cosh\lambda_0(c-u)du + \sin\lambda_0 b\int_0^c f_2(u)\cosh\lambda_0(c-u)du\right], \tag{4.20}$$

$$C_n = \frac{4\cos\lambda_n c}{\gamma_n \sinh\lambda_n(b+l)}\left[\sinh\lambda_n l\int_0^h f_1(u)\cos\lambda_n(c-u)du + \sinh\lambda_n b\int_0^c f_2(u)\cos\lambda_n(c-u)du\right], \tag{4.21}$$

$$D_0 = \frac{4\cosh\lambda_0 c}{\gamma_0 \sin\lambda_0(b-l)}\left[\cos\lambda_0 b\int_0^c f_2(u)\cosh\lambda_0(c-u)du - \cos\lambda_0 l\int_0^h f_3(u)\cosh\lambda_0(c-u)du\right], \tag{4.22}$$

$$D_n = \frac{-4\cos\lambda_n c}{\gamma_n \sinh\lambda_n(b-l)}\left[\cosh\lambda_n b\int_0^c f_2(u)\cos\lambda_n(c-u)du - \cosh\lambda_n l\int_0^h f_3(u)\cos\lambda_n(c-u)du\right] \tag{4.23}$$

$$E_0 = \frac{4\cosh\lambda_0 c}{\gamma_0 \sin\lambda_0(b-l)}\left[\sin\lambda_0 b\int_0^c f_2(u)\cosh\lambda_0(c-u)du - \sin\lambda_0 l\int_0^h f_3(u)\cosh\lambda_0(c-u)du\right], \tag{4.24}$$

$$E_n = \frac{4\cos\lambda_n c}{\gamma_n \sinh\lambda_n(b-l)}\left[\sinh\lambda_n b\int_0^c f_2(u)\cos\lambda_n(c-u)du - \sinh\lambda_n l\int_0^h f_3(u)\cos\lambda_n(c-u)du\right], \tag{4.25}$$

$$T = \frac{-4i\cosh\alpha_0 h}{\delta_0}\int_0^h f_3(u)\cosh\alpha_0(h-u)du, \tag{4.26}$$

$$F_n = \frac{-4\cos\alpha_n h}{\delta_n}\int_0^h f_3(u)\cos\alpha_n(h-u)du \tag{4.27}$$

where $\delta_0 = 2\alpha_0 h + \sinh 2\alpha_0 h$; $\delta_n = 2\alpha_n h + \sin 2\alpha_n h, \gamma_0 = 2\lambda_0 c + \sinh 2\lambda_0 c$; $\gamma_n = 2\lambda_n c + \sin 2\lambda_n c \quad (n = 1, 2, ...)$.
Thus all the unknown constants are expressed in terms of the function $f_j(y)$ and $g_j(y),\ j = 1,\ 2,\ 3$ so that once $f_j(y)$and $g_j(y),\ j = 1,\ 2,\ 3$ are known then the problem is solved. In the next section we proceed to determine $f_j(y),\ j = 1,\ 2,\ 3$ through integral equation formulation.

3.2 Formation of integral equation:

In this section we will derive integral equations for $f_j(y),\ j = 1,\ 2,\ 3$. For this we first consider the continuity of $\phi_j(x, y)$ across the gaps in the boundaries of different regions as given in relation (4.9). This gives

$$\begin{aligned}
\phi_1(-b-0, y) &= \phi_2(-b+0, y), \quad 0 < y < h,\\
\phi_2(l-0, y) - \phi_3(l+0, y) &= -\frac{i}{\alpha_0 G} f_2(y), \quad 0 < y < a,\\
\phi_2(l-0, y) - \phi_3(l+0, y) &= 0, \quad a < y < c,\\
\phi_3(b-0, y) &= \phi_4(b+0, y), \quad 0 < y < h.
\end{aligned} \tag{4.28}$$

These provides the three integral equations given by

$$\int_0^h p_1(u)L_j(y,u)du + \int_0^c p_2(u)M_j(y,u)du + \int_0^h p_3(u)N_j(y,u)du = X_j, j = 1,2,3 \tag{4.29}$$

where

$$X_1 = \psi_0(y),\ X_2 = q_2(y),\quad X_3 = 0$$
$$p_i(u) = \frac{g_i(u)}{1+R},\ i = 1,2,3, \tag{4.30}$$
$$q_2(u) = \frac{f_2(u)}{1+R},$$

$$L_1(y,u) = -\sum_{n=1}^{\infty} \frac{4\cos\alpha_n(h-y)\cos\alpha_n(h-u)}{\delta_n} + \frac{4\cosh\lambda_0(c-y)\cosh\lambda_0(c-u)}{\gamma_0\tan\lambda_0(b+l)} - \sum_{n=1}^{\infty} \frac{4\cos\lambda_n(c-y)\cos\lambda_n(c-u)}{\gamma_n\tanh\lambda_n(b+l)}, \tag{4.31}$$

$$M_1(y,u) = -\frac{4\cosh\lambda_0(c-y)\cosh\lambda_0(c-u)}{\gamma_0\sin\lambda_0(b+l)} + \sum_{n=1}^{\infty} \frac{4\cos\lambda_n(c-y)\cos\lambda_n(c-u)}{\gamma_n\sinh\lambda_n(b+l)}, \tag{4.32}$$

$$N_1(y,u) = 0, \tag{4.33}$$

$$L_2(y,u) = -\frac{4\cosh\lambda_0(c-y)\cosh\lambda_0(c-u)}{\gamma_0\sin\lambda_0(b+l)} + \sum_{n=1}^{\infty} \frac{4\cos\lambda_n(c-y)\cos\lambda_n(c-u)}{\gamma_n\sinh\lambda_n(b+l)}, \tag{4.34}$$

$$M_2(y,u) = \frac{4\cosh\lambda_0(c-y)\cosh\lambda_0(c-u)}{\gamma_0\tan\lambda_0(b-l)} + \frac{4\cosh\lambda_0(c-y)\cosh\lambda_0(c-u)}{\gamma_0\tan\lambda_0(b+l)} - \sum_{n=1}^{\infty}\frac{4\cos\lambda_n(c-y)\cos\lambda_n(c-u)}{\gamma_n\tanh\lambda_n(b-l)} - \sum_{n=1}^{\infty}\frac{4\cos\lambda_n(c-y)\cos\lambda_n(c-u)}{\gamma_n\tanh\lambda_n(b+l)}, \tag{4.35}$$

$$N_2(y,u) = -\frac{4\cosh\lambda_0(c-y)\cosh\lambda_0(c-u)}{\gamma_0\sin\lambda_0(b-l)} + \sum_{n=1}^{\infty}\frac{4\cos\lambda_n(c-y)\cos\lambda_n(c-u)}{\gamma_n\sinh\lambda_n(b-l)}, \tag{4.36}$$

$$L_3(y,u) = 0, \tag{4.37}$$

$$M_3(y,u) = -\frac{4\cosh\lambda_0(c-y)\cosh\lambda_0(c-u)}{\gamma_0\sin\lambda_0(b-l)} + \sum_{n=1}^{\infty}\frac{4\cos\lambda_n(c-y)\cos\lambda_n(c-u)}{\gamma_n\sinh\lambda_n(b-l)}, \tag{4.38}$$

$$N_3(y,u) = \frac{4\cosh\lambda_0(c-y)\cosh\lambda_0(c-u)}{\gamma_0\tan\lambda_0(b-l)} - \sum_{n=1}^{\infty}\frac{4\cos\lambda_n(c-y)\cos\lambda_n(c-u)}{\gamma_n\tanh\lambda_n(b-l)} - \frac{4i\cosh\alpha_0(h-y)\cosh\alpha_0(h-u)}{\delta_0} - \sum_{n=1}^{\infty}\frac{4\cos\alpha_n(h-y)\cos\alpha_n(h-u)}{\delta_n}. \tag{4.39}$$

3.3 Solution of integral equation

We solve the integral equations (4.29) using the multi-term Galerkin approximation

method. For this we write the unknown functions $p_i(y),\ i = 1, 2, 3$ as

$$p_1(y) = \sum_{n=0}^{N} a_n u_n(y), 0 < y < h, \tag{4.40}$$

$$p_2(y) = \sum_{n=0}^{N} b_n z_n(y), 0 < y < c, \tag{4.41}$$

where $z_n(y) = v_n(y)$ for $0 < y < a$ and $z_n(y) = x_n(y)$ for $a < y < c$,

$$p_3(y) = \sum_{n=0}^{N} c_n w_n(y), 0 < y < h, \tag{4.42}$$

$$q_2(y) = \sum_{n=0}^{N} b_n v_n(y), 0 < y < a,$$

where the basis functions $u_n(y)$ for $0 < y < h$ and $w_n(y)$ for $0 < y < h$ are chosen in terms of ultraspherical Gegenbauer polynomials of order $\frac{1}{6}$ and $z_n(y)$ for $0 < y < a$ are chosen in terms of orthogonal Chebyshev's polynomial of order $2n$ with suitable weights respectively. The choice of basis functions depends on the types of singularities at the corners of the trench and at the submerged sharp edge of the barrier as given by the edge condition (4.7). Here we also consider simple polynomial as basis function to solve the integral equation. The basis function in various intervals are given below.

3.4 Basis functions

Approximation of basis functions in terms of orthogonal polynomials

In each integral equation of (4.29) there are three integrals where the unknown functions are $p_1(y),\ p_2(y),\ p_3(y)$ in first, second and third integral respectively. As given in equations (4.40) to (4.42), these unknown function are expanded in terms of suitable basis functions. The choice of basis functions are explained in section 3.3 and are given below. For the first integral in (4.29) we write,

$$u_n(y) = -\frac{d}{dy}[e^{-Ky} \int_y^h e^{Kt} \tilde{u}_n(t) dt], 0 < y < h. \tag{4.43}$$

We choose the basis functions in terms of $\tilde{u}_n(y)$ as follows

$$\tilde{u}_n(y) = \frac{2^{\frac{7}{6}}\Gamma(\frac{1}{6})(2n)!}{\pi\Gamma(2n+\frac{1}{3})(h)^{\frac{1}{3}}(h^2-y^2)^{\frac{1}{3}}} C_{2n}^{\frac{1}{6}}(\frac{y}{h}), 0 < y < h \tag{4.44}$$

where $C_{2n}^{\frac{1}{6}}(\frac{y}{h})$ are Gegenbauer polynomials of order 1/6.

For the second integral in (4.29) we write,

$$\begin{aligned} v_n(y) &= -\frac{d}{dy}[e^{-Ky}\int_0^a e^{Kt}\tilde{v}_n(t)dt], 0 < y < a, \\ x_n(y) &= -\frac{d}{dy}[e^{-Ky}\int_a^c e^{Kt}\tilde{x}_n(t)dt], 0 < y < a. \end{aligned} \tag{4.45}$$

We choose the basis functions in terms of $\tilde{v}_n(y)$ as follows

$$\begin{aligned} \tilde{v}_n(y) &= \frac{2(-1)^n}{\pi(2n+1)ah}(a^2-y^2)^{\frac{1}{2}}U_{2n}(\frac{y}{a}), 0 < y < a, \\ \tilde{x}_n(y) &= \frac{2(-1)^n}{\pi\{(c-y)^2-(c-a)^2\}^{\frac{1}{2}}} T_{2n}(\frac{c-y}{c-a}), a < y < c \end{aligned} \tag{4.46}$$

where $T_{2n}(y)$ and $U_{2n}(y)$ are Chebychev's polynomial of first and second kind of order 2n.

For the third integral in (4.29) we write,

$$w_n(y) = -\frac{d}{dy}[e^{-Ky}\int_y^h e^{Kt}\tilde{w}_n(t)dt], 0 < y < h. \tag{4.47}$$

Here also we choose the $\tilde{w}_n(y)$ in terms of Gegenbauer polynomials of order 1/6 as given below.

$$\tilde{w}_n(y) = \frac{2^{\frac{7}{6}}\Gamma(\frac{1}{6})(2n)!}{\pi\Gamma(2n+\frac{1}{3})(h)^{\frac{1}{3}}(h^2-y^2)^{\frac{1}{3}}} C_{2n}^{\frac{1}{6}}(\frac{y}{h}), 0 < y < h. \tag{4.48}$$

Thus the unknown functions satisfying the integral equation (4.29) are expanded in terms of suitable orthogonal polynomials as shown in equations (4.43) to (4.48).

However the unknown functions satisfying the integral equation (4.29) can also be expanded in terms of simple polynomials as shown below.

Approximation of basis functions in terms of simple polynomials

For the first integral in (4.29) we write,

$$u_n(y) = \left(\frac{h}{h-y}\right)^{\frac{1}{3}} \left(\frac{y}{h}\right)^n, 0 < y < h. \tag{4.49}$$

For the second integral in (4.29) we write,

$$v_n(y) = \left(\frac{a}{a-y}\right)^{\frac{1}{2}} \left(\frac{y}{a}\right)^n, 0 < y < a, \tag{4.50}$$

and

$$x_n(y) = \left(\frac{a}{y-a}\right)^{\frac{1}{2}} \left(\frac{y}{a}\right)^n, a < y < c. \tag{4.51}$$

For the third integral in (4.29) we write,

$$w_n(y) = \left(\frac{h}{h-y}\right)^{\frac{1}{3}} \left(\frac{y}{h}\right)^n, 0 < y < h. \tag{4.52}$$

3.5 Formation of linear system of equations

As the three integral equations given by (4.29) are in different ranges, they can be extended to the range $(0, c)$ as in Morris (1975), by multiplying with appropriate Heaviside unit functions. This gives the linear system of equations as follows

$$\sum_{n=0}^{N} a_n \mathcal{K}_{mn} + \sum_{n=0}^{N} b_n \mathcal{L}_{mn} = d_m, \quad m = 0, 1, ..., N \tag{4.53}$$

$$\sum_{n=0}^{N} a_n \mathcal{M}_{mn} + \sum_{n=0}^{N} b_n \mathcal{N}_{mn} + \sum_{n=0}^{N} c_n \mathcal{P}_{mn} = 0, \quad m = 0, 1, ..., N \tag{4.54}$$

$$\sum_{n=0}^{N} b_n \mathcal{Q}_{mn} + \sum_{n=0}^{N} c_n \mathcal{R}_{mn} = 0, \quad m = 0, 1, ..., N \tag{4.55}$$

where

$$\mathcal{K}_{mn} = \int_0^h \left(\int_0^h L_1(y,u)u_n(u)du \right) u_m(y)dy$$

$$\mathcal{L}_{mn} = -i\alpha_0 G \int_0^h \left(\int_0^a M_1(y,u)v_n(u)du \right) u_m(y)dy + \int_0^h \left(\int_a^c M_1(y,u)x_n(u)du \right) u_m(y)dy$$

$$\mathcal{M}_{mn} = \int_0^c \left(\int_0^h L_2(y,u)u_n(u)du \right) z_m(y)dy$$

$$\mathcal{N}_{mn} = -i\alpha_0 G \int_0^a \left(\int_0^a M_2(y,u)v_n(u)du \right) v_m(y)dy + \int_a^c \left(\int_a^c M_2(y,u)x_n(u)du \right) x_m(y)dy - \int_0^a v_n(y)v_m(y)dy$$

$$\mathcal{P}_{mn} = \int_0^c \left(\int_0^h N_2(y,u)w_n(u)du \right) z_m(y)dy$$

$$\mathcal{Q}_{mn} = -i\alpha_0 G \int_0^h \left(\int_0^a M_3(y,u)v_n(u)du \right) w_m(y)dy + \int_0^h \left(\int_a^c M_3(y,u)x_n(u)du \right) w_m(y)dy$$

$$\mathcal{R}_{mn} = -\int_0^h \left(\int_0^h N_3(y,u)w_n(u)du \right) w_m(y)dy$$

and

$$d_m = \int_0^h \frac{\cosh \alpha_0(h-y)}{\cosh \alpha_0 h} u_m(y)dy$$

with $m, n = 0, 1, 2, ...N$.

Substituting the expression of $f_1(y)$ in terms of $p_1(y)$ in (4.16), we obtain the

reflection coefficient as follows

$$R = \frac{1 + Cs}{1 - Cs} \tag{4.56}$$

where

$$Cs = \frac{4i \cosh \alpha_0 h}{\delta_0} \sum_{n=0}^{N} a_n \int_0^h \cosh \alpha_0 (h - y) u_n(y) dy \tag{4.57}$$

and substituting the expression of $f_3(y)$ in terms of $p_3(y)$ in (4.26), we obtain transmission coefficient as follows

$$T = -\frac{4i(1 + R) \cosh \alpha_0 h}{\delta_0} \sum_{n=0}^{N} c_n \int_0^h \cosh \alpha_0 (h - y) w_n(y) dy. \tag{4.58}$$

3.6 Evaluation of coefficients of linear system of equations

The various coefficients $\mathcal{K}_{mn}$, $\mathcal{M}_{mn}$, $\mathcal{N}_{mn}$, $\mathcal{P}_{mn}$, $\mathcal{Q}_{mn}$ and $\mathcal{R}_{mn}$, occurring in the linear system of algebraic equations (4.53) to (4.55), can be evaluated by choosing the basis functions in terms of simple polynomial as given by equations (4.49) to (4.52) and orthogonal polynomials as given by equations (4.43) to (4.48). The choice of basis functions in terms of orthogonal polynomial simplifies the coefficients of the linear system of equations (4.53) to (4.55) considerably using the properties of the orthogonal polynomials. The simplified form of various coefficients using the properties of orthogonal polynomials are given below.

$$\begin{aligned}
\mathcal{K}_{mn} &= \int_0^h \left(\int_0^h L_1(y, u) u_n(u) du \right) u_m(y) dy \\
&= -\sum_{r=1}^{\infty} \frac{4}{\delta_r} \left(\int_0^h \cos \alpha_r (h - y) u_m(y) dy \right) \left(\int_0^h \cos \alpha_r (h - u) u_n(u) du \right) \\
&\quad + \frac{4}{\gamma_0 \tan \lambda_0 (b + l)} \left(\int_0^h \cosh \lambda_0 (c - y) u_m(y) dy \right) \left(\int_0^h \cosh \lambda_0 (c - u) u_n(u) du \right) \\
&\quad - \sum_{r=1}^{\infty} \frac{4}{\gamma_r \tanh \lambda_r (b + l)} \left(\int_0^h \cos \lambda_r (c - y) u_m(y) dy \right) \left(\int_0^h \cos \lambda_r (c - u) u_n(u) du \right)
\end{aligned}$$

Now,

$$\int_0^h \cos\alpha_r(h-y)u_m(y)dy = \frac{2^{\frac{7}{6}}\Gamma(\frac{1}{6})(2m)!}{\pi\Gamma(2m+\frac{1}{3})(h)^{\frac{1}{3}}}\int_0^h \cos\alpha_r(h-y)\frac{1}{(h^2-y^2)^{\frac{1}{3}}}C_{2n}^{\frac{1}{6}}(\frac{y}{h})dy$$
$$= \frac{2(-1)^m}{(\alpha_r h)^{\frac{1}{6}}}\cos(\alpha_r h)J_{2m+\frac{1}{6}}(\alpha_r h)$$

where $J_n{}'$s are Bessel functions of first kind.

Similarly other integrals in the expression for $\mathcal{K}_{mn}$ can be evaluated. Using this result in the expression for $\mathcal{K}_{mn}$, we get

$$\mathcal{K}_{mn} = -\sum_{r=1}^{\infty}\frac{16(-1)^{m+n}\cos^2\alpha_r h}{\delta_r(\alpha_r h)^{\frac{1}{3}}}J_{2m+\frac{1}{6}}(\alpha_r h)J_{2n+\frac{1}{6}}(\alpha_r h)$$
$$+\frac{16\cosh^2\lambda_0 c}{\gamma_0(\lambda_0 h)^{\frac{1}{3}}\tan\lambda_0(b+l)}I_{2m+\frac{1}{6}}(\lambda_0 h)I_{2n+\frac{1}{6}}(\lambda_0 h)$$
$$-\sum_{r=1}^{\infty}\frac{16(-1)^{m+n}\cos^2\lambda_r c}{\gamma_r(\lambda_r h)^{\frac{1}{3}}\tanh\lambda_r(b+l)}J_{2m+\frac{1}{6}}(\lambda_r h)J_{2n+\frac{1}{6}}(\lambda_r h)$$

where $I_n{}'$s are modified Bessel function of first kind.

$$\mathcal{L}_{mn} = i\alpha_0 G\left[\frac{16\cosh^2\lambda_0 c}{\gamma_0(\lambda_0 c)\sin\lambda_0(b+l)}I_{2m+1}(\lambda_0 a)I_{2n+1}(\lambda_0 a)\right.$$
$$\left.-\sum_{r=1}^{\infty}\frac{16(-1)^{m+n}\cos^2\lambda_r c}{\gamma_r(\lambda_r c)\sinh\lambda_r(b+l)}J_{2m+1}(\lambda_r a)J_{2n+1}(\lambda_r a)\right]$$
$$-\frac{16}{\gamma_0(\lambda_0 c)\sin\lambda_0(b+l)}I_{2m}(\lambda_0(c-a))I_{2n}(\lambda_0(c-a))$$
$$+\sum_{r=1}^{\infty}\frac{16(-1)^{m+n}}{\gamma_r(\lambda_r c)\sinh\lambda_r(b+l)}J_{2m}(\lambda_r(c-a))J_{2n}(\lambda_r(c-a))$$

$$\mathcal{M}_{mn} = -\frac{16\cosh^2\lambda_0 c}{\gamma_0(\lambda_0 h)^{\frac{1}{3}}\sin\lambda_0(b+l)} I_{2m+\frac{1}{6}}(\lambda_0 h) I_{2n+\frac{1}{6}}(\lambda_0 h) + \sum_{r=1}^{\infty} \frac{16(-1)^{m+n}\cos^2\lambda_r c}{\gamma_r(\lambda_r h)^{\frac{1}{3}}\sinh\lambda_r(b+l)} J_{2m+\frac{1}{6}}(\lambda_r h) J_{2n+\frac{1}{6}}(\lambda_r h)$$

$$\begin{aligned}\mathcal{N}_{mn} = i\alpha_0 G \Bigg[& -\frac{16\cosh^2\lambda_0 c}{\gamma_0(\lambda_0 c)\tan\lambda_0(b-l)} I_{2m+1}(\lambda_0 a) I_{2n+1}(\lambda_0 a) \\ & -\frac{16\cosh^2\lambda_0 c}{\gamma_0(\lambda_0 c)\tan\lambda_0(b+l)} I_{2m+1}(\lambda_0 a) I_{2n+1}(\lambda_0 a) \\ & +\sum_{r=1}^{\infty} \frac{16(-1)^{m+n}\cos^2\lambda_r c}{\gamma_r(\lambda_r c)\tanh\lambda_r(b-l)} J_{2m+1}(\lambda_r a) J_{2n+1}(\lambda_r a) \\ & +\sum_{r=1}^{\infty} \frac{16(-1)^{m+n}\cos^2\lambda_r c}{\gamma_r(\lambda_r c)\tanh\lambda_r(b+l)} J_{2m+1}(\lambda_r a) J_{2n+1}(\lambda_r a) \Bigg] \\ & +\frac{16}{\gamma_0(\lambda_0 c)\tan\lambda_0(b+l)} I_{2m}(\lambda_0(c-a)) I_{2n}(\lambda_0(c-a)) \\ & -\sum_{r=1}^{\infty} \frac{16(-1)^{m+n}}{\gamma_r(\lambda_r c)\tanh\lambda_r(b+l)} J_{2m}(\lambda_r(c-a)) J_{2n}(\lambda_r(c-a)) \\ & +\frac{16}{\gamma_0(\lambda_0 c)\tan\lambda_0(b-l)} I_{2m}(\lambda_0(c-a)) I_{2n}(\lambda_0(c-a)) \\ & -\sum_{r=1}^{\infty} \frac{16(-1)^{m+n}}{\gamma_r(\lambda_r c)\tanh\lambda_r(b-l)} J_{2m}(\lambda_r(c-a)) J_{2n}(\lambda_r(c-a)) \\ & -\frac{4(-1)^{m+n}}{\pi^2 a^2 h^2 (2m+1)(2n+1)} \int_0^a (a^2-y^2) U_{2n}(\frac{y}{a}) U_{2m}(\frac{y}{a}) dy\end{aligned}$$

$$\mathcal{P}_{mn} = -\frac{16\cosh^2\lambda_0 c}{\gamma_0(\lambda_0 h)^{\frac{1}{3}}\sin\lambda_0(b-l)} I_{2m+\frac{1}{6}}(\lambda_0 h) I_{2n+\frac{1}{6}}(\lambda_0 h) + \sum_{r=1}^{\infty} \frac{16(-1)^{m+n}\cos^2\lambda_r c}{\gamma_r(\lambda_r h)^{\frac{1}{3}}\sinh\lambda_r(b-l)} J_{2m+\frac{1}{6}}(\lambda_r h) J_{2n+\frac{1}{6}}(\lambda_r h)$$

$$\mathcal{Q}_{mn} = i\alpha_0 G \left[\frac{16\cosh^2\lambda_0 c}{\gamma_0(\lambda_0 c)\sin\lambda_0(b-l)} I_{2m+1}(\lambda_0 a) I_{2n+1}(\lambda_0 a) \right.$$
$$\left. - \sum_{r=1}^{\infty} \frac{16(-1)^{m+n}\cos^2\lambda_r c}{\gamma_r(\lambda_r c)\sinh\lambda_r(b-l)} J_{2m+1}(\lambda_r a) J_{2n+1}(\lambda_r a) \right]$$
$$- \frac{16}{\gamma_0(\lambda_0 c)\sin\lambda_0(b-l)} I_{2m}(\lambda_0(c-a)) I_{2n}(\lambda_0(c-a))$$
$$+ \sum_{r=1}^{\infty} \frac{16(-1)^{m+n}}{\gamma_r(\lambda_r c)\sinh\lambda_r(b-l)} J_{2m}(\lambda_r(c-a)) J_{2n}(\lambda_r(c-a))$$

$$\mathcal{R}_{mn} = -\frac{16i\cosh^2\alpha_0 h}{\delta_0(\alpha_0 h)^{\frac{1}{3}}} I_{2m+\frac{1}{6}}(\alpha_0 h) I_{2n+\frac{1}{6}}(\alpha_0 h)$$
$$- \sum_{r=1}^{\infty} \frac{16(-1)^{m+n}\cos^2\alpha_r h}{\delta_r(\alpha_r h)^{\frac{1}{3}}} J_{2m+\frac{1}{6}}(\alpha_r h) J_{2n+\frac{1}{6}}(\alpha_r h)$$
$$+ \frac{16\cosh^2\lambda_0 c}{\gamma_0(\lambda_0 h)^{\frac{1}{3}}\tan\lambda_0(b-l)} I_{2m+\frac{1}{6}}(\lambda_0 h) I_{2n+\frac{1}{6}}(\lambda_0 h)$$
$$- \sum_{r=1}^{\infty} \frac{16(-1)^{m+n}\cos^2\lambda_r c}{\gamma_r(\lambda_r h)^{\frac{1}{3}}\tanh\lambda_r(b-l)} J_{2m+\frac{1}{6}}(\lambda_r h) J_{2n+\frac{1}{6}}(\lambda_r h)$$

$$d_m = \frac{2I_{2m+\frac{1}{6}}(\alpha_0 h)}{(\alpha_0 h)^{\frac{1}{6}}}$$

3.7 Dynamic wave force:

The dynamic pressure $P(x, y)$ can be obtained according to the Bernoulli equation Li *et al.* (2015)

$$P(x, y) = -i\rho\sigma g_2(y) \tag{4.59}$$

where ρ is the fluid density. The magnitude of horizontal wave force acting on barriers can be obtained by integrating the dynamic pressure along the porous barriers

as follows

$$C_f = -i\rho\sigma \int_0^a g_2(y)dy. \tag{4.60}$$

The non-dimensional form of the horizontal force coefficient on the vertical porous barriers is given by

$$K_f = \frac{K|C_f|}{\rho g}. \tag{4.61}$$

3.8 Energy identity relation:

The energy identity plays an important role in the theoretical study of water waves scattering by barriers. A part of incident wave energy can be dissipated by the porous barriers. The absolute values of the reflection and transmission coefficients are connected by the relation

$$|R|^2 + |T|^2 = 1 - J. \tag{4.62}$$

Here J signifies the amount of dissipated energy due to the permeability of barriers and its expression in terms of the potential differences across the barriers is found to be

$$J = 2KG^r \int_0^a |g_2(y)|^2 dy. \tag{4.63}$$

It is clearly noticed from the expression of J that the integrand in the right-hand side of (4.57) is always positive for a non-zero G^r so that $|R|^2 + |T|^2 < 1$ for the case of permeable barriers, whereas for impermeable barriers the energy identity relation satisfies $|R|^2 + |T|^2 = 1$, which provides the convergence of result in the present study.

4.4 NUMERICAL RESULTS

In this section the numerical results of hydrodynamic quantities viz. reflection coefficient, transmission coefficient, energy dissipation coefficient and hydrodynamic force

are depicted graphically. Here this quantities are non dimensionalized by the water depth h.

Table 4.1: Convergence of $|R|$ with N for $a/h = 0.5, b/h = 1.5, c/h = 1.5, l/h = 0.5, G = 0.5$

Kh	**N**=2	**N**=3	**N**=4	**N**=5
0.00001	0.001271	0.001351	0.001372	0.001377
0.50001	0.090594	0.090595	0.090596	0.090596
1.00001	0.249584	0.251970	0.252254	0.252259
1.50001	0.570622	0.575437	0.577160	0.577165
2.00001	0.179136	0.187224	0.187403	0.187405
2.50001	0.263810	0.251276	0.254864	0.254867

Table 4.2: Comparision of our results with the results of Ray *et al.* (2021) taking $a/h = 0.5, b/h = 1.5, c/h = 1.5, G = 0, l/h = 0$

Kh	$\|R\|(N = 5)$ (Ray *et al.* (2021))	$\|R\|(N = 3)$ (Present Study)	$\|T\|(N = 5)$ (Ray *et al.* (2021))	$\|T\|(N = 3)$ (Present Study)
0.001	0.013015	0.013019	0.999915	0.999915
0.491	0.132204	0.132209	0.991213	0.991221
0.981	0.047433	0.047441	0.998867	0.998874
1.471	0.315932	0.315937	0.947309	0.948780
1.961	0.636024	0.636030	0.783752	0.771664
2.451	0.873816	0.873824	0.474271	0.486242
2.941	0.966781	0.966789	0.262009	0.255576

In Table (4.1), we display the numerical results for $|R|$ showing its convergence with the truncation number N in equations (4.53) to (4.55), taking $N = 2, 3, 4, 5$ for different values of Kh. In this case we see that, for $N = 3, 4, 5$, the numerical values computed here coincide upto 5 decimal places. We have also checked that the present method converges for all other values of the parameters and the wave number when N is 3. So, for all the calculations we have chosen $N = 3$.

Then the accuracy of the numerical results are established in Table (4.2), by comparing our present result with Ray *et al.* (2021). In Table (4.2), the numerical values of $|R|$ computed by present method are compared with those given in Table 1 of Ray *et al.* (2021) for a rigid barrier placed along the y-axis, by considering $\frac{a}{h} = 0.5$, $\frac{b}{h} = 1.5$, $\frac{c}{h} = 1.5$, $\frac{l}{h} = 0$, $G = 0$. Ray *et al.* (2021), used Galerkin technique with simple polynomial as a basis function, whereas in the present work, suitable orthogonal polynomials (Gegenbauer polynomial for 1/3 rd singularity and Chebyshev

polynomial for half singularity) are chosen as a basis function. From Table (4.2), it is clearly noticed that the linear system of equations (4.53) to (4.55), converges for $N = 5$ in Ray *et al.* (2021), where as in the present study the same converges for $N = 3$. Thus the rate of convergence of the linear system taking algebraic polynomials as basis function is slower than the orthogonal polynomials as basis function.

In Table (4.3), the values of reflection coefficient are presented for different wave numbers Kh and fixed values of $a/h = 0.6, b/h = 1.5, c/h = 1.3, l/h = 0, G = 0.5$, and compared by choosing simple polynomials and orthogonal polynomial as basis functions in Galerkin method. It is observed that rate of convergence of the method choosing basis function as orthogonal polynomial (N=3) is faster than taking basis function as simple polynomial (N=5). Also the Table (4.3) shows that the values of $|R|$ choosing orthogonal polynomial as basis function matches with values of $|R|$ choosing simple polynomial as basis function upto five places of decimal. Hence we may infer that the orthogonal polynomials as basis function is a better choice.

Table 4.3: $|R|$ for $a/h = 0.6, b/h = 1.5, c/h = 1.3, l/h = 0, G = 0.5$

Kh	Orthogonal Polynomials(N=3)	Simple Polynomials(N=5)
0.00001	0.000948	0.000945
0.50001	0.024745	0.024751
1.00001	0.344937	0.344935
1.50001	0.379658	0.379654
2.00001	0.956727	0.956721
2.50001	0.265245	0.265241

The numerical values of the reflection coefficient, transmission coefficient, energy dissipation coefficients and the energy identity are presented in Table (4.4) for different values of Kh and fixed values of $a/h = 0.5, b/h = 1.5, c/h = 1.5, l/h = 0.5, G = 1.0$. In this table for all the values of Kh we observe that the energy identity relation $|R|^2 + |T|^2 + J = 1$ is satisfied. This tables provide a partial check on the correctness of the results obtained by the present method.

Validation of the results:-

To check the validity of the analytical solutions obtained in the present work, $|R|$ is compared with the results of Lee and Chwang (2015) considering limiting values of certain parameters in our results. In the present analysis, considering $a/h = 0.5$, $G(=$

Table 4.4: Energy identity for $a/h = 0.5, b/h = 1.5, c/h = 1.5, G = 1.0, l/h = 0.5$

Kh	$\|R\|$	$\|T\|$	J	$\|R\|^2 + \|T\|^2 + J$
0.10001	0.1135310	0.994401	0.00172329	1.00345
1.20001	0.3618910	0.904478	0.05095360	1.00000
2.00001	0.0771846	0.715724	0.48178200	1.00000
2.50001	0.2708460	0.745861	0.37033300	1.00000
2.83001	0.9765090	0.136927	0.02768090	1.00000

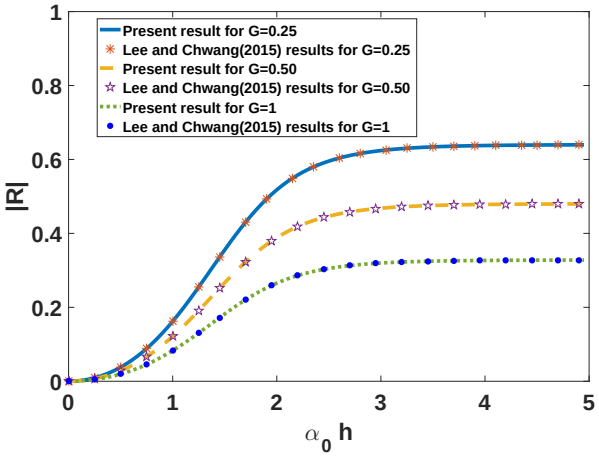

Figure 4.3: Comparison of our results to the Fig.6 of Lee and Chwang(2015) taking $a/h = 0.5, b/h = 0.001, c/h = 1$ and different values of G.

$0.25, 0.5, 1)$ and $c/h = 1, b/h = 0.001$, i.e., in absence of trench, the reflection coefficient $|R|$ is compared with the results of Lee and Chwang (2015) in Figure (4.3). A good matching of $|R|$ is observed in the figure.

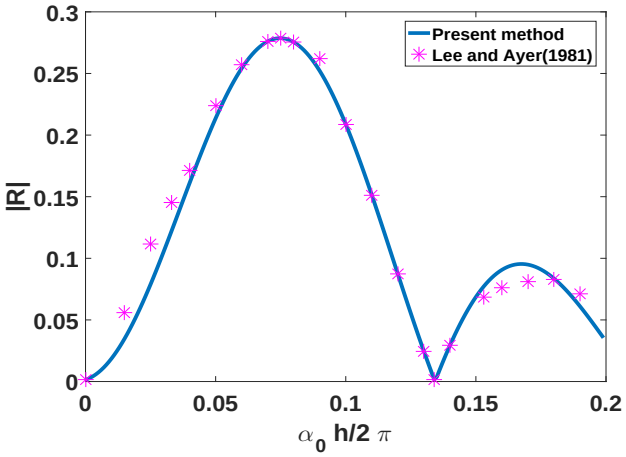

Figure 4.4: Comparison of our results to the Fig.2 of Lee and Ayer (1981) taking $a/h = 0.0001, b/h = 2.5, c/h = 2$ and $G = 0$.

In absence of barrier (i.e., making $a/h \to 0,\ G = 0$ in the present study), the problem reduces to study of wave propagation over a ractangular trench which was studied earlier by Lee and Ayer (1981). Choosing $a/h = 0.0001, b/h = 2.5, c/h = 2$ and $G = 0$, the reflection coefficient $|R|$ is plotted against $\frac{\alpha_0 h}{2\pi}$ in Figure (4.4) and it is observed that our result almost match with the Figure 2 of Lee and Ayer (1981).

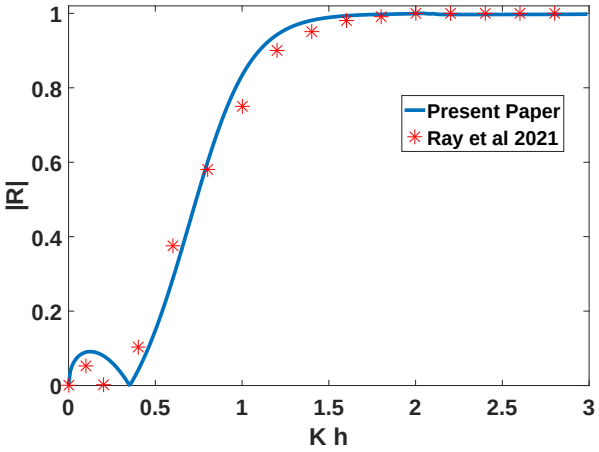

Figure 4.5: Comparison of our results to the Fig.4a of Ray *et al.* (2021) taking $a/h = 0.9, b/h = 1.5, c/h = 1.5$ and $G = 0$.

In Figure (4.5), $|R|$ for rigid barrier, obtained in the present analysis by making $G = 0,\ a/h = 0.9,\ b/h = 1.5,\ c/h = 1.5$, is compared with the results given by Ray *et al.* (2021) (Figure 4a there). A good matching of the results are observed from Figure (4.5).

Effect of various parameters on scattering coefficients($|R|$ and $|T|$)

Figure (4.6) illustrates the effect of width of the trench on the reflection coefficients in presence of porous barrier. Here $|R|$ is plotted against the non-dimensional wave number Kh for three different width of the trench ($b/h = 1.3, 1.4, 1.5$) and fixed values of $a/h = 0.7, c/h = 1.3, l/h = 0.5$ and $G = 0.5$. We observe oscillatory behaviour of $|R|$. Also we observe that for $Kh > 2$, larger width of the trench increases the amount of reflection and the same behavior have shown in Chakraborty and Mandal (2014).

The effect of the length of the partially immersed porous barrier on the reflection coefficient $|R|$ is studied in Figure (4.7) where $|R|$ is plotted against the non-dimensional wave number Kh for various values of the length of the barrier ($a/h = 0.3, 0.6, 0.9$) and fixed values of $b/h = 1.5, c/h = 1.3, l/h = 0.5$ and $G = 0.5$. Figure (4.7) shows that $|R|$ exhibits oscillatory behaviour and the amplitude of oscillation increases with increasing length of the porous barrier. For Kh near about 1.5, there occurs a sharp increase in amplitude of oscillation in $|R|$ showing resonating behaviour of the reflection coefficient.

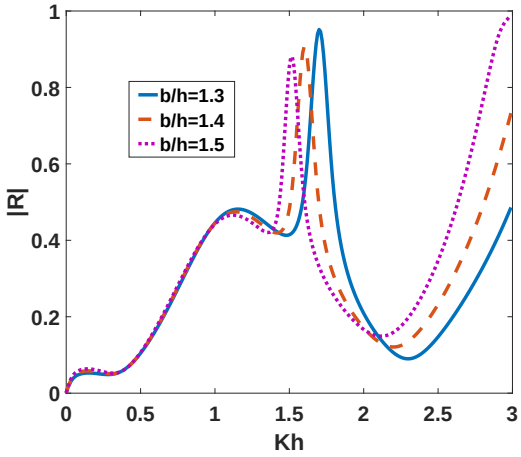

Figure 4.6: Reflection coefficient against Kh for different values of $\frac{b}{h}$ with $\frac{a}{h} = 0.7, \frac{c}{h} = 1.3, G = 0.5, \frac{l}{h} = 0.5$.

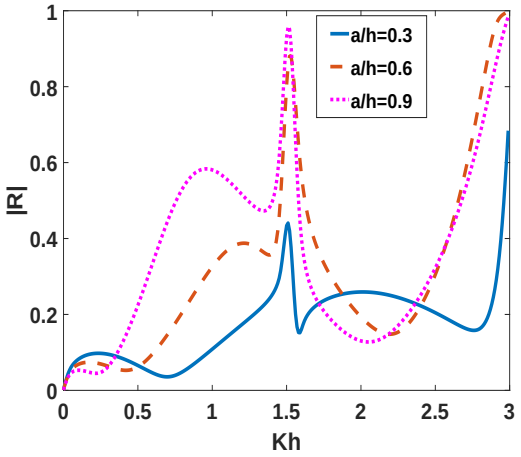

Figure 4.7: Reflection coefficient against Kh for different values of $\frac{a}{h}$ with $\frac{b}{h} = 1.5, \frac{c}{h} = 1.3, G = 0.5, \frac{l}{h} = 0.5$.

Figure (4.8) illustrate the effect of depth of the trench on the reflection coefficient. Here $|R|$ is plotted against the non-dimensional wave number Kh, for $a/h = 0.7$, $b/h = 1.4$, $l/h = 0.5$ and $G = 0.5$ and for various depth of the trench viz, $c/h = 1.1, 1.2, 1.3$. It is observed that $|R|$ shows oscillatory behaviour and amplitude of oscillation increases with the increasing values of the trench depth c/h. Also for $Kh \approx 1.5$, there occur resonance in $|R|$.

In Figure (4.9), reflection coefficient $|R|$ is plotted against the non-dimensional wave number Kh for different values of the porosity parameter $G(= 0.5, 1, 2)$ and for $a/h = 0.7$, $b/h = 1.4$, $l/h = 0.5$, $c/h = 1.3$. It is seen that $|R|$ shows oscillatory behaviour with multiple peaks and for $Kh \approx 1.75$ a resonance occurs in the reflection coefficient $|R|$ for all values of porosity parameter G. This occurs as a consequence

of the interaction between porous barrier, trench and the waves. It is seen that with increasing porosity parameter reflection decreases. This is due to the fact that the pores in the barrier allows water to pass through them and thereby decreasing the reflection.

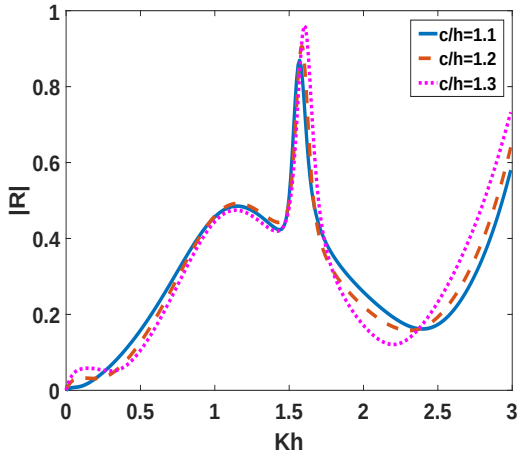

Figure 4.8: Reflection coefficient against Kh for different values of $\frac{c}{h}$ with $\frac{a}{h} = 0.7, \frac{b}{h} = 1.4, G = 0.5, \frac{l}{h} = 0.5$.

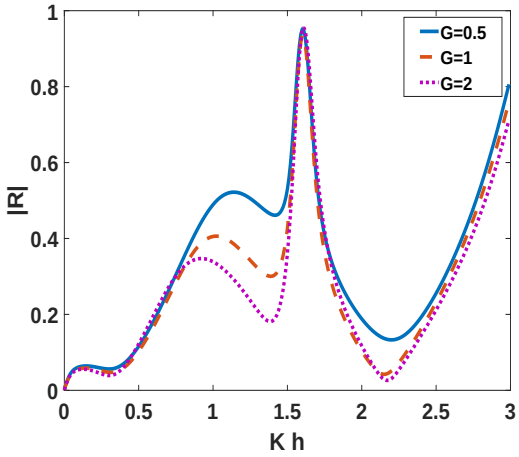

Figure 4.9: Reflection coefficient against Kh for different values of G with $\frac{a}{h} = 0.7, \frac{b}{h} = 1.4, \frac{c}{h} = 1.3, \frac{l}{h} = 0.5$.

In Figure (4.10), reflection coefficient $|R|$ is plotted against the non-dimensional wave number Kh for different values of $l/h(= 0.4, 0.5, 0.6)$ and keeping $a/h = 0.7, b/h = 1.4, l/h = 0.5$ and $c/h = 1.3$ fixed. Here $|R|$ shows oscilltory behaviour. For $Kh < 1.5$, $|R|$ almost coincide for all values of l/h. For $1.5 < Kh < 1.7$, a sharp peak is observed in $|R|$ for each value of l/h and the peaks shift towards left as l/h increases. Thus as the barrier is placed away from the central line of the trench, there is a phase shift in the peak of $|R|$. Also $|R|$ increases with decreasing values of l/h. It means that the reflection coefficient increases when the porous barrier is shifted towards the centre of the trench from the right side of the trench. In all curves, $|R|$ starts from zero near $Kh = 0$ and for large values of Kh, $|R|$ becomes unity.

In Figure (4.11), amplitude of the energy dissipation coefficient J is plotted against the non-dimensional wave number Kh for different values of the porosity parameter $G(= 1, 2, 3)$ and keeping $a/h = 0.7, b/h = 2.0, l/h = 0.5$ and $c/h = 1.3$ fixed. From this figure it is seen that J exhibits oscillatory behaviour and J increases as Kh increases. Initially for small wave number $Kh < 1.2$, the energy dissipation increases with increasing porosity, then for $1.2 < Kh < 2$ energy dissipation decreases with increasing

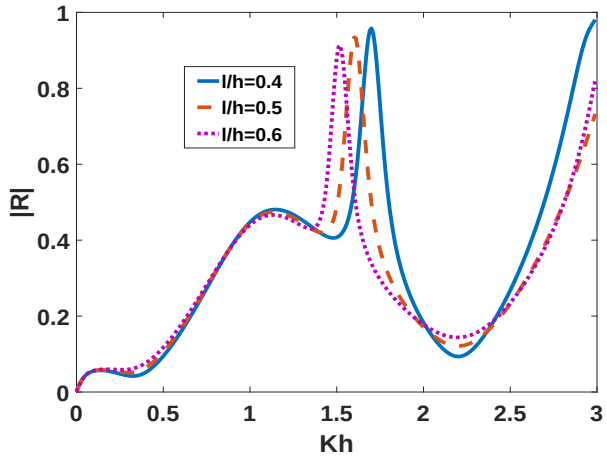

Figure 4.10: Reflection coefficient for different $\frac{l}{h}$ with $\frac{a}{h} = 0.7, \frac{b}{h} = 1.4, \frac{c}{h} = 1.3, G = 0.5$.

porosity. But for large wave number $Kh > 2$, energy dissipation again increases with increasing porosity parameter of the barrier. This may be due to the interaction of waves with the barrier and the trench.

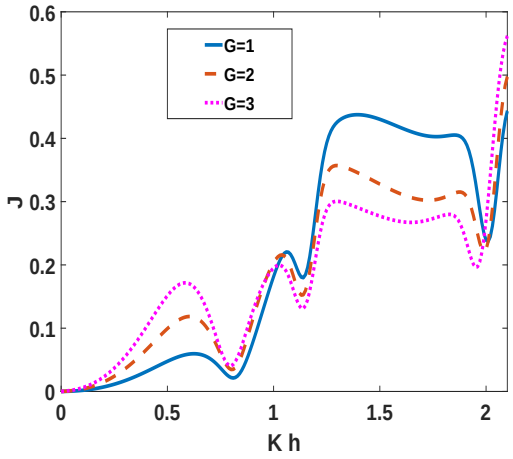

Figure 4.11: Energy dissipation for different G with $\frac{a}{h} = 0.7, \frac{b}{h} = 2.0, \frac{c}{h} = 1.3, \frac{l}{h} = 0.5$.

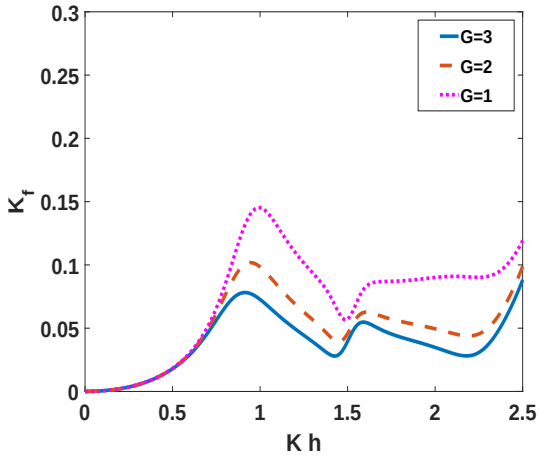

Figure 4.12: Hydrodynamic wave force for different G with $\frac{a}{h} = 0.7, \frac{b}{h} = 1.5, \frac{c}{h} = 1.3, \frac{l}{h} = 0.5$.

In Figure (4.12), non-dimensional horizontal wave force K_f is plotted against the non-dimensional wave number Kh for different values of the porosity parameter $G(= 1, 2, 3)$ and keeping $a/h = 0.7, b/h = 1.5, l/h = 0.5$ and $c/h = 1.3$ fixed. It is observed that the horizontal wave force increases with decreasing porosity G showing that with

the decrease in G, less amount of water can pass through the pores of the barrier and so the horizontal wave force increases.

Partially immersed porous barrier at middle of the trench

The porous barrier is along the y-axis, i.e., along the centre of the trench, when $l/h = 0$. The Figures (4.13-4.18) depicts the behaviour of $|R|,\ J, K_f$ for various values of the parameters $a/h,\ b/h,\ c/h,\ G$.

Figure (4.13) exhibits the effect of width of the trench on the reflection coefficients for three different widths of the trench ($b/h = 0.5, 1.5, 2.5$) and fixed values of $a/h = 0.6, c/h = 1.5$ and $G = 0.5 + i$. In this figure we see that $|R|$ exhibits oscillatory behaviour and the frequency of oscillation increases as the width of the trench b/h increases. Also there occurs resonance in $|R|$ for a particular value of Kh and multiple resonance occurs as the width of the trench increases when the barrier is along the central vertical line of the trench.

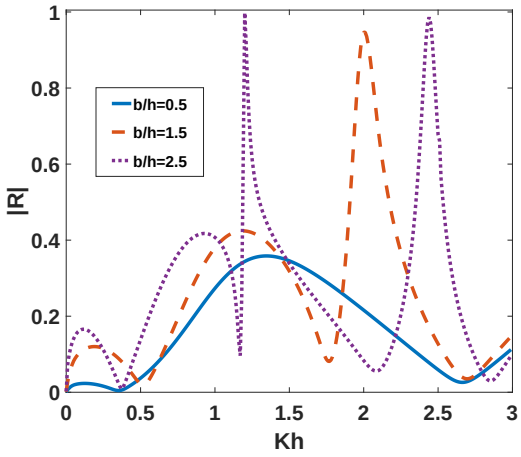

Figure 4.13: Reflection coefficient for different $\frac{b}{h}$ with $\frac{a}{h} = 0.6, \frac{c}{h} = 1.5, G = 0.5 + i$.

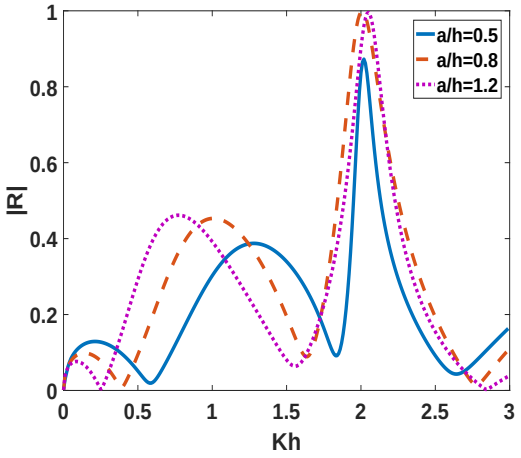

Figure 4.14: Reflection coefficient for different $\frac{a}{h}$ with $\frac{b}{h} = 1.5, \frac{c}{h} = 1.5, G = 0.5 + i$.

The effect of the length of the partially immersed porous barrier a/h on the reflection coefficient $|R|$ is studied in Figure (4.14). Here $|R|$ is plotted against the non-dimensional wave number Kh for various values of the length of the barrier

($a/h = 0.5, 0.8, 1.2$) and fixed values of $b/h = 1.5, c/h = 1.5$ and $G = 0.5 + i$. Figure (4.14) shows oscillatory behaviour in $|R|$ exhibits and the amplitude of oscillation increases with increasing length of the porous barrier.

In Figure (4.15), $|R|$ is depicted against the non-dimensional wave number Kh, keeping $a/h = 0.6, b/h = 1.5$ and $G = 0.5 + i$ fixed and taking $c/h = 1.1, 1.3, 1.5$ to visualize the effect of the trench depth on the reflection coefficient. Here also $|R|$ exhibits oscillatory behaviour and for $Kh \simeq 2.3$, a resonating behaviour in $|R|$ is observed.

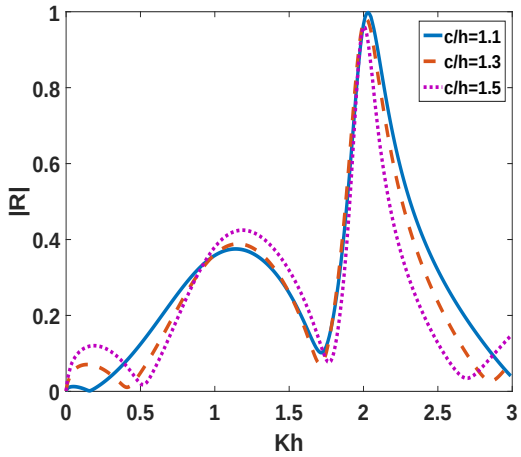

Figure 4.15: Reflection coefficient for different $\frac{c}{h}$ with $\frac{a}{h} = 0.6, \frac{b}{h} = 1.5, G = 0.5 + i$.

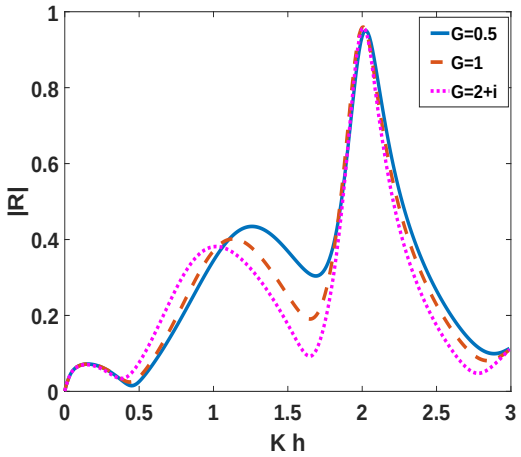

Figure 4.16: Reflection coefficient for different G with $\frac{a}{h} = 0.6, \frac{b}{h} = 1.5, \frac{c}{h} = 1.3$.

In Figure (4.16), reflection coefficient $|R|$ is plotted against the non-dimensional wave number Kh for different values of the porosity parameter $G(= 0.5, 1, 2 + i)$ and keeping $a/h = 0.6, b/h = 1.5$ and $c/h = 1.3$ fixed. It is seen that multiple peaks occur in the reflection coefficient. This phenomena occurs due to the interaction of wave with the porous barrier. It is seen that with as G increases from 0.5 to 1, the reflection coefficient decreases. Also it is seen that $|R|$ is least when $G = 2 + i$. This is due to the fact that presence of inertial force coefficient G_i in G allows the passage of water through the pores which diminishes reflection.

In Figure (4.17), coefficient of energy dissipation J is plotted against the non-dimensional wave number Kh for different values of the porosity parameter $G(= 1, 2, 3)$

and keeping $a/h = 0.5, b/h = 1.5$ and $c/h = 1.5$ fixed. From the figure it is visible that, for small wave numbers ($Kh < 1$), energy dissipation increases as porosity parameter increases while for $Kh > 1$ energy dissipation decreases with increasing porosity parameter G. The occurrence of this phenomena is due to the fact that as Kh increases, the wavelength of the waves decreases. These correspond to the short waves which are near the free surface interact with the porous barrier. Here G is real ($G = G_r$) which means that the inertial force coefficient G_i is much less than the resistance force coefficient G_r of the porous barrier and so as $G = G_r$ increases, the resistance force coefficient of the porous barrier resists the passage of water through the pores and reflects back the short waves thereby reducing the energy dissipation.

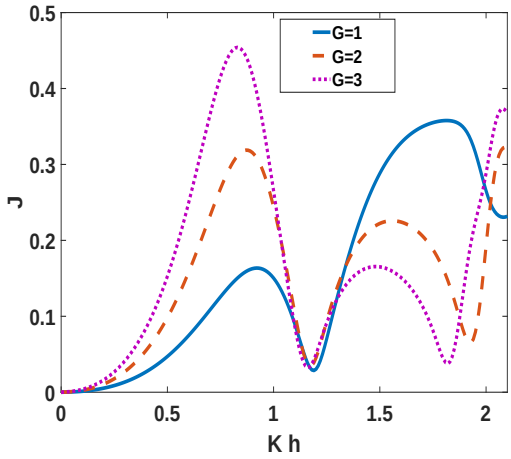

Figure 4.17: Energy dissipation for different G with $\frac{a}{h} = 0.5, \frac{b}{h} = 1.5, \frac{c}{h} = 1.5$.

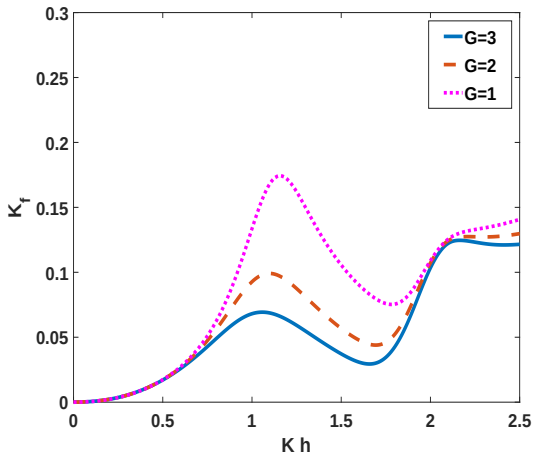

Figure 4.18: Hydrodynamic wave force for different G with $\frac{a}{h} = 0.7, \frac{b}{h} = 1.5, \frac{c}{h} = 1.3$.

In Figure (4.18), non-dimensional horizontal wave force K_f is plotted against the non-dimensional wave number Kh for different values of the porosity parameter $G(= 1, 2, 3)$ and keeping $a/h = 0.7, b/h = 1.5$ and $c/h = 1.3$ fixed. The coefficient of wave force increases with decreasing porosity parameters.

From all these oscillatory behavior of the curves, one can find the values of wave number in which maximum reflection and transmission occurs. Also full reflection of waves occurs for some wave numbers. This behavior may be due to the interaction of waves with the depression of the bottom and the porous barrier. These outcomes are very useful for marine engineers to construct breakwaters to protect sea shore areas.

4.5 CONCLUSIONS

The problem of water waves scattering by thin porous plate over a rectangular trench is discussed here considering linearized theory of water waves. The physical problem is mathematically modeled in terms of a boundary value problem for two different positions of the porous plate. Havelock's expansion of potential function together with its inversion formulae have been employed to the problem which then modified into a system of linear integral equations in terms of horizontal component of velocity function above the trench and below the edge of the vertical barrier. There are two types of integrable singularities that occurred in the unknown function satisfying the integral equations. One is square root singularity at the sharp edge of the thin barrier and the other type is 1/3 rd singularity at the edges of the rectangular trench. To solve the integral equations where the unknown functions satisfy two types of singularities a multi term Galerkin approximation technique with appropriate basis functions is considered. For 1/3 rd singularity, the unknown function is approximated by Gegenbauer polynomial of order 1/6 and for square root singularity, Chebyshev polynomials are utilized to approximate the unknown function. Also we consider simple polynomials as basis function in mathematical computations and compare the rate of convergence of the method taking two types of basis functions in Table (4.3). It is observed that use of special function as basis function produces better rate of convergence of the method than simple polynomial as basis function. The numerical appraise of reflection and transmission coefficients, energy dissipation and horizontal wave force are determined for different parameter values. These results are illustrated in a number of figures. The known results are recovered as depicted in some figures. For both positions of the barrier, effect of porosity decreases the reflection coefficient but increasing length of the barrier reflect more energy and less transmition. Larger width of the trench transmits more energy. Hence form present study, it is clear that scattering nature of surface waves in presence of bottom obstacle in form a rectangular trench is really influenced by thin porous barrier. These changes of surface waves play a crucial role in marine structures in coastal regions.

CHAPTER 5

SCATTERING OF WATER WAVES BY RECTANGULAR THICK BARRIERS IN PRESENCE OF SURFACE TENSION

5.1 INTRODUCTION

The phenomena of water wave scattering by thin vertical barriers submerged in water of finite depth under the assumption of linearized theory are well studied in the literature. Many researchers (cf. Packman and Williams (1972), Losada *et al.* (1992), Porter and Evans (1995), Mandal and Dolai (1994), Kanoria and Mandal (2000), Banerjea *et al.* (1996), Das *et al.* (1997), Das, De and Mandal (2020)) used various mathematical techniques to study the problem of scattering of a normally incident wave train on a thin vertical barrier. However, when the obstacle is in the form of a thick vertical barrier with a rectangular cross-section present in the water of uniform finite depth, the corresponding water wave scattering problems for normally incident wave train

[0]† The content of this chapter is based on the paper " Scattering of water waves by rectangular thick barriers in presence of surface tension", *Journal of University of Shanghai for Science and Technology*, 23(11) (2021), 30-55.

have been investigated by Mei and Black (1969), Kanoria *et al.* (1999). Mei and Black (1969) considered surface piercing and bottom standing thick vertical barriers and used variational method to evaluate the reflection and the transmission coefficients. Later Kanoria *et al.* (1999) and Mandal and Kanoria (1998) considered the problems of scattering of a normally and also a obliquely incident wave train by a thick barrier where they considered four types of barriers configurations such as surface-piercing or bottom standing thick barrier or a submerged block, or a thick wall with a gap. They used the multi-term Galerkin approximation method involving ultraspherical Gegenbauer polynomials for solving first kind integral equations arising in the mathematical analysis to obtain very accurate numerical estimates for the reflection coefficient.

In the above mentioned studies, the effect of surface tension was not considered. The effect of cohesive forces in between water molecule in the free surface of water, i.e., the effect of surface tension on the water wave scattering problems needs special attention. Many researchers such as Evans (1968a, 1968b), Rhodes-Robinson (1970, 1971, 1982), Chakrabarti and Sahoo (1998) included the effect of surface tension in water to study wave scattering problems. However, the scattering problem by a thick rectangular barrier in presence of surface tension has not been investigated yet. The amplitude and the frequency of the wave depend on both the surface tension and gravity. For this reason, it may not be possible to neglect the effect of surface tension while doing experimental study. As mentioned by Hocking and Mahdmina (1991), another important reason for including surface tension is that in the absence of surface tension the transient motion initiated by an impulsive pressure is singular, but when the effect of surface tension is taken into account this singularity is removed.

In the present study, we analyzed the effect of surface tension on oblique wave scattering problem involving thick rectangular barrier. Three types of configurations of the barrier, viz, submerged bottom standing, submerged block and fully submerged block with a gap are considered here. Due to geometrical symmetry about its central line, the scattering problems for all the cases are split into two separate boundary value problems in terms of symmetric and antisymmetric potential functions. Analytically the boundary value problems involving potential functions are reduced in to first kind integral equations using inverse Havelock inversion formula. The integral equations are

solved analytically by using multi term Galerkin approximation technique using the ultra spherical Gegenbauer polynomial as a basis function, as was done by Chakraborty and Mandal (2014, 2015), Newman (1965), Sasmal and De (2021), Paul and De (2021). The analytical results for reflection coefficients is depicted graphically against the non dimensional wave number. In absence of surface tension and for normally incident wave train, the known results in the work of Kanoria *et al.*'s (1999) are recovered. For large width of the barriers, the reflection coefficient exhibits oscillatory behaviour becoming zero for certain values of the wave number which matches with the observation of Kanoria *et al.* (1999) for thick vertical barriers and Newman (1965) for long bottom obstacles. The present study shows that the surface tension has some effect on the reflection coefficient.

5.2 FORMULATION OF THE PROBLEM

We consider two dimensional time harmonic, irrotational motion in an incompressible inviscid fluid (water) with surface tension τ, density ρ, due to interaction of an obliquely incident wave train of angular frequency σ with a thick rectangular barrier of uniform width $2b$ submerged in water of finite depth h.

A rectangular cartesian coordinate system is chosen, where y-axis is taken vertically downwards and the (x, z) plane corresponds to the undisturbed free surface. Here we study three different types of configurations of the barrier as shown in Figure (5.1) and are described below.

I) Type-I: $-b \leq x \leq b,\ y \in L = L_1(= (c, h))$,

II) Type-II: $-b \leq x \leq b,\ y \in L = L_2(= (a, c))$, with $0 \leq a \leq c \leq h$,

III) Type-III: $-b \leq x \leq b,\ y \in L = L_3(= (a, c) + (d, h))$, with $0 \leq a \leq c \leq d \leq h$.

A time harmonic progressive wave from negative infinity, denoted by $\Re\{\phi^{inc}(x, y)\, e^{i(\nu z - \sigma t)}\}$ is incident obliquely on the rectangular barrier at an angle θ with the undisturbed free surface and it is partially reflected by the barrier and partially transmitted. If the resulting motion is described by the velocity potential $\Re\{\phi(x, y)e^{i(\nu z - \sigma t)}\}$, then $\phi(x, y)$

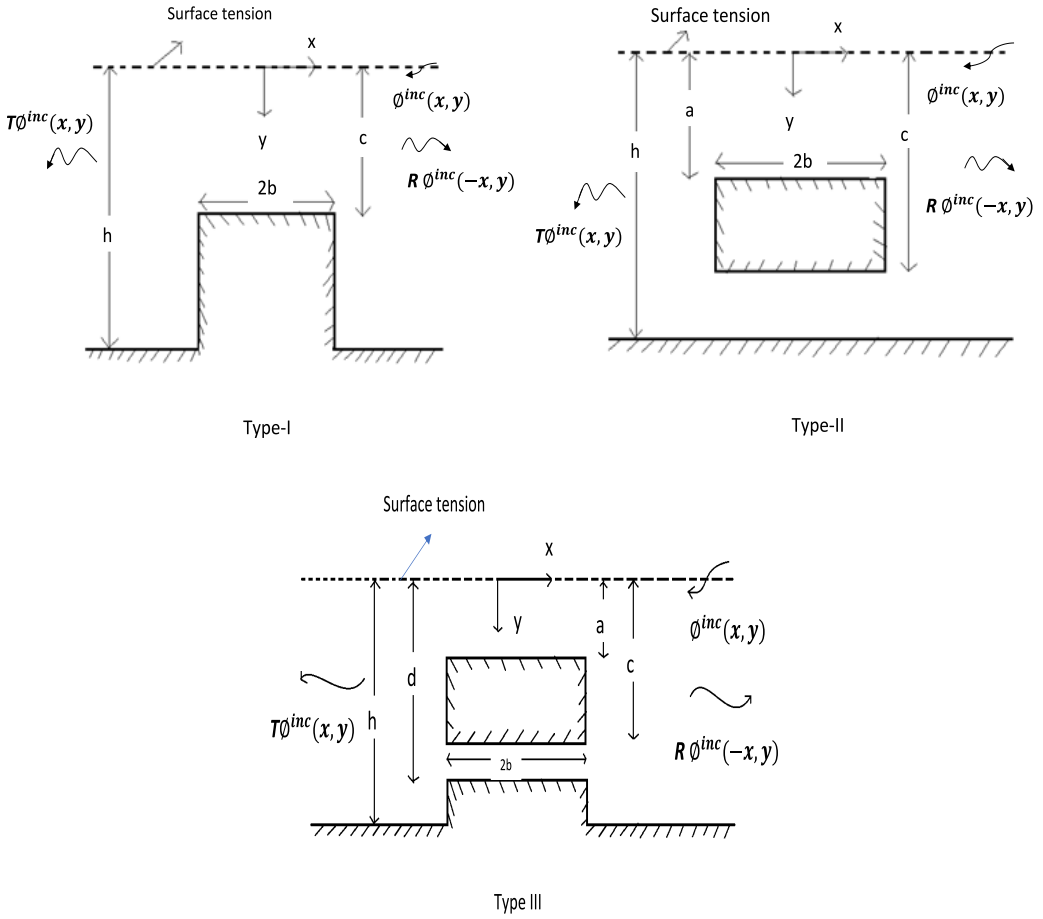

Figure 5.1: Diagram of thick barriers

satisfies the following boundary value problem.

$$(\nabla^2 - \nu^2)\phi = 0 \quad \text{in the fluid region,} \tag{5.1}$$

$$K\phi + \frac{\partial \phi}{\partial y} + M\frac{\partial^3 \phi}{\partial y^3} = 0 \quad \text{on} \;\; y = 0, \quad |x| < \infty, \;\; M = \frac{\tau}{\rho g}, \tag{5.2}$$

τ is the coefficient of surface tension at the free surface of water,

$$\phi_x = 0 \;\; \text{on} \quad x = \pm b, \;\; y \in L_j, \;\; j = 1, 2, 3, \tag{5.3}$$

$$r^{\frac{1}{3}}\nabla\phi \;\; \text{is bounded as} \quad r \to 0, \tag{5.4}$$

r is the distance of any point in the fluid region from a submerged edge of the thick barrier,

$$\phi_y = 0 \quad \text{on} \quad y = L_j, \quad |x| < b, \qquad \text{for j-th type of barrier, } j = 1, 2, 3, \tag{5.5}$$

$$\phi_y = 0 \quad \text{on} \quad y = h, \quad \begin{cases} |x| > b \ \text{ for type I and III barrier,} \\ |x| < \infty \ \text{ for type II barrier,} \end{cases} \tag{5.6}$$

and finally

$$\phi(x, y) \sim \begin{cases} \phi^{inc}(x, y) + R\phi^{inc}(-x, y) \ \text{ as } \ x \to \infty, \\ T\phi^{inc}(x, y) \qquad \text{as } \ x \to -\infty \end{cases} \tag{5.7}$$

where R and T is the unknown reflection and transmission coefficients respectively and is to be determined for each barrier configuration of the barrier. Here

$$\phi^{inc}(x, y) = \frac{2\cosh\gamma_0(h - y)e^{-i\mu(x-b)}}{\cosh\gamma_0 h}, \tag{5.8}$$

$\mu = \gamma_0 \cos\theta, \ \nu = \gamma_0 \sin\theta, \quad 0 < \theta < \pi/2,$
and $\gamma = \gamma_0$ satisfy the transcendental equation

$$\gamma(1 + M\gamma^2)\tanh\gamma h = K, \ K = \frac{\sigma^2}{g}, \tag{5.9}$$

g being the acceleration due to gravity. It may be noted here that the transcendental equation (5.9) has two real roots $\pm\gamma_0$ and infinitely many purely imaginary roots $\pm i\gamma_n, n = 1, 2, ...(\gamma_n > 0)$ (cf. Rhodes Robinson (1971)).

5.3 METHOD OF SOLUTION

The configuration of rectangular barrier is such that it is symmetric about $x = 0$, and so we express $\phi(x, y)$ as a combination of symmetric and antisymmetric components. Let $\phi^{SMM}(x, y)$ and $\phi^{ANSMM}(x, y)$ denote symmetric and antisymmetric components

respectively, so that

$$\phi(x,y) = \phi^{SMM}(x,y) + \phi^{ANSMM}(x,y) \tag{5.10}$$

where

$$\phi^{SMM}(-x,y) = \phi^{SMM}(x,y), \quad \phi^{ANSMM}(-x,y) = -\phi^{ANSMM}(x,y). \tag{5.11}$$

Therefore, we consider only the region $x \geq 0$. Now $\phi^{SMM,ANSMM}(x,y)$ satisfy (5.1) to (5.6) together with

$$\phi_x^{SMM}(0,y) = 0 \quad \text{and} \quad \phi^{ANSMM}(0,y) = 0, \quad 0 < y < h. \tag{5.12}$$

Let the behavior of $\phi^{SMM,ANSMM}(x,y)$ for large x be represented by

$$\phi^{SMM,ANSMM}(x,y) \sim \frac{\cosh\gamma_0(h-y)}{\cosh\gamma_0 h}\{e^{-i\mu(x-b)} + R^{SMM,ANSMM}e^{i\mu(x-b)}\} \quad \text{as} \quad x \to \infty \tag{5.13}$$

where R^{SMM} and R^{ANSMM} are unknown constants which are related to R by

$$R = \frac{1}{2}(R^{SMM} + R^{ANSMM})e^{-2i\mu b}. \tag{5.14}$$

Similarly T is given by

$$T = \frac{1}{2}(R^{SMM} - R^{ANSMM})e^{-2i\mu b}.$$

We divide the region $x > 0$ into two regions viz, Region I: $(x > b,\ 0 < y < h)$ and Region II: $(0 < x < b,\ \ y \in (0,h) - L_j,\ \ j = 1,2,3)$. Now the eigen function expansions of $\phi^{SMM,ANSMM}(x,y)$ satisfying (5.1) to (5.6) and (5.12) for $x > 0$ in the two regions for each barrier configuration are below.

Region I $(x > b,\ 0 < y < h)$**:**

$$\phi^{SMM,ANSMM}(x,y) = \frac{\cosh\gamma_0(h-y)}{\cosh\gamma_0 h}\{e^{-i\mu(x-b)} + R^{SMM,ANSMM}e^{i\mu(x-b)}\}$$

$$+\sum_{n=1}^{\infty}\mathcal{A}_n^{SMM,ANSMM}\frac{\cos\gamma_n(h-y)}{\cos\gamma_n h}e^{-s_n(x-b)} \tag{5.15}$$

where $\gamma_0,\ \pm i\gamma_n$ satisfy the equation (5.9) and $s_n = (\gamma_n^2+\nu^2)^{\frac{1}{2}}$. The unknowns $\mathcal{A}_n^{SMM,ANSMM}$ and $R^{SMM,ANSMM}$ are to be determined.

Region II $(0 < x < b,\quad y \in (0,h) - L_j,\quad j = 1,2,3)$**:**

Barrier of Type I: $-b \le x \le b,\ y \in L = L_1(= (c,h))$

For barrier of this type, the Region II is given by $0 < x < b,\ y \in (0,c)$. In this region a suitable representation of $\phi^{SMM}(x,y)$ and $\phi^{ANSMM}(x,y)$ are given by

$$\begin{pmatrix}\phi^{SMM}(x,y)\\ \phi^{ANSMM}(x,y)\end{pmatrix} = \frac{\cosh\alpha_0(c-y)}{\cosh\alpha_0 c}\begin{pmatrix}\mathcal{B}_0^{SMM}\cos(\alpha_0^2-\nu^2)^{\frac{1}{2}}x\\ \mathcal{B}_0^{ANSMM}\sin(\alpha_0^2-\nu^2)^{\frac{1}{2}}x\end{pmatrix}$$

$$+\sum_{n=1}^{\infty}\begin{pmatrix}\mathcal{B}_n^{SMM}\cosh t_n x\\ \mathcal{B}_n^{ANSMM}\sinh t_n x\end{pmatrix}\frac{\cos\alpha_n(c-y)}{\cos\alpha_n c} \tag{5.16}$$

where $\pm\alpha_0, \pm i\alpha_n (n = 1,2,...)$ satisfy the equation

$$\alpha(1+M\alpha^2)\tanh\alpha c = K, \tag{5.17}$$

$$t_n = (\alpha_n^2+\nu^2)^{\frac{1}{2}}, (n = 1,2,..) \tag{5.18}$$

and $\mathcal{B}_n^{SMM,ANSMM},\ n = 0,1,2,....$ are unknowns to be determined.

Barrier of Type II:$-b \le x \le b,\ y \in L = L_2(= (a,c))$

For barrier of this type of configuration, the Region II is given by $0 < x < b, \;\; y \in (0, a) + (c, h)$. In this region a suitable representation of $\phi^{SMM,ANSMM}(x, y)$ are given by

$$\begin{pmatrix} \phi^{SMM}(x,y) \\ \phi^{ANSMM}(x,y) \end{pmatrix} = \frac{\cosh\beta_0(a-y)}{\cosh\beta_0 a} \begin{pmatrix} \mathcal{D}_0^{SMM}\cos(\beta_0^2-\nu^2)^{\frac{1}{2}}x \\ \mathcal{D}_0^{ANSMM}\sin(\beta_0^2-\nu^2)^{\frac{1}{2}}x \end{pmatrix}$$
$$+\sum_{n=1}^{\infty} \begin{pmatrix} \mathcal{D}_n^{SMM}\cosh u_n x \\ \mathcal{D}_n^{ANSMM}\sinh u_n x \end{pmatrix} \frac{\cos\beta_n(a-y)}{\cos\beta_n a}, \;\; 0 < y < a, \tag{5.19}$$

and

$$\begin{pmatrix} \phi^{SMM}(x,y) \\ \phi^{ANSMM}(x,y) \end{pmatrix} = \begin{pmatrix} E_0^{SMM}\cosh\nu x \\ E_0^{ANSMM}\sinh\nu x \end{pmatrix} + \sum_{n=1}^{\infty} \begin{pmatrix} E_n^{SMM}\cosh\eta_n x \\ E_n^{ANSMM}\sinh\eta_n x \end{pmatrix} \cos\frac{n\pi(h-y)}{h-c}, \tag{5.20}$$

where

$$\eta_n = \sqrt{\left(\frac{n\pi}{h-c}\right)^2 + \nu^2}.$$

Here $\pm\beta_0, \;\; \pm i\beta_n (n = 1, 2, ...)$ satisfy the equation

$$\beta(1 + M\beta^2)\tanh\beta a = K, \tag{5.21}$$

$$u_n = (\beta_n^2 + \nu^2)^{\frac{1}{2}}, (n = 1, 2, ..), \tag{5.22}$$

and $\mathcal{D}_n^{SMM,ANSMM}, \;\; {E_n}^{SMM,ANSMM}, \;\; n = 0, 1, 2, ...$ are unknowns to be determined.

Barrier of Type III: $-b \le x \le b, \;\; y \in L = L_3(= (a, c) + (d, h))$

For barrier of this type of configuration, the Region II is given by $0 < x < b, \;\; y \in (0, a) + (c, d)$. In this region a suitable representation of $\phi^{SMM,ANSMM}(x, y)$ are given below.

For $0 < y < a$ the expressions of $\phi^{SMM,ANSMM}(x,y)$ are given by

$$\begin{pmatrix} \phi^{SMM}(x,y) \\ \phi^{ANSMM}(x,y) \end{pmatrix} = \frac{\cosh\beta_0(a-y)}{\cosh\beta_0 a} \begin{pmatrix} \chi_0^{SMM}\cos(\beta_0^2-\nu^2)^{\frac{1}{2}}x \\ \chi_0^{ANSMM}\sin(\beta_0^2-\nu^2)^{\frac{1}{2}}x \end{pmatrix}$$

$$+\sum_{n=1}^{\infty}\begin{pmatrix} \chi_n^{SMM}\cosh u_n x \\ \chi_n^{ANSMM}\sinh u_n x \end{pmatrix}\frac{\cos\beta_n(a-y)}{\cos\beta_n a}, \quad 0<y<a, \tag{5.23}$$

where $\pm\beta_0, \ \pm i\beta_n (n=1,2,...)$ are the roots of the equation (5.21), u_n are given by (5.22) and ${\chi_n}^{SMM,ANSMM}(x,y), \ n=0,1,2,...$ are unknowns to be determined.

For $c < y < d$ the expressions of $\phi^{SMM,ANSMM}(x,y)$ are given by

$$\begin{pmatrix} \phi^{SMM}(x,y) \\ \phi^{ANSMM}(x,y) \end{pmatrix} = \begin{pmatrix} U_0^{SMM}\cosh\nu x \\ U_0^{ANSMM}\sinh\nu x \end{pmatrix} + \sum_{n=1}^{\infty}\begin{pmatrix} U_n^{SMM}\cosh\zeta_n x \\ U_n^{ANSMM}\sinh\zeta_n x \end{pmatrix}\cos\frac{n\pi(d-y)}{d-c}, \tag{5.24}$$

where

$$\zeta_n = \sqrt{\left(\frac{n\pi}{d-c}\right)^2+\nu^2} \tag{5.25}$$

and ${\chi_n}^{SMM,ANSMM}, \ {U_n}^{SMM,ANSMM}, \ n=0,1,2,....$ are unknowns to be determined.

Evaluation of various unknowns in the expressions for $\phi^{SMM,ANSMM}$ in Regions I and II

In this section we shall evaluate various unknowns in the expression for $\phi^{SMM,ANSMM}$ defined by equations (5.15), (5.16), (5.19), (5.20), (5.23) and (5.24) in Regions I and II.

A. Region I

Now let us define

$$\phi_x^{SMM,ANSMM}(b+0,y)=\phi_x^{SMM,ANSMM}(b-0,y)=f^{SMM,ANSMM}(y),\ 0<y<h, \tag{5.26}$$

then in view of condition (5.3)

$$f^{SMM,ANSMM}(y)=0,\quad for\ y\in L_j, \tag{5.27}$$

and $f^{SMM,ANSMM}(y)$ is unknown for $y\in(0,h)-L_j,\ j=1,2,3$ which is to be determined.

Due to the edge condition described in equation (5.4), we must have the requirement that

$$f^{SMM,ANSMM}(y)=O(|y-l_j|^{-\frac{1}{3}})\quad \text{as}\ \ y\to l_j, j=1,2,3. \tag{5.28}$$

Using $\phi^{SMM,ANSMM}(y)$ from equation (5.15) in (5.26) and applying modified inversion formula Manam *et al.* (2006) we obtain

$$1-R^{SMM,ANSMM}=iV(\gamma_0,h)\left[\int_a^h f^{SMM,ANSMM}(y)\frac{\cosh\gamma_0(h-y)}{\cosh\gamma_0 h}dy -\frac{M}{K}\gamma_0\tanh(\gamma_0 h)f_y^{SMM,ANSMM}(0)\right] \tag{5.29}$$

and

$$\mathcal{A}_n^{SMM,ANSMM}=iV(i\gamma_n,h)\left[\int_a^h f^{SMM,ANSMM}(y)\frac{\cos\gamma_n(h-y)}{\cos\gamma_n h}dy +\frac{M}{K}\gamma_n\tan(\gamma_n h)f_y^{SMM,ANSMM}(0)\right] \tag{5.30}$$

where

$$V(u,h)=\frac{4u(1+Mu^2)\cosh^2(uh)}{\sqrt{u^2-\nu^2}\,[2uh(1+Mu^2)+(1+3Mu^2)\sinh(2uh)]}. \tag{5.31}$$

Thus the unknowns $\mathcal{A}_n^{SMM,ANSMM},\ R^{SMM,ANSMM}$ are obtained from relations (5.29) and (5.30) for each type of configurations of the barrier in Region I.

B. Region II

Here we shall evaluate various unknowns in the the expressions for $\phi^{SMM,ANSMM}$ in Region II for each type of configurations of the barrier.

Barrier of Type I

Substituting the equation (5.16) in condition (5.3) and using modified inversion formula Manam *et al.* (2006), we obtain the constants $\mathcal{B}_n^{SMM,ANSMM},\ n = 0, 1, 2...$ as

$$\mathcal{B}_0^{SMM,ANSMM} = V(\alpha_0, c)(\frac{1}{-\sin(\alpha_0^2 - \nu^2)^{\frac{1}{2}}b}, \frac{1}{\cos(\alpha_0^2 - \nu^2)^{\frac{1}{2}}b})$$
$$\left[\int_0^c f^{SMM,ANSMM}(y)\frac{\cosh\alpha_0(c-y)}{\cosh\alpha_0 c}dy - \frac{M}{K}\alpha_0\tanh(\alpha_0 c)f_y^{SMM,ANSMM}(0)\right], \quad (5.32)$$

$$\mathcal{B}_n^{SMM,ANSMM} = -iV(i\alpha_n, c)(\frac{1}{\sinh t_n b}, \frac{1}{\cosh t_n b})$$
$$\left[\int_0^c f^{SMM,ANSMM}(y)\frac{\cos\alpha_n(c-y)}{\cos\alpha_n c}dy + \frac{M}{K}\alpha_n\tan(\alpha_n c)f_y^{SMM,ANSMM}(0)\right]. \quad (5.33)$$

Barrier of Type II

Here we evaluate the unknowns $\mathcal{D}_n^{SMM,ANSMM}$ and $E_n^{SMM,ANSMM},\ n = 0, 1, 2, ..$ by substituting $\phi^{SMM,ANSMM}$ from equations (5.19) and (5.20) in to the condition (5.3) and using the modified inversion formula suitably Manam *et al.* (2006). These are given as

$$\mathcal{D}_0^{SMM,ANSMM} = V(\beta_0, a)(\frac{1}{-\sin(\beta_0^2 - \nu^2)^{\frac{1}{2}}b}, \frac{1}{\cos(\beta_0^2 - \nu^2)^{\frac{1}{2}}b})$$
$$\left[\int_0^a f^{SMM,ANSMM}(y)\frac{\cosh\beta_0(a-y)}{\cosh\beta_0 a}dy - \frac{M}{K}\beta_0\tanh(\beta_0 a)f_y^{SMM,ANSMM}(0)\right], \quad (5.34)$$

$$\mathcal{D}_n^{SMM,ANSMM} = -iV(i\beta_n, a)(\frac{1}{\sinh u_n b}, \frac{1}{\cosh u_n b})$$
$$\left[\int_0^a f^{SMM,ANSMM}(y)\frac{\cos\beta_n(a-y)}{\cos\beta_n a}dy + \frac{M}{K}\beta_n \tan(\beta_n a) f_y^{SMM,ANSMM}(0)\right], \quad (5.35)$$

$$E_0^{SMM,ANSMM} = \frac{1}{\nu(h-c)}(\frac{1}{\sinh\nu b}, \frac{1}{\cosh\nu b})\int_c^h f^{SMM,ANSMM}(y)dy, \quad (5.36)$$

$$E_n^{SMM,ANSMM} = \frac{2}{\eta_n(h-c)}(\frac{1}{\sinh\eta_n b}, \frac{1}{\cosh\eta_n b})\int_c^h f^{SMM,ANSMM}(y)\cos\frac{n\pi(h-y)}{h-c}dy. \quad (5.37)$$

Barrier of Type III

Here the unknowns $\chi_n^{SMM,ANSMM}$ and $U_n^{SMM,ANSMM}$, $n = 0, 1, 2, ..$ are obtained by substituting $\phi^{SMM,ANSMM}$ from equations (5.24) and (5.25) in to the condition (5.3) and using the modified inversion formula suitably Manam *et al.* (2006). These are given as

$$\chi_0^{SMM,ANSMM} = V(\beta_0, a)(\frac{1}{-\sin(\beta_0^2-\nu^2)^{\frac{1}{2}}b}, \frac{1}{\cos(\beta_0^2-\nu^2)^{\frac{1}{2}}b})$$
$$\left[\int_0^a f^{SMM,ANSMM}(y)\frac{\cosh\beta_0(a-y)}{\cosh\beta_0 a} - \frac{M}{K}\beta_0 \tanh(\beta_0 a) f_y^{SMM,ANSMM}(0)\right], \quad (5.38)$$

$$\chi_n^{SMM,ANSMM} = -iV(i\beta_n, a)(\frac{1}{\sinh u_n b}, \frac{1}{\cosh t_n b})$$
$$\left[\int_0^a f^{SMM,ANSMM}(y)\frac{\cos\beta_n(a-y)}{\cos\beta_n a}dy + \frac{M}{K}\beta_n \tan(\beta_n a) f_y^{SMM,ANSMM}(0)\right], \quad (5.39)$$

and

$$U_0^{SMM,ANSMM} = \frac{1}{\nu(d-c)}(\frac{1}{\sinh\nu b}, \frac{1}{\cosh\nu b})\int_c^d f^{SMM,ANSMM}(y)dy, \tag{5.40}$$

$$U_n^{SMM,ANSMM} = \frac{2}{\zeta_n(d-c)}(\frac{1}{\sinh\zeta_n b}, \frac{1}{\cosh\zeta_n b})\int_c^d f^{SMM,ANSMM}(y)\cos\frac{n\pi(d-y)}{d-c}dy. \tag{5.41}$$

Thus various unknowns in the expressions of $\phi^{SMM,ANSMM}$ are obtained in terms of the unknown functions $f^{SMM,ANSMM}$ for each type of configuration of the barrier in different regions. These unknown functions $f^{SMM,ANSMM}$ for each type of configuration of the barrier can be determined by solving an integral equation for $f^{SMM,ANSMM}$.

Formation of integral equation:

The integral equations for $f^{SMM,ANSMM}s$ can be derived by using the following matching conditions for $\phi^{SMM,ANSMM}(x,y)$ at $x = b \pm 0,\ \ y \in (0,h) - L_j,\ j = 1,2,3.$

$$\phi^{SMM,ANSMM}(b+0,y) = \phi^{SMM,ANSMM}(b-0,y). \tag{5.42}$$

Using the expressions for $\phi^{SMM,ANSMM}(x,y)$, the following integral equations are obtained for $y \in (0,h) - L_j, j = 1,2,3.$

$$\int_{(0,h)-L_j} F^{SMM,ANSMM}(u)N^{SMM,ANSMM}(y,u)du = \frac{\cosh\gamma_0(h-y)}{\cosh\gamma_0 h}, \quad \text{for } y \in (0,h) - L_j,\ j = 1,2,3, \tag{5.43}$$

$$\text{where}\ \ F^{SMM,ANSMM}(y) = \frac{f^{SMM,ANSMM}(y)}{(1+R^{SMM,ANSMM})}, \tag{5.44}$$

and the kernel $N^{SMM,ANSMM}(y,u)(y,u \in (0,h) - L_j)$ $(j = 1,2,3)$ are given below for each type of barrier configuration.

Barrier of Type I

For configuration of barrier of Type I,

$$N^{SMM}(y,u) = V(\alpha_0,c)(-\cot(\alpha_0^2-\nu^2)^{\frac{1}{2}}b)\left[\frac{\cosh\alpha_0(c-y)\cosh\alpha_0(c-u)}{\cosh^2\alpha_0 c} - \frac{M}{K}\alpha_0\tanh(\alpha_0 c)F_y^{SMM}(0)\frac{\cosh\alpha_0(c-y)}{\cosh\alpha_0 c}\right] - \sum_{n=1}^{\infty} iV(i\alpha_n,c)\coth(t_n b)\left[\frac{\cos\alpha_n(c-y)\cos\alpha_n(c-u)}{\cos^2\alpha_n c} + \frac{M}{K}\alpha_n\tan(\alpha_n c)F_y^{SMM}(0)\frac{\cos\alpha_n(c-y)}{\cos\alpha_n c}\right] - \sum_{n=1}^{\infty} iV(i\gamma_n,h)\left[\frac{\cos\gamma_n(h-y)\cos\gamma_n(h-u)}{\cos^2\gamma_n h} + \frac{M}{K}\gamma_n\tan(\gamma_n h)F_y^{SMM}(0)\frac{\cos\gamma_n(h-y)}{\cos\gamma_n h}\right], \quad (5.45)$$

$$N^{ANSMM}(y,u) = V(\alpha_0,c)(\tan(\alpha_0^2-\nu^2)^{\frac{1}{2}}b)\left[\frac{\cosh\alpha_0(c-y)\cosh\alpha_0(c-u)}{\cosh^2\alpha_0 c} - \frac{M}{K}\alpha_0\tanh(\alpha_0 c)F_y^{ANSMM}(0)\frac{\cosh\alpha_0(c-y)}{\cosh\alpha_0 c}\right] - \sum_{n=1}^{\infty} iV(i\alpha_n,c)\tanh(t_n b)\left[\frac{\cos\alpha_n(c-y)\cos\alpha_n(c-u)}{\cos^2\alpha_n c} + \frac{M}{K}\alpha_n\tan(\alpha_n c)F_y^{ANSMM}(0)\frac{\cos\alpha_n(c-y)}{\cos\alpha_n c}\right] - \sum_{n=1}^{\infty} iV(i\gamma_n,h)\left[\frac{\cos\gamma_n(h-y)\cos\gamma_n(h-u)}{\cos^2\gamma_n h} + \frac{M}{K}\gamma_n\tan(\gamma_n h)F_y^{ANSMM}(0)\frac{\cos\gamma_n(h-y)}{\cos\gamma_n h}\right]. \quad (5.46)$$

Barrier of Type II

For configuration of the barrier of Type II, we get three different expressions for

$N^{SMM,ANSMM}(y,u)$ depending on the interval where $y,\ u$ belong.

Case I:

For $y,u \in (0,a)$

$$\begin{aligned}N^{SMM}(y,u) = V(\beta_0,a)(-\cot(\beta_0^2-\nu^2)^{\frac{1}{2}}b)\left[\frac{\cosh\beta_0(a-y)\cosh\beta_0(a-u)}{\cosh^2\beta_0 a}\right.\\ \left.-\frac{M}{K}\beta_0\tanh(\beta_0 a)F_y^{SMM}(0)\frac{\cosh\beta_0(a-y)}{\cosh\beta_0 a}\right]\\ -\sum_{n=1}^{\infty}iV(i\beta_n,a)\coth(u_n b)\left[\frac{\cos\beta_n(a-y)\cos\beta_n(a-u)}{\cos^2\beta_n a}\right.\\ \left.+\frac{M}{K}\beta_n\tan(\beta_n a)F_y^{SMM}(0)\frac{\cos\beta_n(a-y)}{\cos\beta_n a}\right]\\ -\sum_{n=1}^{\infty}iV(i\gamma_n,h)\left[\frac{\cos\gamma_n(h-y)\cos\gamma_n(h-u)}{\cos^2\gamma_n h}\right.\\ \left.+\frac{M}{K}\gamma_n\tan(\gamma_n h)F_y^{SMM}(0)\frac{\cos\gamma_n(h-y)}{\cos\gamma_n h}\right],\end{aligned}\tag{5.47}$$

$$\begin{aligned}N^{ANSMM}(y,u) = V(\beta_0,a)(\tan(\beta_0^2-\nu^2)^{\frac{1}{2}}b)\left[\frac{\cosh\beta_0(a-y)\cosh\beta_0(a-u)}{\cosh^2\beta_0 a}\right.\\ \left.-\frac{M}{K}\beta_0\tanh(\beta_0 a)F_y^{ANSMM}(0)\frac{\cosh\beta_0(a-y)}{\cosh\beta_0 a}\right]\\ -\sum_{n=1}^{\infty}iV(i\beta_n,a)\tanh(u_n b)\left[\frac{\cos\beta_n(a-y)\cos\beta_n(a-u)}{\cos^2\beta_n a}\right.\\ \left.+\frac{M}{K}\beta_n\tan(\beta_n a)F_y^{ANSMM}(0)\frac{\cos\beta_n(a-y)}{\cos\beta_n a}\right]\\ -\sum_{n=1}^{\infty}iV(i\gamma_n,h)\left[\frac{\cos\gamma_n(h-y)\cos\gamma_n(h-u)}{\cos^2\gamma_n h}\right.\\ \left.+\frac{M}{K}\gamma_n\tan(\gamma_n h)F_y^{ANSMM}(0)\frac{\cos\gamma_n(h-y)}{\cos\gamma_n h}\right].\end{aligned}\tag{5.48}$$

Case II:

For $y,u \in (c,h)$,

$$N^{SMM}(y,u) = \frac{\coth \nu b}{(h-c)\nu} + \sum_{n=1}^{\infty} \frac{2\coth \eta_n b}{(h-c)\eta_n} \cos\frac{n\pi(h-y)}{h-c} \cos\frac{n\pi(h-u)}{h-c} - \sum_{n=1}^{\infty} iV(i\gamma_n, h) \left[\frac{\cos\gamma_n(h-y)\cos\gamma_n(h-u)}{\cos^2\gamma_n h} + \frac{M}{K}\gamma_n \tan(\gamma_n h) F_y^{SMM}(0) \frac{\cos\gamma_n(h-y)}{\cos\gamma_n h} \right], \quad (5.49)$$

$$N^{ANSMM}(y,u) = \frac{\tanh \nu b}{(h-c)\nu} + \sum_{n=1}^{\infty} \frac{2\tanh \eta_n b}{(h-c)\eta_n} \cos\frac{n\pi(h-y)}{h-c} \cos\frac{n\pi(h-u)}{h-c} - \sum_{n=1}^{\infty} iV(i\gamma_n, h) \left[\frac{\cos\gamma_n(h-y)\cos\gamma_n(h-u)}{\cos^2\gamma_n h} + \frac{M}{K}\gamma_n \tan(\gamma_n h) F_y^{ANSMM}(0) \frac{\cos\gamma_n(h-y)}{\cos\gamma_n h} \right]. \quad (5.50)$$

Case III:

For $y \in (0,a), u \in (c,h)$ *or* $y \in (c,h), u \in (0,a)$

$$N^{SMM,ANSMM}(y,u) = -\sum_{n=1}^{\infty} iV(i\gamma_n, h) \left[\frac{\cos\gamma_n(h-y)\cos\gamma_n(h-u)}{\cos^2\gamma_n h} + \frac{M}{K}\gamma_n \tan(\gamma_n h) F_y^{SMM,ANSMM}(0) \frac{\cos\gamma_n(h-y)}{\cos\gamma_n h} \right]. \quad (5.51)$$

Barrier of Type III

For configuration of the barrier of Type III, we get three different expressions for $N^{SMM,ANSMM}(y,u)$ depending on the interval where $y,\ u$ belong.

Case I:

For $y, u \in (0, a)$

$$N^{SMM}(y,u) = V(\beta_0,a)(-\cot(\beta_0^2-\nu^2)^{\frac{1}{2}}b)\left[\frac{\cosh\beta_0(a-y)\cosh\beta_0(a-u)}{\cosh^2\beta_0 a} - \frac{M}{K}\beta_0\tanh(\beta_0 a)F_y^{SMM}(0)\frac{\cosh\beta_0(a-y)}{\cosh\beta_0 a}\right] - \sum_{n=1}^{\infty} iV(i\beta_n,a)\coth(u_n b)\left[\frac{\cos\beta_n(a-y)\cos\beta_n(a-u)}{\cos^2\beta_n a} + \frac{M}{K}\beta_n\tan(\beta_n a)F_y^{SMM}(0)\frac{\cos\beta_n(a-y)}{\cos\beta_n a}\right] - \sum_{n=1}^{\infty} iV(i\gamma_n,h)\left[\frac{\cos\gamma_n(h-y)\cos\gamma_n(h-u)}{\cos^2\gamma_n h} + \frac{M}{K}\gamma_n\tan(\gamma_n h)F_y^{SMM}(0)\frac{\cos\gamma_n(h-y)}{\cos\gamma_n h}\right], \quad (5.52)$$

$$N^{ANSMM}(y,u) = V(\beta_0,a)(\tan(\beta_0^2-\nu^2)^{\frac{1}{2}}b)\left[\frac{\cosh\beta_0(a-y)\cosh\beta_0(a-u)}{\cosh^2\beta_0 a} - \frac{M}{K}\beta_0\tanh(\beta_0 a)F_y^{ANSMM}(0)\frac{\cosh\beta_0(a-y)}{\cosh\beta_0 a}\right] - \sum_{n=1}^{\infty} iV(i\beta_n,a)\tanh(u_n b)\left[\frac{\cos\beta_n(a-y)\cos\beta_n(a-u)}{\cos^2\beta_n a} + \frac{M}{K}\beta_n\tan(\beta_n a)F_y^{ANSMM}(0)\frac{\cos\beta_n(a-y)}{\cos\beta_n a}\right] - \sum_{n=1}^{\infty} iV(i\gamma_n,h)\left[\frac{\cos\gamma_n(h-y)\cos\gamma_n(h-u)}{\cos^2\gamma_n h} + \frac{M}{K}\gamma_n\tan(\gamma_n h)F_y^{ANSMM}(0)\frac{\cos\gamma_n(h-y)}{\cos\gamma_n h}\right]. \quad (5.53)$$

Case II

For $y, u \in (c, d)$

$$N^{SMM}(y,u) = \frac{\coth \nu b}{(d-c)\nu} + \sum_{n=1}^{\infty} \frac{2\coth \zeta_n b}{(d-c)\zeta_n} \cos\frac{n\pi(d-y)}{d-c} \cos\frac{n\pi(d-u)}{d-c} - \sum_{n=1}^{\infty} iV(i\gamma_n, h) \left[\frac{\cos\gamma_n(h-y)\cos\gamma_n(h-u)}{\cos^2\gamma_n h} + \frac{M}{K}\gamma_n \tan(\gamma_n h) F_y^{SMM}(0) \frac{\cos\gamma_n(h-y)}{\cos\gamma_n h} \right], \tag{5.54}$$

$$N^{ANSMM}(y,u) = \frac{\tanh \nu b}{(d-c)\nu} + \sum_{n=1}^{\infty} \frac{2\tanh \zeta_n b}{(d-c)\zeta_n} \cos\frac{n\pi(d-y)}{d-c} \cos\frac{n\pi(d-u)}{d-c} - \sum_{n=1}^{\infty} iV(i\gamma_n, h) \left[\frac{\cos\gamma_n(h-y)\cos\gamma_n(h-u)}{\cos^2\gamma_n h} + \frac{M}{K}\gamma_n \tan(\gamma_n h) F_y^{ANSMM}(0) \frac{\cos\gamma_n(h-y)}{\cos\gamma_n h} \right]. \tag{5.55}$$

Case III

For $y \in (0,a), u \in (c,d)$ *or* $y \in (c,d), u \in (0,a)$

$$N^{SMM,ANSMM}(y,u) = -\sum_{n=1}^{\infty} iV(i\gamma_n, h) \left[\frac{\cos\gamma_n(h-y)\cos\gamma_n(h-u)}{\cos^2\gamma_n h} + \frac{M}{K}\gamma_n \tan(\gamma_n h) F_y^{SMM,ANSMM}(0) \frac{\cos\gamma_n(h-y)}{\cos\gamma_n h} \right]. \tag{5.56}$$

Now if we define

$$C^{SMM,ANSMM} = -i\frac{1-R^{SMM,ANSMM}}{1+R^{SMM,ANSMM}}, \tag{5.57}$$

then by using the relation (5.44), we obtain from equation (5.29)

$$C^{SMM,ANSMM} = iV(\gamma_0, h)\left[\int_{(0,h)-L_j} F^{SMM,ANSMM}(y)\frac{\cosh\gamma_0(h-y)}{\cosh\gamma_0 h}dy - \frac{M}{K}\gamma_0\tanh(\gamma_0 h)F_y^{SMM,ANSMM}(0)\right]. \quad (5.58)$$

Thus if the integral equations (5.43) can be solved for each type of configurations of the barrier, then these solutions can be used to evaluate $C^{SMM,ANSMM}$ from the relations (5.58), and hence the reflection and transmission coefficients $|R|$ and $|T|$ can be obtained from relations (5.14) and (5.57) by using

$$|R| = \frac{|1 + C^{SMM}C^{ANSMM}|}{\triangle} \quad \text{and} \quad |T| = \frac{|C^{SMM} - C^{ANSMM}|}{\triangle} \quad (5.59)$$

with

$$\triangle = \{1 + (C^{SMM})^2 + (C^{ANSMM})^2 + (C^{SMM}C^{ANSMM})^2\}^{\frac{1}{2}}. \quad (5.60)$$

Solution of integral equation

In this section we will proceed to solve integral equation (5.43) by utilizing Galerkin technique. For this, we approximate $F^{SMM,ANSMM}(y)$ as

$$F^{SMM,ANSMM}(y) \approx \mathcal{F}^{SMM,ANSMM}(y),\ y \in (0,h) - L_j, j = 1,2,3. \quad (5.61)$$

Now $\mathcal{F}^{SMM,ANSMM}(y)$ is expanded in terms of multi-term Galerkin expansions with a suitable choice of basis function for three types of configurations of the barrier which are given below.

For barrier of Type-I,

$$\mathcal{F}^{SMM,ANSMM}(y) = \sum_{n=0}^{N} a_n^{SMM,ANSMM} f_n^{SMM,ANSMM}(y), y \in (0,c). \quad (5.62)$$

Here $f_n^{SMM,ANSMM}(y)$ are basis functions and $a_n^{SMM,ANSMM}$ are the unknown coeffi-

cients.

For barrier of Type-II,

$$\mathcal{F}^{SMM,ANSMM}(y) = \begin{cases} \sum_{n=0}^{N} a_n^{SMM,ANSMM} p_n^{SMM,ANSMM}(y), 0 < y < a, \\ \sum_{n=0}^{N} b_n^{SMM,ANSMM} q_n^{SMM,ANSMM}(y), c < y < h. \end{cases} \tag{5.63}$$

Here $p_n^{SMM,ANSMM}(y)$ and $q_n^{SMM,ANSMM}(y)$ are basis functions and $a_n^{SMM,ANSMM}$, $b_n^{SMM,ANSMM}$ are the unknown coefficients.

For barrier of Type-III,

$$\mathcal{F}^{SMM,ANSMM}(y) = \begin{cases} \sum_{n=0}^{N} a_n^{SMM,ANSMM} p1_n^{SMM,ANSMM}(y), 0 < y < a, \\ \sum_{n=0}^{N} b_n^{SMM,ANSMM} q1_n^{SMM,ANSMM}(y), c < y < d. \end{cases} \tag{5.64}$$

The basis functions in the expansions (5.62) to (5.64) can be chosen as ultraspherical Gegenbauer polynomials of order 1/6 with suitable weights [cf. Porter (1995)]. The advantage of this choice is that all odd order derivatives of ultraspherical Gegenbauer polynomials of order 1/6 vanishes at zero (cf. Gradshteyn Rhyzhik). This gives $\mathcal{F}_y^{SMM,ANSMM}(0) = 0$ i.e., $f_y^{SMM,ANSMM}(0) = 0$. This simplifies the evaluation of various unknown constants occurring in the expressions for $\phi^{SMM,ANSMM}(x, y)$. It may be mentioned here that due to occurrence of the term $f_y^{SMM,ANSMM}(0)$ in the various unknowns occurring in the expressions for $\phi^{SMM,ANSMM}(x, y)$, Rhodes Robinson (1971) stated that Havelock's expansion of water wave potential $\phi^{SMM,ANSMM}(x, y)$ for wave-barrier interaction problems in water of finite depth is not unique.
Now the expressions for $\mathcal{F}^{SMM,ANSMM}(y)$ for different types of configurations of the barrier are substituted in the integral equation (5.43) to reduce it to a system of linear algebraic equations in the coefficients $a_n^{SMM,ANSMM}$, $b_n^{SMM,ANSMM}$. This system of linear algebraic equations is solved to determine the coefficients and hence the integral equation (5.43). We now evaluate the basis functions for each type of barrier configuration which given below.

Basis functions

Barrier of Type-I :

For this type of bottom standing barrier, noting the edge condition (5.4) and the free surface condition (5.2), we write the function $f_m^{SMM,ANSMM}(y)$ as

$$f_m^{SMM}(y) = f_m^{ANSMM}(y) = f_m(y) = -\frac{d}{dy}[e^{\frac{-Ky}{\gamma+M\gamma^3}} \int_y^c e^{\frac{Kt}{\gamma+M\gamma^3}} \tilde{f}_m(t)dt], 0 < y < c \quad (5.65)$$

where the functions $\tilde{f}_m(y)$ are chosen in terms of ultraspherical Gegenbauer polynomials $C_{2m}^{\frac{1}{6}}(\frac{y}{c})$ of order 1/6 as

$$\tilde{f}_m(y) = \frac{2^{\frac{7}{6}}\Gamma(\frac{1}{6})(2m)!}{\pi\Gamma(2m+\frac{1}{3})(c)^{\frac{1}{3}}(c^2-y^2)^{\frac{1}{3}}} C_{2m}^{\frac{1}{6}}(\frac{y}{c}), 0 < y < c. \quad (5.66)$$

Barrier of Type II:

In this case also, we note the free surface and edge conditions (5.2) and (5.4) and write

$$p_m^{SMM}(y) = p_m^{ANSMM}(y) = p_m(y) = -\frac{d}{dy}[e^{\frac{-Ky}{\gamma+M\gamma^3}} \int_y^a e^{\frac{Kt}{\gamma+M\gamma^3}} \tilde{p}_m(t)dt], \ 0 < y < a \quad (5.67)$$

where

$$\tilde{p}_m(y) = \frac{2^{\frac{7}{6}}\Gamma(\frac{1}{6})(2m)!}{\pi\Gamma(2m+\frac{1}{3})(a)^{\frac{1}{3}}(a^2-y^2)^{\frac{1}{3}}} C_{2m}^{\frac{1}{6}}(\frac{y}{a}), 0 < y < a, \quad (5.68)$$

$$q_m^{SMM}(y) = g1_{m+1}^{(1)}(y), m = 0, 1, 2, ...,$$

$$q_m^{ANSMM}(y) = g1_m^{(1)}(y), m = 0, 1, 2, ..., \quad (5.69)$$

and

$$g1_m^{(1)}(y) = \frac{2^{\frac{7}{6}}\Gamma(\frac{1}{6})(2m)!}{\pi\Gamma(2m+\frac{1}{3})(h-c)^{\frac{1}{3}}((h-c)^2-(h-y)^2)^{\frac{1}{3}}} C_{2m}^{\frac{1}{6}}(\frac{h-y}{h-c}),\ c<y<h. \quad (5.70)$$

Barrier of Type III:

Here we choose two different basis functions for two disjoint intervals as

$$p1_m^{SMM}(y) = p1_m^{ANSMM}(y) = p1_m(y) = -\frac{d}{dy}[e^{\frac{-Ky}{\gamma+M\gamma^3}} \int_y^a e^{\frac{Kt}{\gamma+M\gamma^3}} \tilde{x}_m(t)dt],\ 0<y<a \quad (5.71)$$

where

$$\tilde{x}_m(y) = \frac{2^{\frac{7}{6}}\Gamma(\frac{1}{6})(2m)!}{\pi\Gamma(2m+\frac{1}{3})(a)^{\frac{1}{3}}(a^2-y^2)^{\frac{1}{3}}} C_{2m}^{\frac{1}{6}}(\frac{y}{a}), 0<y<a \quad (5.72)$$

and

$$q1_m^{SMM,ANSMM}(y) = \frac{2^{\frac{7}{6}}\Gamma(\frac{1}{6})(m)!}{\pi\Gamma(m+\frac{1}{3})(\frac{d-c}{2})^{\frac{1}{3}}((y-c)(d-y))^{\frac{1}{3}}} C_m^{\frac{1}{6}}(\frac{2y-c-d}{d-c}),\ c<y<d. \quad (5.73)$$

Formation of linear system of equations for solution of integral equation

Barrier of type I

Here we use (5.62) in the integral equation (5.43), and then multiplying both side by appropriate basis function $f_m^{SMM,ANSMM}(y)$ and integrating over $(0,c)$, to obtain the following linear system of equations.

$$\sum_{n=0}^{N} a_n^{SMM,ANSMM} \mathcal{V}_{mn}^{SMM,ANSMM} = \omega_m^{SMM,ANSMM}, \quad m = 0,1,...,N \quad (5.74)$$

where

$$\mathcal{V}_{mn}^{SMM,ANSMM} = \int_0^c \int_0^c N^{SMM,ANSMM}(y,u) f_n^{SMM,ANSMM}(u) f_m^{SMM,ANSMM}(y) du\, dy,$$

$$m, n = 0, 1, 2, ..., N, \tag{5.75}$$

and

$$\omega_m^{SMM,ANSMM} = \int_0^c \frac{\cosh\gamma_0(h-y)}{\cosh\gamma_0 h} f_m^{SMM,ANSMM}(y) dy, m = 0, 1, ..., N. \tag{5.76}$$

The integrals (5.75) and (5.76) can be evaluated explicitly, as in Kanoria *et al.* (1999) by using the different properties and standard results on Gegenbaur polynomials. These are given in APPENDIX A. Thus the constants $a_n^{SMM,ANSMM}(n = 0, 1, ...N)$ are obtained by solving the linear equations (5.74). The relation (5.58) produce

$$C^{SMM,ANSMM} = iV(\gamma_0, h) \sum_{n=0}^{N} a_n^{SMM,ANSMM} \omega_n^{SMM,ANSMM} \tag{5.77}$$

so that using $C^{SMM,ANSMM}$, $|R|$ and $|T|$ can be evaluated from the relations (5.59).

Barrier of type II

Here we use the equation (5.63) in the integral equation (5.43) and multiplying both sides first by $p_m^{SMM,ANSMM}(y)$ for $(0 < y < a)$ and then by $q_m^{SMM,ANSMM}(y)$ for $(c < y < h)$ and then integrate over $(0, a)$ and (c, h) respectively, to get the following linear system of equations.

$$\sum_{n=0}^{N} a_n^{SMM,ANSMM} \begin{pmatrix} \mathcal{G}_{mn}^{SMM,ANSMM} \\ \mathcal{P}_{mn}^{SMM,ANSMM} \end{pmatrix} + \sum_{n=0}^{N} b_n^{SMM,ANSMM} \begin{pmatrix} \mathcal{H}_{mn}^{SMM,ANSMM} \\ \mathcal{Q}_{mn}^{SMM,ANSMM} \end{pmatrix}$$

$$= \begin{pmatrix} \omega_m^{(1)SMM,ANSMM} \\ \omega_m^{(2)SMM,ANSMM} \end{pmatrix}, \quad m = 0, 1, ..., N \tag{5.78}$$

where

$$\mathcal{G}_{mn}^{SMM,ANSMM} = \int_0^a \left(\int_0^a N^{SMM,ANSMM}(y,u) p_n^{SMM,ANSMM}(u) du \right) p_m^{SMM,ANSMM}(y) dy,$$

$$\mathcal{H}_{mn}^{SMM,ANSMM} = \int_0^a \left(\int_c^h N^{SMM,ANSMM}(y,u) q_n^{SMM,ANSMM}(u) du \right) p_m^{SMM,ANSMM}(y) dy,$$

$$\mathcal{P}_{mn}^{SMM,ANSMM} = \int_c^h \left(\int_0^a N^{SMM,ANSMM}(y,u) p_n^{SMM,ANSMM}(u) du \right) q_m^{SMM,ANSMM}(y) dy,$$

$$\mathcal{Q}_{mn}^{SMM,ANSMM} = \int_c^h \left(\int_c^h N^{SMM,ANSMM}(y,u) q_n^{SMM,ANSMM}(u) du \right) q_m^{SMM,ANSMM}(y) dy,$$

$$m, n = 0, 1, 2, ..., N, \tag{5.79}$$

and

$$\omega_m^{(1)SMM,ANSMM} = \int_0^a \frac{\cosh \gamma_0 (h-y)}{\cosh \gamma_0 h} p_m^{SMM,ANSMM}(y) dy,$$

$$\omega_m^{(2)SMM,ANSMM} = \int_c^h \frac{\cosh \gamma_0 (h-y)}{\cosh \gamma_0 h} q_m^{SMM,ANSMM}(y) dy,$$

$$m = 0, 1, ..., N. \tag{5.80}$$

The integrals in the relations (5.79) and (5.80) can be evaluated explicitly and are given in APPENDIX A. Thus the constants, $a_n^{SMM,ANSMM}$ *and* $b_n^{SMM,ANSMM}$ $(n =$

$0, 1, 2, ..N$) can be obtained by solving the linear equations (5.63). We evaluate $C^{SMM,ANSMM}$ as

$$C^{SMM,ANSMM} = iV(\gamma_0, h)\left[\sum_{n=0}^{N} a_n^{SMM,ANSMM}\omega_n^{(1)SMM,ANSMM} + \sum_{n=0}^{N} b_n^{SMM,ANSMM}\omega_n^{(2)SMM,ANSMM}\right] \tag{5.81}$$

so as to obtain $|R|$ and $|T|$.

Barrier of type III

In this case, we substitute the equation (5.64) in the integral equation (5.43) and multiplying both sides first by $p1_m^{SMM,ANSMM}(y)$ for $(0 < y < a)$ and then by $q1_m^{SMM,ANSMM}(y)$ for $(c < y < d)$ and then integrate over $(0, a)$ and (c, d) respectively, we get the linear system of equations as follows:

$$\sum_{n=0}^{N} a_n^{SMM,ANSMM}\begin{pmatrix} R_{mn}^{SMM,ANSMM} \\ X_{mn}^{SMM,ANSMM} \end{pmatrix} + \sum_{n=0}^{N} b_n^{SMM,ANSMM}\begin{pmatrix} S_{mn}^{SMM,ANSMM} \\ Y_{mn}^{SMM,ANSMM} \end{pmatrix} = \begin{pmatrix} \omega 1_m^{(1)SMM,ANSMM} \\ \omega 1_m^{(2)SMM,ANSMM} \end{pmatrix}, \quad m = 0, 1, ..., N \tag{5.82}$$

where

$$R_{mn}^{SMM,ANSMM} = \int_0^a \left(\int_0^a N^{SMM,ANSMM}(y, u) p1_n^{SMM,ANSMM}(u)du \right) p1_m^{SMM,ANSMM}(y)dy,$$

$$S_{mn}^{SMM,ANSMM} = \int_0^a \left(\int_c^d N^{SMM,ANSMM}(y, u) q1_n^{SMM,ANSMM}(u)du \right) p1_m^{SMM,ANSMM}(y)dy,$$

$$X_{mn}^{SMM,ANSMM} = \int_c^d \left(\int_0^a N^{SMM,ANSMM}(y,u) p1_n^{SMM,ANSMM}(u) du \right) q1_m^{SMM,ANSMM}(y) dy,$$

$$Y_{mn}^{SMM,ANSMM} = \int_c^d \left(\int_c^d N^{SMM,ANSMM}(y,u) q1_n^{SMM,ANSMM}(u) du \right) q1_m^{SMM,ANSMM}(y) dy,$$

$$m, n = 0, 1, 2, ..., N, \tag{5.83}$$

$$\omega 1_m^{(1)SMM,ANSMM} = \int_0^a \frac{\cosh \gamma_0 (h-y)}{\cosh \gamma_0 h} p1_m^{SMM,ANSMM}(y) dy,$$

$$\omega 1_m^{(2)SMM,ANSMM} = \int_c^d \frac{\cosh \gamma_0 (h-y)}{\cosh \gamma_0 h} q1_m^{SMM,ANSMM}(y) dy,$$

$$m = 0, 1, ..., N. \tag{5.84}$$

The integrals in the relations (5.82) to (5.84) can be evaluated explicitly and are given in APPENDIX A. Thus the constants, $a_n^{SMM,ANSMM}$ *and* $b_n^{SMM,ANSMM}$ $(n = 0, 1, 2, ..N)$ can be obtained from linear equations (5.64) and hence $C^{SMM,ANSMM}$ are given by

$$C^{SMM,ANSMM} = iV(\gamma_0, h) \left[\sum_{n=0}^{N} a_n^{SMM,ANSMM} \omega 1_n^{(1)SMM,ANSMM} + \sum_{n=0}^{N} b_n^{SMM,ANSMM} \omega 1_n^{(2)SMM,ANSMM} \right]. \tag{5.85}$$

Thus knowing $C^{SMM,ANSMM}$, one can evaluate $|R|$ and $|T|$.

5.4 NUMERICAL RESULTS AND DISCUSSIONS

The numerical results in this section depicts the behaviour of reflection coefficient $|R|$ for the non dimensional wave numbers Kh for different values of the parameters $b/h, c/h, a/h,\ M/h^2$ and different values of incident angle θ. For numerical computation of three type of barriers, we consider $N = 8$ in equation (5.74), (5.78) and (5.82) respectively. In the Table (5.1), we study the convergence of values of $|R|$ for different values of Kh for $N = 2, 5, 7, 8$ of the series (5.74) for Type I barrier. From this table it is seen that the results for $|R|$ converge very rapidly with N. For $N = 7$, an accuracy of almost five decimal places is achieved.

Table 5.1: Convergence of $|R|$ with N for Type I Barrier with $b/h = 0.5, c/h = 0.5, \theta = 25^0, M/h^2 = 0.5$

Kh	**N**=2	**N**=5	**N**=7	**N**=8
0.2	0.603525	0.623054	0.623670	0.623672
1.0	0.423256	0.441943	0.442309	0.442312
1.8	0.305412	0.326481	0.326831	0.326834

Table (5.2) shows the convergence of the numerical values of $|R|$ for different values of Kh with the truncation size $N = 2, 5, 7, 8$ of the finite series (5.78) for Type II barrier. Here also a five figure accuracy is achieved for $N = 7$. In a similar manner the convergence analysis of $|R|$ for Type III barrier has been done, although it is not presented in tabular form here. Thus, from these two tables, we can say the present method is quite efficient for the numerical calculation of $|R|$ (and $|T|$).

Table 5.2: Convergence of $|R|$ with N for Type II Barrier with $\frac{(c-a)}{h} = 0.5, b/h = 1, \theta = 25^0, M/h^2 = 0.5$

Kh	**N**=2	**N**=5	**N**=7	**N**=8
0.2	0.179421	0.197454	0.197475	0.197478
1.0	0.601245	0.628014	0.628047	0.628049
1.8	0.572983	0.597452	0.597674	0.597676

In Table (5.3), the energy identity $|R|^2 + |T|^2 = 1$ are verified for different values of the dimensionless wavenumber Kh for Type I barrier with fixed values of

$c/h = 0.8, \theta = 25^0, M/h^2 = 0.5$ which authenticated the correctness of the results. Simarly the energy balance relation is verified for barrier configurations of Type II and III, although not presented here.

Table 5.3: Energy identity, Type I barrier for $b/h = 0.5, c/h = 0.5, \theta = 25^0, M/h^2 = 0.5$

Kh	$\|R\|$	$\|T\|$	$\|R\|^2 + \|T\|^2$
0.1	0.660504	0.750823	1.0000
0.5	0.539024	0.842291	1.0000
1.0	0.439943	0.898026	1.0000
1.5	0.363089	0.931754	1.0000
2.0	0.299241	0.954178	1.0000
2.5	0.245141	0.969487	1.0000
2.9	0.207693	0.978194	1.0000

In Figure (5.2), the reflection coefficient $|R|$ is depicted against the non dimensional wave number Kh for Type I and Type II barriers when the non dimensional surface tension M/h^2 is very small, i.e., $M/h^2 = 0.0001$. These results are compared with the results for $|R|$ in Kanoria *et al* (1999) (Figure 4 and 5 there) and a very good matching of the results are observed from Figure (5.2). This shows the correctness of the results obtained by present method.

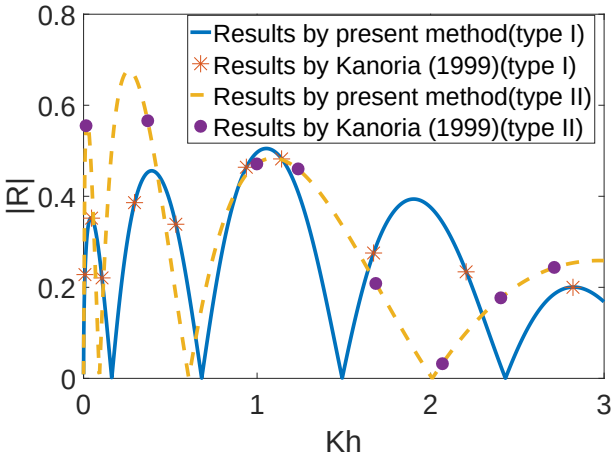

Figure 5.2: Reflection coefficients for two types of barriers without surface tension

We now discuss about the behaviour of $|R|$ associated with Type I, Type II and Type III barriers.

Barrier of Type I

The Figures (5.3), (5.4), (5.5) and (5.6) exhibit the behaviour of reflection coefficient $|R|$ of bottom standing thick barrier of Type I, against non-dimensional wave number (Kh), for various values of non dimensional parameters $\frac{b}{h}$, $\frac{c}{h}$, $\frac{M}{h^2}$ and θ.
In Figure (5.3), $|R|$ is plotted against Kh for different values of width of the barrier $\frac{b}{h} = 0.5, 1.0, 1.5,\ 2$ and for $\frac{c}{h} = 0.5,\ \frac{M}{h^2} = 0.5,\ \theta = 25^0$. It is seen that $|R|$ exhibits oscillatory behaviour and the frequency of oscillation in $|R|$ increases as the width of the barrier increases. Also for certain values of Kh, there occurs no reflection of wave energy.

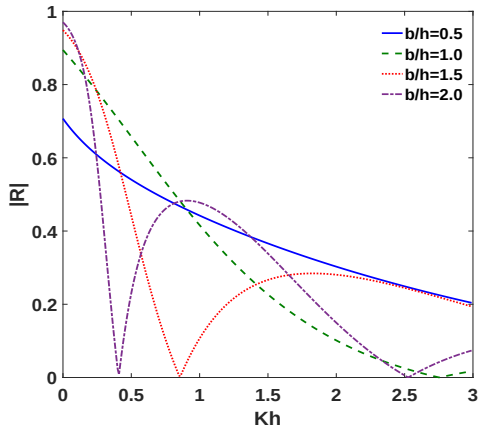

Figure 5.3: Reflection coefficient for type I barrier for different $\frac{b}{h}$ with $\frac{c}{h} = 0.5, \frac{M}{h^2} = 0.5, \theta = 25^0$.

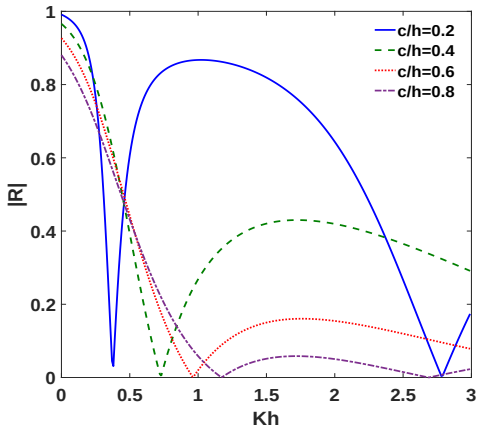

Figure 5.4: Reflection coefficient for type I barrier for different $\frac{c}{h}$ with $\frac{b}{h} = 1.5, \frac{M}{h^2} = 0.5, \theta = 25^0$.

In Figure (5.4), $|R|$ is depicted against Kh for different length of the barrier, viz, $\frac{c}{h}(= 0.2, 0.4, 0.6, 0.8)$ and for fixed values of $\frac{b}{h} = 1.5, \frac{M}{h^2} = 0.5, \theta = 25^0$. Here also it is observed that $|R|$ exhibits oscillatory behaviour and the frequency and amplitude of oscillation increases as the length of the barrier increases. This shows that longer barrier induces more reflection of wave energy. Also, for certain values of Kh there occurs no reflection of wave energy.

The effect of surface tension on reflection coefficient is depicted in Figure (5.5). In this figure, $|R|$ is plotted against Kh for different values of surface tension factor $\frac{M}{h^2} = 0.5, 1.0, 1.5$ and 2.0 and for fixed values of $\frac{b}{h} = 1.5, \frac{c}{h} = 0.5, \theta = 25^0$. In this figure

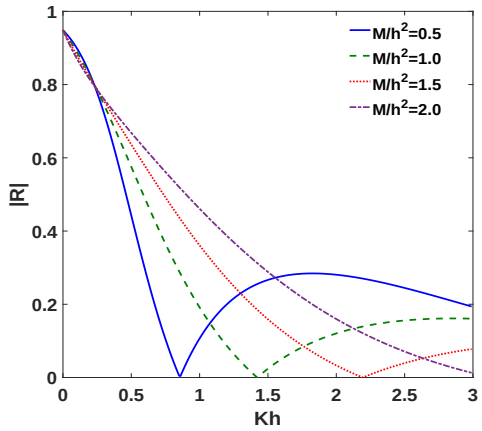

Figure 5.5: Reflection coefficient for type I barrier for different $\frac{M}{h^2}$ with $\frac{b}{h} = 1.5, \frac{c}{h} = 0.5, \theta = 25^0$.

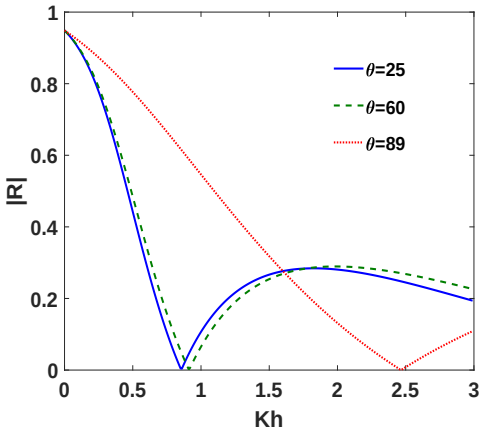

Figure 5.6: Reflection coefficient for type I barrier for different θ with $\frac{b}{h} = 1.5, \frac{c}{h} = 0.5, \frac{M}{h^2} = 0.5$.

the oscillatiory behaviour of $|R|$ is observed and the amplitude of oscillation decreases with Kh as the surface tension increases showing a damping effect of surface tension on the reflected wave. Also there occurs phase shift in the oscillation of $|R|$ as the surface tension increases and for some values of the wave number Kh, there occurs no reflection.

The Figure (5.6) depicts reflection coefficients against wave numbers with fixed values of $\frac{b}{h} = 1.5, \frac{c}{h} = 0.5$, $\frac{M}{h^2} = 0.5$ and for different values of angle of incidence $\theta = 25^0, 60^0, 89^0$. This figure shows oscillatory behaviour of $|R|$. It is also noticed that when θ is almost 90^0, the frequency of oscillation of $|R|$ decreases compared to other angles of incidence.

Barrier of Type II

In Figures (5.7), (5.8), (5.9) and (5.10), the behaviour of reflection coefficient $|R|$ is depicted against non dimensional wave number Kh for barrier of Type II (submerged rectangular block) for various values of non dimensional parameters $\frac{(c-a)}{h}, \frac{b}{h}$, $\frac{M}{h^2}$ and θ.

In Figure (5.7), $|R|$ is plotted against Kh for different values of $\frac{(c-a)}{h} = 0.5, 0.6, 0.7$ and for fixed values of $\frac{b}{h} = 1$, $\frac{M}{h^2} = 0.5$ and $\theta = 25^0$. It is seen that $|R|$ exhibits oscillatory behaviour and as $\frac{(c-a)}{h}$ increases, $|R|$ increases. This is due to the reason

that as $\frac{(c-a)}{h}$ increases, the length of the barrier increases, so the longer barrier induces more reflection of waves.

Figure (5.8) shows the effect of variation in width of the barrier on reflection coefficients by considering $\frac{b}{h} = 0.5,\ 1.0,\ 1.5$ and $\frac{(c-a)}{h} = 0.5, \frac{M}{h^2} = 0.5,\ \theta = 25^0$. It is seen that $|R|$ exhibits oscillatory behaviour with no reflection for some values of Kh and frequency of oscillation increases as the width of the barrier increases.

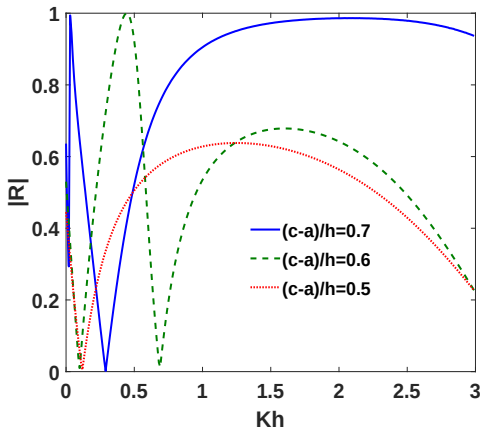

Figure 5.7: Reflection coefficient for type II barrier for different $\frac{(c-a)}{h}$ with $\frac{b}{h} = 1, \frac{M}{h^2} = 0.5, \theta = 25^0$.

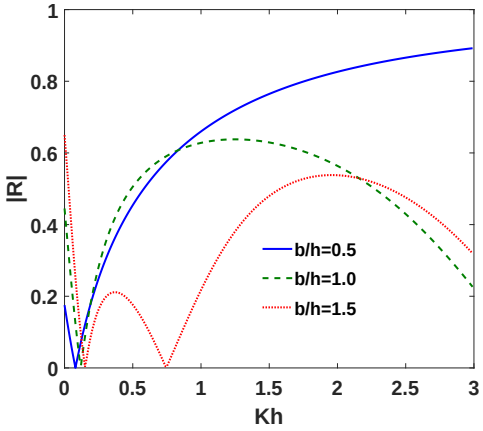

Figure 5.8: Reflection coefficient for type II barrier for different $\frac{b}{h}$ with $\frac{(c-a)}{h} = 0.5, \frac{M}{h^2} = 0.5, \theta = 25^0$.

In Figure (5.9), $|R|$ is depicted against Kh for with different values of $\frac{M}{h^2} = 0.5,\ 1.0,\ 1.5$ and fixed values of $\frac{(c-a)}{h} = 0.5,\ \frac{b}{h} = 1$ and $\theta = 25^0$. Here $|R|$ exhibits oscillatory behaviour. The presence of surface tension decreases $|R|$.

In Figure (5.10) the variation of reflection coefficient $|R|$ for different angles of incidence $\theta(= 25^0, 60^0, 89^0)$ and for fixed values of $\frac{(c-a)}{h} = 0.5, \frac{b}{h} = 1$ and $\frac{M}{h^2} = 0.5$ is shown. Figure shows that $|R|$ exhibits oscillatory behaviour. However, when θ is 89^0, the frequency of oscillation in $|R|$ decreases.

Type III barrier

Figures (5.11), (5.12), (5.13), (5.14) depict the behavior of $|R|$ against non dimensional wave numbers Kh, for Type III barrier.
In Figure (5.11), $|R|$ is plotted against Kh for different values of width ($\frac{b}{h} = 0.4,\ 0.7,\ 1.5$)

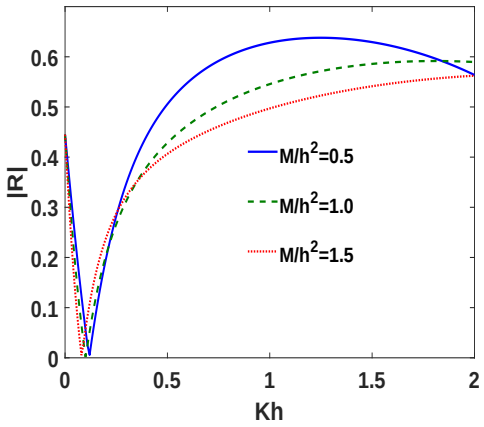

Figure 5.9: Reflection coefficient for type II barrier for different $\frac{M}{h^2}$ with $\frac{(c-a)}{h} = 0.5, \frac{b}{h} = 1, \theta = 25^0$.

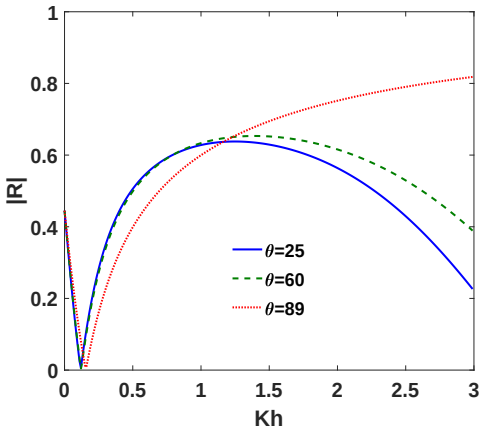

Figure 5.10: Reflection coefficient for type II barrier for different θ with $\frac{(c-a)}{h} = 0.5, \frac{b}{h} = 1, \frac{M}{h^2} = 0.5$

of the thick barrier and fixed values of $\frac{a}{h} = 0.2$, $\frac{M}{h^2} = 0.5$, $\frac{(d-c)}{h} = 0.3$, $\theta = 25^0$. The figure shows that $|R|$ exhibits oscillatory behaviour for wide barrier.

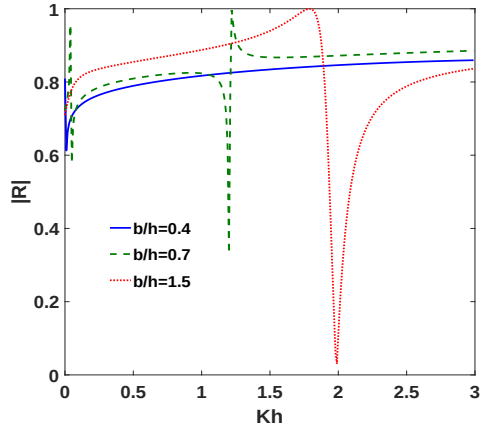

Figure 5.11: Reflection coefficient for type III barrier for different $\frac{b}{h}$ with $\frac{a}{h} = 0.2, \frac{M}{h^2} = 0.5, \frac{(d-c)}{h} = 0.3, \theta = 25^0$.

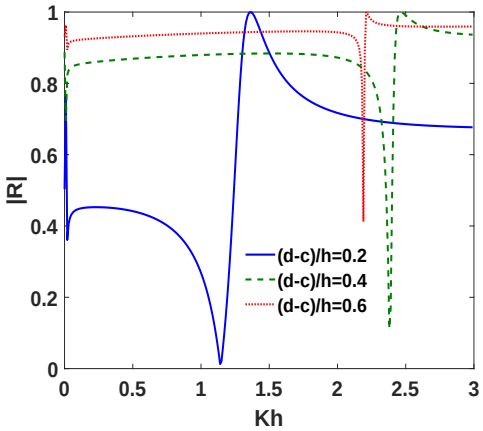

Figure 5.12: Reflection coefficient for type III barrier for different $\frac{d-c}{h}$ with $\frac{a}{h} = 0.1, \frac{b}{h} = 0.5, \frac{M}{h^2} = 0.5, \theta = 25^0$.

In Figure (5.12), $|R|$ is depicted for various values of the gap in between the barrier ($\frac{d-c}{h} = 0.2,\ 0.4,\ 0.6$) and fixed values of $\frac{a}{h} = 0.1, \frac{b}{h} = 0.5, \frac{M}{h^2} = 0.5, \theta = 25^0$. This figure shows oscillatory behaviour in $|R|$ due to interaction of barrier with the waves and there occurs no reflection for some values of Kh and as the gap length increases,

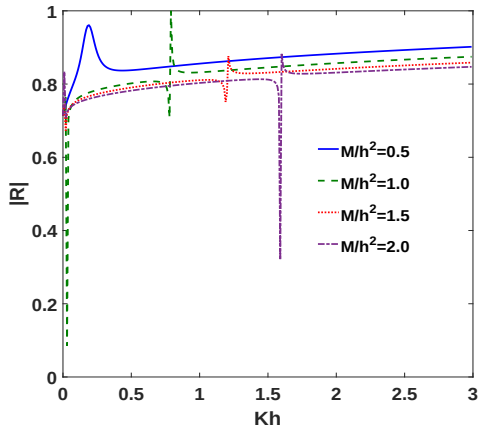

Figure 5.13: Reflection coefficient for type III barrier for different $\frac{M}{h^2}$ with $\frac{a}{h} = 0.2, \frac{b}{h} = 1, \frac{(d-c)}{h} = 0.3, \theta = 25^0$.

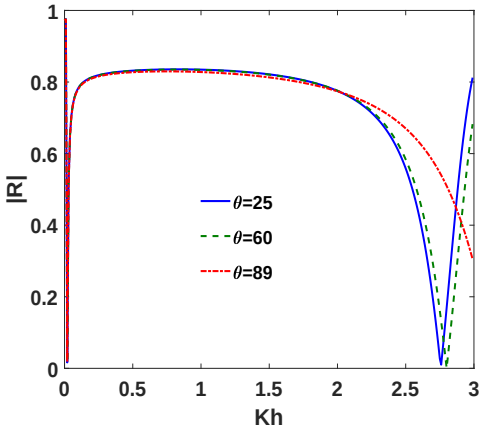

Figure 5.14: Reflection coefficient for type III barrier for different θ with $\frac{a}{h} = 0.2, \frac{b}{h} = 1, \frac{M}{h^2} = 0.5, \frac{(d-c)}{h} = 0.3$.

$|R|$ increases. Also for certain Kh, $|R|$ becomes almost unity showing total reflection of waves.

Figure (5.13) shows the behavior of $|R|$ for different values of $\frac{M}{h^2} = 0.5,\ 1.0,\ 1.5,\ 2.0$ with fixed values of $\frac{a}{h} = 0.2, \frac{b}{h} = 1, \frac{(d-c)}{h} = 0.3, \theta = 25^0$. In case of Type III barrier, the figure shows that increase in surface tension decreases the reflection of wave energy.

Figure (5.14) shows the behavior of $|R|$ for different values of $\theta = 25^0,\ 60^0,\ 89^0$ with fixed values of $\frac{a}{h} = 0.2, \frac{b}{h} = 0.5, \frac{(d-c)}{h} = 0.4, \frac{M}{h} = 0.5$ for Type III barrier. Here $|R|$ exhibits oscillatory behaviour. For large angle of incidence, $\theta = 89^0$, the frequency of oscillation decreases.

5.5 CONCLUSIONS

Oblique wave scattering by thick rectangular barrier in presence of surface tension at the upper surface have been studied here by employing multi-term Galerkin approximation technique. Three different geometrical positions of the barrier are considered here. The numerical estimate of reflection coefficient for different values of wave numbers and other parameters involved in the physical problem have been obtained and

exemplify graphically. The numerical results also satisfy the energy balance relation. The results without surface tension have been recovered from present result by considering very small values of M. From the present study, it is concluded that presence of surface tension decreases the amplitude of reflected waves. The reflection coefficient exhibits oscillatory behaviour as the width and height of the thick barriers increases and a total transmission of waves of certain wavelength are observed.

APPENDIX A

Coefficients of linear system of equations

Barrier of type I

$$\mathcal{V}_{mn}^{SMM} = \Bigg[4(-1)^{m+n}\sum_{r=1}^{\infty}\Bigg\{-\frac{iV(i\gamma_r,h)}{(\gamma_r c)^{\frac{1}{3}}}J_{2m+\frac{1}{6}}(\gamma_r c)J_{2n+\frac{1}{6}}(\gamma_r c) - \coth t_r b\frac{iV(i\alpha_r,c)}{(\alpha_r c)^{\frac{1}{3}}}J_{2m+\frac{1}{6}}(\alpha_r c)J_{2n+\frac{1}{6}}(\alpha_r c)\Bigg\} + (-\cot(\alpha_0^2-\nu^2)^{\frac{1}{2}}b)\frac{V(\alpha_0,c)}{(\alpha_0 c)^{\frac{1}{3}}}I_{2m+\frac{1}{6}}(\alpha_0 c)I_{2n+\frac{1}{6}}(\alpha_0 c)\Bigg] \tag{5.86}$$

$$\mathcal{V}_{mn}^{ANSMM} = \Bigg[4(-1)^{m+n}\sum_{r=1}^{\infty}\Bigg\{-\frac{iV(i\gamma_r,h)}{(\gamma_r c)^{\frac{1}{3}}}J_{2m+\frac{1}{6}}(\gamma_r c)J_{2n+\frac{1}{6}}(\gamma_r c) - \tanh t_r b\frac{iV(i\alpha_r,c)}{(\alpha_r c)^{\frac{1}{3}}}J_{2m+\frac{1}{6}}(\alpha_r c)J_{2n+\frac{1}{6}}(\alpha_r c)\Bigg\} + (\tan(\alpha_0^2-\nu^2)^{\frac{1}{2}}b)\frac{V(\alpha_0,c)}{(\alpha_0 c)^{\frac{1}{3}}}I_{2m+\frac{1}{6}}(\alpha_0 c)I_{2n+\frac{1}{6}}(\alpha_0 c)\Bigg] \tag{5.87}$$

$$\omega_m^{SMM,ANSMM} = \frac{I_{2m+\frac{1}{6}}(\gamma_0 c)}{(\gamma_0 c)^{\frac{1}{6}}}, \quad m = 0,1,...,N. \tag{5.88}$$

Barrier of type II

$$\mathcal{G}_{mn}^{SMM} = \Bigg[4(-1)^{m+n}\sum_{r=1}^{\infty}\Bigg\{-\frac{iV(i\gamma_r,h)}{(\gamma_r a)^{\frac{1}{3}}}J_{2m+\frac{1}{6}}(\gamma_r a)J_{2n+\frac{1}{6}}(\gamma_r a) - \coth u_r b\frac{iV(i\beta_r,a)}{(\beta_r a)^{\frac{1}{3}}}J_{2m+\frac{1}{6}}(\beta_r a)J_{2n+\frac{1}{6}}(\beta_r a)\Bigg\} + (-\cot(\beta_0^2-\nu^2)^{\frac{1}{2}}b)\frac{V(\beta_0,a)}{(\beta_0 a)^{\frac{1}{3}}}I_{2m+\frac{1}{6}}(\beta_0 a)I_{2n+\frac{1}{6}}(\beta_0 a)\Bigg] \tag{5.89}$$

$$\mathcal{G}_{mn}^{ANSMM} = \Bigg[4(-1)^{m+n}\sum_{r=1}^{\infty}\Bigg\{-\frac{iV(i\gamma_r,h)}{(\gamma_r a)^{\frac{1}{3}}}J_{2m+\frac{1}{6}}(\gamma_r a)J_{2n+\frac{1}{6}}(\gamma_r a) - \tanh u_r b\frac{iV(i\beta_r,a)}{(\beta_r a)^{\frac{1}{3}}}J_{2m+\frac{1}{6}}(\beta_r a)J_{2n+\frac{1}{6}}(\beta_r a)\Bigg\} + (\tan(\beta_0^2-\nu^2)^{\frac{1}{2}}b)\frac{V(\beta_0,a)}{(\beta_0 a)^{\frac{1}{3}}}I_{2m+\frac{1}{6}}(\beta_0 a)I_{2n+\frac{1}{6}}(\beta_0 a)\Bigg] \tag{5.90}$$

$$\mathcal{H}_{mn}^{SMM} = -4(-1)^{m+n}\sum_{r=1}^{\infty}\frac{iV(i\gamma_r,h)}{(\gamma_r a)^{\frac{1}{6}}}$$

$$\frac{1}{(\gamma_r(h-c))^{\frac{1}{6}}}J_{2m+\frac{1}{6}}(\gamma_r a)J_{2n+\frac{13}{6}}(\gamma_r(h-c)) \tag{5.91}$$

$$\mathcal{H}_{mn}^{ANSMM} = \mathcal{H}_{m,n-1}^{SMM} \tag{5.92}$$

$$\mathcal{P}_{mn}^{SMM} = \mathcal{H}_{nm}^{SMM} \tag{5.93}$$

$$\mathcal{P}_{mn}^{ANSMM} = \mathcal{P}_{m-1,n}^{SMM} \tag{5.94}$$

$$\mathcal{Q}_{mn}^{SMM} = \Bigg[\frac{12\pi b}{h-c}\frac{2^{\frac{1}{3}}}{\Gamma(\frac{1}{3})^4}\frac{\coth\nu b}{\nu}\delta_{0n}\delta_{0m}$$

$$+(-1)^{m+n}\sum_{r=1}^{\infty}\left\{-\frac{4iV(i\gamma_r,h)}{(\gamma_r(h-c))^{\frac{1}{3}}}\ J_{2m+\frac{13}{6}}(\gamma_r(h-c))J_{2n+\frac{13}{6}}(\gamma_r(h-c))\right.$$

$$\left.+\ \frac{2}{r\pi}\frac{\coth\eta_r b}{(h-c)\eta_r}\frac{J_{2m+\frac{13}{6}}(r\pi)J_{2n+\frac{13}{6}}(r\pi)}{(r\pi)^{\frac{1}{3}}}\right\}\Bigg] \tag{5.95}$$

$$\mathcal{Q}_{mn}^{ANSMM}=\Bigg[\frac{12\pi b}{h-c}\frac{2^{\frac{1}{3}}}{\Gamma(\frac{1}{3})^4}\frac{\tanh\nu b}{\nu}\delta_{0n}\delta_{0m}$$

$$+(-1)^{m+n}\sum_{r=1}^{\infty}\left\{-\frac{4iV(i\gamma_r,h)}{(\gamma_r(h-c))^{\frac{1}{3}}}\ J_{2m+\frac{13}{6}}(\gamma_r(h-c))J_{2n+\frac{13}{6}}(\gamma_r(h-c))\right.$$

$$\left.+\ \frac{2}{r\pi}\frac{\tanh\eta_r b}{(h-c)\eta_r}\frac{J_{2m+\frac{13}{6}}(r\pi)J_{2n+\frac{13}{6}}(r\pi)}{(r\pi)^{\frac{1}{3}}}\right\}\Bigg] \tag{5.96}$$

where $\delta_{0n}=1$ for $n=0$, and $\delta_{0n}=0$ for $n\geq 1$ and $J's$ are Bessel functions of first kind and

$$\omega_m^{(1)SMM}=\frac{I_{2m+\frac{1}{6}}(\gamma_0 a)}{(\gamma_0 a)^{\frac{1}{6}}},\quad m=0,1,...,N. \tag{5.97}$$

$$\omega_m^{(1)ANSMM}=\omega_m^{(1)SMM} \tag{5.98}$$

$$\omega_m^{(2)SMM}=\frac{I_{2m+\frac{13}{6}}(\gamma_0(h-c))}{(\gamma_0(h-c))^{\frac{1}{6}}},m=0,1,...,N. \tag{5.99}$$

$$\omega_m^{(2)ANSMM}=\omega_{m-1}^{(2)SMM} \tag{5.100}$$

Barrier of type III

$$R^{SMM}=\Bigg[4(-1)^{m+n}\sum_{r=1}^{\infty}\left\{-\frac{iV(i\gamma_r,h)}{(\gamma_r a)^{\frac{1}{3}}}J_{2m+\frac{1}{6}}(\gamma_r a)J_{2n+\frac{1}{6}}(\gamma_r a)\right.$$

$$\left.-\ \coth u_r b\frac{iV(i\beta_r,a)}{(\beta_r a)^{\frac{1}{3}}}J_{2m+\frac{1}{6}}(\beta_r a)J_{2n+\frac{1}{6}}(\beta_r a)\right\}$$

$$+(-\cot(\beta_0^2-\nu^2)^{\frac{1}{2}}b)\frac{V(\beta_0,a)}{(\beta_0 a)^{\frac{1}{3}}}I_{2m+\frac{1}{6}}(\beta_0 a)I_{2n+\frac{1}{6}}(\beta_0 a)\Bigg] \tag{5.101}$$

$$R_{mn}^{ANSMM}=\Bigg[4(-1)^{m+n}\sum_{r=1}^{\infty}\Bigg\{-\frac{iV(i\gamma_r,h)}{(\gamma_r a)^{\frac{1}{3}}}J_{2m+\frac{1}{6}}(\gamma_r a)J_{2n+\frac{1}{6}}(\gamma_r a)$$

$$-\tanh u_r b\frac{iV(i\beta_r,a)}{(\beta_r a)^{\frac{1}{3}}}J_{2m+\frac{1}{6}}(\beta_r a)J_{2n+\frac{1}{6}}(\beta_r a)\Bigg\}$$

$$+(\tan(\beta_0^2-\nu^2)^{\frac{1}{2}}b)\frac{V(\beta_0,a)}{(\beta_0 a)^{\frac{1}{3}}}I_{2m+\frac{1}{6}}(\beta_0 a)I_{2n+\frac{1}{6}}(\beta_0 a)\Bigg] \tag{5.102}$$

$$S_{mn}^{SMM,ANSMM}=-4\sum_{r=1}^{\infty}\frac{iV(i\gamma_r,h)}{(\gamma_r a)^{\frac{1}{6}}}$$

$$\frac{\cos(\frac{n\pi}{2}-\gamma_r(h-\frac{c+d}{2}))}{\cos(\gamma_r h)(\gamma_r\frac{d-c}{2})^{\frac{1}{6}}}J_{2m+\frac{1}{6}}(\gamma_r a)J_{n+\frac{1}{6}}(\gamma_r\frac{d-c}{2}) \tag{5.103}$$

$$S_{mn}^{SMM,ANSMM}=X_{nm}^{SMM,ANSMM} \tag{5.104}$$

$$Y_{mn}^{SMM}=\Bigg[2\sum_{r=1}^{\infty}\{-2iV(i\gamma_r,h)\ \cos(\frac{n\pi}{2}-\gamma_r(h-\frac{c+d}{2}))$$

$$\frac{\cos(\frac{m\pi}{2}-\gamma_r(h-\frac{c+d}{2}))}{\cos(\gamma_r h)^2}\frac{J_{m+\frac{1}{6}}(\gamma_r\frac{d-c}{2})J_{n+\frac{1}{6}}(\gamma_r\frac{d-c}{2})}{(\gamma_r\frac{d-c}{2})^{\frac{1}{3}}}$$

$$+\frac{coth\zeta_r b}{(d-c)\zeta_r}\cos\Big\{\frac{m\pi}{2}-\frac{r\pi}{2}\Big\}\cos\Big\{\frac{n\pi}{2}-\frac{r\pi}{2}\Big\}\frac{J_{m+1/6}(\frac{r\pi}{2})J_{n+1/6}(\frac{r\pi}{2})}{(\frac{r\pi}{2})^{1/3}}\Bigg\}$$

$$+\frac{12\pi}{(d-c)}\frac{2^{1/3}}{(\Gamma(1/3))^4}\frac{\coth\nu b}{\nu}\delta_{0m}\delta_{0n}\Bigg] \tag{5.105}$$

where $\delta_{0n}=1$ for $n=0$, and $\delta_{0n}=0$ for $n\geq 1$.

$$Y_{mn}^{ANSMM}=\Bigg[2\sum_{r=1}^{\infty}\{-2iV(i\gamma_r,h)\ \cos(\frac{n\pi}{2}-\gamma_r(h-\frac{c+d}{2}))$$

$$\frac{\cos(\frac{m\pi}{2}-\gamma_r(h-\frac{c+d}{2}))}{\cos(\gamma_r h)^2}\frac{J_{m+\frac{1}{6}}(\gamma_r\frac{d-c}{2})J_{n+\frac{1}{6}}(\gamma_r\frac{d-c}{2})}{(\gamma_r\frac{d-c}{2})^{\frac{1}{3}}}$$

$$+\frac{\tanh\zeta_r b}{(d-c)\zeta_r}\cos\left\{\frac{m\pi}{2}-\frac{r\pi}{2}\right\}\cos\left\{\frac{n\pi}{2}-\frac{r\pi}{2}\right\}\frac{J_{m+1/6}(\frac{r\pi}{2})J_{n+1/6}(\frac{r\pi}{2})}{(\frac{r\pi}{2})^{1/3}}\Bigg\}$$

$$+\frac{12\pi}{(d-c)}\frac{2^{1/3}}{(\Gamma(1/3))^4}\frac{\tanh\nu b}{\nu}\delta_{0m}\delta_{0n}\Bigg] \tag{5.106}$$

$$\omega 1_m^{(1)SMM,ANSMM}=\frac{I_{2m+1/6}(\gamma_0 a)}{(\gamma_0 a)^{\frac{1}{6}}} \tag{5.107}$$

$$\omega 1_m^{(2)SMM,ANSMM}=\frac{(-1)^m e^{\gamma_0(h-\frac{c+d}{2})}e^{-\gamma_0(h-\frac{c+d}{2})}}{2\cosh\gamma_0 h}\frac{I_{m+1/6}(\gamma_0\frac{d-c}{2})}{(\gamma_0\frac{d-c}{2})^{\frac{1}{6}}} \tag{5.108}$$

where $I's$ are modified Bessel function of first kind.

CHAPTER 6

WATER WAVE SCATTERING BY THICK RECTANGULAR SLOTTED BARRIERS IN PRESENCE OF ICE COVER

6.1 INTRODUCTION

Breakwater type coastal structures are designed to dissipate the wave energy so that they protect the harbours and mariners from the effect of rough sea. Breakwaters also reduce the intensity of wave action in inshore waters and thereby provide safe harbourage. Breakwaters in form of slotted barrier provides a number of desirable features such as the wave energy reflected by them is small which is very useful for navigating vessels within the harbour near them, and also they permit the circulation of water and so as to assist in maintenance of the water quality in the harbour [cf. Bennet *et*

[0]† The content of this chapter is based on the paper " Water wave scattering by thick rectangular slotted barriers in presence of ice cover".

al. 1992] . These usefulness of slotted breakwaters motivated us to consider slotted thick barrier as models of breakwaters in the present study. Here two types of slotted barriers are considered, one is bottom standing and other is submerged in the form of submerged slotted thick barrier.

Many researchers studied the problem of water wave scattering by thin vertical slotted barriers in deep water or water of finite depth by using various mathematical techniques, assuming linear theory. Lewin (1963) studied the propagation of water waves in presence of N-vertical barriers present in deep water. Porter (1972) used integral equation formulation based on reduction method to study the wave motion in presence of barrier with a gap. Porter (1974) considered a problem of wave propagation in presence of an arbitrarily arranged barriers which perform small rolling or swaying oscillations.

Scattering of waves by vertical barriers in water of finite-depth were studied by Porter and Evans (1995). They used multi-term Galerkin approximation to get the accurate estimated of reflection and transmission coefficients. Issacson *et al.* (1998) considered wave interaction with a thin vertical slotted barrier and used eigenfunction expansion method to study the problem. Kanoria *et al.* (1999) considered the problem of water wave scattering by four types of barrier configurations namely surface piercing and partially immersed, or bottom-standing and submerged, or in the form of a submerged rectangular block, or in the form of a thick vertical wall with a submerged gap. They used multi-term Galerkin approximation to solve the integral equations arising in the problem.

Oblique water wave diffraction by thin vertical barriers in water of uniform finite depth was studied by Mandal and Dolai (1994). They considered four different types of the barrier configurations namely partially immersed, bottom standing, submerged plate, a thin vertical wall with a submerged gap. They used an appropriate one-term Galerkin approximation to get a very accurate upper and lower bounds for the reflection and transmission coefficients. Banerjea *et al.* (1996) considered the problem of oblique wave scattering by a single and two submerged thin verical wall(s) with a gap present in water of finite-depth. They used both one-term and multi-term Galerkin

approximation to study the problem. Das *et al.* (1997) studied the problem of oblique water wave diffraction by two parallel thin barriers with gaps.

In cold regions, floating ice sheets constitute an integral part of the human activities like airstrips and other transportation links. Obviously there is a need to establish a reliable safety criterion, which can only be accomplished by systematic studies of the response of the ice sheet. Chakrabarti (2000) solved the mixed boundary-value problem arising in the study of scattering of two dimensional time harmonic surface water waves by a discontinuity on the surface boundary conditions, separating the free surface and an ice-covered surface when the depth of water is infinite. Interaction of ocean waves with shore fast sea ice modelled as a thin elastic plate was first considered by Fox and Squire (1990). Later, Fox and Squire (1994) reported a mathematical model describing the oblique reflecion and penetration of ocean waves into shore fast ice sheet. Scattering of an obliquely incident flexural-gravity wave by a narrow straight-line crack separating two semi-infinite thin elastic plates floating on water of finite depth were studied by Evans and Porter (2003). The reflection and transmission of waves under an ice sheet of variable thickness were studied by Vaughan and Squire (2006). They used piecewise polynomials to solve this problem. Das and Mandal (2008) investigated the problem of radiation of water waves by a sphere submerged in deep water as well as uniform finite depth water with an ice cover. They used multipole method to solve this problem. Squire (2007) described the general area of ocean wave or sea ice interactions in his review paper. In a regime of linear theory, Sturova (2011) studied the two dimensional problem of steady oscillations of a horizontal cylinder submerged in a linearly stratified fluid layer whose upper boundary is ice cover. She used Boussinesq approximation for solving this problem. Assuming small amplitude linear wave theory, Bhattacharjee and Soares (2012) studied the behavior of flexural gravity waves propagating over a semi-infinite floating ice sheet.

In the present study, we consider the problem of water wave scattering by a thick rectangular slotted barrier present in water of finite depth with ice cover. Here, the slotted barrier has arbitrary number of slots of unequal lengths along the vertical direction. Two types of barrier configuration are considered, one is bottom standing and the other is in the form of a submerged slotted thick block. We consider the train of surface wave which is obliquely incident on the slotted barriers. Exploiting the geometrical symmetry of the rectangular slotted barrier about its center line taken, the

problem for all the cases is split into two separate boundary value problems involving the symmetric and antisymmetric potential functions describing the resultant motion in the fluid region. The eigenfunction expansion of the potential function is used to reduce the problem into a first kind integral equation in disjoint intervals. The integral equation is solved analytically using multi-term Galerkin approximations involving ultraspherical Gegenbauer polynomials. Numerical estimates for the reflection and transmission coefficients are obtained for different values of the parameters. Numerical results of the reflection coefficients are studied graphically against the non-dimensional wave number.

6.2 FORMULATION OF THE PROBLEM

We consider a long thick barrier of rectangular cross section of width $2b$ with $q-1(q \geq 2)$ number of slots present in water of uniform finite depth h. We choose y-axis vertically downwards along the vertical line of symmetry of the barrier and xz-plane coinciding with the ice cover surface at rest. Two types of barrier configuration are considered, one is bottom standing (Type I) and the other is in the form of a submerged slotted thick block (Type II). In both types of barrier, the barrier is placed at a depth a_1 from the ice cover surface and for Type II barrier there is a gap (a_{2q}, h) above the bottom of the water region. The wetted part of the barrier occupies the region $-b \leq x \leq b, y \in L = L_j(j = 1, 2)$. Here

$$L_1 = \bigcup_{l=0}^{q-1}(a_{2l+1}, a_{2l+2})(0 < a_1 < a_2 < ... < a_{2q} = h),$$

$$L_2 = \bigcup_{l=0}^{q-1}(a_{2l+1}, a_{2l+2})(0 < a_1 < a_2 < ... < a_{2q} < h).$$

L_1 and L_2 corresponds, respectively, to the Type I and Type II barrier configurations and the slot in the barrier is given by

$$G_1 = \bigcup_{l=1}^{q-1}(a_{2l}, a_{2l+1}), \text{ for Type I and Type II barrier.}$$

The length of the each slot is $2y_l$, then

$$2y_l = a_{2l+1} - a_{2l} \tag{6.1}$$

where $l = 1, 2, ..., q-1$ for Type I barrier and Type II barrier and the length of the gap above the bottom of the water region for Type II barrier is

$$2y_q = h - a_{2q}.$$

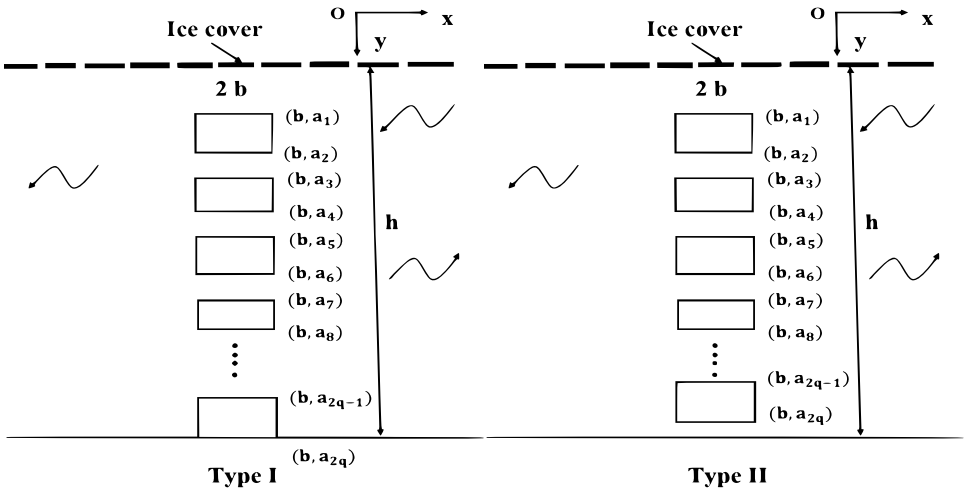

Figure 6.1: Schematic diagram of the problem

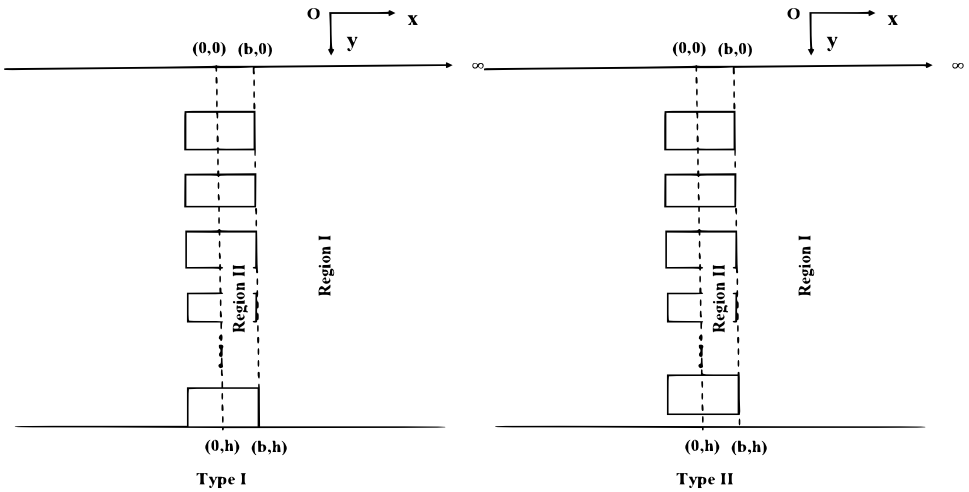

Figure 6.2: Subregions of the problem

A train of surface water waves of frequency σ, from positive infinity is incident obliquely on a thick slotted barrier and is partially reflected by the barrier and partially

transmitted through the slotted barrier. The wave makes an angle θ with the plane $y = 0$. Under the assumption of linear theory, the resulting motion is described by the velocity potential $\Phi(x, y, z, t)$ which may be expressed as

$$\Phi(x, y, z, t) = Re\{\phi(x, y)e^{i\nu z - i\sigma t}\} \tag{6.2}$$

where ν is the wave number in the z-direction. Then $\phi(x, y)$ satisfies

$$(\nabla^2 - \nu^2)\phi = 0 \quad \text{in the fluid region,} \tag{6.3}$$

$$\left\{ D(\frac{\partial^2}{\partial x^2} - \nu^2)^2 + 1 - \epsilon K \right\} \phi_y + K\phi = 0 \quad \text{on y=0}, -\infty < x < \infty, \tag{6.4}$$

with $K = \sigma^2/g$ (g being the acceleration due to gravity),

$$\phi_x = 0 \ \text{ on } \ x = \pm b, \ \ y \in L_i, \ i = 1, 2, \tag{6.5}$$

$$r^{\frac{1}{3}} \nabla\phi \ \text{ is bounded as } \ r \to 0, \tag{6.6}$$

where r is the distance from any submerged edge of the thick barrier,

$$\phi_y = 0 \quad \text{on} \quad y = a_i (i = 1, 2, ..., m_j; j = 1, 2), \ \ |x| < b, \tag{6.7}$$

where $m_1 = 2q - 1, m_2 = 2q$,

$$\phi_y = 0 \quad \text{on} \quad y = h, \ \begin{cases} |x| > b \ \text{ for Type I barrier,} \\ |x| < \infty \ \text{ for Type II barrier,} \end{cases} \tag{6.8}$$

$$\phi(x, y) \sim \begin{cases} (e^{-i\mu(x-b)} + Re^{i\mu(x-b)})\psi_0(y) \ \text{ as } \ x \to \infty, \\ Te^{-i\mu(x-b)}\psi_0(y) \qquad \text{as } \ x \to -\infty. \end{cases} \tag{6.9}$$

Here R and T denote, respectively, the complex reflection and transmission coefficients and are to be determined. Here $\mu = (\lambda_0^2 - \nu^2)^{\frac{1}{2}} = \lambda_0 \cos\theta, \nu = \lambda_0 \sin\theta$, where λ_0

denotes the positive real roots of the usual dispersion relation

$$\lambda(1-\epsilon K+D\lambda^4)\tanh\lambda h=K. \tag{6.10}$$

It may be noted that (6.10) has a real positive root λ_0, four complex roots $\pm\lambda_1$ and $\pm\lambda_2(\lambda_1$ has positive real and imaginary parts with $\lambda_2=\bar{\lambda_1})$ and a set of countably infinite purely imaginary roots $\pm i\lambda_n^*(\lambda_n^*>0, n=1,2,...)$, where

$$(n-\frac{1}{2})\pi<\lambda_n^* h<n\pi$$

and

$$\lambda_n^* h\to n\pi \quad \text{as} \quad n\to\infty$$

and also

$$\psi_0(y)=\mathcal{P}_0^{-\frac{1}{2}}\cosh\lambda_0(h-y) \tag{6.11}$$

with

$$\mathcal{P}_0=\frac{1}{2}(1+\frac{\sinh 2\lambda_0 h}{2\lambda_0 h}).$$

6.3 METHOD OF SOLUTION

Due to geometrical symmetry about $x=0$, we may consider symmetric and antisymmetric motion independently, defined by the potentials $\phi^{1,2}(x,y)$ respectively, satisfying Eqs. (6.2)-(6.8) and

$$\phi^1(x,y)=\phi^1(-x,y);\quad \phi^2(x,y)=-\phi^2(-x,y). \tag{6.12}$$

Thus we may restrict our analysis to the region $x\geq 0$ only with additional boundary conditions

$$\phi_x^1(0,y)=0, \phi^2(0,y)=0 \tag{6.13}$$

and recover the wave field in the region $x < 0$ from relation (6.12).

Let the behaviours of $\phi^{1,2}(x, y)$ as $x \to \infty$ be represented by

$$\phi^{1,2}(x, y) \sim [e^{-i\mu(x-b)} + R^{1,2}e^{i\mu(x-b)}]\psi_0(y) \tag{6.14}$$

where $R^{1,2}$ are unknown constants related to R and T by

$$R, T = \frac{1}{2}(R^1 \pm R^2)e^{-2i\mu b} \tag{6.15}$$

obtained after using (6.14) in (6.9).

We now divide the region $0 < x < \infty;\ 0 < y < h$ into two regions, viz, Region I: $x > b;\ 0 < y < h$ and Region II: $0 < x < b,\ y \in \bar{L}_j = (0, h) - L_j,\ j = 1, 2.$

The eigenfunction expansions of $\phi^{1,2}(x, y)$ satisfying Equations (6.3)-(6.5), (6.7) and (6.8)(for $x \geq 0$) and Equations (6.13) and (6.14) in the different regions are given below.

Region I $(x > b, 0 < y < h)$:

In this region a suitable eigen function expansion for $\phi^{1,2}(x, y)$ are given by

$$\phi^{1,2}(x, y) = [e^{-i\mu(x-b)} + R^{1,2}e^{i\mu(x-b)}]\psi_0(y) + \sum_{n=1}^{2} A_n^{1,2} e^{i\xi_n(\lambda_n^2-\nu^2)^{\frac{1}{2}}(x-b)}\psi_n(y)$$

$$+ \sum_{n=1}^{\infty} A_n^{*1,2} e^{-s_n(x-b)}\psi_n^*(y) \tag{6.16}$$

where

$$\xi_n = \begin{cases} 1, n = 1, \\ -1, n = 2, \end{cases} \tag{6.17}$$

$$\psi_n(y) = \mathcal{P}_n^{-\frac{1}{2}} \cosh \lambda_n(h - y) \tag{6.18}$$

with

$$\mathcal{P}_n = \frac{1}{2}(1 + \frac{\sinh 2\lambda_n h}{2\lambda_n h}), n = 1, 2, \tag{6.19}$$

and

$$\psi_n^*(y) = (\mathcal{P}_n^*)^{-\frac{1}{2}} \cos \lambda_n^*(h-y) \tag{6.20}$$

with

$$\mathcal{P}_n^* = \frac{1}{2}(1 + \frac{\sin 2\lambda_n^* h}{2\lambda_n^* h}), n = 1, 2, ..., \tag{6.21}$$

where $\lambda_n^*(n = 1, 2, ..)$ are the positive roots of the equation

$$\lambda(1 - \epsilon K + D\lambda^4) \tan \lambda h + K = 0 \tag{6.22}$$

and

$$s_n = ((\lambda_n^*)^2 + \nu^2)^{\frac{1}{2}}.$$

It may be noted here that $\{\psi_n(y)\}'s$ are orthogonal functions and so are $\{\psi_n^*(y)\}'s$. However, $\psi_n(y)$ and $\psi_n^*(y)$ satisfy modified orthogonality relation as given in Manam *et al.* (2006). These orthogonality relations are required to determine the constants $A_n^{1,2}$, $A_n^{*1,2}$ which are evaluated in later section.

Region II $(0 < x < b, y \in \bar{L} \equiv \bar{L_j} = (0, h) - L_j, j = 1, 2)$:

In this region, we have considered two subregions, namely a region bounded above by the ice cover surface and below by the upper rigid plane surface of the uppermost rectangular block and another region is the gap between the uppermost rectangular block and the lowermost rectangular block/bottom surface of water region as shown in Figure 6.2.

For the region defined by $0 < x < b, 0 < y < a_1$, the eigen function expansion is given by

$$\left\{ \begin{array}{c} \phi^1(x,y) \\ \phi^2(x,y) \end{array} \right\} = \sum_{n=0}^{2} \left\{ \begin{array}{c} E_n^1 \cos{(\beta_n^2 - \nu^2)^{\frac{1}{2}}x} \\ E_n^2 \xi_n \sin{(\beta_n^2 - \nu^2)^{\frac{1}{2}}x} \end{array} \right\} \bar{\psi}_n(y) + \sum_{n=1}^{\infty} \left\{ \begin{array}{c} E_n^{*1} \cosh t_n x \\ E_n^{*2} \sinh t_n x \end{array} \right\} \bar{\psi}_n^*(y) \tag{6.23}$$

where $\xi_0 = 1,\ \xi_n,\ n = 1, 2$ are defined in equation (6.17),

$$t_n = ((\beta_n^*)^2 + \nu^2)^{\frac{1}{2}}, n = 1, 2, ..., \tag{6.24}$$

$$\bar{\psi}_0(y) = \mathcal{M}_0^{-\frac{1}{2}} \cosh \beta_0(a_1 - y),$$

$$\mathcal{M}_0 = \frac{1}{2}(1 + \frac{\sinh 2\beta_0 a_1}{2\beta_0 a_1}), \tag{6.25}$$

$$\bar{\psi}_n(y) = \mathcal{M}_n^{-\frac{1}{2}} \cosh \beta_n(a_1 - y),$$

$$\mathcal{M}_n = \frac{1}{2}(1 + \frac{\sinh 2\beta_n a_1}{2\beta_n a_1}), n = 1, 2, \tag{6.26}$$

$$\bar{\psi}_n^*(y) = (\mathcal{M}_n^*)^{-\frac{1}{2}} \cos \beta_n^*(a_1 - y),$$

$$\mathcal{M}_n^* = \frac{1}{2}(1 + \frac{\sin 2\beta_n^* a_1}{2\beta_n^* a_1}), n = 1, 2, ..., \tag{6.27}$$

$\beta_0, \beta_1, \beta_2$ satisfies

$$\beta(1 - \epsilon K + D\beta^4) \tanh \beta a_1 = K \tag{6.28}$$

and β_n^* satisfies

$$\beta(1 - \epsilon K + D\beta^4) \tan \beta a_1 + K = 0, n = 1, 2, ... \tag{6.29}$$

For the region defined by $0 < x < b, a_{2l} < y < a_{2l+1}$, where $l = 1, 2, ..., q-1$ for Type I barrier and $l = 1, 2, ..., q$ for Type II barrier, the normalised eigenfunctions are

$$\kappa_n(l, y) = \epsilon_n^{\frac{1}{2}} \cos \frac{n\pi}{2y_l}(a_{2l+1} - y) \tag{6.30}$$

where $\epsilon_0 = 1, \epsilon_n = 2, n \geq 1$.

Thus the representation of $\phi^{1,2}$ in this region is

$$\left\{ \begin{array}{l} \phi^1(x,y) \\ \phi^2(x,y) \end{array} \right\} = \left\{ \begin{array}{l} B_0^1(l)\cosh\nu x \\ B_0^2(l)\sinh\nu x \end{array} \right\} \kappa_0(l,y) + \sum_{n=1}^{\infty} \left\{ \begin{array}{l} B_n^1(l)\cosh\xi_n(l)x \\ B_n^2(l)\sinh\xi_n(l)x \end{array} \right\} \kappa_n(l,y) \tag{6.31}$$

where

$$\xi_n(l) = \left\{ \left(\frac{n\pi}{2y_l}\right)^2 + \nu^2 \right\}^{\frac{1}{2}}, n = 1, 2, ... \tag{6.32}$$

We now define

$$\phi_x^{1,2}(b+0,y) = f^{1,2}(y), 0 < y < h. \tag{6.33}$$

Then

$$f^{1,2}(y) = 0 \quad for \quad y \in L_j, j = 1, 2 \tag{6.34}$$

and

$$\phi_x^{1,2}(b-0,y) = f^{1,2}(y) \quad for \quad y \in \bar{L}. \tag{6.35}$$

Also due to the edge conditions (6.6),

$$f^{1,2}(y) = O(|(y-a_i)|^{-\frac{1}{3}}) \quad as \quad y \to a_i, (i = 1, 2, ...m_j; j = 1, 2). \tag{6.36}$$

Using the expansion (6.16) in (6.33) followed by Havelock's inversion formula produces, after noting (6.34),

$$\begin{aligned} A_n^{1,2} = i\xi_n U(\lambda_n) \Bigg[& \int_{\bar{L}} f^{1,2}(y)\psi_n(y)dy \\ & -\frac{D}{K}\lambda_n \tanh(\lambda_n h) \left\{ \lambda_n^2 f_y^{1,2}(0) + f_{yyy}^{1,2}(0) \right\} \Bigg], n = 0, 1, 2, \end{aligned} \tag{6.37}$$

with

$$A_0^{1,2} = 1 - R^{1,2}$$

and

$$A_n^{*1,2} = iU(i\lambda_n^*)\left[\int_{\bar{L}} f^{1,2}(y)\psi_n^*(y)dy - \frac{D}{K}\lambda_n^*\tan(\lambda_n^* h)\left\{(\lambda_n^*)^2 f_y^{1,2}(0) - f_{yyy}^{1,2}(0)\right\}\right], n = 1, 2, ..., \quad (6.38)$$

where

$$U(u) = \frac{4u(Du^4 + 1 - \epsilon K)\cosh^2 uh}{\sqrt{(u^2 - \nu^2)}\left\{(Du^4 + 1 - \epsilon K)2uh + (5Du^4 + 1 - \epsilon K)\sinh 2uh\right\}}. \quad (6.39)$$

Again, use of the expansion (6.31) in (6.35) followed by Fourier inversion formula produces

$$B_0^1(l) = \frac{1}{2y_l}\frac{1}{\nu\sinh\nu b}\int_{a_{2l}}^{a_{2l+1}} f^1(u)\kappa_0(l,u)du, \quad (6.40)$$

$$B_n^1(l) = \frac{1}{2y_l}\frac{1}{\xi_n(l)\sinh\xi_n(l)b}\int_{a_{2l}}^{a_{2l+1}} f^1(u)\kappa_n(l,u)du, n = 1, 2, ..., \quad (6.41)$$

$$B_0^2(l) = \frac{1}{2y_l}\frac{1}{\nu\cosh\nu b}\int_{a_{2l}}^{a_{2l+1}} f^2(u)\kappa_0(l,u)du, \quad (6.42)$$

$$B_n^2(l) = \frac{1}{2y_l}\frac{1}{\xi_n(l)\cosh\xi_n(l)b}\int_{a_{2l}}^{a_{2l+1}} f^2(u)\kappa_n(l,u)du, n = 1, 2, ... \quad (6.43)$$

The constants $E_n^{1,2}$, $E_n^{*1,2}$ in (6.23) are obtained similarly as

$$E_n^{1,2} = V(\beta_n)\left(-\frac{1}{\sin(\beta_n^2 - \nu^2)^{\frac{1}{2}}b}, \frac{1}{\cos(\beta_n^2 - \nu^2)^{\frac{1}{2}}b}\right) \left[\int_0^{a_1} f^{1,2}(y)\bar{\psi}_n(y)dy - \frac{D}{K}\beta_n\tanh(\beta_n a_1)\left\{\beta_n^2 f_y^{1,2}(0) + f_{yyy}^{1,2}(0)\right\}\right], n = 0, 1, 2, \quad (6.44)$$

$$E_n^{*1,2} = iV(i\beta_n^*)\left(\frac{1}{\sinh t_n b}, \frac{1}{\cosh t_n b}\right)$$
$$\left[\int_0^{a_1} f^{1,2}(y)\bar{\psi}_n^*(y)dy - \frac{D}{K}\beta_n^*\tan(\beta_n^* a_1)\left\{(\beta_n^*)^2 f_y^{1,2}(0) - f_{yyy}^{1,2}(0)\right\}\right], n = 1, 2, ... \quad (6.45)$$

where

$$V(u) = \frac{4u(Du^4 + 1 - \epsilon K)\cosh^2 ua_1}{\sqrt{(u^2 - \nu^2)}\left\{(Du^4 + 1 - \epsilon K)2ua_1 + (5Du^4 + 1 - \epsilon K)\sinh 2ua_1\right\}}. \quad (6.46)$$

Now, matching of $\phi^{1,2}(x, y)$ across the line $x = b$ through the right corner points of the gaps, produces the relations

$$\phi^{1,2}(b + 0, y) = \phi^{1,2}(b - 0, y), y \in \bar{L} \quad (6.47)$$

which eventually give rise to the integral equations

$$\int_{\bar{L}} M^{1,2}(y, u)F^{1,2}(u)du = \psi_0(y), y \in \bar{L} \quad (6.48)$$

where

$$F^{1,2}(y) = \frac{1}{1 + R^{1,2}} f^{1,2}(y) \quad (6.49)$$

and $M^{1,2}(y, u)(y, u \in \bar{L})$ are real and symmetric in y and u, and their expressions for $\bar{L} = \bar{L}_j(j = 1, 2)$ are given in Appendix A.

If we now define the constants $c^{1,2}$ by

$$c^{1,2} = -i\frac{1 - R^{1,2}}{1 + R^{1,2}} \quad (6.50)$$

then, by using the relations (6.37) and (6.50), we find that

$$\int_{\bar{L}} F^{1,2}(y)\psi_0(y)dy = c^{1,2}. \quad (6.51)$$

It is important to note that $F^{1,2}(y)$ and $c^{1,2}$ are all real quantities. Thus, if the inte-

gral equation (6.48) are solved, then these solutions can be utilized to obtain $c^{1,2}$ from the relations (6.51), which in turn produce the reflection and transmission coefficients $|R|$ and $|T|$, respectively, by using

$$|R| = \frac{|1 + c^1 c^2|}{\Delta}, |T| = \frac{|c^1 - c^2|}{\Delta} \tag{6.52}$$

where

$$\Delta = \left\{1 + (c^1)^2 + (c^2)^2 + (c^1 c^2)^2\right\}^{\frac{1}{2}}$$

so that $|R|^2 + |T|^2 = 1$ as expected from the energy consideration. We shall now proceed to solve the integral equation (6.48) by two methods, viz, Galerkin approximation method and Boundary Element method.

Galerkin approximation method

Galerkin approximation method is employed to find approximate solution of integral equation (6.48). The functions $F^{1,2}$ are approximated as

$$F^{1,2}(y) \approx \mathcal{F}^{1,2}(y), y \in \bar{L} \tag{6.53}$$

where $\mathcal{F}^{1,2}(y)$ have the expansions given by

$$\mathcal{F}^{1,2}(y) = \begin{cases} \sum_{n=0}^{N} p_n^{1,2} f_n(y), 0 < y < a_1, & \text{for Type I,II barrier,} \\ \sum_{n=0}^{N} b_n^{1,2}(l) g_n^{1,2}(l, y), a_{2l} < y < a_{2l+1}, l = 1, 2, ..., q-1, & \text{for Type I,II barrier,} \\ \sum_{n=0}^{N} w_n^{1,2} h_n^{1,2}(y), a_{2q} < y < h, & \text{for Type II barrier.} \end{cases} \tag{6.54}$$

In equation (6.54), $\mathcal{F}^{1,2}(y)$ is approximated by suitable basis functions $f_n(y), g_n^{1,2}(l, y)$ and $h_n^{1,2}(y)$ which are ultraspherical Gegenbauer polynomials and the details are given in Appendix B. The constants $p_n^{1,2}, b_n^{1,2}(l)$ *and* $w_n^{1,2}(n = 0, 1, 2, ..., N)$ are unknown which are to be determined. We note that in $(0, a_1)$, we use the same set of basis functions for the symmetric and antisymmetric cases.

We substitute the expansions (6.54) in the integral equation (6.48) for $\bar{L} = \bar{L_j}(j = 1, 2)$ and using orthogonality properties of the basis functions, we obtain this following

system of linear equations for determination of the unknown constants $p_n^{1,2}, b_n^{1,2}(l)$ *and* $w_n^{1,2}(n = 0, 1, 2, ..., N)$

$$\sum_{n=0}^{N} p_n^{1,2} G_{mn}^{1,2} + \sum_{l=1}^{q-1} \sum_{n=0}^{N} b_n^{1,2}(l) K_{mn}^{1,2}(l) + \sum_{n=0}^{N} w_n^{1,2} H_{mn}^{1,2} = d_m, m = 0, 1, 2, ..., N,$$

$$\sum_{n=0}^{N} p_n^{1,2} P_{mn}^{1,2}(l) + \sum_{l_1=1, l_1 \neq l}^{q-1} \sum_{n=0}^{N} b_n^{1,2}(l_1) R_{mn}^{1,2}(l, l_1) + \sum_{n=0}^{N} b_n^{1,2}(l) Q_{mn}^{1,2}(l)$$

$$+ \sum_{n=0}^{N} w_n^{1,2} T_{mn}^{1,2}(l) = d_m^{1,2}(l), m = 0, 1, 2, ..., N; l = 1, 2, ..., q-1,$$

$$\sum_{n=0}^{N} p_n^{1,2} X_{mn}^{1,2} + \sum_{l=1}^{q-1} \sum_{n=0}^{N} b_n^{1,2}(l) Y_{mn}^{1,2}(l) + \sum_{n=0}^{N} w_n^{1,2} Z_{mn}^{1,2} = d_m^{1,2}(q), m = 0, 1, 2, ..., N; \text{for Type II barrier.} \tag{6.55}$$

It is noted that $H_{mn}^{1,2}, T_{mn}^{1,2}(l), X_{mn}^{1,2}, Y_{mn}^{1,2}(l), Z_{mn}^{1,2}$ *and* $d_m^{1,2}(q)$ does not exist for Type I barrier because it is bottom standing barrier so that there is no gap between the lowermost block and the bottom of water region. The expressions $G_{mn}^{1,2}, K_{mn}^{1,2}(l)$ etc. are given in Appendix C.

The constants $c^{1,2}$ in this case are now approximately obtained by using relation (6.51) and are given by

$$c^{1,2} = \sum_{n=0}^{N} p_n^{1,2} d_n + \sum_{l_1=1}^{q-1} \sum_{n=0}^{N} b_n^{1,2}(l_1) d_n^{1,2}(l_1) + \sum_{n=0}^{N} w_n^{1,2} d_n^{1,2}(q). \tag{6.56}$$

Boundary Element Method

In this method, the unknown function in the integral equation (6.48) is $F^{1,2}(y)$ which has one third singularity in the points $a_i (i = 1, 2, ..., m_j; j = 1, 2)$ where $m_1 = 2q - 1, m_2 = 2q$. So, we define

$$F^{1,2}(y) = \sqrt[3]{(y - a_1)(y - a_2)...(y - m_j)} \mathcal{F}^{1,2}(y) \tag{6.57}$$

where $\mathcal{F}^{1,2}(y)$ is a regular function in $\bar{L}$.

Substituting (6.57) in the I.E. (6.48), we reformulate the integral equation as

$$\int_{\bar{L}} \mathcal{M}^{1,2}(y,u)\mathcal{F}^{1,2}(u)du = \psi_0(y),\ y \in \bar{L} \tag{6.58}$$

where

$$\mathcal{M}^{1,2}(y) = \sqrt[3]{(y-a_1)(y-a_2)...(y-m_j)}M^{1,2}(y). \tag{6.59}$$

Now we divide the intervals $[a_{2l}, a_{2l+1}]$ in $\bar{L}$ into n_l subintervals such that $[a_{2l}, a_{2l+1}] = \cup_{i=1}^{n_l}[b_{l,i-1}, b_{l,i}]$ with $b_{l,0} = a_{2l}, b_{l,i} = b_{l,0} + ir_l, r_l = \frac{a_{2l+1}-a_{2l}}{n_l}, l = 0, 1, 2, ...q-r;\ r = 1$ for Type I barrier and $r = 0$ for Type II barrier with $a_{2q+1} = h$.

Now we take $u = u1_{l,i} \in [b_{l,i-1}, b_{l,i}],\ y = y1_{m,K_v} \in [b_{m,K_v-1}, b_{m,K_v}], i, K_v = 1, 2, ..., n_l,$ $l, m = 0, 1, 2, ..., q-r$, so

$$\begin{aligned} u1_{l,i} &= (1-\omega)b_{l,i-1} + \omega\ b_{l,i}; 0 \le \omega \le 1; \\ y1_{m,K_v} &= (1-\zeta)b_{m,K_v-1} + \zeta b_{m,K_v}; 0 \le \zeta \le 1. \end{aligned} \tag{6.60}$$

Using (6.60) in (6.58), we have

$$\sum_{l=0}^{q-r}\sum_{i=1}^{n_l}\int_0^1 \mathcal{F}^{1,2}(u1_{l,i})\mathcal{M}(y1_{m,K_v}, u1_{l,i})r_l d\omega = \psi_0(y1_{m,K_v}) \tag{6.61}$$

where $K_v = 1, 2, ..., n_l; m = 0, 1, ..., q-r$.

Now in boundary element method, we assume that the unknown function $\mathcal{F}^{1,2}(u1_{l,i})$ satisfying integral equation is constant in each small sub-interval. So writing $\mathcal{F}^{1,2}(u1_{l,i}) = \mathcal{F}^{1,2}(l,i), i = 1, 2, ..., n_l; l = 0, 1, ..., q-r$ and using this approximation in (6.61), we get

$$\sum_{l=0}^{q-r}\sum_{i=1}^{n_l}\mathcal{F}^{1,2}(l,i)\mathcal{M}(m,K_v;l,i) = \psi_0(m,K_v) \tag{6.62}$$

where

$$\mathcal{M}(m, K_v; l, i) = \int_0^1 \mathcal{M}(y1_{m,K_v}, u1_{l,i}) r_l d\omega$$
$$\psi_0(m, K_v) = \psi_0(y1_{m,K_v}). \tag{6.63}$$

Solving the system of linear equation (6.62), we get the unknown functions $\mathcal{F}^{1,2}(l,i); l = 0, 1, ..., q-r; i = 1, 2, ..., n_l$. Now substituting these solution in (6.51), we get

$$c^{1,2} = \sum_{l=0}^{q-r} \sum_{i=1}^{n_l} \mathcal{F}^{1,2}(l,i) \int_0^1 \sqrt[3]{(y1_{l,i} - a_1)(y1_{l,i} - a_2)...(y1_{l,i} - m_j)} \psi_0(y1_{l,i}) r_l d\zeta. \tag{6.64}$$

6.4 NUMERICAL DISCUSSION

In this section, the reflection and transmission coefficients are numerically calculated for two types of barrier and plotted in different graphs choosing various values of the parameters. In the numerical calculations, we have chosen $q = 2, 3$ where q denotes the number of rectangular blocks in the slotted barrier so that there are $q-1$ number of slots in between the barrier.

For Type I barrier, for Figures 6.3 to 6.5 and for the tables, we have chosen the following

i) For $q = 3$, $a_1/h = 0.2$, $a_2/h = 0.4$, $a_3/h = 0.6$, $a_4/h = 0.7$, $a_5/h = 0.8$, $a_6/h = 1.0$.

ii) For $q = 2$, $a_1/h = 0.2$, $a_2/h = 0.4$, $a_3/h = 0.6$, $a_4/h = 1.0$.

For Type II barrier, for Figures 6.7 to 6.9 and for the tables, we have chosen the following

i) For $q = 3$, $a_1/h = 0.2$, $a_2/h = 0.3$, $a_3/h = 0.4$, $a_4/h = 0.5$, $a_5/h = 0.6$, $a_6/h = 0.7$.

ii) For $q = 2$, $a_1/h = 0.2$, $a_2/h = 0.5$, $a_3/h = 0.6$, $a_4/h = 0.9$.

4.1 *Validation of the numerical results*

4.1.1 *Comparison of Galerkin Method and BEM*

In Tables 6.1 and 6.2, $|R|$ obtained by solving the integral equation by Galerkin

Table 6.1: $|R|$ for Type I barrier for $\frac{b}{h} = 0.5, \frac{D}{h^4} = 0.5, \frac{\epsilon}{h} = 0.01, \theta = 45^0, q = 3$

Kh	Galerkin Method	BEM
0.10001	0.327196	0.327192
1.20001	0.753769	0.753762
1.90001	0.810377	0.810374
2.30001	0.828095	0.828089
2.80001	0.843610	0.843601

Table 6.2: $|R|$ for Type II barrier for $\frac{b}{h} = 0.3, \frac{D}{h^4} = 0.5, \frac{\epsilon}{h} = 0.01, \theta = 25^0, q = 3$

Kh	Galerkin Method	BEM
0.10001	0.038554	0.038552
1.10001	0.788240	0.788235
2.00001	0.876571	0.876564
2.50001	0.837173	0.837168
2.83001	0.829227	0.829221

method and BEM are compared for barrier of Type I and Type II respectively choosing the values of different parameters suitably. In Table 6.1, it is observed that for Type I barrier, $|R|$ obtained by using Galerkin method coincides with $|R|$ obtained by using BEM up to 4/5 places of decimal for $\frac{b}{h} = 0.5, \frac{D}{h^4} = 0.5, \frac{\epsilon}{h} = 0.01, \theta = 45^0, q = 3$. Table 6.2 shows that for Type II barrier, values of $|R|$ obtained by Galerkin method and BEM coincide up to 5/6 decimal places for $\frac{b}{h} = 0.3, \frac{D}{h^4} = 0.5, \frac{\epsilon}{h} = 0.01, \theta = 25^0, q = 3$. This confirms the correctness of the method.

For both types of the barriers, it is necessary to truncate the infinite series given in (6.55) and (6.56) to a finite number of terms. Table 6.3 shows the values of reflection coefficient for Type I barrier with different values of the wave number Kh. Here we consider $\frac{b}{h} = 0.5, \frac{D}{h^4} = 0.5, \frac{\epsilon}{h} = 0.01, \theta = 45^0, q = 3$ for different values of $N = 2, 3, 4$ and 5. From the table, one can easily observe that for $N = 4, 5$, the values of $|R|$ almost match upto 5 decimal places.

Table 6.4 corresponds the reflection coefficient for Type II barrier with fixed values of $\frac{b}{h} = 0.3, \frac{D}{h^4} = 0.5, \frac{\epsilon}{h} = 0.01, \theta = 25^0, q = 3$ and different $N = 2, 3, 4$ and 5. In this case, the values of $|R|$ match with each other upto 5 decimal places for $N = 4$ and 5. Thus for further numerical computation it is quite sufficient to consider $N = 5$ which gives accurate result up to desired number of terms. Thus the tabulated values shows

that the method converges for $N = 5$.

Tables 6.5 and 6.6 correspond the reflection coefficient $|R|$ for Type I barrier for fixed values of $\frac{b}{h} = 0.5, \frac{D}{h^4} = 0.5, \frac{\epsilon}{h} = 0.01, \theta = 45^0, q = 3$ and Type II barrier for fixed values of $\frac{b}{h} = 0.3, \frac{D}{h^4} = 0.5, \frac{\epsilon}{h} = 0.01, \theta = 25^0, q = 3$ respectively. In both cases, the values of $|R|$ match with each other upto 4/5 decimal places for $N = 7$ and 8.

Table 6.3: Convergence of Galerkin Method for $|R|$ with N for Type I Barrier with $\frac{b}{h} = 0.5, \frac{D}{h^4} = 0.5, \frac{\epsilon}{h} = 0.01, \theta = 45^0, q = 3$

Kh	**N**=2	**N**=3	**N**=4	**N**=5
0.00001	0.003585	0.003613	0.003632	0.003634
0.50001	0.593426	0.593551	0.593583	0.593586
1.00001	0.724853	0.725021	0.725069	0.725071
1.50001	0.783893	0.783943	0.783980	0.783983
2.00001	0.815381	0.815433	0.815471	0.815473
2.50001	0.834826	0.834919	0.834947	0.834949

Table 6.4: Convergence of Galerkin Method for $|R|$ with N for Type II Barrier with $\frac{b}{h} = 0.3, \frac{D}{h^4} = 0.5, \frac{\epsilon}{h} = 0.01, \theta = 25^0, q = 3$

Kh	**N**=2	**N**=3	**N**=4	**N**=5
0.00001	0.000645	0.000716	0.000743	0.000746
0.50001	0.008115	0.008174	0.008193	0.008195
1.00001	0.570869	0.571043	0.571076	0.571079
1.50001	0.979954	0.980035	0.980069	0.980071
2.00001	0.876952	0.877017	0.877045	0.877047
2.50001	0.842943	0.843034	0.843073	0.843076

Table 6.5: Convergence of BEM for $|R|$ with N for Type I Barrier with $\frac{b}{h} = 0.5, \frac{D}{h^4} = 0.5, \frac{\epsilon}{h} = 0.01, \theta = 45^0, q = 3$

Kh	**N**=3	**N**=6	**N**=7	**N**=8
0.10001	0.308539	0.327163	0.327189	0.327192
1.20001	0.729458	0.753723	0.753760	0.753762
1.90001	0.791421	0.810351	0.810371	0.810374
2.30001	0.812693	0.828045	0.828088	0.828089
2.80001	0.823528	0.843565	0.843599	0.843601

Table 6.6: Convergence of BEM for $|R|$ with N for Type II Barrier with $\frac{b}{h} = 0.3, \frac{D}{h^4} = 0.5, \frac{\epsilon}{h} = 0.01, \theta = 25^0, q = 3$

Kh	**N**=3	**N**=6	**N**=7	**N**=8
0.10001	0.021537	0.038523	0.038550	0.038552
1.20001	0.771254	0.788213	0.788234	0.788235
1.90001	0.855125	0.876541	0.876561	0.876564
2.50001	0.817854	0.837141	0.837165	0.837168
2.83001	0.805468	0.829197	0.829218	0.829221

4.1.2 *Energy Identity*

Tables 6.7 and 6.8 show the validation of the energy identity $|R|^2 + |T|^2 = 1$ for two types of barrier for various values of the parameters. Table 6.7 corresponds data for Type I barrier for $\frac{b}{h} = 0.5, \frac{D}{h^4} = 0.5, \frac{\epsilon}{h} = 0.01, \theta = 45^0, q = 3$ and Table 6.8 for Type II barrier for $\frac{b}{h} = 0.3, \frac{D}{h^4} = 0.5, \frac{\epsilon}{h} = 0.01, \theta = 25^0, q = 3$. In both tables the energy identity is perfectly satisfied which is a partial check of the correctness of the present method.

Table 6.7: Energy identity, Type I barrier for $\frac{b}{h} = 0.5, \frac{D}{h^4} = 0.5, \frac{\epsilon}{h} = 0.01, \theta = 45^0, q = 3$

Kh	$\lvert R\rvert$	$\lvert T\rvert$	$\lvert R\rvert^2 + \lvert T\rvert^2$
0.10001	0.327196	0.944956	1.00000
1.20001	0.753769	0.657139	1.00000
1.90001	0.810377	0.585909	1.00000
2.30001	0.828095	0.560587	1.00000
2.80001	0.843610	0.536956	1.00000

Table 6.8: Energy identity, Type II barrier for $\frac{b}{h} = 0.3, \frac{D}{h^4} = 0.5, \frac{\epsilon}{h} = 0.01, \theta = 25^0, q = 3$

Kh	$\lvert R\rvert$	$\lvert T\rvert$	$\lvert R\rvert^2 + \lvert T\rvert^2$
0.10001	0.038554	0.999257	1.00000
1.10001	0.788240	0.615368	1.00000
2.00001	0.876571	0.481273	1.00000
2.50001	0.837173	0.546938	1.00000
2.83001	0.829227	0.558912	1.00000

4.2 *Effect of various parameters on reflection coefficients*

In this section we discuss the behaviour of $|R|$ for different wave numbers (Kh) as-

sociated with Type I and Type II barriers considering various values of the parameters.

4.2.1 *Type I barrier*

Figures 6.3 to Figure 6.6 depict $|R|$ against Kh for Type I barrier.

Figure 6.3 depicts the effect of different width b/h of the slotted barriers of Type I with 3 rectangular blocks with two slots in between, on the reflection coefficient. Here we choose the different values of $\frac{b}{h}(= 0.1, 0.5, 0.7, 1.5)$ keeping $\frac{D}{h^4} = 0.5, \frac{\epsilon}{h} = 0.01, \theta = 45^0, q = 3$ fixed. It is noted that, as the width of the barrier is increased, the value of reflection coefficient $|R|$ also increases. For large width of the barrier, the almost total reflection of short crested waves occurs except for wave number $Kh \sim 0.6$. At $Kh \sim 0.6$, a sudden decrease in $|R|$ occurs which may be due to the interaction of waves with very wide barrier.

In Figure 6.4, we plot the graph of reflection coefficient $|R|$ against non-dimensional wavenumber Kh for different values of $\frac{D}{h^4} = 0.01, 0.5, 2.0$ keeping $\frac{b}{h} = 0.5, \frac{\epsilon}{h} = 0.01, \theta = 45^0, q = 3$ fixed. Here also slotted barrier of Type I is chosen with three rectangular blocks. In this case we observed that as $\frac{D}{h^4}$ increases $|R|$ also increases for $0.2 < Kh < 2.4$. This is due to the interaction of waves with the barrier. For $Kh > 2.4$, $|R|$ for different Kh coincide. This is due to the reason that for bottom standing barrier, the short waves which are at the ice cover surface do not feel the presence of the barrier.

Figure 6.5 illustrates the effect of angle of incidence of the waves on the reflection coefficient against wave number. Here we take four different values of $\theta = 0^0, 45^0, 60^0, 85^0$ keeping $\frac{b}{h} = 0.5, \frac{\epsilon}{h} = 0.01, \frac{D}{h^4} = 0.5, q = 3$ fixed. The reflection coefficient $|R|$ decreases corresponding to increasing values of the incident angle θ. But when we take the incident angle $\theta = 85$, we see that reflection increases. This pecularity in the behaviour of $|R|$ happens because when θ is close to 90^0, the wave interacts with the barrier almost tangentially to the vertical wall of the barrier.

In Figure 6.6, we plot the graph of reflection coefficient $|R|$ against non-dimensional wave number Kh for different values of the rectangular block of the barrier, i.e., $q = 2, 3$ keeping $\frac{b}{h} = 0.5, \frac{D}{h^4} = 0.5, \frac{\epsilon}{h} = 0.01, \theta = 45^0$ fixed. Here, $\frac{a_1}{h} = 0.2, \frac{a_2}{h} = 0.4, \frac{a_3}{h} =$

0.6, $\frac{a_4}{h} = 1$ (for q=2) and $\frac{a_1}{h} = 0.2, \frac{a_2}{h} = 0.4, \frac{a_3}{h} = 0.6, \frac{a_4}{h} = 0.7, \frac{a_5}{h} = 0.9, \frac{a_6}{h} = 1.0$ (for q=3). Here for $q = 3$, the number of slots is 2 and for $q = 2$, the number of slot is 1 and the slot lengths are chosen to be equal. The graph shows that the reflection coefficient $|R|$ decreases for increasing values of q. This happens because for increasing number of the slots, the wave finds more space for transmission which results in decreasing reflection.

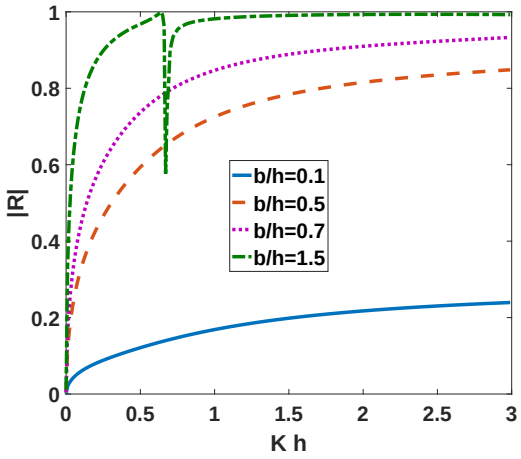

Figure 6.3: Reflection coefficient for Type I barrier for different $\frac{b}{h}$ with $\frac{D}{h^4} = 0.5, \frac{\epsilon}{h} = 0.01, \theta = 45, q = 3$.

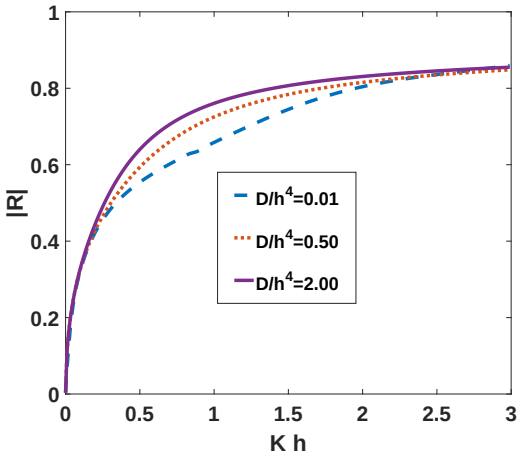

Figure 6.4: Reflection coefficient for Type I barrier for different $\frac{D}{h^4}$ with $\frac{b}{h} = 0.5, \frac{\epsilon}{h} = 0.01, \theta = 45, q = 3$.

4.2.2 *Type II barrier*

Figure 6.7 to Figure 6.10 illustrate the behaviour of $|R|$ against Kh for Type II barrier for different values of various parameters. In these figures $|R|$ exhibits oscillatory behaviour. This oscillatory phenomena occurs for Type II barrier as the waves can interact with the bottom of water region and the barrier. This nature of $|R|$ is observed in Figures 6.7 to 6.10. However for Type I barrier which is a bottom standing barrier, this oscillatory nature of $|R|$ is absent.

In Figure 6.7, the numerical estimates of the reflection coefficients ($|R|$) for Type II barrier are depicted against the wave number Kh for different width of the barrier, viz, $\frac{b}{h} = 0.3, 0.7$ and 1.0 keeping $\frac{D}{h^4} = 0.1, \frac{\epsilon}{h} = 0.01, \theta = 25^0, q = 3$ fixed. In this case we observe that the reflection coefficients $|R|$ exhibits oscillatory behaviour and for certain

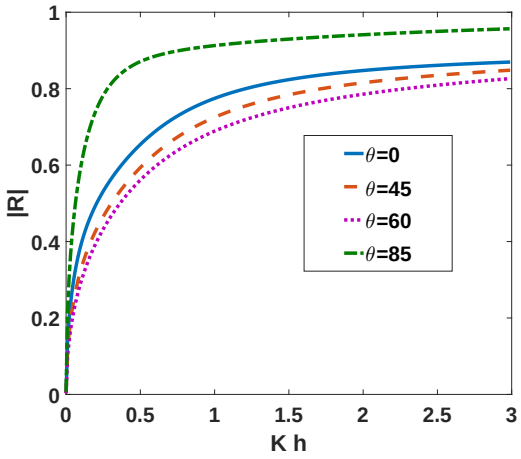

Figure 6.5: Reflection coefficient for Type I barrier for different θ with $\frac{b}{h} = 0.5, \frac{D}{h^4} = 0.5, \frac{\epsilon}{h} = 0.01, q = 3$.

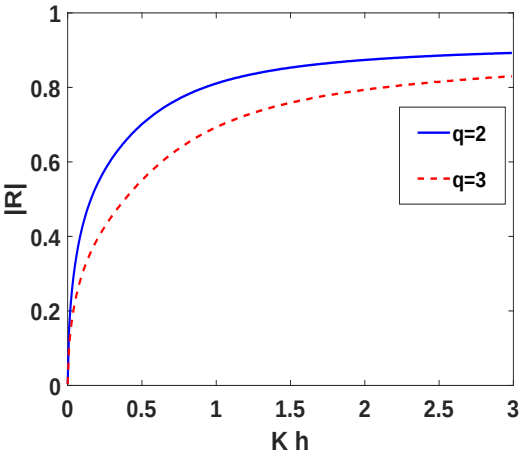

Figure 6.6: Reflection coefficient for Type I barrier for different q with $\frac{b}{h} = 0.5, \frac{D}{h^4} = 0.5, \frac{\epsilon}{h} = 0.01, \theta = 45$.

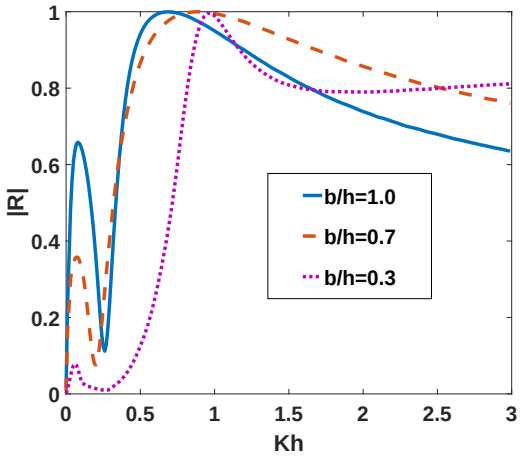

Figure 6.7: Reflection coefficient for Type II barrier for different $\frac{b}{h}$ with $\frac{D}{h^4} = 0.1, \frac{\epsilon}{h} = 0.01, \theta = 25, q = 3$.

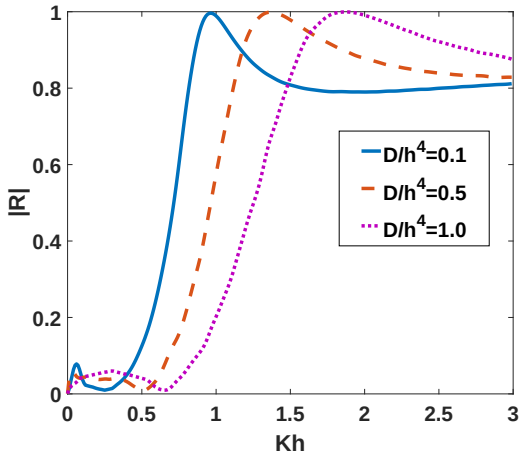

Figure 6.8: Reflection coefficient for Type II barrier for different $\frac{D}{h^4}$ with $\frac{b}{h} = 0.3, \frac{\epsilon}{h} = 0.01, \theta = 25, q = 3$.

value of Kh, $|R|$ almost becomes unity. Also, this figure reveals that for small values of Kh, $|R|$ increases as the width of the slotted barriers increases. However for large wave number, $|R|$ increases as the width of the barrier decreases for $\frac{b}{h} = 0.7$ and 1.0. However, $|R|$ for $\frac{b}{h} = 0.3$ exceeds $|R|$ for $\frac{b}{h} = 0.7$ and 1.0. This happens because the small values of Kh corresponds to waves with longer wavelength which are towards the bottom of the water region and these waves find less space for transmission as

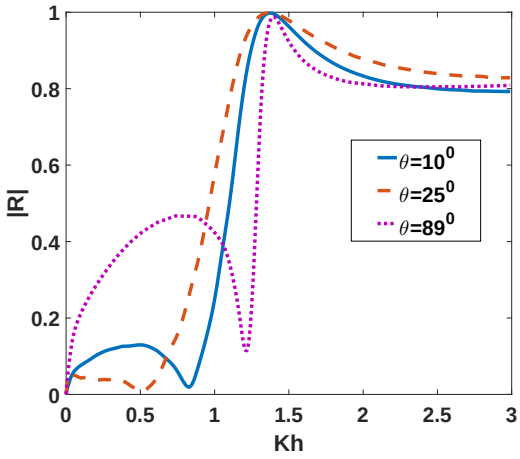

Figure 6.9: Reflection coefficient for Type II barrier for different θ with $\frac{b}{h} = 0.3, \frac{D}{h^4} = 0.5, \frac{\epsilon}{h} = 0.01, q = 3$.

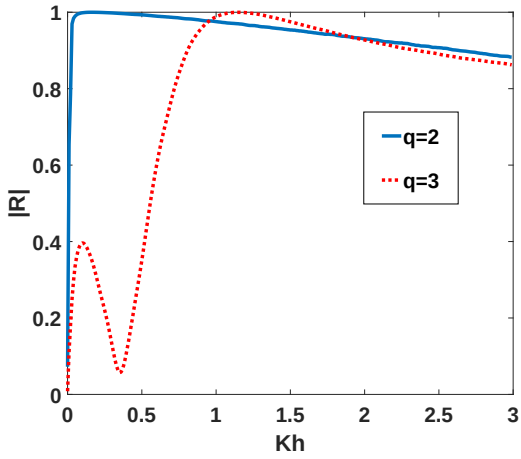

Figure 6.10: Reflection coefficient for Type II barrier for different q with $\frac{b}{h} = 0.3, \frac{D}{h^4} = 0.5, \frac{\epsilon}{h} = 0.01, \theta = 25$.

the width of the barrier increases. However, larger values of Kh corresponds to the surface waves which does not much feel the presence of the barrier and gets transmitted.

In Figure 6.8, the numerical estimates of the reflection coefficients $|R|$ for Type II barrier are depicted against the wave number Kh for different values of elastic parameter $\frac{D}{h^4} = 0.1, 0.5$ and 1.0 keeping $\frac{b}{h} = 0.3, \frac{\epsilon}{h} = 0.01, \theta = 25^0, q = 3$ fixed. It is observed that, in this case, the reflection coefficients $|R|$ shows oscillatory behaviour and become zero between Kh = 0.2 and 0.7 and reaches to near unity for $0.8 < Kh < 1.7$. There occurs phase shift in $|R|$ as $\frac{D}{h^4}$ increases.

The graphs depicted in Figure 6.9 are the reflection coefficients against wave numbers with fixed values of $\frac{b}{h} = 0.3, \frac{D}{h^4} = 0.5, \frac{\epsilon}{h} = 0.01, q = 3$ and different values of angle of incidence $\theta = 10^0, 25^0, 89^0$. Here we observed that $|R|$ exhibits oscillatory behaviour and becomes unity near $Kh = 1.5$.

In Figure 6.10 , $|R|$ is depicted against the non-dimensional wave number Kh by considering $\frac{b}{h} = 0.3, \frac{D}{h^4} = 0.5, \frac{\epsilon}{h} = 0.01, \theta = 25$ and $\frac{a_1}{h} = 0.1, \frac{a_2}{h} = 0.2, \frac{a_3}{h} = 0.3, \frac{a_4}{h} = 0.4$ (for q=2) and $\frac{a_1}{h} = 0.1, \frac{a_2}{h} = 0.2, \frac{a_3}{h} = 0.3, \frac{a_4}{h} = 0.4, \frac{a_5}{h} = 0.5, \frac{a_5}{h} = 0.6$ (for q=3). Here for $q = 3$, the number of slots is 2 and for $q = 2$, the number of slot is 1 and the slot lengths are chosen to be equal. From this figure it is clear that when there are two slots

then $|R|$ shows oscillatory behaviour and decreases as Kh increases. However, for one slot barrier, $|R|$ does not exhibit oscillatory behaviour and increases sharply to unity for small Kh and then decreases as Kh increases.

6.5 CONCLUSIONS

Oblique wave scattering by thick rectangular slotted barrier present in water with ice cover surface have been studied here by employing multi-term Galerkin approximation technique as well as boundary element method. Two different geometrical configurations of the barrier are considered here. The numerical estimates of reflection coefficient for different values of wave numbers and other parameters involved in the physical problem have been obtained and exemplified graphically. The energy balance relation is authenticated numerically. From the present study, the following observation is made.

1. For Type II barrier, the reflection coefficient exhibits oscillatory behaviour which is in contrast with bottom standing Type I barrier.
2. An increase in width of the barrier increases reflection coefficient for Type I barrier.
3. An increase in elastic coefficient of the ice cover decreases the reflection coefficient for Type I barrier but for Type II barrier a phase shift in reflection coefficient occurs.
4. As the angle of incidence θ increases reflection coefficient decreases for Type I barrier.
5. As the slots in the barrier increases reflection coefficient decreases for Type I barrier. For Type II barrier, an increase in number of slots increase the frequency of oscillation in the behaviour of reflection coefficient.

Appendix A

For $y, u \in (a_{2l}, a_{2l+1})$, where $l = 1, ..., q-1$ for Type I and $l = 1, ..., q$ for Type II barrier configuration,

$$M^1(y,u) = \frac{\coth \nu b}{2\nu y_l}\kappa_0(l,u)\kappa_0(l,y) + \sum_{n=1}^{\infty}\frac{\coth \xi_n(l)b}{2\xi_n(l)y_l}\kappa_n(l,u)\kappa_n(l,y) - \sum_{n=1}^{2} i\xi_n U(\lambda_n)\left[\psi_n(u)\psi_n(y) - \frac{D}{K}\lambda_n \tanh(\lambda_n h)\left\{\lambda_n^2 F_y^{1,2}(0) + F_{yyy}^{1,2}(0)\right\}\psi_n(y)\right] - \sum_{n=1}^{\infty} iU(i\lambda_n^*)\left[\psi_n^*(u)\psi_n^*(y) - \frac{D}{K}\lambda_n^* \tan(\lambda_n^* h)\left\{(\lambda_n^*)^2 F_y^{1,2}(0) - F_{yyy}^{1,2}(0)\right\}\psi_n^*(y)\right], \tag{6.65}$$

$$M^2(y,u) = \frac{\tanh \nu b}{2\nu y_l}\kappa_0(l,u)\kappa_0(l,y) + \sum_{n=1}^{\infty}\frac{\tanh \xi_n(l)b}{2\xi_n(l)y_l}\kappa_n(l,u)\kappa_n(l,y) - \sum_{n=1}^{2} i\xi_n U(\lambda_n)\left[\psi_n(u)\psi_n(y) - \frac{D}{K}\lambda_n \tanh(\lambda_n h)\left\{\lambda_n^2 F_y^{1,2}(0) + F_{yyy}^{1,2}(0)\right\}\psi_n(y)\right] - \sum_{n=1}^{\infty} iU(i\lambda_n^*)\left[\psi_n^*(u)\psi_n^*(y) - \frac{D}{K}\lambda_n^* \tan(\lambda_n^* h)\left\{(\lambda_n^*)^2 F_y^{1,2}(0) - F_{yyy}^{1,2}(0)\right\}\psi_n^*(y)\right]. \tag{6.66}$$

For $y, u \in (0, a_1)$,

$$M^1(y,u) = \sum_{n=0}^{2} -\cot((\beta_n^2-\nu^2)^{\frac{1}{2}}b)V(\beta_n)\left[\bar{\psi}_n(u)\bar{\psi}_n(y) - \frac{D}{K}\beta_n \tanh(\beta_n a_1)\left\{\beta_n^2 F_y^{1,2}(0) + F_{yyy}^{1,2}(0)\right\}\bar{\psi}_n(y)\right] - \sum_{n=1}^{\infty} iV(i\beta_n^*)\coth(t_n b)\left[\bar{\psi}_n^*(u)\bar{\psi}_n^*(y) - \frac{D}{K}\beta_n^* \tan(\beta_n^* a_1)\left\{(\beta_n^*)^2 F_y^{1,2}(0) - F_{yyy}^{1,2}(0)\right\}\bar{\psi}_n^*(y)\right] - \sum_{n=1}^{2} i\xi_n U(\lambda_n)\left[\psi_n(u)\psi_n(y) - \frac{D}{K}\lambda_n \tanh(\lambda_n h)\left\{\lambda_n^2 F_y^{1,2}(0) + F_{yyy}^{1,2}(0)\right\}\psi_n(y)\right] - \sum_{n=1}^{\infty} iU(i\lambda_n^*)\left[\psi_n^*(u)\psi_n^*(y) - \frac{D}{K}\lambda_n^* \tan(\lambda_n^* h)\left\{(\lambda_n^*)^2 F_y^{1,2}(0) - F_{yyy}^{1,2}(0)\right\}\psi_n^*(y)\right], \tag{6.67}$$

$$M^2(y,u) = \sum_{n=0}^{2} \tan((\beta_n^2-\nu^2)^{\frac{1}{2}}b)V(\beta_n)\left[\bar{\psi}_n(u)\bar{\psi}_n(y) - \frac{D}{K}\beta_n \tanh(\beta_n a_1)\left\{\beta_n^2 F_y^{1,2}(0) + F_{yyy}^{1,2}(0)\right\}\bar{\psi}_n(y)\right] - \sum_{n=1}^{\infty} iV(i\beta_n^*)\tanh(t_n b)\left[\bar{\psi}_n^*(u)\bar{\psi}_n^*(y) - \frac{D}{K}\beta_n^* \tan(\beta_n^* a_1)\left\{(\beta_n^*)^2 F_y^{1,2}(0) - F_{yyy}^{1,2}(0)\right\}\bar{\psi}_n^*(y)\right] - \sum_{n=1}^{2} i\xi_n U(\lambda_n)\left[\psi_n(u)\psi_n(y) - \frac{D}{K}\lambda_n \tanh(\lambda_n h)\left\{\lambda_n^2 F_y^{1,2}(0) + F_{yyy}^{1,2}(0)\right\}\psi_n(y)\right] - \sum_{n=1}^{\infty} iU(i\lambda_n^*)\left[\psi_n^*(u)\psi_n^*(y) - \frac{D}{K}\lambda_n^* \tan(\lambda_n^* h)\left\{(\lambda_n^*)^2 F_y^{1,2}(0) - F_{yyy}^{1,2}(0)\right\}\psi_n^*(y)\right]. \tag{6.68}$$

For $y \in (a_{2l}, a_{2l+1})$ and $u \in (a_{2l_1}, a_{2l_1+1})(l_1 \neq l)$ and vice-versa

$$M^{1,2}(y,u) = -\sum_{n=1}^{2} i\xi_n U(\lambda_n)\left[\psi_n(u)\psi_n(y) - \frac{D}{K}\lambda_n \tanh(\lambda_n h)\left\{\lambda_n^2 F_y^{1,2}(0) + F_{yyy}^{1,2}(0)\right\}\psi_n(y)\right] - \sum_{n=1}^{\infty} iU(i\lambda_n^*)\left[\psi_n^*(u)\psi_n^*(y) - \frac{D}{K}\lambda_n^* \tan(\lambda_n^* h)\left\{(\lambda_n^*)^2 F_y^{1,2}(0) - F_{yyy}^{1,2}(0)\right\}\psi_n^*(y)\right]. \tag{6.69}$$

Appendix B

For $y \in (0, a_1)$, the choice of the basis functions for both symmetric and antisymmetric cases are

$$f_n(y) = -\frac{d}{dy}[e^{\frac{-Ky}{1-\epsilon K+D\lambda^4}} \int_y^{a_1} e^{\frac{Kt}{1-\epsilon K+D\lambda^4}} \hat{f}_n(t)dt] \tag{6.70}$$

where

$$\hat{f}_n(y) = \frac{2^{7/6}\Gamma(1/6)(2n)!}{\pi\Gamma(2n+1/3)(a_1)^{1/3}(a_1^2-y^2)^{1/3}} C_{2n}^{1/6}(\frac{y}{a_1})$$

and $C_n^{1/6}$ is an ultraspherical Gegenbauer polynomial of order 1/6.

For $y \in (a_{2l}, a_{2l+1})(l = 1, 2, ..., q-1)$, the basis functions for both symmetric and antisymmetric cases are chosen as

$$g_n^{1,2}(l, y) = g_n(l, y) = \frac{2^{1/6}\Gamma(1/6)(n)!}{\pi\Gamma(n+1/3)\left\{2y_l(y-a_{2l})(a_{2l+1}-y)\right\}^{1/3}} C_n^{1/6}(\frac{y-x_l}{y_l}) \tag{6.71}$$

where $x_l = (1/2)(a_{2l+1} - a_{2l})$.

For $y \in (a_{2q}, h)$,the basis functions are chosen as

$$h_n^{1,2}(y) = h_n(y) = \frac{2^{7/6}\Gamma(1/6)(2n)!}{\pi\Gamma(2n+1/3)(h-a_{2q})^{1/3}\left\{(h-a_{2q})^2-(h-y)^2\right\}^{1/3}} C_{2n}^{1/6}(\frac{h-y}{h-a_{2q}}). \tag{6.72}$$

Appendix C

$$
\begin{aligned}
&G^1_{mn} = \\
&-\sum_{r=0}^{2} V(\beta_r)\frac{\cot(\beta_r^2-\nu^2)^{1/2}b\cosh^2(\beta_r a_1)}{\mathcal{M}_r}\frac{I_{2m+1/6}(\beta_r a_1)I_{2n+1/6}(\beta_r a_1)}{(\beta_r a_1)^{1/3}} \\
&-\sum_{r=1}^{2} i\xi_r U(\lambda_r)\frac{\cosh^2(\lambda_r h)}{\mathcal{P}_r}\frac{I_{2m+1/6}(\lambda_r a_1)I_{2n+1/6}(\lambda_r a_1)}{(\lambda_r a_1)^{1/3}} \\
&-4(-1)^{m+n}\sum_{r=1}^{\infty} iU(i\lambda_r^*)\frac{\cos^2(\lambda_r^* h)}{\mathcal{P}_r^*}\frac{J_{2m+1/6}(\lambda_r^* a_1)J_{2n+1/6}(\lambda_r^* a_1)}{(\lambda_r^* a_1)^{1/3}} \\
&+4(-1)^{m+n}\sum_{r=1}^{\infty} iV(i\beta_r^*)\frac{\coth(t_r b)\cos^2(\beta_r^* a_1)}{\mathcal{M}_r^*}\frac{J_{2m+1/6}(\beta_r^* a_1)J_{2n+1/6}(\beta_r^* a_1)}{(\beta_r^* a_1)^{1/3}}
\end{aligned}
\tag{6.73}
$$

where J_n denotes the Bessel function of first kind of order n and I_n denotes the modified Bessel function of first kind of order n. G^2_{mn} is obtained from (6.73) by replacing 'coth' by 'tanh' and '-cot' by 'tan'.

$$
\begin{aligned}
&K^{1,2}_{mn}(l) = \\
&-\sum_{r=1}^{2} i\xi_r U(\lambda_r)\frac{\cosh(\lambda_r h)}{\mathcal{P}_r}\frac{(-1)^n e^{\lambda_r(h-x_l)}+e^{-\lambda_r(h-x_l)}}{2}\frac{I_{2m+1/6}(\lambda_r a_1)I_{n+1/6}(\lambda_r y_l)}{(\lambda_r a_1)^{1/6}(\lambda_r y_l)^{1/6}} \\
&-\sum_{r=1}^{\infty} 4(-1)^m iU(i\lambda_r^*)\frac{\cos(\lambda_r^* h)}{\mathcal{P}_r^*}\cos\left\{\frac{n\pi}{2}-(\lambda_r^*(h-x_l))\right\}\frac{J_{2m+1/6}(\lambda_r^* a_1)J_{n+1/6}(\lambda_r^* y_l)}{(\lambda_r^* a_1)^{1/6}(\lambda_r^* y_l)^{1/6}}
\end{aligned}
\tag{6.74}
$$

$$
\begin{aligned}
&H^{1,2}_{mn} = \\
&-\sum_{r=1}^{2} i\xi_r U(\lambda_r)\frac{\cosh(\lambda_r h)}{\mathcal{P}_r}\frac{I_{2m+1/6}(\lambda_r a_1)I_{2n+1/6}(\lambda_r(h-a_{2q}))}{(\lambda_r a_1)^{1/6}(\lambda_r(h-a_{2q}))^{1/6}} \\
&-4(-1)^{m+n}\sum_{r=1}^{\infty} iU(i\lambda_r^*)\frac{\cos(\lambda_r^* h)}{\mathcal{P}_r^*}\frac{J_{2m+1/6}(\lambda_r^* a_1)J_{2n+1/6}(\lambda_r^*(h-a_{2q}))}{(\lambda_r^* a_1)^{1/6}(\lambda_r^*(h-a_{2q}))^{1/6}}
\end{aligned}
\tag{6.75}
$$

$$
P^{1,2}_{mn}(l) = K^{1,2}_{nm}(l) \tag{6.76}
$$

$$
\begin{aligned}
&R^{1,2}_{mn}(l,l_1) = \\
&-\sum_{r=1}^{2}\frac{i\xi_r U(\lambda_r)}{\mathcal{P}_r}\frac{(-1)^m e^{\lambda_r(h-x_l)}+e^{-\lambda_r(h-x_l)}}{2}\frac{(-1)^n e^{\lambda_r(h-x_{l_1})}+e^{-\lambda_r(h-x_{l_1})}}{2}\frac{I_{m+1/6}(\lambda_r y_l)I_{n+1/6}(\lambda_r y_{l_1})}{(\lambda_r y_l)^{1/6}(\lambda_r y_{l_1})^{1/6}} \\
&-\sum_{r=1}^{\infty}\frac{4iU(i\lambda_r^*)}{\mathcal{P}_r^*}\cos\left\{\frac{m\pi}{2}-(\lambda_r^*(h-x_l))\right\}\cos\left\{\frac{n\pi}{2}-(\lambda_r^*(h-x_{l_1}))\right\}\frac{J_{m+1/6}(\lambda_r^* y_l)J_{n+1/6}(\lambda_r^* y_{l_1})}{(\lambda_r^* y_l)^{1/6}(\lambda_r^* y_{l_1})^{1/6}}
\end{aligned}
\tag{6.77}
$$

$$
\begin{aligned}
&Q^1_{mn}(l) = \\
&\tfrac{24\pi}{y_l}\tfrac{2^{1/3}}{(\Gamma(1/3))^4}\tfrac{\coth\nu b}{\nu}\delta_{0m}\delta_{0n} \\
&+\sum_{r=1}^{\infty}\tfrac{4\coth(\xi_r(l)b)}{\xi_r(l)y_l}\cos\left\{\tfrac{m\pi}{2}-\tfrac{r\pi}{2}\right\}\cos\left\{\tfrac{n\pi}{2}-\tfrac{r\pi}{2}\right\}\tfrac{J_{m+1/6}(\frac{r\pi}{2})J_{n+1/6}(\frac{r\pi}{2})}{(\frac{r\pi}{2})^{1/3}} \\
&-\sum_{r=1}^{2}\tfrac{i\xi_r U(\lambda_r)}{\mathcal{P}_r}\tfrac{(-1)^m e^{\lambda_r(h-x_l)}+e^{-\lambda_r(h-x_l)}}{2}\tfrac{(-1)^n e^{\lambda_r(h-x_l)}+e^{-\lambda_r(h-x_l)}}{2}\tfrac{I_{m+1/6}(\lambda_r y_l)I_{n+1/6}(\lambda_r y_l)}{(\lambda_r y_l)^{1/3}} \\
&-\sum_{r=1}^{\infty}\tfrac{4iU(i\lambda^*_r)}{\mathcal{P}^*_r}\cos\left\{\tfrac{m\pi}{2}-(\lambda^*_r(h-x_l))\right\}\cos\left\{\tfrac{n\pi}{2}-(\lambda^*_r(h-x_l))\right\}\tfrac{J_{m+1/6}(\lambda^*_r y_l)J_{n+1/6}(\lambda^*_r y_l)}{(\lambda^*_r y_l)^{1/3}}
\end{aligned}
\tag{6.78}
$$

and Q^2_{mn} is obtained from (6.78) by replacing 'coth' by 'tanh'.

$$
\begin{aligned}
&T^{1,2}_{mn}(l) = \\
&-\sum_{r=1}^{2}\tfrac{i\xi_r U(\lambda_r)}{\mathcal{P}_r}\tfrac{(-1)^m e^{\lambda_r(h-x_l)}+e^{-\lambda_r(h-x_l)}}{2}\tfrac{I_{2n+1/6}(\lambda_r(h-a_{2q}))I_{m+1/6}(\lambda_r y_l)}{(\lambda_r(h-a_{2q}))^{1/6}(\lambda_r y_l)^{1/6}} \\
&-\sum_{r=1}^{\infty}\tfrac{4(-1)^n iU(i\lambda^*_r)}{\mathcal{P}^*_r}\cos\left\{\tfrac{m\pi}{2}-(\lambda^*_r(h-x_l))\right\}\tfrac{J_{2n+1/6}(\lambda^*_r(h-a_{2q}))J_{m+1/6}(\lambda^*_r y_l)}{(\lambda^*_r(h-a_{2q}))^{1/6}(\lambda^*_r y_l)^{1/6}}
\end{aligned}
\tag{6.79}
$$

$$
X^{1,2}_{mn} = H^{1,2}_{nm} \tag{6.80}
$$

$$
Y^{1,2}_{mn}(l) = T^{1,2}_{nm}(l) \tag{6.81}
$$

$$
\begin{aligned}
&Z^1_{mn} = \\
&\tfrac{48\pi}{h-a_{2q}}\tfrac{2^{1/3}}{(\Gamma(1/3))^4}\tfrac{\coth\nu b}{\nu}\delta_{0m}\delta_{0n} \\
&+\sum_{r=1}^{\infty}\tfrac{8(-1)^{m+n}\coth(\xi_r(q)b)}{\xi_r(q)(h-a_{2q})}\tfrac{J_{2m+1/6}(r\pi)J_{2n+1/6}(r\pi)}{(r\pi)^{1/3}} \\
&-\sum_{r=1}^{2}\tfrac{i\xi_r U(\lambda_r)}{\mathcal{P}_r}\tfrac{I_{2m+1/6}(\lambda_r(h-a_{2q}))I_{2n+1/6}(\lambda_r(h-a_{2q}))}{(\lambda_r(h-a_{2q}))^{1/3}} \\
&-\sum_{r=1}^{\infty}\tfrac{4(-1)^{m+n}iU(i\lambda^*_r)}{\mathcal{P}^*_r}\tfrac{J_{2m+1/6}(\lambda^*_r(h-a_{2q}))J_{2n+1/6}(\lambda^*_r(h-a_{2q}))}{(\lambda^*_r(h-a_{2q}))^{1/3}}
\end{aligned}
\tag{6.82}
$$

and Z^2_{mn} is obtained from (6.82) by replacing 'coth' by 'tanh'.

$$
d_m = \frac{\cosh\lambda_0 h}{\mathcal{P}_0^{1/2}}\frac{I_{2m+1/6}(\lambda_0 a_1)}{(\lambda_0 a_1)^{1/6}} \tag{6.83}
$$

$$
d^{1,2}_m(l) = \frac{(-1)^m e^{\lambda_0(h-x_l)}+e^{-\lambda_0(h-x_l)}}{2\mathcal{P}_0^{1/2}}\frac{I_{m+1/6}(\lambda_0 y_l)}{(\lambda_0 y_l)^{1/6}} \tag{6.84}
$$

$$d_m^{1,2}(q) = \frac{\cosh \lambda_0 h}{\mathcal{P}_0^{1/2}} \frac{I_{2m+1/6}(\lambda_0(h-a_{2q}))}{(\lambda_0(h-a_{2q}))^{1/6}} \tag{6.85}$$

CHAPTER 7

EFFECT OF NONUNIFORM POROSITY IN CURVED BREAKWATER ON WATER WAVES

7.1 INTRODUCTION

Breakwaters, also known as wave attenuator, are coastal structures built out into the sea to protect a coast or harbour from the force of waves. These are usually bottom founded rigid structures which are expensive to construct, particularly for deep water and also these prevent the natural water circulation, leading to environmental issues. Floating breakwaters are useful alternatives which are cost effective and have low impact on environment. These type of breakwaters are usually kept floating by using proper mooring system [cf. Sobhani *et al.* (1988), Dai *et al.* (2018)]. Floating breakwaters can be of various shapes and configurations. A floating breakwater in form of an arc of a circle, encountering water waves is an important because it is known that the increase in arc length of a circular arc-shaped rigid breakwater reduces the reflection

[0]† The content of this chapter is based on the paper " Effect of nonuniform porosity in curved breakwater on water waves", (communicated after revision).

of waves [cf. Parsons and Martin (1994)] so that most of wave energy can be utilised. This has an important bearing on construction of wave energy device. An important application of a circular arc shaped breakwater is semi-circular caisson whose major advantage is its stability against sliding [cf. Liu and Li (2012)]. As reported in Liu and Li (2012) many experimentalists studied the effect of waves on circular arc shaped barrier for construction of coastal structures in form of curved breakwaters and verified the experimental result with the theoretical one.

The phenomena of wave encounter with barrier in form of a circular arc shaped rigid structure submerged in water under linear theory was studied by many researchers using various mathematical tools. Notable among them are Parsons and Martin (1994) , McIver and Urka (1995), Kanoria and Mandal (2002), Mondal *et al.* (2021).

Recently, there is a surge in number of studies on porous breakwaters as the pores are dissipators of energy which reduces wave action and maintain water circulation. Wave propagation over a porous circular arc shaped barriers are studied by many researchers like Liu and Li (2012), Mondal *et al.* (2017), Mondal and Banerjea (2016), Samanta *et al.* (2023).

A study of wave interaction with barriers with nonuniform porosity is limited in the literature although, studies in connection with the problem of wave interaction with a perforated cylindrical breakwater with nonuniform porosity in the circumferential direction and uniform porosity in the vertical direction was initiated by Tao *et al.* (2009) using eigen function expansion method. Song and Tao (2010) adopted an efficient numerical method to study water wave interaction with a cylinder with a nonuniform porosity and their numerical experiments established the efficacy and accuracy of their numerical method. In these studies the authors mention that two dimensional studies on the interaction of ocean surface waves with a porous breakwater have limitations as in reality, the ocean waves are more complex, and better described by three-dimensional short-crested waves. They also found that by making the porosity nonuniform, the various features of wave motion become more complex than its counterpart of uniform porosity. In recent past, the problem related to wave interaction with dual porous barrier with non uniform porosity was studied by Gupta

and Gayen (2019) and Sarkar *et al.* (2020) using coupled integral equation formulation. Later, Singh *et al.* (2022) studied the phenomena of water wave propagation in the presence of an inclined flexible plate with variable porosity using hypersingular integral equation formulation. Recently Mondal *et al.* (2024) and Banerjee et al [**?**] studied the effect of non uniform porosity of a porous vertical barrier on an obliquely incident wave train by using Fredholm integral equation formulation. Banerjee *et al.* (2024) in their study showed that for certain choice of porosity distribution, the wave energy dissipation by a barrier with nonuniform porosity is more than that of a barrier with uniform porosity. This choice of porosity distribution in a barrier with nonuniform makes enhances its efficiency as a breakwater than a barrier with uniform porosity.

In the present paper we study the behaviour of water waves in presence of thin circular arc shaped porous barrier with variable porosity. Based on a judicious application of Green's integral theorem, the corresponding boundary value problem is reduced to a second kind hypersingular integral equation.

Hypersingular integral equation is a powerful mathematical tool which are very useful in studying scattering problems involving barriers of different geometry. Usually the problem of scattering by a rigid barrier can be formulated in terms of first kind hypersingular integral equation whereas the scattering problems involving porous barriers give rise to second kind hypersingular integral equation. Parsons and Martin (1994) were pioneers in applying collocation method to solve hypersingular integral equation where they approximated the unknown function by Tchebychev's polynomial. In recent past Samanta *et al.* (2023) used boundary element method to solve hypersingular integral equation in a very simple manner. This is an useful alternative method of solution.

In the present study, following Samanta *et al.* (2023), Mondal *et al.* (2021), the second kind hypersingular integral equation was solved by using boundary element method as well as the collocation method. We may mention here that the kernel of the hypersingular integral equation in case of finite depth is more complicated than that of for infinite depth and as such the numerical solution of the hypersingular integral equation arising in case of finite depth is more time consuming than its counterpart for infinite depth. So the solution of the integral equation in both cases are interesting from the mathematical and numerical point of view. Also, the collocation method

converges faster than the boundary element method but the advantage of boundary element method is that it is very simple computationally, particularly when the kernel is complicated. The convergence of boundary element method is discussed in detail in Samanta *et al.* (2023). Using the solution of the hypersingular integral equation, the quantities of physical interest, viz, the reflection coefficient and amount of energy dissipated are determined and depicted graphically considering two types of distribution of porosity in the barrier. It was observed that the reflection coefficient obtained by using the solution of hypersingular integral equation by the two methods are in good agreement up to a desired degree of accuracy. In the present study we have chosen the distribution of nonuniform porosity in the barrier as a linear function and also as quadratic function of the parameter which varies along the arc length of the curved barrier. The physical quantities like reflection and transmission coefficients and energy dissipation are evaluated for these two types of chosen porosity distributions. Other types of distribution of porosity may be considered for which the physical quantities of interest can be evaluated from the present method. The advantage of nonuniform porosity distribution in the barrier over uniform porosity distribution is that a proper choice of nonuniform porosity distribution in the barrier can enhance the wave energy dissipation than a barrier with uniform porosity. This is useful in reduction of wave power and thereby protecting the coastal region from the effect of rough sea. This is illustrated graphically for a particular choice of porosity distribution in the barrier. We mention here that the results concerning the physical quantities of interest viz., reflection coefficient, transmission coefficient and energy dissipation for deep water can be recovered from the results of the finite depth case by making the water depth large. However it is not easy to reduce the hypersingular integral equation for finite depth to the one for infinite depth case by making water depth tending to infinity. Thus it is interesting to study mathematically the hypersingular integral equation both for deep water and for water of finite depth. In the present study we recovered the numerical results for reflection coefficient for deep water from the results for finite depth depth by making the depth very large.

7.2 PROBLEM FORMULATION

Under the assumption of linearised theory, we study two dimensional irrotational motion in water due to scattering of a normally incident wave train by a thin porous circular arc shaped barrier submerged in water. A rectangular cartesian coordinate system is chosen where the y-axis is taken vertically downwards into the fluid and the x-axis is along the undisturbed free surface. Two dimensional motion is justified due to the reason that motion in every cross section $z = c$, c being an arbitrary contant, is similar [cf. Mandal and Chakrabarti (2000)]. Here we study the motion for two cases when the water region is infinitely deep and also when water is of finite depth H. The water occupies the region $-\infty < x < \infty;\ 0 < y < \infty$ for deep water (DW) and the region $-\infty < x < \infty;\ 0 < y < H$ when the depth of water is finite (FDW). The circular arc shaped barrier C of radius u is placed symmetrically about y-axis, with center at $(0, v + u)$ and the radius through end points make an angle θ with y-axis. Schematic diagram of the problem is given by the Figure 7.1.

A train of time harmonic surface waves from negative infinity, with circular frequency σ represented by $Re\{\phi^{inc}(x, y)e^{-i\sigma\tau}\}$, when incident on the porous thin circular arc shaped barrier C, a part of it is reflected and a part is transmitted above and below the barrier as shown in Figure 7.1.

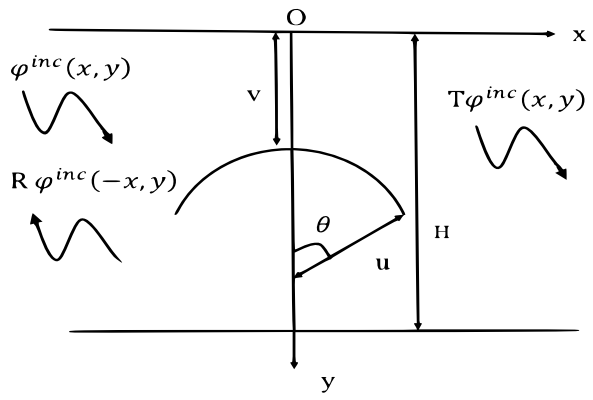

Figure 7.1: Schematic diagram of the problem

The resulting motion is described by the velocity potential $Re\{\phi(x, y)e^{-i\sigma\tau}\}$, where $\phi(x, y)$ satisfies the following boundary value problem.

$$\nabla^2\phi = 0; \qquad \text{in the fluid region,} \tag{7.1}$$

$$K\phi + \phi_y = 0 \ \text{ on } \ y = 0, \tag{7.2}$$

$$r^{1/2}\nabla\phi \qquad \text{is bounded as } r \to 0 \tag{7.3}$$

where r is the distance of any point in the fluid region from the either sharp ends of the barrier.

$$\begin{aligned} \nabla\phi &\to 0 \quad \text{as } y \to \infty \quad \text{for DW,} \\ \frac{\partial\phi}{\partial y} &= 0 \quad \text{on } \ y = H \qquad \text{for FDW.} \end{aligned} \tag{7.4}$$

The boundary condition on the curved plate surface C is given by

$$\frac{\partial\phi(q+)}{\partial n} = \frac{\partial\phi(q-)}{\partial n} = -i\kappa\lambda(q)\ [\phi](q) \ \text{ on } \ C, \tag{7.5}$$

where

$$\kappa = \begin{cases} K = \frac{\sigma^2}{g} & \text{for DW,} \\ k_0 & \text{for FDW,} \end{cases}$$

and k_0 is the unique real positive root of the transcendental equation $k\tanh kH = K$.

Here $[\phi](q) = \phi(q+) - \phi(q-)$ $(q \in C)$ is the difference of the potential function across the curved barrier C where

$$\begin{aligned} q+ &= \{(x,y) \in C \mid x^2 + (y-v-u)^2 > u^2\} \\ q- &= \{(x,y) \in C \mid x^2 + (y-v-u)^2 < u^2\} \end{aligned} \tag{7.6}$$

and $\frac{\partial}{\partial n}$ denotes the normal derivative at a point on C and $\lambda(q) = \lambda_r(q) + i\lambda_i(q)$ rep-

resents the nonuniform porosity parameter [cf. Singh *et al.* (2022)] which varies along the arc length of the barrier C. Here $\lambda_r(q)$ denotes resistance force coefficient and $\lambda_i(q)$ denotes inertial force coefficient of the porous barrier and if $\lambda_r >> \lambda_i$, then λ is taken to be real. It may be mentioned that the resistance force coefficient $\lambda_r(q)$ resists the passage of water through the pores while the inertial force coefficient $\lambda_i(q)$ allows the flow of water through the pores [cf. Yu (1995)].

The far field condition is

$$\phi(x,y) \sim \begin{cases} \phi^{inc}(x,y) + R\phi^{inc}(-x,y) \text{ as } x \to -\infty, \\ T\phi^{inc}(x,y) \text{ as } x \to \infty \end{cases} \tag{7.7}$$

where R and T are the reflection and transmission coefficients respectively, which are to be determined. Here the barrier C is represented parametrically as

$$C: \ x = u\sin s\theta; \ y = v + u - u\cos s\theta; \ \ -1 \le s \le 1; \ \ -\pi < \theta < \pi \tag{7.8}$$

and

$$\phi^{inc}(x,y) = g(y)e^{i\kappa x} \tag{7.9}$$

where

$$g(y) = \begin{cases} e^{-Ky} & \text{for DW} \\ \frac{\cosh k_0(H-y)}{\cosh k_0 H} & \text{for FDW.} \end{cases}$$

7.3 METHOD OF SOLUTION

Let $G(x,y;\xi,\eta)$ be the Green's function which is the velocity potential due to the presence of a line source at (ξ,η) in the fluid region whose expression is given below [cf. Mandal and Chakrabarti (2000)].

For DW,

$$G(x,y;\xi,\eta) = \log\left(\frac{r_-}{r_+}\right) - 2\int_0^\infty \frac{e^{-k(y+\eta)}}{k-K}\cos k(x-\xi)\, dk. \tag{7.10}$$

For FDW,

$$G(x,y;\xi,\eta) = \log\left(\frac{r_-}{r_+}\right) - 2\int_0^\infty \left[\frac{\cosh k(H-y)\cosh k(H-\eta)}{k\sinh kH - K\cosh kH} + \frac{e^{-kH}\sinh k\eta \sinh ky}{k}\right]\frac{\cos k(x-\xi)}{\cosh kH}dk, \tag{7.11}$$

where $r_\mp = \sqrt{(x-\xi)^2+(y\mp\eta)^2}$ and the infinite integrals in (7.10) and (7.11) can be evaluated by standard procedure [cf. Parsons and Martin (1994)].

We apply the Green's Integral theorem to the scattered potential $(\phi - \phi^{inc})(x,y)$ and the source potential $G(x,y;\xi,\eta)$ on the region (as shown in Figure 7.2) bounded externally by the lines $y=0, -X_1 \le x \le X_1;\ x=-X_1, 0\le y\le Y_1;\ y=Y_1,\ -X_1 \le x \le X_1;\ x=X_1, 0\le y\le Y_1$; internally by a very small circle of radius δ centering (ξ,η) and a contour enclosing curve barrier C. It may be noted that for FDW, $Y_1 = H$ and for DW, Y_1 will tend to infinity. Making $X_1\to\infty,\ \delta\to 0$ and $Y_1\to\infty$ for DW and $Y_1\to H$ for FDW respectively, a representation of the potential function in terms of the unknown function $[\phi(p)]$ is obtained as

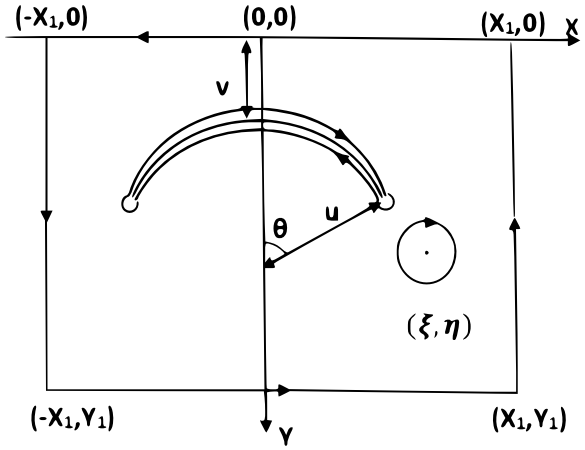

Figure 7.2: Contour for Green's Integral Theorem

$$\phi(q) = \phi^{inc}(q) - \frac{1}{2\pi}\int_C [\phi](p)\frac{\partial}{\partial n_p}G(p,q)ds_p. \tag{7.12}$$

In obtaining the above representation we have used equation (7.1) and the fact that

$\nabla^2 G = 0$ except at (ξ, η). Also it can be noted that the line integrals over all outer boundaries are zero because of the fact that both $(\phi - \phi^{inc})(x, y)$ and G satisfy similar boundary conditions on all the outer boundaries. The only contribution comes from the contour C enclosing the barrier and the small circle of radius δ enclosing the point (ξ, η) [cf. Figure 7.2 and Mandal and Chakrabarti (2000)]. In the equation (7.12), $q = (\xi, \eta)$ is a field point, $p \equiv (x, y)$ is a point on barrier C, $[\phi](p)$ is the discontinuity of potential function $\phi(x, y)$ across C and $\frac{\partial}{\partial n_p}$ is the normal derivative at the point p on C. It may be noted that the unknown function $[\phi](p)$ vanishes at the end points of the arc shaped barrier [cf. Mandal and Chakrabarti (2000)].

Using the boundary condition (7.5) on the barrier to the equation (7.12) we obtain the following second kind hypersingular integral equation as

$$\frac{1}{2\pi} \neg\!\!\!\!\int_C [\phi](p) \frac{\partial^2}{\partial n_q \partial n_p} G(p, q) ds_p \; - \; i\kappa \; \lambda(q) \; [\phi](q) \; = \frac{\partial \phi^{inc}}{\partial n_q}(q), \; q \; \epsilon \; C \tag{7.13}$$

where $\frac{\partial}{\partial n_q}$ is the normal derivative at the point q on C. The parametric equation of C at the points $p = (x, y)$ and $q = (\xi, \eta)$ in (7.13) is given by

$$\begin{aligned} x(s) &= u \sin s\theta, \quad y(s) = v + u - u \cos s\theta; \quad -1 \le s \le 1, \\ \xi(t) &= u \sin t\theta, \quad \eta(t) = v + u - u \cos t\theta; \quad -1 \le t \le 1. \end{aligned} \tag{7.14}$$

Thus, with the help of the parametrisation given by equation (7.14) along with the introduction of a new unknown function $f(s) = [\phi](p(s))$; the integral equation (7.13) can be rewritten as

$$\int_{-1}^{1} f(s) \left[\frac{1}{(s-t)^2} + u^2 \theta^2 \mathcal{L}(s, t) \right] ds + 2\pi i u \theta \kappa \lambda(t) f(t) = 2\pi u \theta g_1(t) \tag{7.15}$$

where

$$g_1(t) = \begin{cases} K e^{-K\eta(t) + i(K\xi(t) + t\theta)} & \text{for DW,} \\ \frac{k_0 e^{ik_0 \xi(t)} \sinh\left(k_0(H - \eta(t)) + \imath t\theta\right)}{\cosh k_0 H} & \text{for FDW.} \end{cases} \tag{7.16}$$

The expression of $\mathcal{L}(s, t)$ is given as follows.

For DW,

$$\mathcal{L}(s,t) = \left[\frac{1}{4u^2\sin^2\frac{(s-t)\theta}{2}} - \frac{1}{u^2\theta^2(s-t)^2}\right] + \cos(s-t)\theta\left[\frac{Y^2-X^2}{(X^2+Y^2)^2} + \frac{2KY}{X^2+Y^2} + 2K^2\Phi_0(X,Y)\right] + 2\sin(s-t)\theta\left[K\frac{\partial\Phi_0}{\partial X} - \frac{XY}{(X^2+Y^2)^2}\right] \tag{7.17}$$

with

$$X = x-\xi = u(\sin s\theta - \sin t\theta);\ Y = y+\eta = 2v+2u-u(\cos s\theta + \cos t\theta);$$

$$\Phi_0(X,Y) = \imath\pi e^{-KY+\imath K|X|} + \int_0^\infty \frac{e^{-k|X|}}{k^2+K^2}\{k\cos kY - K\sin kY\}\,dk.$$

For FDW,

$$\begin{aligned}\mathcal{L}(s,t) = \left[\frac{1}{4u^2\sin^2\frac{(s-t)\theta}{2}} - \frac{1}{u^2\theta^2(s-t)^2}\right] &+ \frac{X^2-Y^2}{(X^2+Y^2)^2}\ \cos(s-t)\theta\ - \frac{2XY}{(X^2+Y^2)^2}\ \sin(t-s)\theta \\ &+2\sin t\theta\sin s\theta\int_0^\infty \mu(k)\sinh k\eta\sinh ky\cos kX\,dk \\ &-2\sin t\theta\cos s\theta\int_0^\infty \mu(k)\sinh k\eta\cosh ky\sin kX\,dk \\ &+2\cos t\theta\sin s\theta\int_0^\infty \mu(k)\cosh k\eta\sinh ky\sin kX\,dk \\ &+2\cos t\theta\cos s\theta\int_0^\infty \mu(k)\cosh k\eta\cosh ky\cos kX\,dk \\ +\sin t\theta\sin s\theta\Bigg[\zeta i\cosh k_0(H-y)\cosh k_0(H-\eta)\ e^{ik_0|X|} &- \sum_{n=1}^\infty \omega_n\cos k_n(H-y)\cos k_n(H-\eta)\ e^{-k_n|X|} \\ &+\frac{2\pi}{H}\sum_{n=0}^\infty \alpha_n\sin\alpha_n y\sin\alpha_n\eta\ e^{-\alpha_n|X|}\Bigg]\end{aligned}$$

$$+\cos t\theta\cos s\theta\Bigg[\zeta i\sinh k_0(H-y)\sinh k_0(H-\eta)\ e^{ik_0|X|}+\sum_{n=1}^{\infty}\omega_n\sin k_n(H-y)\sin k_n(H-\eta)\ e^{-k_n|X|}$$
$$-\frac{2\pi}{H}\sum_{n=0}^{\infty}\alpha_n\cos\alpha_n y\cos\alpha_n\eta\ e^{-\alpha_n|X|}\Bigg]$$
$$+\sin t\theta\cos s\theta\Bigg[\zeta\sinh k_0(H-y)\cosh k_0(H-\eta)\ e^{ik_0|X|}-\sum_{n=1}^{\infty}\omega_n\sin k_n(H-y)\cos k_n(H-\eta)\ e^{-k_n|X|}$$
$$+\frac{2\pi}{H}\sum_{n=0}^{\infty}\alpha_n\cos\alpha_n y\sin\alpha_n\eta\ e^{-\alpha_n|X|}\Bigg]$$
$$-\cos t\theta\sin s\theta\Bigg[\zeta\cosh k_0(H-y)\sinh k_0(H-\eta)\ e^{ik_0|X|}-\sum_{n=1}^{\infty}\omega_n\cos k_n(H-y)\sin k_n(H-\eta)\ e^{-k_n|X|}$$
$$+\frac{2\pi}{H}\sum_{n=0}^{\infty}\alpha_n\sin\alpha_n y\cos\alpha_n\eta\ e^{-\alpha_n|X|}\Bigg] \tag{7.18}$$

where k_0 and ik_n are roots of the transcendental equations $k\tanh kH-K=0$ and $i\alpha_n$'s are roots of the equation $\cosh kH=0$ and

$$\mu(k)=\frac{k\ e^{-kH}}{\cosh kH};\quad \zeta=\frac{4\pi k_0^2}{2k_0H+\sinh(2k_0H)};\quad \omega_n=\frac{4\pi k_n^2}{2k_nH+\sin(2k_nH)}.$$

It may be noted here that if $\lambda(t)=0$ then the hypersingular integral equation of second kind (7.15) reduces to hypersingular integral equation of first kind. Also for $\lambda(t)=0$, the condition (7.5) on the porous barrier reduces to the condition on rigid barrier. This shows that wave interaction with porous barrier produces second kind hypersingular integral equation while that with rigid barrier produces first kind hypersingular integral equation. It is also interesting to observe that the kernel of the hypersingular integral equation for water of finite depth is quite complicated in comparison to the kernel in case of deep water.

The unknown physical quantities R and T are evaluated by making $\xi\to\mp\infty$ in equation (7.12) and comparing with far field condition for $\phi(\xi,\eta)$ as given by equation

(7.7).This yields

$$R = \begin{cases} -iKu\theta \int_{-1}^{1} f(s) e^{-Ky(s)+iKx(s)s\theta} ds & \text{for DW,} \\ -\frac{2u\theta ik_0 \cosh k_0 H}{2k_0 H + \sinh 2k_0 H} \int_{-1}^{1} f(s) \sinh(k_0(H - y(s)) + is\theta)\ e^{ik_0 x(s)}\ ds & \text{for FDW} \end{cases} \tag{7.19}$$

and

$$T = \begin{cases} 1 - iKu\theta \int_{-1}^{1} f(s) e^{-Ky(s)-iKx(s)s\theta} ds & \text{for DW,} \\ 1 - \frac{2u\theta ik_0 \cosh k_0 H}{2k_0 H + \sinh 2k_0 H} \int_{-1}^{1} f(s) \sinh(k_0(H - y(s)) - is\theta)\ e^{-ik_0 x(s)}\ ds & \text{for FDW.} \end{cases} \tag{7.20}$$

Thus from equations (7.19) and (7.20) we observe that R and T are expressed in terms of the unknown function $f(s)$ which can be obtained by solving the integral equation (7.15).

SOLUTION OF THE INTEGRAL EQUATION

This section illustrates the boundary element method and the collocation method of solution of the second kind hypersingular integral equation (7.15). We may mention here that numerical solution of hypersingular integral equation is limited in the literature due to the reason that hypersingular integrals are not amenable to the numerical methods. Application of collocation method using Chebychev's polynomial in solving hypersingular integral equation was initiated by Parsons and Martin (1994). Later Samanta *et al.* (2023) applied boundary element method to solve hypersingular integral equation. Boundary element method is a simple method computationally but the convergence of collocation method is faster than boundary element method. The present analysis demonstrates the application of two methods.

Boundary Element Method

We will solve the integral equation (7.15) numerically using boundary element method (BEM). The method of solution of hypersingular integral equation using BEM and the convergence study is described in detail in Samanta *et al.* (2023). Since $[\phi] = 0$

at the ends of the barrier, so we have $f(s) = 0$ at $s = \pm 1$. This behaviour asserts that we may assume

$$f(s) = \sqrt{1 - s^2}\psi(s) \tag{7.21}$$

where $\psi(s)$ is a regular function in $[-1, 1]$. Noting (7.21) the hypersingular equation (7.15) takes the form

$$\int_{-1}^{1} \sqrt{1-s^2}\left[\frac{1}{(s-t)^2} + u^2\theta^2\mathcal{L}(s,t)\right]\psi(s)\,ds + 2\pi i u\theta\kappa\lambda(t)\sqrt{1-t^2}\psi(t) = 2\pi u\theta g_1(t), \quad -1 \le t \le 1. \tag{7.22}$$

As per boundary element method, the range of integration $[-1, 1]$ is divided into m number of equal line elements i.e. $[-1, 1] = \bigcup_{j=1}^{m}[a_{j-1}, a_j]$, where a_{j-1} and a_j are the end points of jth line element and $a_0 = -1$, $a_m = 1$ and $a_j = a_0 + jr'$, $r' = \frac{a_m - a_0}{m}$. Writing $s = s_j$ where $s_j \in [a_{j-1}, a_j]$, and $t = t_i$ where $t_i \in [a_{i-1}, a_i]$, $\quad i,\ j = 1, 2...., m$ we have

$$s_j = (1-\tau)a_{j-1} + \tau a_j, \quad 0 \le \tau \le 1; \quad t = t_i = (1-\gamma)a_{i-1} + \gamma a_i,\ 0 \le \gamma \le 1. \tag{7.23}$$

Thus equation (7.22) takes the form

$$\sum_{j=1}^{m}\int_0^1 \sqrt{1-s_j^2}\left\{\frac{1}{(s_j - t_i)^2} + u^2\theta^2\mathcal{L}(s_j, t_i)\right\}\psi(s_j)\ r'\ d\tau + 2\pi i u\theta\kappa\lambda(t_i)\sqrt{1-t_i^2}\psi(t_i) = 2\pi u\theta g_1(t_i)\ ,\ i = 1, 2, ..., m. \tag{7.24}$$

Assuming the unknown function $\psi(s_j) = \psi_j$ is a constant for jth line element, $j = 1, 2, ..., m$, the integral equation (7.24) is reduced to the following system of linear algebraic equations [cf. Samanta *et al.* (2023)].

$$\sum_{j=1}^{m} a_{ij}\ \psi_j = 2\pi u\theta g_{1i}\ ,\ i = 1, 2, ..., m \tag{7.25}$$

where

$$a_{ij} = \int_0^1 \sqrt{1-s_j^2}\left\{\frac{1}{(s_j-t_i)^2} + u^2\theta^2\mathcal{L}(s_j,t_i)\right\} r'\, d\tau \;\; + \delta_{ij} 2\pi i u\theta\kappa\lambda(t_i)\sqrt{1-t_i^2}, \quad i = 1,2,....,m; \quad j = 1,2,.....,m, \tag{7.26}$$

$$g_{1i} = g_1(t_i)\ , \quad i = 1,2,.....,m. \tag{7.27}$$

Now solving the system of linear equations (7.25), we obtain the unknown coefficients $\psi_j,\ j = 1,2,....,m$ and then we approximate the solution of $f(s)$ in each line interval to evaluate the value of R and T from equations (7.19) and (7.20).

Collocation Method

In this method, the unknown function $f(s)$ is approximated as Parsons and Martin (1994)

$$f(s) \approx \sqrt{1-s^2}\sum_{n=0}^{N} d_n U_n(s) \tag{7.28}$$

where N is an integer, $U_n(s)$ is the nth order Chebyshev polynomial of second kind and d_n are unknown complex constants for each $n = 0,1,2.....,N$.
Substituting $f(s)$ from (7.28) into hypersingular integral equation (7.15), we obtain the following system of algebraic equation [cf. Parsons and Martin (1994)].

$$\sum_{n=0}^{N} d_n\ B_n(t) \;\; = 2\pi u\theta g_1(t)\ , \quad -1 \le t \le 1 \tag{7.29}$$

where

$$B_n(t) = -\ \pi(n+1)U_n(t) \;\; + \;\; u^2\theta^2 \int_{-1}^{1} \sqrt{1-s^2}\ U_n(s)\ \mathcal{L}(s,t)\ ds \\ +2\pi i u\theta\kappa\lambda(t)\sqrt{1-t^2}\ U_n(t). \tag{7.30}$$

The collocation points $t = t_j$ can be taken as

$$t_j = \cos\left(\frac{2j+1}{2N+2}\right)\pi, \quad j = 0,1,2,....,N \tag{7.31}$$

so that the equation (7.29) yields the following system of linear equations

$$\sum_{n=0}^{N} d_n \; B_n(t_j) \; = 2\pi u\theta \; g_1(t_j) \; , \quad j = 0, 1, 2, ..., N \tag{7.32}$$

where d_ns are unknown constants to be determined.
Now we can approximate the solution $f(s)$ of the integral equation (7.15) by substituting d_ns in (7.28) and then using it in the equations (7.19) and (7.20) we can evaluate the value of reflection coefficient R and transmission coefficient T respectively.

ENERGY IDENTITY

The energy dissipation due to porosity yields $|R|^2 + |T|^2 < 1$ and this can be mathematically justified by applying Greens Integral theorem to the functions ϕ and $\bar{\phi}$ in the suitable chosen region which results the energy identity as

$$|R|^2 + |T|^2 = 1 - J$$

where

$$J = \begin{cases} 2Ku\theta \; \int_{-1}^{1} |f(t)|^2 \; \lambda_r(t) \; dt & \text{for DW,} \\ \frac{2Ku\theta \cosh k_0 H}{k_0 H + \frac{1}{2} \sinh 2k_0 H} \; \int_{-1}^{1} |f(t)|^2 \; \lambda_r(t) \; dt & \text{for FDW} \end{cases} \tag{7.33}$$

is the energy dissipation coefficient.

7.4 NUMERICAL RESULTS

In this section, the numerical estimates for reflection coefficients $|R|$ and energy dissipation coefficients J are studied graphically for deep water as well as finite depth of water. For deep water (DW), $|R|$ and J are depicted graphically against the dimensionless wave number Ku for different values of non-dimensional parameters v/u, θ, $\lambda(t)$. When water region is of finite depth H (FDW), $|R|$ and J are plotted graphically against the wave number KH for different values of non-dimensional parameters v/H, u/H, θ, $\lambda(t)$.

The porosity parameter $\lambda(t) = \lambda_r(t) + i\lambda_i(t), \ -1 \leq t \leq 1$ is chosen here as i) $\lambda(t) = (1+t)/2$, *ii)* $(1+i/2)(1+t)/2$, *iii)* $\lambda(t) = t^2$, *iv)* $t^2(1+i/2), \ -1 \leq t \leq 1$. We may mention here that when the inertial force coefficient is negligible as compared to the resistance force coefficient, then $\lambda(t)$ is taken to be real. The distribution of pores in each of the cases is described below.

a) When $\lambda(t) = (1+t)/2, \quad \lambda_i(t) = 0$ and $\lambda_r(t) = (1+t)/2$ so that $\lambda(t) = \lambda_r(t)$ is real. In this case, the distribution of pores in the barrier is such that $\lambda(t) = 0$ for $t = -1$, i.e., at the one end of the barrier and increases as t increases till $\lambda_r(t)$ reaches maximum value $\lambda_r(t) = 1$ at $t = 1$.

b) When $\lambda(t) = (1+i/2)(1+t)/2$, then $\lambda_r(t) = (1+t)/2$ and $\lambda_i(t) = (1+t)/4$. In this case at $t = -1$, $\lambda_r(t) = \lambda_i(t) = 0$, i.e., at one end of the plate porosity is zero. As t increases, $\lambda_r(t)$ and $\lambda_i(t)$ increase and reach maximum values $\lambda_r(t) = 1$ and $\lambda_i(t) = 1/2$. So $\lambda(t) = (1+i/2)(1+t)/2$ suggests that the distribution of pores in the barrier is such that the barrier is rigid at one end and the porosity increases along the barrier in the sense that resistance force coefficient $\lambda_r(t)$ and inertial force coefficient $\lambda_i(t)$ increases linearly along the barrier, till at the other end, the resistance force coefficient and the inertial force coefficient reaches a maximum value.

Similarly the distribution of pores in the barrier for $\lambda(t) = t^2, \ t^2(1+i/2)$ is such that $\lambda(t) = 0$ for $t = 0$, i.e., the barrier is rigid at the centre. The resistance force coefficient $\lambda_r(t)$ and inertial force coefficient $\lambda_i(t)$ increases towards the two ends of the barrier till they reach maximum values at $t = \pm 1$, i.e., at the two ends of the barrier.

The reflection coefficient $|R|$ and the amount of wave energy dissipated J can be computed numerically from (7.19) and (7.33) respectively, by solving the integral equations (7.15). For numerical computation, the value of m (number of elements) in (7.25) is chosen as $m = 45$ and the value of N (number of collocation points) in (7.32) is taken as 15. We may say here that the convergence of collocation method is faster than BEM but computation execution of BEM is simpler than collocation method.

In Tables 7.1 and 7.2 show a comparison of the values of $|R|$ obtained from boundary element method and collocation method for DW for $Ku = \{0.5, 1.0, 1.5, 2.0\}, \ \theta = \pi/10$, $v/u = 0.1$ and for $\lambda(t) = \{t^2, t^2(1+i/2)\}$.

Similar comparison of $|R|$ are presented in Tables 7.3 and 7.4 for FDW with $KH = \{0.5, 1.0, 1.5, 2.0\}$,
$\theta = \pi/10$, $v/H = 0.3$, $u/H = 0.5$ for $\lambda(t) = \{t^2, t^2(1 + i/2)\}$.
It is observed from Tables 7.1, 7.2, 7.3 and 7.4 that values of $|R|$ agree with each other upto 3 or 4 decimal places. The accuracy can be improved by increasing the number of line elements in the boundary element method and the number of collocation points N in the collocation method.
It may be noted here that the energy identity $|R|^2 + |T|^2 = 1$ has been verified for the rigid curve barrier, i.e., $\lambda = 0$. Also, the energy identity $|R|^2 + |T|^2 + J = 1$ for a porous curve barriers has been verified.

Table 7.1: Reflection coefficient for $\theta = \frac{\pi}{10}$; $\frac{v}{u} = 0.1$; $\lambda(t) = t^2$

Ku	BEM	Collocation Method
0.5	0.110823	0.110881
1.0	0.393708	0.393773
1.5	0.585003	0.585089
2.0	0.628177	0.628244

Table 7.2: Reflection coefficient for $\theta = \frac{\pi}{10}$; $\frac{v}{u} = 0.1$; $\lambda(t) = t^2(1 + \frac{i}{2})$

Ku	BEM	Collocation Method
0.5	0.106467	0.106530
1.0	0.368472	0.368526
1.5	0.554586	0.554646
2.0	0.606203	0.606259

Table 7.3: Reflection coefficient for $\theta = \frac{\pi}{10}$; $\frac{v}{H} = 0.3$; $\frac{u}{H} = 0.5$; $\lambda(t) = t^2$

KH	BEM	Collocation Method
0.5	0.0065013	0.00655601
1.0	0.0213352	0.0213885
1.5	0.0412981	0.0413128
2.0	0.0603015	0.0603288

The reflection coefficient $|R|$ for rigid barrier, i.e., for $\lambda = 0$ in deep water are compared with the results of Parsons and Martin (1994) in Figure 7.3 and in Figure 7.4, $|R|$ for rigid barrier, i.e., for $\lambda = 0$ in finite depth water are compared with the Table 1 of Liu and Li (2012). It is observed that both results are in good agreement with each

Table 7.4: Reflection coefficient for $\theta = \frac{\pi}{10}$; $\frac{v}{H} = 0.3$; $\frac{u}{H} = 0.5$; $\lambda(t) = t^2(1 + \frac{i}{2})$

KH	BEM	Collocation Method
0.5	0.0064481	0.00647615
1.0	0.0208257	0.0208765
1.5	0.0393671	0.0398722
2.0	0.0573542	0.0576478

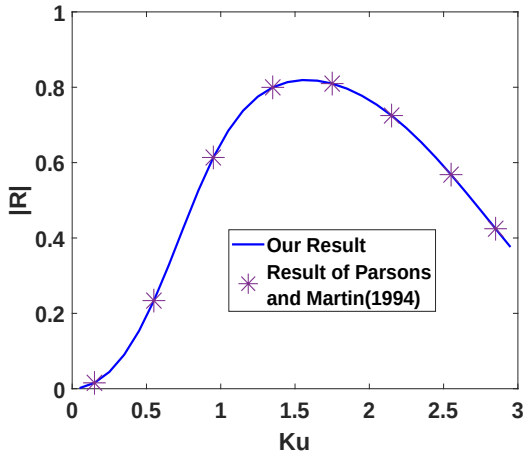

Figure 7.3: Comparison between our result and the results of Parsons and Martin(1994) for $v/u = 0.1, \theta = \pi/2$.

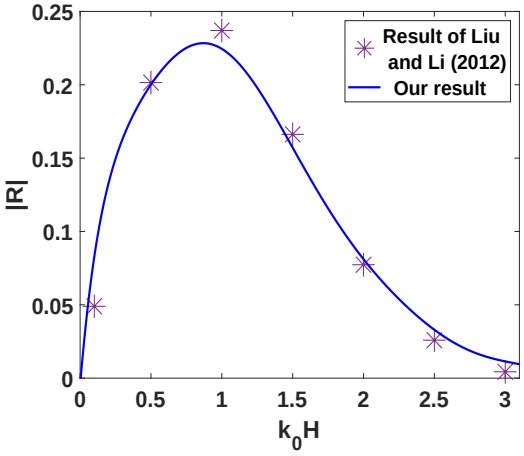

Figure 7.4: Comparison between our result and the results of Liu and Li (2012) for $v/H = 0.5, u/H = 0.5$ and $\theta = \pi/2$.

other.

In Figure 7.5, $|R|$ for deep water is compared with $|R|$ for water of finite depth, for large depth, i.e., $H/u = 3$, $v/u = 0.1$, $\theta = \pi/10$. A good matching of $|R|$ is observed for both infinite and finite depth of water region.

Behaviour of $|R|$ and J for deep water

In Figures 7.6 - 7.8 and 7.9 - 7.11, the reflection coefficient $|R|$ and the wave energy dissipation coefficient J are computed numerically for barrier in deep water (DW) and depicted graphically against the wave number Ku, for $v/u = 0.1$, the porosity parameter $\lambda(t) = \{1, 1+i/2, (1+t)/2, (1+i/2)(1+t)/2, t^2, t^2(1+i/2)\}$ and $\theta = \{\pi/10, 3\pi/10, \pi/2\}$. In Figures 7.12-7.14 and 7.15 - 7.17, the reflection coefficient $|R|$ and the wave energy dissipation coefficient J are computed numerically for barrier in water of finite depth (FDW) and depicted graphically against the wave number KH, for $v/H = 0.3, u/H = 0.5$, the porosity parameter $\lambda(t) = \{1, 1+i/2, (1+t)/2, (1+i/2)(1+t)/2, t^2, t^2(1+i/2)\}$

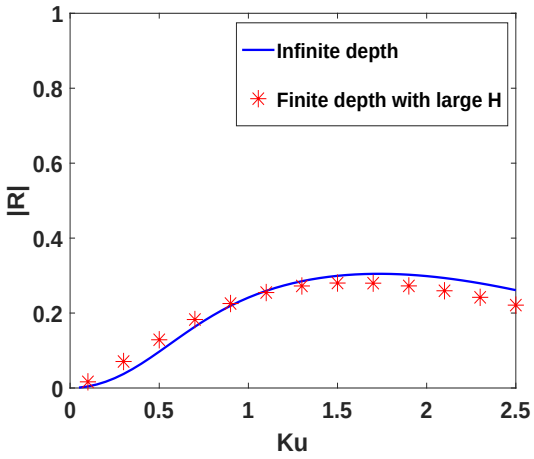

Figure 7.5: $|R|$ against Ku for deep water and for water of finite depth where $v/u = 0.1$, $\theta = \pi/10$, $H/u = 3$

and $\theta = \{\pi/10, 3\pi/10, \pi/2\}$.

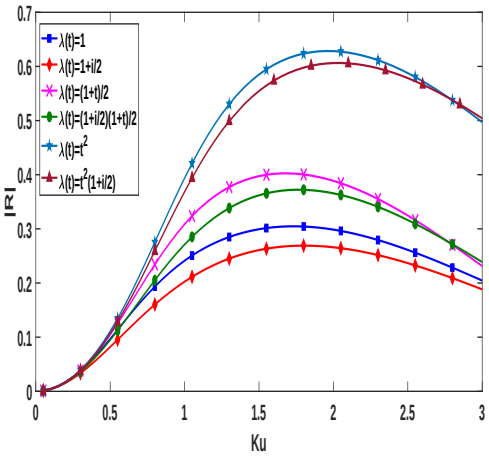

Figure 7.6: $|R|$ against Ku for constant as well as variable porosity where $v/u = 0.1$, $\theta = \pi/10$

In Figures 7.6, 7.7, 7.8, the reflection coefficient $|R|$ is plotted against wave numbers Ku for DW, for $v/u = 0.1$, the porosity parameter $\lambda(t) = \{1, 1 + i/2, (1 + t)/2, (1 + i/2)(1 + t)/2, t^2, t^2(1 + i/2)\}$ and $\theta = \{\pi/10, 3\pi/10, \pi/2\}$.

It is observed from Figures 7.6 - 7.8 that for each $\theta = \{\pi/10, 3\pi/10, \pi/2\}$, $|R|_{\lambda(t)=t^2} >$

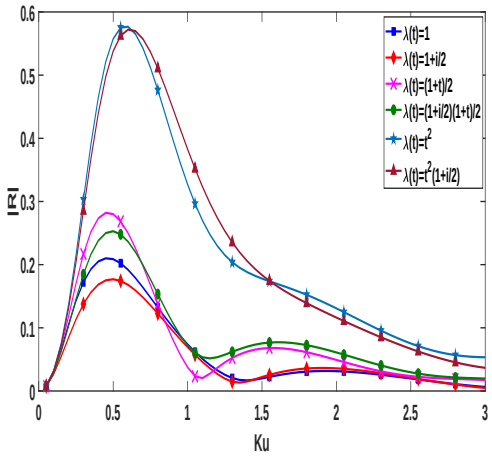

Figure 7.7: $|R|$ against Ku for constant as well as variable porosity where $v/u = 0.1$, $\theta = 3\pi/10$

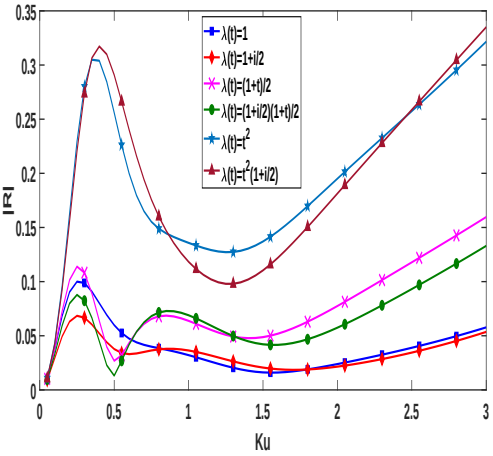

Figure 7.8: $|R|$ against Ku for constant as well as variable porosity where $v/u = 0.1$, $\theta = \pi/2$

$|R|_{\lambda(t)=(1+t)/2} > |R|_{\lambda(t)=1}$ and $|R|_{\lambda(t)=t^2(1+i/2)} > |R|_{\lambda(t)=(1+t)(1+i/2)/2} > |R|_{\lambda(t)=1+i/2}$, $-1 < t < 1$ in general. This shows that barrier with these particular choice of non uniform porosity induces more reflection than that of barrier with constant porosity.

In Figures 7.9, 7.10, 7.11, the amount of wave energy dissipated J is plotted against wave numbers Ku for DW, for $v/u = 0.1$, the porosity parameter $\lambda(t) = \{1, 1 + i/2, (1 + t)/2, (1 + i/2)(1 + t)/2, t^2, t^2(1 + i/2)\}$ and $\theta = \{\pi/10, 3\pi/10, \pi/2\}$.

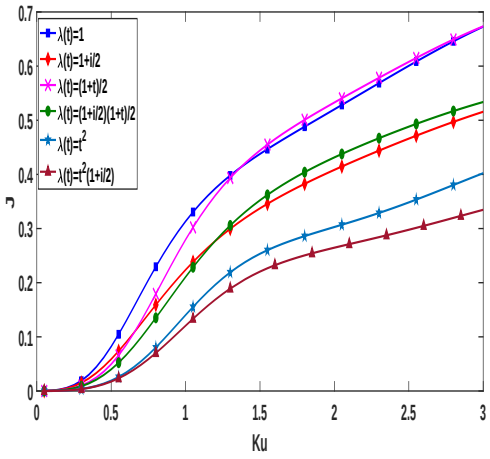

Figure 7.9: J against Ku for constant as well as variable porosity where $v/u = 0.1$, $\theta = \pi/10$

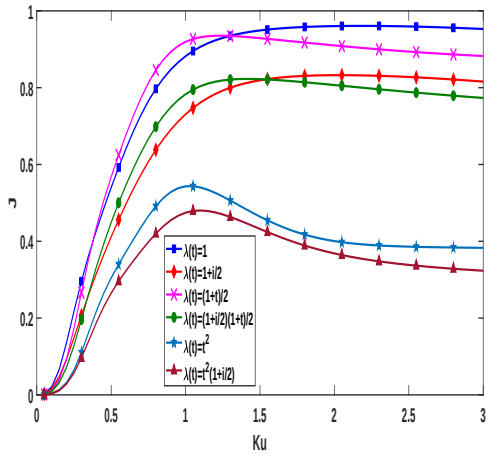

Figure 7.10: J against Ku for constant as well as variable porosity where $v/u = 0.1$, $\theta = 3\pi/10$

From the Figures 7.9-7.11, the following observation is made.

i) For short barrier, $\theta = \pi/10$, $J_{\lambda(t)=(1+t)/2} > J_{\lambda(t)=1}$ for $Ku > 1.4$. This shows that nonuniform porous barrier whose porosity increases circumferentially from one end to the other end, dissipates energy of short crested surface waves more than for barrier with uniform porosity distribution. This confirms the efficacy of a nonuniform porous barrier with this particular porosity distribution over a uniform porous barrier as model for breakwater. As the length of the barrier increases, the energy dissipation for short crested waves is more for barrier with uniform porosity than for barrier with nonuni-

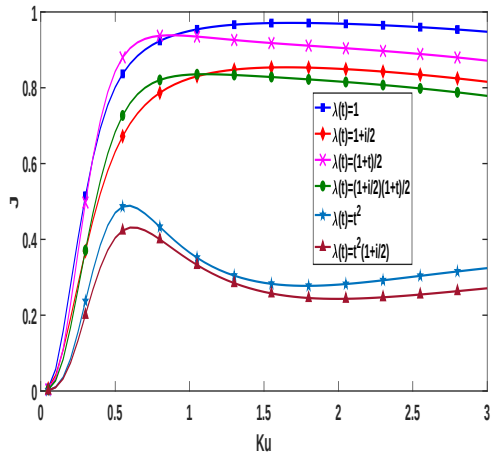

Figure 7.11: J against Ku for constant as well as variable porosity where $v/u = 0.1$, $\theta = \pi/2$

form porosity.

ii) For any length of the barrier, the energy dissipation coefficient J for barrier which is rigid at the centre and porous towards the end, is least.

iii) $J_{\lambda_{real}} > J_{\lambda_{complex}}$ showing that inertial force coefficient of the porous barrier allows the passage of water through the pores of the barrier and thereby prevents dissipation of wave energy.

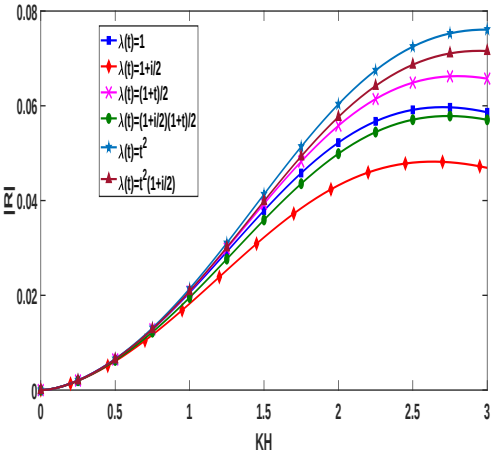

Figure 7.12: $|R|$ against KH for constant as well as variable porosity where $v/H = 0.3$, $u/H = 0.5$, $\theta = \pi/10$

Behaviour of $|R|$ and J for water of finite depth

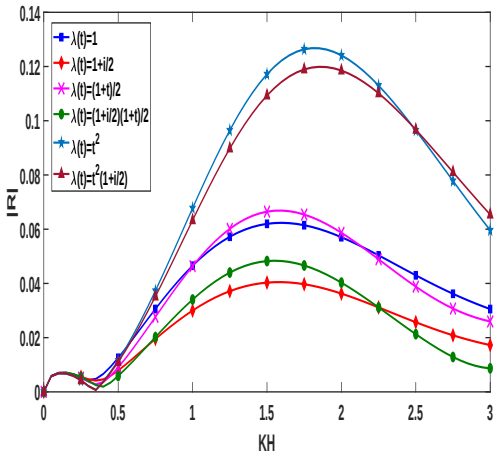

Figure 7.13: $|R|$ against KH for constant as well as variable porosity where $v/H = 0.3$, $u/H = 0.5$, $\theta = 3\pi/10$

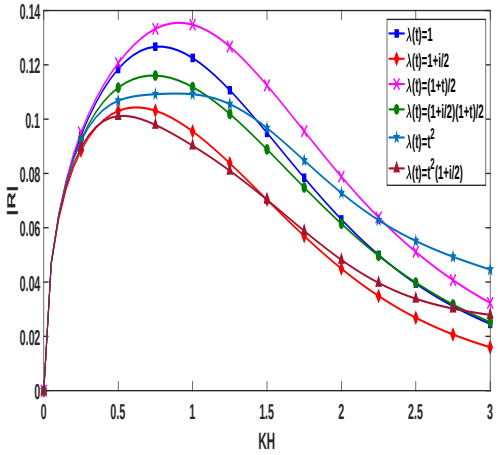

Figure 7.14: $|R|$ against KH for constant as well as variable porosity where $v/H = 0.3$, $u/H = 0.5$, $\theta = \pi/2$

In Figures 7.12-7.14, the reflection coefficient $|R|$ for FDW is plotted against the wave number KH, for $v/H = 0.3, u/H = 0.5$, the porosity parameter $\lambda(t) = \{1, 1 + i/2, (1 + t)/2, (1 + i/2)(1 + t)/2, t^2, t^2(1 + i/2)\}$ and $\theta = \{\pi/10, 3\pi/10, \pi/2\}$.

From these figures, we make the following observations.

1. From Figures 7.12, 7.13 and 7.14, it is observed in general that $|R|_{\lambda_r} > |R|_{\lambda_r + i\lambda_i}$ for all values of $\lambda(t) = \{1, 1 + i/2, (1 + t)/2, (1 + i/2)(1 + t)/2, t^2, t^2(1 + i/2)\}$ which shows that presence of inertial force coefficient in the porous barrier allows the passage

of water through it and thereby reduces the reflection.

2. Figure 7.12 show that for $KH > 1$, $|R|_{\lambda(t)=t^2} > |R|_{\lambda(t)=(1+t)/2} > |R|_{\lambda(t)=1}$ and $|R|_{\lambda(t)=t^2(1+i/2)} > |R|_{\lambda(t)=(1+i/2)(1+t)/2} > |R|_{\lambda(t)=(1+i/2)}$ which infers that for small arc length of the barrier ($\theta = \pi/10,\ 3\pi/10$), the reflection of waves with moderate to short wavelength, is more for the barrier which is rigid at the center and porous towards the ends ($\lambda(t) = t^2,\ t^2(1 + i/2)$) than by the barrier which is rigid at one end and becomes porous towards the other end ($\lambda(t) = (1+t)/2,\ (1+i/2)(1+t)/2$). Moreover reflection coefficient for these waves for barrier with constant porosity is less than the barrier with variable porosity. Also for $KH < 1$, i.e., the long waves which are towards the bottom, do not feel the presence of the barrier. Almost similar behaviour is observed from Figure 7.13 when $\theta = 3\pi/10$. It may be mentioned that for $KH > 2.2$, $|R|_{\lambda(t)=1} > |R|_{\lambda(t)=(1+t)/2}$.

However when the length of the barrier increases to $\pi/2$, the change in the behaviour of $|R|$ can be observed from Figure 7.14. For $KH < 0.3$, $|R|$ coincides for all values of $\lambda(t)$ showing that the long waves do not feel the presence of the barrier. For $0.3 < KH < 1.5$, $|R|_{\lambda(t)=(1+t)/2} > |R|_{\lambda(t)=1} > |R|_{\lambda(t)=t^2}$. For $1.5 < KH < 2.3$, $|R|_{\lambda(t)=(1+t)/2} > |R|_{\lambda(t)=t^2} > |R|_{\lambda(t)=1}$ and for $KH > 2.3$, $|R|_{\lambda(t)=t^2} > |R|_{\lambda(t)=(1+t)/2} > |R|_{\lambda(t)=1}$. Almost similar behaviour in $|R|$ is observed when the inertial force coefficient if present in the porous material of the barrier.

Thus for these choice of porosity distribution of the barrier, the behaviour of $|R|$ in the case of finite depth of water region (FDW) is different from the behaviour of $|R|$ for deep water (DW) and may be attributed to the interaction of waves with the porous barrier and the bottom of the water region.

In Figures 7.15, 7.16 and 7.17 captures the behaviour of wave energy dissipation coefficient J for FDW for various values of the wave number KH, depth of the barrier below the mean free surface, i.e., $v/H = 0.3$, radius of the barrier i.e., $u/H = 0.5$, and the porosity parameter $\lambda(t) = \{1, 1 + i/2, (1 + t)/2, (1 + i/2)(1 + t)/2, t^2, t^2(1 + i/2)\}$ and $\theta = \{\pi/10, 3\pi/10, \pi/2\}$.

1. It is observed from these figures that $J_{\lambda(t)=t^2} < J_{\lambda(t)=(1+t)/2} < J_{\lambda(t)=1}$ and $J_{\lambda(t)=t^2(1+i/2)} < J_{\lambda(t)=(1+t)(1+i/2)/2} \leq J_{\lambda(t)=1+i/2}$, $-1 < t < 1$ for $\theta = \{\pi/10, 3\pi/10, \pi/2\}$. This shows that energy dissipation for barrier with constant porosity is more than that of barrier with variable porosity. Also the energy dissipation is least for $\lambda(t) = t^2,\ t^2(1 + i/2)$.

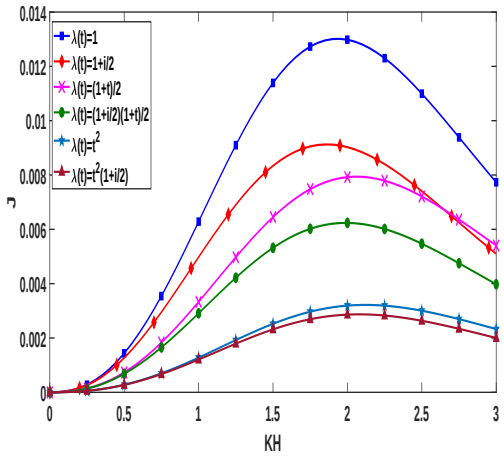

Figure 7.15: J against KH for constant as well as variable porosity where $v/H = 0.3$, $u/H = 0.5$, $\theta = \pi/10$

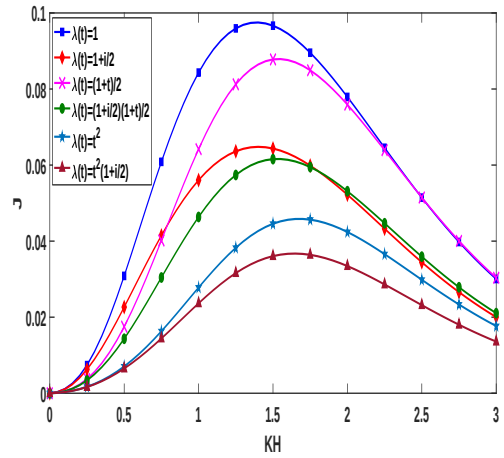

Figure 7.16: J against KH for constant as well as variable porosity where $v/H = 0.3$, $u/H = 0.5$, $\theta = 3\pi/10$

2. From these figures, it is seen that for a particular value of KH, J increases as θ increases. This shows that the dissipation of wave energy increases with length of the curved barrier.

3. Also from these figures, $J_{\lambda_r} > J_{\lambda_r + i\lambda_i}$ for any length of the barrier. So the inertial force coefficient of the porous barrier increases transmission and prevents dissipation of the wave energy.

Comparison of uniform and nonuniform porosity distribution

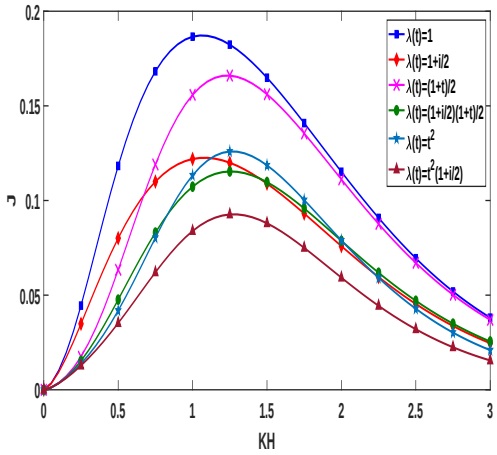

Figure 7.17: J against KH for constant as well as variable porosity where $v/H = 0.3$, $u/H = 0.5$, $\theta = \pi/2$

Figure 7.18 depicts $|R|$ and J against Ku for $v/u = 0.1$, $\theta = \pi/5$ for deep water while Figure 7.19 depicts $|R|$ and J against Ku for $v/u = 0.1$, $H/u = 1.2$ $\theta = \pi/5$ for water of finite depth for uniform porosity distribution given by $\lambda(t) = 1$ and for nonuniform porosity distribution $\lambda(t) = (0.5 + t^2)$. This particular choice of nonuniform porosity distribution shows that the porosity is less near the middle of the barrier and increases towards the ends of the barrier. From both figures it is seen that energy dissipation J for nonuniform porosity is more than that of uniform porosity. In particular, the J for barrier with nonuniform porosity is significantly more than J for barrier with uniform porosity when the water is of finite depth. This shows that barrier with porosity distribution $\lambda(t) = (0.5+t^2)$ reduces the wave power by dissipating the energy and thus serves as a better model for breakwater than a barrier with uniform porosity. This phenomena is also observed in Figure 7.9.

7.5 CONCLUSIONS

The present work is concerned with a study of phenomenon of scattering of incident waves by a porous curve barrier in water with finite and infinite depth. The problem is formulated in terms of hypersingular integral equation of second kind where the

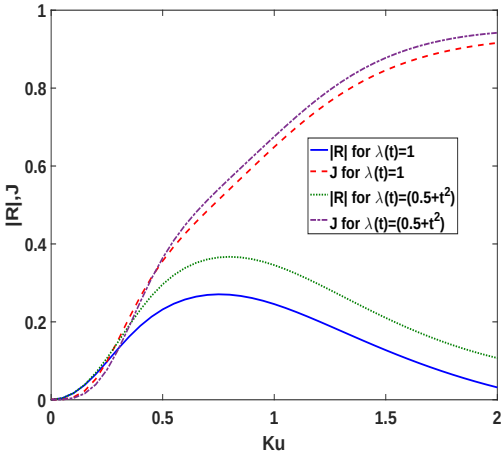

Figure 7.18: $|R|$ and J against Ku for $v/u = 0.1$, $\theta = \pi/5$ for deep water.

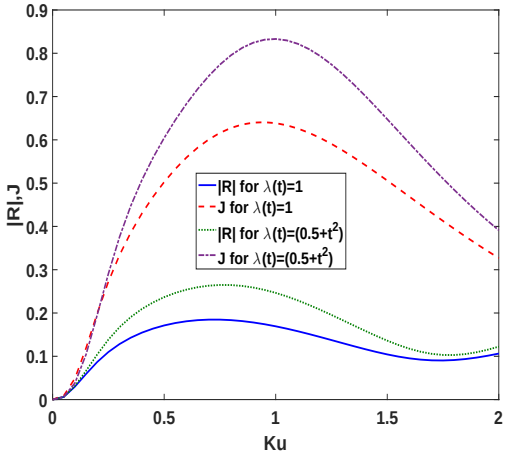

Figure 7.19: $|R|$ and J against Ku for $v/u = 0.1$, $H/u = 1.2$ $\theta = \pi/5$ for water of finite depth.

unknown function represents the difference of potentials across the curve barrier. The integral equation is then solved by two methods viz, the boundary element method and the collocation method. Using the solution of the integral equation the reflection coefficient and the amount of wave energy dissipated are obtained which are depicted graphically against the wave number choosing different types of porosity distribution in the barrier. An important observation from the graphical representation is that for a certain choice of nonuniform porosity distribution in the barrier, the energy dissipation can be enhanced and thereby the wave power can be reduced, making the barrier a better model for breakwater.

The behaviour of reflected waves and the energy dissipation coefficient in the case of finite depth of water region is some what different from the behaviour of the same for deep water and may be attributed to the interaction of waves with the porous barrier and the bottom of the water region.

CHAPTER 8

WATER WAVE INTERACTION WITH A VERTICAL WALL WITH A GAP SUBMERGED IN DEEP WATER

8.1 INTRODUCTION

The problem of scattering of water waves by a submerged wall with a gap present in deep water was studied by Banerjea and Mandal in 1998 using singular integral equation formulation. Using Havelock's expansion of water wave potential, they reduced the corresponding boundary value problem to the solution of singular integral equation in double interval whose kernel involves i) Cauchy type singularity ii) a combination of Cauchy and logarithmic singularity. In their study the unknown function satisfying the integral equation has square root singularity at the end points of the domain of definition of the integral equation. The integral equation was solved by using function theoretic method. The reflection coefficient was evaluated using the solutions of the two types of integral equations and they were found to match with each other. We

[0]† The content of this chapter is based on the paper " Water wave interaction with a vertical wall with a gap submerged in deep water", (communicated).

may mention here that the solution of Cauchy integral equation in double interval (also termed as Tricomi integral equation), where the unknown function satisfying the integral equation has square root singularity at the end points of the domain of definition was solved by Tricomi (1951) using a simple method. Also the solution of Cauchy integral equation in multiple intervals was given in the book of Gakhov (1966) when the unknown function satisfying the integral equation has i) square root singularity at the end points of the domain of definition, ii) square root zero at the end points of the domain of definition, iii) square root zero at some end points of the domain of definition and square root singularity at other end points. Gakhov used function theoretic method to solve this integral equation for various end point behaviour of the unknown function. For the case ii) and iii) the solution exists if the forcing function satisfies some solvability conditions.

Banerjea (1996) used singular integral equation formulation to study water wave scattering problem by a vertical barrier with multiple gaps submerged in deep water. The kernel of the singular integral equation obtained in Banerjea (1996) has Cauchy type singularity and the unknown function satisfying the integral equation has square root singularity at the end points of the domain of definition. The reflection coefficient was obtained in terms of the solution of the integral equation.

In the present study we used Cauchy type singular integral equation formulation to investigate the wave scattering problem by a submerged wall with a gap which was studied by Banerjea and Mandal in 1998 . Following Williams (1966), Jarvis and Taylor (1969) and Mandal (1998), we reduced the corresponding boundary value problem to a Cauchy singular integral equation in two disjoint intervals where the unknown function satisfying the integral equation is bounded at all end points of the domain of integration. In this case the solution of the integral equation exists if the forcing function satisfies two solvability conditions. It is mentioned apriori that the unknown function satisfying the Cauchy integral equation obtained in Banerjea and Mandal (1998) was unbounded at all end points of the interval of definition. In the present case the forcing function involved two unknown constants, one of which is the reflection coefficient. These unknowns were obtained from the two solvability conditions without solving the integral equation. The reflection coefficient was found to match with the

result in Banerjea and Mandal (1998).

8.2 FORMULATION OF THE PROBLEM

We consider two dimensional irrotational motion of an incompressible inviscid fluid occupying the region $y \geq 0$, where y-axis is taken vertically downwards into the fluid and the plane $y = 0$ represents the undisturbed free surface. A train of time harmonic surface waves with circular frequency σ is incident from negative infinity on a thin vertical submerged wall with a gap. The wall occupies the position $x = 0, y \in B$ where $B = (\alpha, \beta) \cup (\gamma, \infty)$ while the gap in the wall has the position $x = 0, \beta < y < \gamma$. If the fluid motion is described by the velocity potential $\Re\{\Phi(x, y)e^{-i\sigma t}\}$, then assuming linear theory, Φ satisfies (cf. Banerjea and Mandal (1998))

$$\nabla^2\Phi = 0 \text{ in } y \geq 0, \tag{8.1}$$

$$\frac{\partial\Phi}{\partial y} + K\Phi = 0 \text{ in } y = 0, \tag{8.2}$$

where $K = \frac{\sigma^2}{g}$, with g being the acceleration due to gravity.

$$\frac{\partial\Phi}{\partial x} = 0 \text{ on } x = 0, y \in B, \tag{8.3}$$

$$\nabla\Phi \to 0 \text{ as } y \to \infty, \tag{8.4}$$

$$r^{1/2}\nabla\Phi \to 0 \text{ as } r \to 0, \tag{8.5}$$

where r is the distance of any field point from sharp edges of the barrier,

$$\Phi(x, y) \sim \begin{cases} e^{-Ky+iKx} + Re^{-Ky-iKx} \text{ as } x \to -\infty, \\ Te^{-Ky+iKx} \text{ as } x \to \infty. \end{cases} \tag{8.6}$$

Here R and T are the reflection and transmission coefficients respectively, which are

to be determined.

To solve this boundary value problem, we introduce a new function $\phi(x, y)$ defined by,

$$\phi(x, y) = e^{Ky} \int_{\infty}^{y} \Phi(x, \eta) e^{-K\eta} d\eta. \tag{8.7}$$

Then clearly from (8.7), we have

$$\Phi(x, y) = \frac{\partial \phi}{\partial y} - K\phi. \tag{8.8}$$

Using relation (8.7) in equations (8.1), (8.2), (8.5) (8.6) we find that $\phi(x, y)$ satisfies

$$\frac{\partial^2 \phi}{\partial x^2} + \frac{\partial^2 \phi}{\partial y^2} = 0 \quad (y \geq 0), \tag{8.9}$$

$$\frac{\partial^2 \phi}{\partial x^2} + K^2 \phi = 0 \quad (y = 0), \tag{8.10}$$

$$\nabla \phi \sim r^{1/2} \quad \text{as} \quad r \to 0, \tag{8.11}$$

$$\begin{aligned} \phi(x, 0) &= -\frac{1}{2K} e^{iKx} - \frac{R}{2K} e^{-iKx} \quad (x < 0), \\ \phi(x, 0) &= -\frac{T}{2K} e^{iKx} \quad (x > 0). \end{aligned} \tag{8.12}$$

Since $\frac{\partial \Phi}{\partial x}$ is continuous across $x = 0$, the relation (8.7) shows that $\frac{\partial \phi}{\partial x}$ is also continuous across $x = 0$. Hence relation (8.12) implies that

$$R + T = 1. \tag{8.13}$$

We now define a function $\psi(x, y)$ by,

$$\psi(x, y) \sim \begin{cases} \phi(x, y) + \frac{1}{2K} e^{-Ky + iKx} + \frac{R}{2K} e^{-Ky - iKx} & (x < 0), \\ \phi(x, y) + \frac{T}{2K} e^{-Ky + iKx} & (x > 0). \end{cases} \tag{8.14}$$

Then from (8.9) to (8.12), we find that $\psi(x,y)$ satisfies

$$\frac{\partial^2\psi}{\partial x^2}+\frac{\partial^2\psi}{\partial y^2}=0 \quad (y\geq 0), \tag{8.15}$$

$$\psi(x,0)=0 \quad (-\infty<x<\infty), \tag{8.16}$$

$$\psi(+0,y)-\psi(-0,y)=\begin{cases}\frac{2R}{K}\sinh Ky, & y\in(0,\alpha),\\ \frac{2A}{K}e^{-K(\gamma-y)}-\frac{2R}{K}e^{-K\gamma}\sinh K(\gamma-y), & y\in(\beta,\gamma),\end{cases} \tag{8.17}$$

where

$$A=\frac{K}{2}\left\{\psi(+0,\gamma)-\psi(-0,\gamma)\right\},$$

is an unknown constant to be determined,

$$\frac{\partial\psi}{\partial x}(+0,y)-\frac{\partial\psi}{\partial x}(-0,y)=0, \quad y\in G\equiv(0,\alpha)\cup(\beta,\gamma), \tag{8.18}$$

$$\nabla\psi\sim r^{1/2} \quad \text{as} \quad r\to 0, \tag{8.19}$$

$$\frac{\partial\psi}{\partial x}(0,y)=\frac{i}{2}(1-R)e^{-Ky}, \quad y\in B. \tag{8.20}$$

Following Jarvis and Taylor (1969), we apply Greens integral theorem to the function $\psi(x,y)$ and the Green's function

$$G_1(x,y;\xi,\eta)=\frac{1}{4\pi}\log\frac{\{(x-\xi)^2+(y-\eta)^2\}\{(x+\xi)^2+(y-\eta)^2\}}{\{(x-\xi)^2+(y+\eta)^2\}\{(x+\xi)^2+(y+\eta)^2\}} \tag{8.21}$$

in the region bounded by $y=0, 0\leq x\leq X_1$; $x=0, 0\leq y\leq Y_1$; $y=Y_1$, $0\leq x\leq X_1$; $x=X_1, 0\leq y\leq Y_1$ and internally by a very small circle of radius δ centering (ξ,η), $\xi>0$ and ultimately making $X_1\to\infty$, $Y_1\to\infty$ and $\delta\to 0$ and taking $x>0$,

we represent $\psi(x,y)$ as

$$\psi(x,y) = \int_0^\infty \frac{\partial \psi}{\partial \xi}(+0,\eta) G_1(x,y;0,\eta) d\eta, \quad x > 0.$$

Similarly applying Greens integral theorem to the functions $\psi(x,y)$ and $G_1(x,y,\xi,\eta)$ in the region bounded by $y = 0, -X_1 \le x \le 0$; $x = 0, 0 \le y \le Y_1$; $y = Y_1$, $-X_1 \le x \le 0$; $x = -X_1, 0 \le y \le Y_1$ and internally by a very small circle of radius δ centering (ξ,η), $\xi < 0$ and ultimately making $X_1 \to \infty$, $Y_1 \to \infty$ and $\delta \to 0$, we represent $\psi(x,y)$ in the the region $x < 0$ as

$$\psi(x,y) = -\int_0^\infty \frac{\partial \psi}{\partial \xi}(-0,\eta) G_1(x,y;0,\eta) d\eta \quad x < 0.$$

Using relations (8.17), (8.18) and (8.20), we obtain

$$\int_0^\infty \frac{\partial \psi}{\partial \xi}(0,\eta) G_1(0,y;0,\eta) d\eta = \begin{cases} \frac{R}{K} \sinh Ky, & y \in (0,\alpha), \\ \frac{A}{K} e^{-K(\gamma - y)} - \frac{R}{K} e^{-K\gamma} \sinh K(\gamma - y), & y \in (\beta,\gamma), \end{cases}$$

where A is an unknown constant to be determined. Further simplification gives

$$\begin{aligned} &\frac{1}{\pi} \int_{\eta \in G} f(\eta) \log \left| \frac{y-\eta}{y+\eta} \right| d\eta \\ &= \begin{cases} \frac{R}{K} \sinh Ky - \frac{i}{2\pi}(1-R) \int_{\eta \in B} e^{-K\eta} \log \left| \frac{y-\eta}{y+\eta} \right| d\eta, & y \in (0,\alpha), \\ \frac{A}{K} e^{-K(\gamma-y)} - \frac{R}{K} e^{-K\gamma} \sinh K(\gamma - y) - \frac{i}{2\pi}(1-R) \int_{\eta \in B} e^{-K\eta} \log \left| \frac{y-\eta}{y+\eta} \right| d\eta, & y \in (\beta,\gamma), \end{cases} \end{aligned} \tag{8.22}$$

where

$$f(y) = \frac{\partial \psi}{\partial x}(0,y). \tag{8.23}$$

Noting the relations (8.23) and (8.19) we state that

$$f(y) \sim r^{1/2} \quad \text{as} \quad r \to 0 \tag{8.24}$$

where r is the distance from sharp edges of the barrier. Now Differentiating (8.22)

with respect to y, we have the following Cauchy type integral equation in two disjoint intervals

$$\frac{1}{\pi}\int_{\eta\in G} f(\eta)\frac{2\eta}{y^2-\eta^2}d\eta = g(y), \quad y\in G, \tag{8.25}$$

where

$$g(y) = \begin{cases} R\cosh Ky - \frac{i}{2\pi}(1-R)\int_{\eta\in B} e^{-K\eta}\frac{2\eta}{y^2-\eta^2}d\eta, \ y\in(0,\alpha), \\ Ae^{-K(\gamma-y)} + Re^{-K\gamma}\cosh K(\gamma-y) - \frac{i}{2\pi}(1-R)\int_{\eta\in B} e^{-K\eta}\frac{2\eta}{y^2-\eta^2}d\eta, \ y\in(\beta,\gamma). \end{cases} \tag{8.26}$$

Thus the forcing function $g(y)$ involves two unknown constants A and R.

The solution of the integral equation (8.25) with $f(\eta)$ satisfying the condition (8.24) is given in Gakhov (1966) and also in Chapter 2.6.1, (2.97) and it is also noted that the solution of (8.25) exists if $g(y)$ satisfies two solvability conditions given by (cf (2.98), (2.99), Chapter 2.6.1)

$$\left(\int_0^\alpha - \int_\beta^\gamma\right)\frac{g(u)}{\rho(u)}du = 0 \tag{8.27}$$

and

$$\left(\int_0^\alpha - \int_\beta^\gamma\right)\frac{u^2 g(u)}{\rho(u)}du = 0, \tag{8.28}$$

$$\text{where} \quad \rho(u) = |(u^2-\alpha^2)(\beta^2-u^2)(\gamma^2-u^2)|^{\frac{1}{2}}.$$

It is interesting to note that the function $g(y)$ contains two unknown constants R and A which can be evaluated from two relations (8.27) and (8.28). Now substituitng the value of $g(y)$ from (8.26) in relations (8.27) and (8.28) and solving them, we obtain the value of R and A. The expression for R is given by

$$R = \frac{C(K)\gamma_3(K) - D(K)\gamma_1(K)}{\gamma_3(K)\left[\alpha_1(K) - \alpha_3(K) + C(K)\right] - \gamma_1(K)\left[\beta_1(K) - \beta_3(K) + D(K)\right]} \tag{8.29}$$

where

$$\alpha_1(K) = \int_0^\alpha \frac{\cosh Ky}{\rho(y)} dy, \qquad \alpha_3(K) = e^{-Kc} \int_\beta^\gamma \frac{\cosh K(c-y)}{\rho(y)} dy,$$

$$\beta_1(K) = \int_0^\alpha \frac{y^2 \cosh Ky}{\rho(y)} dy, \qquad \beta_3(K) = e^{-Kc} \int_\beta^\gamma \frac{y^2 \cosh K(c-y)}{\rho(y)} dy,$$

$$\gamma_1(K) = -\int_\beta^\gamma \frac{e^{-K(c-y)}}{\rho(y)} dy, \qquad \gamma_3(K) = -\int_\beta^\gamma \frac{y^2 e^{-K(c-y)}}{\rho(y)} dy,$$

$$C(K) = \frac{i}{2\pi} \left[A_{12}(-K) + A_{14}(-K) - A_{32}(-K) - A_{34}(-K) \right],$$

$$D(K) = \frac{i}{2\pi} \left[B_{12}(-K) + B_{14}(-K) - B_{32}(-K) - B_{34}(-K) \right],$$

$$A_{12}(K) = \int_0^\alpha \frac{1}{\rho(y)} \left(\int_\alpha^\beta \frac{2\eta e^{K\eta}}{\eta^2 - y^2} d\eta \right) dy, \qquad A_{14}(K) = \int_0^\alpha \frac{1}{\rho(y)} \left(\int_\gamma^\infty \frac{2\eta e^{K\eta}}{\eta^2 - y^2} d\eta \right) dy,$$

$$A_{32}(K) = \int_\beta^\gamma \frac{1}{\rho(y)} \left(\int_\alpha^\beta \frac{2\eta e^{K\eta}}{\eta^2 - y^2} d\eta \right) dy, \qquad A_{34}(K) = \int_\beta^\gamma \frac{1}{\rho(y)} \left(\int_\gamma^\infty \frac{2\eta e^{K\eta}}{\eta^2 - y^2} d\eta \right) dy,$$

$$B_{12}(K) = \int_0^\alpha \frac{y^2}{\rho(y)} \left(\int_\alpha^\beta \frac{2\eta e^{K\eta}}{\eta^2 - y^2} d\eta \right) dy, \qquad B_{14}(K) = \int_0^\alpha \frac{y^2}{\rho(y)} \left(\int_\gamma^\infty \frac{2\eta e^{K\eta}}{\eta^2 - y^2} d\eta \right) dy,$$

$$B_{32}(K) = \int_\beta^\gamma \frac{y^2}{\rho(y)} \left(\int_\alpha^\beta \frac{2\eta e^{K\eta}}{\eta^2 - y^2} d\eta \right) dy, \qquad B_{34}(K) = \int_\beta^\gamma \frac{y^2}{\rho(y)} \left(\int_\gamma^\infty \frac{2\eta e^{K\eta}}{\eta^2 - y^2} d\eta \right) dy.$$

8.3 NUMERICAL RESULTS

The graphical representation of the reflection coefficient $|R|$ obtained from the condition (8.29) in the present study and $|R|$ obtained by Banerjea and Mandal (1998) are represented in Figure (8.1) for $\frac{\beta}{\alpha} = 1.1$, $\frac{\gamma}{\alpha} = 1.49$ and in Figure (8.2) for $\frac{\beta}{\alpha} = 1.3$, $\frac{\gamma}{\alpha} = 1.35$. Here we see that $|R|$ obtained from the solvability condition almost matches with the reflection coefficient obtained from Banerjea and Mandal (1998) .

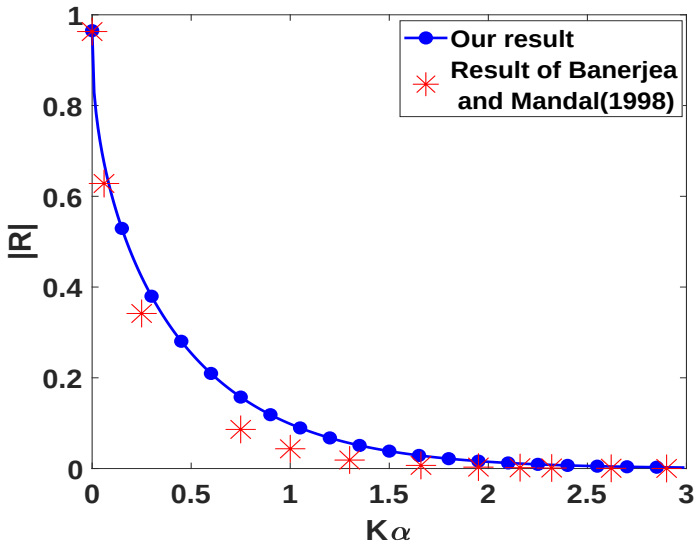

Figure 8.1: Comparison of our results with the results of Banerjea and Mandal (1998) for $\frac{\beta}{\alpha} = 1.1$, $\frac{\gamma}{\alpha} = 1.49$

8.4 CONCLUSIONS

In the present study, we considered the problem of scattering of water waves by a thin vertical wall with a gap submerged in deep ocean. The corresponding boundary value problem is reduced to a Cauchy integral equation in double intervals where the unknown function satisfying the integral equation is bounded at all four end points of the domain of definition of the integral equation. It is known that when this unknown function is bounded at all the said end points then certain solvability conditions need to be satisfied for the solution to exist. The forcing function in this integral equation

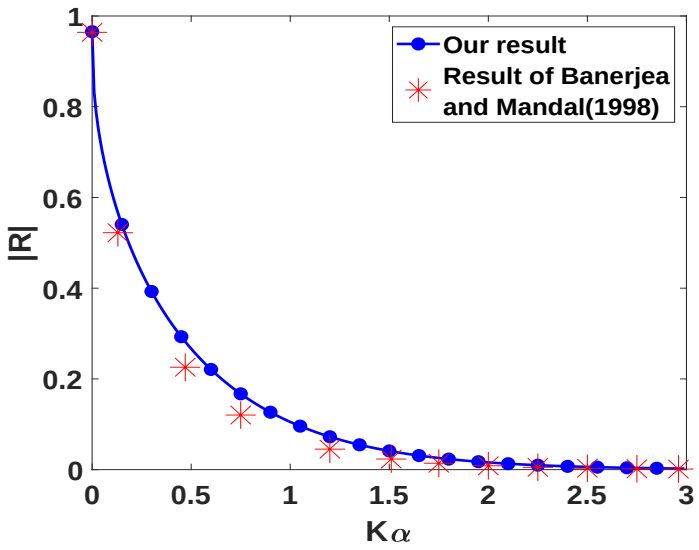

Figure 8.2: Comparison of our results with the results of Banerjea and Mandal (1998) for $\frac{\beta}{\alpha} = 1.3$, $\frac{\gamma}{\alpha} = 1.35$

contains two unknown constants A and $|R|$, which are determined from the aforesaid two solvabilty conditions withot solving the integral equation. The reflection coefficient $|R|$ thus obtained is compared with the results in Banerjea and Mandal (1998) and an almost matching of two results are observed.

FUTURE SCOPE OF WORK

The present thesis is concerned with a study of wave interaction with barriers of various configurations viz., rigid wall with a gap, elastic plate, thick rectangular barrier, thick slotted barrier, porous curved barrier present in water with free surface or water with ice cover. These problems constitute an important class of problems known as scattering problems.

Water wave scattering problems involving barrier present in water with various bathymetry is important from the point of view of coastal engineering. The interaction of water waves with non uniform bottom topography is important in understanding the wave induced mass transport. This class of problems involving barriers present in water region of nonuniform bathymetry can be studied.

It is well known that the problem of scattering of water waves by porous coastal structures like rubble mound breakwaters are important in coastal engineering as the pores in the barrier attenuates wave action by dissipating the wave energy and thereby protects the coast line or harbour. Many researchers used sophisticated mathematical techniques to study scattering problems involving porous barrier with constant porosity. However when the porosity of the barrier is non uniform, then for certain choice of porosity distribution in the barrier, the energy dissipation can be made more than a barrier with uniform porosity. This phenomena has an important bearing in the construction of breakwater. The literature concerning these scattering problems

involving barrier with non uniform porosity is rather limited. There is much scope to study water wave propagation problems in presence of barriers with variable porosity when the water bed is non uniform.

The scattering problems involving barriers in water with poro-ealstic bed is interesting from the physical and mathematical point of view. There is much scope to study wave structure interaction problems in water region with poro-elastic bed.

The three dimensional scattering problems involving perforated cylinder or sphere serve as a model for fish cage in fish farming in deep sea. These problems can be studied using various sophisticated mathematical techniques.

BIBLIOGRAPHY

1. Banerjea, S., (1996). Scattering of water waves by a vertical wall with gaps, *The ANZIAM Journal*, **37(4)**, 512-529.

2. Banerjea, S., Kanoria, M., Dolai, D.P. and Mandal, B.N. (1996). Oblique wave scattering by a submerged thin wall with gap in finite depth water, *Appl Ocean Res.*, **18**, 319-327.

3. Banerjea, S. and Mandal, B.N. (1998). Scattering of water waves by a submerged thin vertical wall with a gap, *The ANZIAM Journal*, **39(3)**, pp.318-331.

4. Banerjee, S., Mondal, D. and Banerjea, S. (2024). Wave response to a non uniform porous vertical plate, *J. Mar. Sci. Applcs.*

5. Bennett, G. S., McIver, P. and Smallman, J.U. (1992). A mathematical model of slotted wave screen breakwater, *Coastal Engng*, **18**, 231-249.

6. Bhattacharjee, J. and Soares, C. G. (2012). Flexural gravity wave over a floating ice sheet near a vertical wall, *J. Eng. Math.*, **75**, 29-48.

7. Chakrabarti, A. (2000) On the solution of the problem of scattering of surface water waves by the edge of an ice-cover, *Proc. R. Soc. Lond. A*, **456**, 1087-1099.

8. Chakrabarti, A. and Mandal, B. N. (1998). Derivation of the solution of a simple hypersingular integral equation, *Int. J. Math. Educ. Sci. Technol.*, **29**, 47-53.

9. Chakrabarti, A. and Sahoo, T. (1998). The effect of surface tension in porous wave maker problems, *Journal of the Australian Mathematical Society*, **B 39**, 539-556.

10. Chakraborty, R., Mandal, B.N. (2013). Water waves scattering by an elastic thin vertical plate submerged in finite depth water, *J. Mar. Sci. Appl.* , **12**, 393-399 .

11. Chakraborty, R. and Mandal B.N. (2014). Water wave scattering by rectangular trench, *J. Eng. Math.*, **89**, 101-112.

12. Chakraborty, R. and Mandal, B.N. (2015). Oblique water wave scattering by a rectangular submarine trench, *ANZIAM J.*, **56**, 286-298.

13. Chakraborty, R., Mondal, A. and Gayen, R. (2016). Interaction of surface water waves with a vertical elastic plate: a hypersingular integral equation approach, *Z. Angew. Math. Phys.*, **67**, 115.

14. Chung, H., and Fox., C., (2002). Calculation of wave-ice interaction using the WienerHopf technique. *New Zealand J. Math.*, **31(1)**, 1-18.

15. Chwang, A. T. (1983). A porous-wavemaker theory, *J. Fluid Mech.*, **132**, 395-406.

16. Crapper, G. D. (1984). Introduction to Water Waves, *Ellis Horwood*.

17. Dai, J., Wang, C.M., Utsunomiya, T. and Duan, W (2018). Review of Recent Research and Developments on Floating Breakwaters, *Ocean Engineering*, **158**, 132-151.

18. Das, B.C., De, S. and Mandal, B.N. (2020). Oblique water waves scattering by a thick barrier with rectangular cross section in deep water, *Journal of Engineering Mathematics*, **122**, 81-99.

19. Das, D. and Mandal, B. N. (2008). Water Wave Radiation by a Sphere Submerged in Water with an Ice-Cover, *Arch. Appl. Mech.*, **78**, 649661.

20. Das, P., Dolai, D.P. and Mandal, B.N. (1997). Oblique wave diffraction by two parallel thin barriers with gaps, *J. Waterw. Port Coast Ocean Eng.*, **123** , 163-171.

21. Dean, R. G. and Ursell, F. (1959). Interaction of a fixed semi-immersed circular cylinder with a train of surface waves, *M. I. T. Hydrodynamics Laboratory, Tech. Rep. no.* **37**.

22. Dean, W. R. (1945). On the reflection of surface waves by a submerged plane barrier, *Proceedings of Cambridge Philosophical Society*, **41**, 231-238.

23. Evans, D. V. (1968a). The effect of surface tension on the waves produced by a heaving circular cylinder, *In Proceedings of Cambridge Philosophical Society*, **64** , 833-847.

24. Evans, D. V. (1968b). The influence of surface tension on the reflection of water waves by a plane vertical barrier, *In Proceedings of Cambridge Philosophical Society*, **64** , 795-810.

25. Evans, D. V. (1970). Diffraction of surface waves by a submerged vertical plate, *Journal of Fluid Mechanics*, **40**, 433-451.

26. Evans, D . V. and Morris, C. A. N. (1972). Complementary approximations of the solution of a problem in water waves, *J. Inst. Maths Applics.*, **10**, 1-9.

27. Evans, D. V. and Porter, R. (2003). Wave scattering by narrow cracks in ice sheets floating on water of finite depth, *Journal of Fluid Mechanics*, **484**, 143-165.

28. Fox, C. and Squire, V. A. (1990). Reflection and transmission characteristics at the edge of shore fast sea ice, *J. Geophys. Res.*, **95**,11629-11639.

29. Fox, C. and Squire, V. A. (1994). On the oblique reflection and transmission of ocean waves at shore fast sea ice, *Phil Trans R Soc.*, **347**, 185-218.

30. Gakhov, F. D. (1966). Boundary value problems, Courier Corporation, Pergamon Press.

31. Gayen, R. (2004). Water wave scattering by obstacles and surface discontinuities, *J. Eng. Math.*, **53**, 21-37.

32. Gayen, R., Mandal, B. N. and Chakrabarti, A. (2005). Water wave scattering by an ice-strip, *J. Eng. Math.*, **53**, 21-37.

33. Gayen, R. and Mandal, B. N. (2009). Scattering of Surface Water Waves by a Floating Elastic Plate in Two Dimensions, *SIAM J. Appl. Math.*, **69(6)**, 1520-1541.

34. Gayen, R. and Mondal, A. (2014). A hypersingular integral equation approach to the porous plate problem, *Applied Ocean Research*, **46**, 70-78.

35. Goswami, S. K. (1983). Scattering of surface waves by a submerged fixed vertical plate in water of finite depth, *J. Indian Inst. Sci.*, **64B**, 79-88.

36. Gradshteyn, I.S. and Ryzhik, I.M. (2014). Table of integrals, series, and products, Academic press.

37. Gupta, S. and Gayen, R. (2019). Water wave interaction with dual asymmetric non-uniform permeable plates using integral equations, *Applied Mathematics and Computation*, **346**, 436-451.

38. Hassan, M., Meylan, M. H. and Peter, M. A. Q. (2009). Water-wave scattering by submerged elastic plates, *The Quarterly Journal of Mechanics and Applied Mathematics*, **62 (3)**, 321-344.

39. Havelock, T. H. (1929). Forced waves in water, *Philos. Mag.*, **8**, 569-576.

40. Havelock, T. H. (1963), Collected Papers, *Government Printing Office*, Washington, DC: U.S.

41. Hocking, L. and Mahdmina, D. (1991). *Journal of Fluid Mechanics*, **224**, 217-226.

42. Issacson, M., Premasiri, S. and Yang, G. (1998). Wave interactions with vertical slotted barriers, *J. Wtry Port, Coastal Ocean Engng* , **124**, 118-126.

43. Jarvis, R.J. and Taylor, B.S. (1969, September). The scattering of surface waves by a vertical plane barrier, *In Mathematical Proceedings of the Cambridge Philosophical Society, Cambridge University Press*, **66(2)**, 417-422.

44. Kaligatla, R. B. and Manam, S. R. (2014). Flexural gravity wave scattering by a nearly vertical porous wall, *J. Eng. Math.*, **88**, 49-66.

45. Kanoria, M., Dolai D.P. and Mandal B.N. (1999). Water wave scattering by thick vertical barriers, *J. Eng. Math.*, **35**, 361-384.

46. Kanoria, M. and Mandal, B.N. (2002). Water wave scattering by a submerged circular-arc-shaped plate, *Fluid dynamics research*, **31**, 317.

47. Kashiwagi, M. (2004). Transient responses of a VLFS during landing and take-off of an airplane, *J. Mar. Sci. Technol.*, **9**, 14-23.

48. Kirby, J.T. and Dalrymple, R.A. (1983). Propagation of obliquely incident water waves over a trench, *J. Fluid Mech.*, **133**, 47-63.

49. Kirby, J.T., Dalrymple, R.A. and Seo S.N. (1987). Propagation of obliquely incident water waves over a trench. Part 2. Currents flowing along the trench, *J. Fluid Mech.*, **176**, 95-116.

50. Kohout, A. L. and Meylan, M. H. (2008). An elastic plate model for wave attenuation and ice floe breaking in the marginal ice zone, *Jour. of Geophys. Res.*, **113**.

51. Kuznetsov, N., McIver, P. and Linton, C. M. (2001). On uniqueness and trapped modes in the water-wave problem for vertical barriers, *Wave Motion*, **33**, 283-307.

52. Lamb, H. (1932). Hydrodynamics, *Cambridge University Press,* England.

53. Lassiter, J.B. (1972). The propagation of water waves over sediment pockets. Doctoral dissertation, M.I.T.

54. Lee J.J. and Ayer R.M. (1981). Wave propagation over a rectangular trench, *J. Fluid Mech.*, **110** , 335-347.

55. Lee, M. M. and Chwang, A. T.(2000). Scattering and radiation of water waves by permeable barriers, *Physics of Fluids*, **12**, 54-65.

56. Levine, H. and Rodemich, E. (1958). Scattering of surface waves on an ideal fluid, Stanford Univ. Tech. Rep. No. 78, Math. and Stat. Lab..

57. Lewin, L. (1975). Theory of Waveguides. Newness-Butterworths, London.

58. Li, A.J., Liu Y. and Li, H.J. (2015). Accurate solutions to water wave scattering by vertical thin porous barriers, *Math Probl Eng.*, **2015**, 985731.

59. Lighthill, M. J. (1978). Waves in Fluids, *Cambridge University Press*.

60. Linton, C. M. and Chung, H.(2003). Reflection and transmission at the ocean/sea-ice boundary, *Wave Motion*, **38**, 43-52.

61. Linton, C. M. and McIver, P. (2001). Handbook of mathematical techniques for wave/structure introductions *Chapman and Hall/CRC,* Boca Raton, FL.

62. Liu, Y. and Li, H.J. (2012). Analysis of wave interaction with a submerged perforated semicircular breakwater through multipole method, *Appl. Ocean Res.*, **34**, 164-172.

63. Liu, Y. and Li, H.J. (2013). Wave reflection and transmission by porous breakwaters: A new analytical solution, *Coastal Engineering*, **78**, 46-52.

64. Losada, I. J., Losada, M. A. and Roldan, A. J. (1992). Propagation of oblique incident waves past rigid vertical thin barrier, *Applied Ocean Research*, **14**, 191-199.

65. Maiti, P., Rakshit P. and Banerjea, S. (2015). Wave motion in an ice covered ocean due to small oscillations of a submerged thin vertical plate, *J. Mar. Sci. Appl.*, **14**, 355-365.

66. Manam, S. R., Bhattacharjee, J. and Sahoo, T. (2006). Expansion formulae in wave structure interaction problems, *Proc. Roy. Soc. A.*, **462**, 263287.

67. Manam, S. R. and Sivanesan, M. (2016). Scattering of water waves by vertical porous barriers: An analytical approach, *Wave Motion*, **67**, 89-101.

68. Mandal, B. N. (1987). A note on construction of potentials due to line multipoles in the theory of water waves, *Int. J. Math. Edu. Sci. Technol.*, **18**, 561-565.

69. Mandal, B.N. (1988). A note on the evaluation of reflection coefficients in the scattering of water waves by fixed vertical barriers, *International Journal of Mathematical Education in Science and Technology*, **19(4)**, 581-585.

70. Mandal, B.N. and Banerjea, S. (1992). The expansion method of solution to the problem of water wave diffraction by a submerged nearly vertical plate, *Indian J. Theo. Phys.*, **40**, 23-38.

71. Mandal, B. N. and Banerjea, S. (1993). Solution of a boundary value problem associated with diffraction of water waves by a submerged nearly vertical barrier, *Bull. Cal. Math. Soc.*, **85**, 209-214.

72. Mandal, B. N. and Chakrabarti, A. (1989). A note on diffraction of water waves by a nearly vertical barrier, *IMA J. Appl. Math.*, **43**, 635-644.

73. Mandal, B. N. and Chakrabarti, A. (2000). Water Wave Scattering By Barriers, *WIT Press*, Southampton, Boston.

74. Mandal, B.N. and Chakrabarti, A. (2016). Applied singular integral equations, *CRC Press*.

75. Mandal, B. N. and Dolai, D. P. (1994). Oblique water wave diffraction by thin vertical barriers in water of uniform finite depth, *Applied Ocean Research*, **16**, 195-203.

76. Mandal, B. N. and Kanoria, M. (1998). Oblique wave scattering by thick barriers. Proceedings of 17th International Conference on Offshore Mechanics and Arctic Engineering, ASME, Lisbon, Portugal.

77. Mandal, B.N. and Kanoria, M. (2000). Oblique wave-scattering by thick horizontal barrier, *J. Offshore Mech. Arctic Eng.*, **122(2)**, 100-108.

78. Martin, P.A. (1992). Exact solution of a simple hyper singular integral equation. *J. Integral Equation Appl.*, **4**, 197-204.

79. McIver, P.(1999). Water-wave diffraction by thin porous breakwater, *Journal of Water-way Port Coastal and Ocean Engineering*, **125**, 66-70.

80. McIver, M. and Urka, U. (1995). Wave scattering by circular are shaped plates. *Journal of engineering mathematics*, **29(6)**, 575-589.

81. Mei, C. C. (1983). The Applied Dynamics of Ocean Surface Waves, *Wiley*, New York.

82. Mei, C. C. and Black, J. L. (1969). Scattering of surface waves by rectangular obstacles in water of finite depth, *J. Fluid Mech.*, **38**, 499-511.

83. Meylan, M. (1995). A flexible vertical sheet in waves, *Int. J. Offshore Polar Eng.*, **5**, 105-110.

84. Meylan, M.H. and Peter, M.A. (2009). Water-wave scattering by submerged elastic plates, *The Quarterly Journal of Mechanics and Applied Mathematics*, **62(3)**, 321-344.

85. Meylan, M., Squire, V. A. (1994). The response of ice floes to ocean waves, *J. Geophys. Res.*, **99** , 891-900.

86. Michele, S., Sammarcoa, P., dErricoa, M., Renzib, E., Abdolalic, A., Bellottic, G. and Dias, F.(2015). Flap gate farm: From Venice lagoon defense to resonating waveenergy production. Part 2: Synchronous response to incident waves in open sea, *Appl. Ocean Res.*, **52**, 43-61.

87. Miles, J.W. (1982). On surface wave diffraction by a trench, *J. Fluid Mech.*, **115**, 315-325.

88. Mondal, A., Panda, S. and Gayen, R. (2017). Flexural-gravity wave scattering by a circular-arc-shaped porous plate, *Studies in Applied Mathematics*, **138(1)**, 77-102.

89. Mondal, D. and Banerjea, S. (2016a). Scattering of water waves by an inclined porous plate submerged in ocean with ice cover, *Quarterly Journal of Mechanics and Applied Mathematics*, **69**, 195-213.

90. Mondal, D. and Banerjea, S. (2016b). Scattering of water waves by a porous circular arc- shaped barrier submerged in Ocean, *International Journal of Computational Methods and Experimental Measurements*, **4(4)**, 523-542.

91. Mondal, D., Banerjee, S. and Banerjea, S. (2024). Effect of thin vertical porous barrier with variable permeability on an obliquely incident wave train, *Wave Motion*, **126**, 103262.

92. Mondal, D., Samanta, A. and Banerjea, S. (2021). Hypersingular Integral Equation Formulation of the Problem of Water Wave Scattering by A Circular Arc Shaped Impermeable Barrier Submerged in Water of Finite Depth, *The Quarterly J of Mech and Appl Math.*, **74(4)**, 491-505.

93. Newman, J.N. (1965). Propagation of water waves over an infinite step, *J. Fluid Mech.*, **23**, 23-29.

94. Newman, J.N. (1977). Marine Hydrodynamics, *MIT Press*, Cambridge.

95. Packham, B.A. and Williams, W.E. (1972). A Note on the Transmission of Water Waves Through Small Apertures, *J. Inst. Maths Applics.*, **10**, 176-184.

96. Parsons, N. F. and Martin, P. A. (1992). Scattering of water waves by submerged plates using hypersingular integral equations, *Applied Ocean Research*, **14**, 313-321.

97. Parsons, N. F. and Martin, P. A. (1994). Scattering of water waves by submerged curved plate sand by surface-piercing flat plates, *Applied Ocean Research*, **16**, 129-139.

98. Paul, S. and De, S. (2021). Interaction of flexural gravity wave in ice cover with a pair of bottom-mounted rectangular barriers, *Ocean Engineering*, **220**, 108449.

99. Paul, S., Sasmal, A. and Dey, S. (2019). Interaction of oblique waves with an ice sheet over an asymmetric trench, *Ocean Engineering*, **193**, 106613 (1-8).

100. Peter, M.A. and Meylan, M.H. (2010). A general spectral approach to the time-domain evolution of linear water waves impacting on a vertical elastic plate, *SIAM J. Appl. Math.*, **70**, 2308-2328.

101. Porter, D., (1972). The transmission of surface waves through a gap in a vertical barrier, *Proc Camb Phil. Soc.*, **71**, 411-421.

102. Porter, D., (1974). The radiation and scattering of surface waves by vertical barriers, *J. Fluid Mech.*, **63**, 625-634.

103. Porter, R., (1953). Surface wave scattering by submerged cylinders of arbitrary cross-section, *Proc. Camb. Phil. Soc.*, **49**, 707-716.

104. Porter, R. and Evans, D. A. (1995). Complementary approximations to wave scattering by vertical barriers, *J. Fluid Mech.*, **294**, 155-180.

105. Ray, S., De, S. and Mandal, B.N. (2021). Wave propagation over a rectangular trench in the presence of a partially immersed barrier, *Fluid Dyn. Res.*, **53**, 035509.

106. Roy, R., Basu, U. and Mandal, B.N. (2016). Oblique water scattering by two unequal vertical barriers, *J Eng Math.*, **97**, 119-133.

107. Roy, R., Basu, U. and Mandal, B.N. (2016). Water wave scattering by two submerged thin vertical unequal plates, *Arch. Appl. Mech.*, **86**, 1681-1692.

108. Roy, R., Chakraborty, R. and Mandal, B. N.(2017). Propagation of water waves over an asymmetrical rectangular trench, *Q. J. Mech. Appl. Math.*, **70**, 49-64.

109. Rhodes Robinson, P. F. (1970). Fundamental Singularities in the theory of Water waves with surface tension, *Bull. Austral. Math. Soc.*, **2**, 317-333.

110. Rhodes Robinson, P. F.(1971). On the forced surface waves due to a vertical wave-maker in the presence of surface tension, *Math. Proc. Camb. Phil. Soc.*, **70**, 323-337.

111. Rhodes Robinson, P. F. (1982). Note on the reflexion of water waves at a wall in the presence of surface tension, *Math. Proc. Camb. Phil. Soc.*, **92**, 369-374.

112. Renzi, E. and Dias F. (2012A). Resonant behaviour of an oscillating wave energy converter in a channel, *J.Fluid Mech.*, **701**, 482-510.

113. Renzi, E. and Dias F. (2012B). Relations for a periodic array of flap-type wave energy converters, *Appl. Ocean Res.*, **39**, 31-39.

114. Renzi, E. and Dias F. (2013). Hydrodynamics of the oscillating wave surge converter in the open ocean, *European Journal of Mechanics B/Fluids*, **41**, 1-10.

115. Sahoo, T., On the Scattering of Water Waves by Porous Barriers, *ZAMM*, **78(5)**, 1998, 364-370.

116. Sahoo, T., Yip, T.L. and Chwang, A.T. (2001). Scattering of surface waves by a semi-infinite floating elastic plate, *Physics of Fluids*, **13(11)**, 3215-3222.

117. Samanta A., Chakraborty R. and Banerjea S. (2021). Line element method of solving singular integral equations, *Indian J pure appl math.*, **53(2)**, 528-541.

118. Samanta, A., Mondal, D. and Banerjea, S. (2023). Water wave interaction with a circular arc shaped porous barrier submerged in a water of finite depth, *J. Engng. Math.*, **138 (4)**, 1-23.

119. Sarkar, B., De, S. and Roy, R. (2021). Oblique wave scattering by two thin non-uniform permeable vertical walls with unequal apertures in water of uniform finite depth, *Waves in Random and Complex Media*, **31(6)**, 2021-2039.

120. Sarkar, B., Paul, S. and De, S. (2021). Water wave propagation over multiple porous barriers with variable porosity in the presence of an ice cover, *Meccanica*, **56(7)**, 1771-1788.

121. Sasmal, B., and De, S. (2021). Propagation of oblique water waves by an asymmetric trench in the presence of surface tension, *Journal of Ocean Engineering and Science*, **6(2)**, 206-214.

122. Sasmal A., Paul S. and De S. (2019). The influence of surface tension on oblique wave scattering by a rectangular trench, *J. Appl. Fluid Mech.*, **12**, 233-241.

123. Shaw, D. C. (1985). Perturbational results for diffration of water waves by nearly vertical barrier, *IMA J. Appl. Math.*, **34**, 99-117.

124. Singh, M., Gayen, R. and Kundu, S. (2022). Linear water wave propagation in the presence of an inclined flexible plate with variable porosity, *Archive of Applied Mechanics*, **92**, 2593-2615.

125. Sobhani, S. M., Lee, J. J. and Wellford, L. C. (1988). Interaction of periodic waves with inclined portable barrier,. *J. Waterway, Port, Coastal, ocean Engng.*, **114**, 745-761.

126. Sollitt, C. K. and Cross, R. H. (1972). Wave transmission through permeable breakwaters, *Coastal Engineering Proceedings*, **1(13)**, 1827-1846.

127. Song, H. and Tao, L.(2010). An efficient scaled boundary FEM model for wave interaction with a nonuniform porous cylinder, *International journal for numerical methods in fluids*, **63(1)**, 96-118.

128. Sretensky, L. N. (1977). The Theory of Wave Motions of a Fluid, *Nauka*, Moscow.

129. Squire, V. A. (2007). Review of ocean and sea ice revisited, *Cold Regions Science and Technology*, **49**, 110-133.

130. Stoker, J. J. (1957). Water waves: the mathematical theory with applications. *Interscience Publishers, Inc.*, New York, 149-187.

131. Sturova, I. V. (2003). The action of an unsteady load on a circular elastic plate floating on shallow water, *J. Appl Math. Mech.*, **67**, 407-416.

132. Sturova, I. V. (2011). Hydrodynamic Loads Acting on an Oscillating Cylinder Submerged in a Stratified Fluid with Ice Cover, *J. Appl. Mech. Tech. Phys.*, **52 (3)**, 415426.

133. Tao, L., Song, H. and Chakrabarti, S. (2009). Wave interaction with a perforated circular breakwater of non-uniform porosity, *Journal of Engineering Mathematics*, **65**, 257-271.

134. Thorne, C. (1953). Multipole expansions in the theory of surface waves, *Proc. Camb. Phil. Soc.*, **49**, 231-238.

135. Torri, T., Okubo, H., Hayashi, N., Matsuoka, K. and Kanai, H. (2000). Development of a very large floating structure, *Nippon Steel Technical Report*, **82**, 23-34.

136. Tricomi, F.G. (1951). The airfoil equation for a double interval, *Zeitschrift fr angewandte Mathematik und Physik ZAMP*, **2(5)**, 402-406.

137. Ursell, F. (1947). The effect of a fixed vertical barrier on surface waves in deep water, *Proceedings of Cambridge Philosophical Society*, **43**, 374-382.

138. Ursell, F. (1994). Collected Papers, *World Scientific*, Vol. 1, Singapore.

139. Ursell, F., Dean, R.G. and Yu, Y.S. (1960). Forced small-amplitude water waves: a comparison of theory and experiment, *Journal of Fluid Mechanics*, **7(1)**, 33-52.

140. Vaughan, G. L. and Squire, V. A. (2006). Scattering of Ice-Coupled Wave by Variable Sea-Ice Terrain, *Ann. Glaciology*, **44**, 8894.

141. Wadhams, P. (1978). Wave decay in the mrginal ice zone measured from submarine, *Deep-sea Res.*, **25**, 23-40.

142. Wang, C. M., Tay, Z. Y., Takagi, K. and Utsunomiya, T. (2010). Review of Methods for Mitigating Hydroelastic Response of VLFS Under Wave Action, *Appl. Mech. Reviews*, **63**, 030802-18.

143. Wehausen, J. V. (1971). The motion of floating bodies, *Ann. Rev. Fluid Mech*, **3**, 237-268.

144. Wehausen, J. V. and Laitone, E. V. (1960). Surface Waves, *Handbuch Der Physik, Springer*, Vol. IX.

145. Weitz, M. and Keller, J. B.(1950). Reflection of Water Waves from Floating Ice in Water of Finite Depth, *Comm. Pure Appl. Math.*, **3 (3)**, 305318.

146. Whitham, G. B. (1979). Lectures on Wave Propagation, *Springer-verlag*, New York.

147. Williams, W.E. (1966, July). Note on the scattering of water waves by a vertical barrier, *In Mathematical Proceedings of the Cambridge Philosophical Society, Cambridge University Press*, **62(3)**, 507-509.

148. Yu, X. (1995). Diffraction of Water Waves by Porous Breakwaters, *Journal of Waterway, Port, Coastal and Engineering*, **121(6)**, 275-282.

149. Yu, Y. S. and Ursell, F. (1961). Surface waves generated by an oscillating circular cylinder on shallow water : theory and experiments, *J. Fluid Mech.*, **11**, 529-551.

Archive of Applied Mechanics (2023) 93:1507–1524
https://doi.org/10.1007/s00419-022-02342-8

ORIGINAL

Rumpa Chakraborty · **Gour Das**

Propagation of surface gravity waves by a submerged thin elastic plate beneath an ice cover

Received: 17 June 2022 / Accepted: 4 December 2022 / Published online: 16 December 2022

Abstract A theoretical analysis involving surface gravity waves propagation by oblique incidence wave due to a thin elastic plate submerged in finite depth water in the presence of ice cover has been studied extensively in this paper employing Green's function technique. The edges of the elastic plate are considered to be free. The boundary conditions on the elastic plate and on the ice cover are derived from the Bernoulli–Euler's beam equation. Applying Green's function technique, the boundary condition satisfied on the elastic plate is converted into integral involving the difference in velocity potentials (unknown) across the plate multiplied by an appropriate Green's function. Utilizing Green's integral theorem, the reflection and transmission energy coefficients are explained in terms of integrals involving combinations of the unknown velocity potential on the two sides of the plate, which satisfy three simultaneous integral equations and are solved numerically. The effect of different values of physical parameters, such as flexural rigidity of ice, elastic coefficient of the barrier, and height and depth of the barrier, on the numerical assessment of magnitude of reflection and transmission coefficients is explained graphically in a number of figures. The energy balance relation is satisfied numerically. The results for a rigid plate are recovered when the parameters characterizing the elastic plate are chosen negligibly small. The influence of ice cover is clearly shown in the behavior of reflection and transmission coefficients curves. The hydrodynamic force, elastic plate deflection, shear force, and shear strain of the elastic plate are analyzed and computed analytically and graphically in a number of figures to understand the effect of ice cover on the wave motion.

Keywords Oblique wave · Vertical elastic plate · Ice cover · Green's function technique · Reflection and Transmission coefficients · Hydrodynamic force · Plate deflection · Shear force · Shear strain

1 Introduction

The considerable research interest has been driven toward the wave–structure interaction problems involving fixed or floating obstacles of various geometrical shapes for the past few decades. Vertical thin barriers are importantly used to construct break waters. These are helpful to protect marine constructions from the direct attack by water waves. Various researchers have studied the wave propagation problems by thin vertical rigid barriers situated in different positions in the water (cf. Evans [5], Porter and Evans [20], Goswami [10] and Mandal and Dolai [15]). Assuming linear theory and irrotational motion, the two-dimensional problem of water wave scattering by a thin vertical rigid plate of finite height submerged in deep water initially studied long back

R. Chakrabortya (✉)
Department of Mathematics, Diamond Harbour Women's University, South 24, Parganas 743368, India
E-mail: chak.rumpa@gmail.com

G. Das
Department of Mathematics, Jadavpur University, Kolkata 700032, India

by Evans [5] using a method based on the theory of complex variable. Porter and Evans [20] considered oblique wave scattering by a thin vertical rigid barrier in uniform finite depth water having four basic configurations, namely a surface piercing barrier, a bottom standing barrier, a barrier with a gap, and a totally submerged barrier. For each case, they used an approximate method based on the Galerkin approximation and numerical estimates for the reflection and transmission coefficients were obtained for different values of wave numbers. Also, earlier Goswami [10] employed Green's function technique to reduce the scattering problem involving a fixed vertical rigid plate submerged in uniform finite depth water and solved it approximately by using a perturbation method. Mandal and Dolai [15] later obtained very accurate upper and lower bounds for the reflection and transmission coefficients for the problem of water wave scattering by a thin vertical rigid barrier present in uniform finite depth water by using the Galerkin approximation method. In all the aforementioned problems, the obstacle bodies are considered to be rigid so that the bending effect of the barrier is not included. In a number of cases, a barrier (floating or submerged) is adept of appreciable flexure. So it becomes crucial to investigate the problem of wave scattering by floating or submerged elastic barriers. A very small number of studies have been done in wave–structure interaction problems involving elastic bodies.

The wave scattering problems due to elastic or viscoelastic structures have been utilized as a floating breakwater, and it is given in Stoker [22]. Though the problem is considered for long waves in shallow water, explicit results for these problems were not given. Later, utilizing the linearized theory in deep water, Fox and Squire [7] investigated the problem of water wave scattering by a floating ice sheet modeled as an elastic beam. Then, scattering problem involving horizontal floating elastic plate is considered by Meylan and Squire [17] and the problem is solved using Green's function technique. More currently, water wave problems involving elastic plates of different geometrical shapes are studied by a number of authors. For example, Sturova [23] investigated the unsteady motion due to a circular elastic plate floating on shallow water under the action of an external load. A floating rectangular elastic plate simulates a floating airport, and by doing this, one can determine the effects of periodic surface pressure on a rectangular floating elastic plate, which is important to engineers engaged in the construction of these types of airports. Gayen and Mandal [9] studied water wave scattering problem by a thin elastic plate of arbitrary width floating in deep water after reducing the problem to solving singular integral equations of the Carleman type.

All these problems involve horizontal elastic plates, floating or submerged in deep or finite depth water. A water wave problem involving a vertical thin elastic plate was studied for the first time by Meylan [16] who considered the scattering problem by a surface piercing thin vertical elastic plate in finite depth water. The time-dependent version of this problem was solved by Peter and Meylan [19] using a generalized eigenfunction expansion. Utilizing Green's function technique, Chakraborty and Mandal [2,3] investigated the wave scattering problem by an elastic plate fully submerged in infinitely deep water and finite depth water. They also established the relevant energy balance relation and coefficient of energy dissipation occurred by elastic plate. For both clamped and free ends of the elastic plate, floating in finite depth water was studied by Chakraborty et al. [4] by using hypersingular integral equation method.

Due to considerable interest increase in different types of scientific and industrial activities in polar regions and arctic oceans toward the later half of the last century, the study of wave propagation problems in polar oceans covered by floating ice has become very attractive to many researchers. The floating ice cover is modeled as a thin elastic plate. A floating thin elastic plate can also be regarded as a practical model for the frozen ocean or for a large floating structure such as a floating airport or quite a number of models for the ice cover have been proposed for the purpose of mathematical investigation of wave propagation problems (cf. Maiti et. al. [14] and Mondal and Banerjea [18]). In the case when the ice sheet is thin and continuous, it is modeled as a thin elastic plate with uniform elastic properties. This model has become very attractive for the purpose of mathematical analysis of water wave problems in water with an ice cover, since under the assumption of linear theory and irrotational motion, the linearized ice cover condition involves fifth-order partial derivative of the potential function, while the free surface condition involves only the first-order derivative.

Interaction of ocean waves with shore fast sea ice modeled as a thin elastic plate was first considered by Fox and Squire [7,8]. Scattering of an oblique wave caused by a narrow crack in ice sheets floating on water of finite depth was studied by Evans and Porter [6]. Vaughan and Squire [26] studied the propagation of waves under an ice sheet of variable thickness, which was interpolated by using low-order piecewise polynomials. The topics in the general area of ocean wave or sea ice interactions, especially in relation to mathematical modeling, were described in the review paper of Squire [21]. Later, Sturova [24] considered steady oscillations of a horizontal cylinder submerged in a linearly stratified fluid layer with an ice cover using the Boussinesq approximation. Bhattacharjee and Soares [1] investigated the behavior of flexural gravity waves propagating over a semi-infinite floating ice sheet under the assumptions of the small-amplitude linear wave theory. The

problems involving wave interaction with floating ice present on the upper surface of water become more accepted among engineers and researchers due to their effective scientific activities in Arctic and cold ocean regions.

Also, the importance of investigation of the problems involving wave interaction with submerged elastic plate is a class of problems that stem from their applications in the construction of very large floating structures (cf. Kashiwagi [13]). A vertical elastic plate may serve as a model for a seawall, wave damper, or a breakwater. Submerged plates are mainly used as the protectors of shoreward area of the breakwater from actions of rough sea by means of diminishing the effect of incoming waves. Such structures are useful as they allow the free exchange of water mass through them so that the pollution of water in the sheltered area is minimized. The submerged structures are also capable of absorbing some wave energy caused due to premature breakup of waves, and thus, they control the beach erosion.

As far as author's knowledge, such work, when a vertical body with elastic properties is present in water in an ice-covered ocean, has not been done before. Our main motivation is to study the combined effect of two elastic bodies on ocean waves. In the marginal ice zone, wave propagation into and through a field of ice flow is definitely a key canonical problem for engineers. The presence of elastic body effects the wave propagation through Marginal Ice Zone in the Arctic oceans. Thus, in the present paper, wave scattering by a thin vertical elastic plate submerged in water of uniform finite depth in the presence of ice cover is studied. The problem is formulated in terms of a boundary value problem for the velocity potential function where the boundary condition over the plate is derived from the Bernoulli–Euler's equation of motion satisfied by the elastic plate. By using the Green's function technique, from the Bernoulli–Euler's equation of motion, the normal velocity (unknown) of the plate is expressed in terms of an integral involving the difference of velocity potentials (unknown) on the two sides of the plate multiplied by an appropriate Green's function. Using the Green's integral theorem in the fluid region, we obtain two more integral equations involving the velocity potentials on either sides of the plate and a normal derivative of the potential. These three integral equations are solved numerically. Also, the reflection and transmission coefficients are obtained in terms of integrals involving a combination of the unknown velocity potentials on either sides of the plate and a normal derivative of the potential over the plate. Then, these coefficients were computed numerically for various values of different non-dimensional parameters and presented graphically in a number of figures. The energy balance relation involving reflection and transmission coefficients is derived by using Green's integral theorem. The hydrodynamic force, plate deflection, shear force, and shear strain are computed for the elastic plate, and they are graphically plotted for different values of rigidity coefficients of ice cover. These graphs show the effect of ice cover on the scattering problem by an elastic plate.

2 Formulation of the boundary value problem

We consider linearized two-dimensional motion of surface waves under the action of gravity only. Water is assumed to be an inviscid, incompressible, and homogeneous liquid with irrotational motion and is of uniform density ρ_1 and finite depth h. A rectangular Cartesian coordinate system (x, y) is chosen wherein the y-axis is taken vertically downward into the fluid region and the plane $y = 0$ represents the undisturbed ice cover surface. The position of the submerged thin elastic vertical plate is given by $x = 0, c < y < d$ and is shown in the schematic diagram of the problem (Fig. 1). It is assumed that a monochromatic flexural gravity wave is obliquely incident from the negative x direction on the elastic barrier with the angle of incidence θ and it is partially reflected and transmitted by and over or below the obstacle. The time-harmonic motion with angular frequency σ is explained in terms of velocity potential function $\Phi(x, y, t) = Re\{\phi(x, y)e^{-i\kappa z+i\sigma t}\}$, where $\kappa = \xi_0 \sin\theta$ and then $\phi(x, y)$ satisfies the Laplace's equation

$$(\nabla^2 - \kappa^2)\phi = 0, \quad \text{in the fluid region,} \tag{1}$$

The boundary condition on ice-covered upper surface (cf. Fox [8])

$$\left\{ D\left(\frac{\partial^2}{\partial x^2} - \kappa^2\right)^2 + 1 - \epsilon K \right\} \phi_y + K\phi = 0 \quad \text{on } y = 0 \tag{2}$$

where $K = \frac{\sigma^2}{g}$, σ being the circular frequency of incoming wave train and g being the gravitational acceleration, and $D = \frac{\mathcal{Y}h_0^3}{12(1-\nu^2)\rho_1 g}$, $\epsilon = \frac{\rho_0 h_0}{\rho_1}$, where ρ_0 is the density of ice, h_0 is the small thickness of the ice cover and

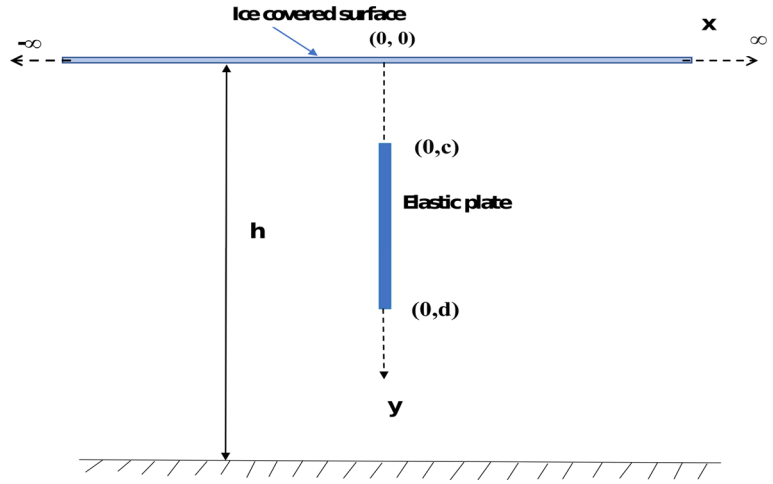

Fig. 1 Schematic diagram of the problem

$\mathcal{Y}$, υ are, respectively, the Young's modulus and Poisson's ratio of the ice regarded as an elastic material. There is no flow at the rigid bottom boundary and the condition is

$$\frac{\partial \phi}{\partial y} = 0 \quad \text{on } y = h \tag{3}$$

The Bernoulli–Euler's equation of motion for the submerged thin vertical elastic plate can be written as:

$$\frac{\partial^2 \mathrm{W_E}}{\partial t^2} + \upsilon^2 \frac{\partial^4 \mathrm{W_E}}{\partial y^4} = \frac{P_1 - P_2}{\rho' h'} \quad \text{on} \quad x = 0, \quad c < y < d \tag{4}$$

where $\upsilon^2 = \frac{E' h'^2}{12\rho'(1-\nu'^2)}$, E' is the Young's modulus and ν' is Poisson's ratio of the material of the elastic plate and $\mathrm{W_E}(y, t)$ represents the deflection of the elastic plate from its mean vertical position $x = 0$ and ρ' denotes the density of the elastic plate and h' is its small thickness,

$$P_{1,2} = P(\pm 0, y, t), \quad c < y < d, \tag{5}$$

$P(x, y, t)$ is the pressure at a point (x, y) of the fluid region at time t .

Thus, the boundary condition on the elastic plate surface satisfies (cf. Chakraborty and Mandal [2])

$$D' \frac{\mathrm{d}^4 \phi_x}{\mathrm{d}y^4} - \epsilon' K \phi_x = K[\phi] \quad \text{on} \quad x = 0, c < y < d \tag{6}$$

where

$$[\phi] = (\phi_1 - \phi_2), \quad \text{and} \quad \phi_{1,2} = \phi(\mp 0, y),$$
$$D' = \frac{E' h'^3}{12(1-\nu'^2)\rho_1 g}, \epsilon' = \frac{\rho' h'}{\rho_1}, \phi_x = \frac{\partial \phi}{\partial x}(0, y).$$

In the vicinity of sharp submerged edges, velocity potential function satisfies (cf. Hassan et al. [11])

$$\nabla \phi \sim O(r^{-\frac{1}{2}}) \text{ as } r \to 0 \tag{7}$$

where r denotes the space length between any point in the fluid and either sharp edge of the elastic plate. If the two ends of the submerged elastic plate are assumed to be free, then the conditions at the two ends of the submerged plate can be obtained as (cf. Meylan and Squire [17])

$$\frac{\partial^2 \phi_x}{\partial y^2} = 0 = \frac{\partial^3 \phi_x}{\partial y^3} \quad \text{at } y = c, d \tag{8}$$

Now, if $\phi_0(x, y)$ represents incident velocity potential for a train of surface waves incident on the plate, then

$$\phi_0(x, y) = Ae^{i\omega x}\frac{\cosh \xi_0(h - y)}{\cosh \xi_0 h}, \tag{9}$$

where $\omega = \xi_0 \cos\theta$ and ξ_0 is the unique positive root of

$$\xi(1 - \epsilon K + D\xi^4)\tanh \xi h = K. \tag{10}$$

Also, $\phi(x, y)$ satisfies the infinity requirements that

$$\phi(x, y) \sim \begin{cases} \phi_0(x, y) + R\phi_0(-x, y) & \text{as } x \to -\infty, \\ T\phi_0(x, y) & \text{as } x \to \infty \end{cases} \tag{11}$$

3 Method of solution

Green's function approach

The problem is to solve for $\phi(x, y)$ satisfying (1), (2), (3), (6), (7) and (8). The condition (6) on the plate $x = 0, c < y < d$ can be rewritten as

$$\frac{\mathrm{d}^4\phi_x}{\mathrm{d}y^4} - \beta^4\phi_x = \frac{K}{D'}[\phi], \quad \text{on } c < y < d \tag{12}$$

where

$$\beta^4 = \frac{\epsilon' K}{D'},$$

Here, a Green's function $g1(\tau, y)$ is established and it satisfies the following (cf. Meylan [16]). This construction helps to express ϕ_x, satisfying fourth-degree differential equation (8) in terms of difference between velocity potential across the elastic plate.

$$\frac{\mathrm{d}^4 g1}{\mathrm{d}\tau^4} - \beta^4 g1 = \delta(\tau - y), \ c < \tau, y < d \tag{13}$$

and $g1(\tau, y)$ also satisfies the following conditions:

$$\frac{\partial^2 g1}{\partial \tau^2} = 0 = \frac{\partial^3 g1}{\partial \tau^3}, \quad \text{at } \tau = c, d$$

$$g1, g1_\tau, g1_{\tau\tau} \text{ to be continuous at } \tau = y \tag{14}$$

$$g1_{\tau\tau\tau}(y + 0, y) - g1_{\tau\tau\tau}(y - 0, y) = -1. \tag{15}$$

As $g1$ is to be symmetric in y and τ, then the general solution of (14) becomes (cf. Meylan [16])

$$g1(\tau, y) = \begin{cases} P_1 e^{i\beta\tau} + Q_1 e^{-i\beta\tau} + R_1 e^{\beta\tau} + S_1 e^{-\beta\tau} & \text{as } c < \tau < y < d, \\ P_2 e^{i\beta\tau} + Q_2 e^{-i\beta\tau} + R_2 e^{\beta\tau} + S_2 e^{-\beta\tau} & \text{as } c < y < \tau < d, \end{cases} \tag{16}$$

where $P_1, Q_1, R_1, S_1; P_2, Q_2, R_2, S_2$ are functions of y only. Using the end conditions (14) and the matching and jump conditions (15), P_1, Q_1, R_1, and S_1 are determined from the following linear system:

$$\begin{bmatrix} -e^{i\beta c} & -e^{-i\beta c} & e^{\beta c} & e^{-\beta c} \\ -ie^{i\beta c} & ie^{-i\beta c} & e^{\beta c} & -e^{-\beta c} \\ -e^{i\beta d} & -e^{-i\beta d} & e^{\beta d} & e^{-\beta d} \\ -ie^{i\beta d} & ie^{-i\beta d} & e^{\beta d} & -e^{-\beta d} \end{bmatrix} \begin{bmatrix} P_1 \\ Q_1 \\ R_1 \\ S_1 \end{bmatrix} = \frac{1}{4\beta^3} \begin{bmatrix} 0 \\ 0 \\ -ie^{i\beta(d-y)} + ie^{-i\beta(d-y)} + e^{\beta(d-y)} - e^{-\beta(d-y)} \\ e^{i\beta(d-y)} + e^{-i\beta(d-y)} + e^{\beta(d-y)} + e^{-\beta(d-y)} \end{bmatrix}. \tag{17}$$

while P_2, Q_2, R_2 and S_2 are given by

$$P_2 = P_1 - \frac{i}{4\beta^3}e^{-i\beta y}; \ Q_2 = Q_1 + \frac{i}{4\beta^3}e^{i\beta y}$$

$$R_2 = R_1 - \frac{1}{4\beta^3} e^{-\beta y};\ S_2 = S_1 + \frac{1}{4\beta^3} e^{\beta y} \tag{18}$$

From (12), the condition on the plate becomes

$$\phi_x(0, y) = \frac{K}{D'} \int_c^d g1(\tau, y)[\phi](\tau) \mathrm{d}\tau, \quad c < y < d \tag{19}$$

Again, since $\phi(x, y)$ is continuous past the gaps over and under the plate, we have

$$\phi_1(\tau) = \phi_2(\tau), \quad \text{for } 0 < y < c \text{ and } d < y < h. \tag{20}$$

Also, $\phi_1(\tau) = \phi_2(\tau)$ at two edges of the plate

Now, a Green's integral theorem is employed to the functions $\psi(\gamma, \tau)$ and $G(\gamma, \tau; x, y)(x < 0)$, where

$$\begin{aligned} G(\gamma, \tau; x, y) = -4\pi \sum_{n=1}^{\infty} & \frac{\xi_n (D\xi_n^4 + 1 - \epsilon K) \cos \xi_n (h - y) \cos \xi_n (h - \tau)}{2\xi_n h (D\xi_n^4 + 1 - \epsilon K) + (5D\xi_n^4 + 1 - \epsilon K) \sin 2\xi_n h} \frac{e^{-(\xi_n^2 + \kappa^2)^{\frac{1}{2}} |x - \gamma|}}{(\xi_n^2 + \kappa^2)^{\frac{1}{2}}} \\ - 4\pi i \Bigg[& \frac{\xi_0 (D\xi_0^4 + 1 - \epsilon K) \cosh \xi_0 (h - y) \cosh \xi_0 (h - \tau)}{2\xi_0 h (D\xi_0^4 + 1 - \epsilon K) + (5D\xi_0^4 + 1 - \epsilon K) \sinh 2\xi_0 h} \frac{e^{i(\xi_0^2 - \kappa^2)^{\frac{1}{2}} |x - \gamma|}}{(\xi_0^2 - \kappa^2)^{\frac{1}{2}}} \\ & + \frac{\mu (D\mu^4 + 1 - \epsilon K) \cosh \mu (h - y) \cosh \mu (h - \tau)}{2\mu h (D\mu^4 + 1 - \epsilon K) + (5D\mu^4 + 1 - \epsilon K) \sinh 2\mu h} \frac{e^{i(\mu^2 - \kappa^2)^{\frac{1}{2}} |x - \gamma|}}{(\mu^2 - \kappa^2)^{\frac{1}{2}}} \\ & + \frac{\bar{\mu} (D\bar{\mu}^4 + 1 - \epsilon K) \cosh \bar{\mu} (h - y) \cosh \bar{\mu} (h - \tau)}{2\bar{\mu} h (D\bar{\mu}^4 + 1 - \epsilon K) + (5D\bar{\mu}^4 + 1 - \epsilon K) \sinh 2\bar{\mu} h} \frac{e^{-i\{(-\bar{\mu})^2 - \kappa^2\}^{\frac{1}{2}} |x - \gamma|}}{\{(-\bar{\mu})^2 - \kappa^2\}^{\frac{1}{2}}} \Bigg], \end{aligned} \tag{21}$$

$\pm\xi_0, i\xi_n, \pm\mu, \pm\bar{\mu}$ are the roots of the equation (10), in the regions bounded externally by the lines

$$\tau = 0, -X \le \gamma \le 0;\ \gamma = 0, 0 \le \tau \le h;\ \tau = h, -X \le \gamma \le 0;\ \gamma = -X, 0 \le \tau \le h$$

and internally by a circle with very small radius δ with center at (x, y) where

$$\psi(\gamma, \tau) = \phi(\gamma, \tau) - e^{i\omega\gamma} \frac{\cosh \xi_0 (h - \tau)}{\cosh \xi_0 h}.$$

By making $X \to \infty$ and $\delta \to 0$, we obtain

$$\phi(x, y) = e^{i\omega x} \frac{\cosh \xi_0 (h - y)}{\cosh \xi_0 h} + \int_0^h \left[\frac{\partial G}{\partial \gamma}(0, \tau; x, y)\phi_1(\tau) - G(0, \tau; x, y)\phi_x(\tau) \right] \mathrm{d}\tau, \text{ for } x < 0 \tag{22}$$

It may be noted that G is symmetric in (γ, τ) and (x, y) and behaves as an outgoing wave as $|\gamma - x| \to \infty$. Derivation of G may be found in Thorne [25]. Equation (22) gives a representation of $\phi(x, y)$ for $x < 0$, and hence the reflection coefficient R is obtained by making $x \to -\infty$ in (22) and comparing with (11). This produces

$$R = 2 \int_0^h (\xi_0 \phi_1(\tau) - i\phi_x(\tau)) \frac{(D\xi_0^4 + 1 - \epsilon K) \cosh \xi_0 (h - \tau) \cosh \xi_0 h}{2\xi_0 h (D\xi_0^4 + 1 - \epsilon K) + (5D\xi_0^4 + 1 - \epsilon K) \sinh 2\xi_0 h} d\tau \tag{23}$$

Again, if we choose $x = -0$, then in the region which is used in the Green's integral theorem mentioned above, we have to take a half circle of small radius δ with the center at $(-0, y)$, so that we obtain after making $\delta \to 0$,

$$\frac{1}{2}\phi_1(y) = \frac{\cosh \xi_0 (h - y)}{\cosh \xi_0 h} + \frac{1}{2\pi} \int_0^h \left[\frac{\partial G}{\partial \gamma}(0, \tau; 0, y)\phi_1(\tau) - G(0, \tau; 0, y)\phi_x(\tau) \right] \mathrm{d}\tau, 0 < y < h \tag{24}$$

This serves as an integral equation for $\phi_1(y)$ in $(0, h)$.

Similarly, applying Green's integral theorem to the functions $\phi(\gamma, \tau)$ and $G(\gamma, \tau; x, y)(x > 0)$ in the regions bounded externally by the lines

$$\tau = 0, 0 \le \gamma \le X;\ \gamma = 0, 0 \le \tau \le h;\ \tau = h, 0 \le \gamma \le X;\ \gamma = X, 0 \le \tau \le h$$

and internally by a circle of very small radius δ with center at (x, y) and ultimately making $X \to \infty$ and $\delta \to 0$, we obtain

$$\phi(x, y) = \int_0^h \left[\frac{\partial G}{\partial \gamma}(0, \tau; x, y)\phi_2(\tau) - G(0, \tau; x, y)\phi_x(\tau)\right] \mathrm{d}\tau,\ \text{for } x > 0 \tag{25}$$

Equation (25) gives a representation of $\phi(x, y)$ for $x > 0$, and hence the transmission coefficient T is obtained by making $x \to \infty$ in Eq. (25) and comparing with Eq. (11), we find

$$T = 2\int_0^h (\xi_0\phi_2(\tau) + i\phi_x(\tau))\frac{(D\xi_0^4 + 1 - \epsilon K)\cosh\xi_0(h - \tau)\cosh\xi_0 h}{2\xi_0 h(D\xi_0^4 + 1 - \epsilon K) + (5D\xi_0^4 + 1 - \epsilon K)\sinh 2\xi_0 h} d\tau \tag{26}$$

Again, if we choose $x = +0$, then in the region which is used in the Green's integral theorem mentioned above, we have to take a half circle of small radius δ with the center at $(+0, y)$, so that we obtain after making $\delta \to 0$,

$$\phi_2(y) = -\frac{1}{\pi}\int_0^h \left[\frac{\partial G}{\partial \gamma}(0, \tau; 0, y)\phi_2(\tau) - G(0, \tau; 0, y)\phi_x(\tau)\right] \mathrm{d}\tau, 0 < y < h \tag{27}$$

This serves as an integral equation for $\phi_2(y)$ in $(0, h)$.

Equations (24), (27), (19), and (20) together construct three simultaneous integral equations in terms of three unknowns $\phi_1(y)$, $\phi_2(y)$, and $\phi_x(y)$ in $(0, h)$. By solving these integral equations numerically and utilizing the solutions in (23) and (26), we obtain reflection and transmission coefficients $|R|$ and $|T|$ numerically for various values of different parameters.

Dynamic force:

In this paragraph, we determine the mathematical expression for dynamic wave force. From the linear Bernoulli's equation, the dynamic pressure jump across the elastic barrier can be written in the following form:

$$p(x, y) = -i\rho_1\sigma\,(\phi_1 - \phi_2)\,,\ \text{for } y \in [c, d]. \tag{28}$$

The magnitude of horizontal wave force per unit width acting on barrier is then obtained after integrating the dynamic pressure jump along the elastic barriers which is given by

$$\mathcal{F} = -i\rho_1\sigma\int_c^d (\phi_1 - \phi_2)\,\mathrm{d}y \tag{29}$$

The non-dimensional form of the horizontal force coefficient on the elastic plate becomes

$$F1 = \frac{K|\mathcal{F}|}{\rho_1 g} \tag{30}$$

The deflection of the plate:

We have

$$\frac{\partial \mathrm{W_E}}{\partial t} = \frac{\partial \phi}{\partial x}\ \text{at } x = 0, c < y < d, \tag{31}$$

The non-dimensional form of the plate deflection becomes

$$|\mathrm{W1_E(y)}| = |\sigma \mathrm{W_E(y)}| = |\frac{\partial \phi}{\partial x}(0, y)|, c < y < d \tag{32}$$

where $\mathrm{W_E(y, t)} = Re\{\mathrm{W_E(y)}e^{i\sigma t}\}$ and $\mathrm{W_E(y)}$ is the time-independent part (cf. Hassan et al. [11]).

Shear force and shear strain:

The shear force along the elastic barrier in terms of horizontal displacement is given by the relation (cf. Kaligatla and Manam [12])

$$\zeta(y) = -D'\rho g \frac{\partial^3}{\partial y^3} \mathrm{W_E}(0, y, t),\ c \le y \le d \tag{33}$$

Then, the non-dimensional form of shear force can be written as

$$|\zeta 1(y)| = |-\frac{D'\rho_1\, g}{\rho_1}\frac{4K}{\rho_1\,(d-c)g}\frac{\mathrm{d}^3\phi_x(0,y,t)}{\mathrm{d}y^3}|,\ c \le y \le d \tag{34}$$

The shear strain of the elastic plate is given by

$$\eta_{sh}(y) = -\frac{ih}{2\sigma}\frac{d^2\phi_x}{d^2y},\ c \le y \le d \tag{35}$$

Then, the magnitude of the shear strain becomes

$$|\eta 1(y)| = |-16\frac{i\beta K D'}{(d-c)h}\eta_{sh}(y)|,\ c \le y \le d \tag{36}$$

4 Numerical results and discussion

The three integral equations (24), (27), and (19) together with (20), involving $\phi_1(y)$, $\phi_2(y)$, and $\phi_x(y)$, have the finite range $(0, h)$. For numerical evaluation of the integrals in a finite interval, we employ the Gauss quadrature rule in the form

$$\int_A^B f(\eta)\mathrm{d}\eta \equiv \frac{B-A}{2}\sum_{j=1}^{N} l_j f\left(\frac{B-A}{2}y_j + \frac{B+A}{2}\right) \tag{37}$$

in each of the integrals mentioned above, where l_j, $y_j (j = 1, 2, ..., N)$ are defined below.

For numerical calculations, we non-dimensionalize the variables y, τ and the other parameters with the help of h, and $y_j (j = 1, 2, ..., N)$ in (37) are the zeros of Legendre polynomial $P_N(y)$ of degree N and $l_j (j = 1, 2, ..., N)$ are the corresponding weight functions given by

$$l_j = \frac{2}{(1-y_j)^2(P'_N(y_j))^2} \tag{38}$$

$P'_N(y)$ being the derivative of $P_N(y)$. There will be $3N$ unknowns $\phi_1(y_j)$, $\phi_2(y_j)$ and $\phi_x(y_j)(j = 1, 2, ..., N)$ in the approximation of the three integral equations.

Substituting $y = y_k (k = 1, 2, ..., N)$ in each of the integral equations, we obtain $3n$ linear equations for determining $3n$ unknowns $\phi_1(y_j)$, $\phi_2(y_j)$ and $\phi_x(y_j)(j = 1, 2, ..., N)$.

Using these values, we calculate the approximate form of R and T from the relations (23) and (26), respectively. Here, the energy balance relation $|R|^2 + |T|^2 = 1$ satisfies numerically.

In this section, we present numerical results for the reflection and the transmission coefficients $|R|$ and $|T|$, horizontal hydrodynamic force $F1$, shear force $\zeta 1$, shear strain $\eta 1$ of the thin elastic plate, taking some typical parameter sets. Here, we make different physical quantities dimensionless with respect to h.

Accuracy and validation of the result

To find the accuracy of the present result, it is compared with Chakraborty and Mandal's [2] result by considering the ice cover parameters to be very small ($\frac{D}{d^4} = 0.0005$, $\frac{\epsilon}{d} = 0.0001$)and $\theta = 0$. Chakraborty and Mandal [2] considered the wave scattering problem involving thin elastic plate with free surface of water. In the paper, they have non-dimensionalized the parameters by lower end depth of elastic plate from free surface. Now for accurate comparison, here also we consider the same parameter values $\frac{c}{d} = 0.05$, $\frac{D'}{d^4} = 1$, $\frac{\epsilon'}{d} = 0.01$, $\frac{h}{d} = 2$ as chosen by Chakraborty and Mandal [2]. These values of $|R|$ are given in Table 1, and the data set almost matched with each other up to four-figure accuracy. This provides a check on the validation of the present method.

Table 1 Comparison between present result, considering ice cover coefficient $\frac{D}{d^4} = 0.0005, \theta = 0$ (very small value and Chakraborty and Mandal's [2] result without ice cover with $\frac{c}{d} = 0.05$, $\frac{D'}{d^4} = 1$, $\frac{\epsilon'}{d} = 0.01$, $\frac{h}{d} = 2$)

Kd	Present result ($\|R\|$)	Chakraborty and Mandal's result [2] ($\|R\|$)
0.1	0.00325571	0.00327487
1.2	0.82359812	0.82861321
2.2	0.09871319	0.09824339
3.5	0.0056131	0.00569314

Table 2 Convergence of $|R|$ with N at $(d-c)/h = 0.2$, $D/h^4 = 0.5$, $D'/h^4 = 0.1$, $\epsilon/\epsilon' = 0.01$, $\theta = 0$

Truncation number (N)	$Kh = 0.5$	$Kh = 1$	$Kh = 1.5$	$Kh = 2$	$Kh = 2.5$	$Kh = 3$
5	0.539225	0.375438	0.300753	0.261398	0.237335	0.221137
7	0.539361	0.375623	0.300948	0.261568	0.237514	0.221253
10	0.539574	0.375816	0.301087	0.261754	0.237668	0.221417
12	0.539574	0.375816	0.301087	0.261754	0.237668	0.221417
14	0.539574	0.375816	0.301087	0.261754	0.237668	0.221417

Convergence analysis

The convergence of the numerical results depends on the truncation number of Gauss quadrature formula given in (37). In Table 2, $|R|$ is tabulated for different wave numbers $Kh(= 0.5, 1.0, 1.5, 2.0, 2.5$ and $3)$ with fixed values of $(d-c)/h = 0.2$, $D/h^4 = 0.5$, $D'/h^4 = 0.1$, $\epsilon/\epsilon' = 0.01$ and $\theta = 0$. Here, different truncation numbers $N(= 5, 7, 10, 12$ and $14)$ are considered and it is observed that for $N = 10, 12$ and 14 , the numerical values of $|R|$ coincide up to 4 decimal places. Also, the present method is checked for all other values of the parameters and wave numbers and it almost converges up to 4 decimal places when $N = 10$ (Table 2).

Effect of variation of length of the elastic barrier on reflection and transmission coefficients

In the present study, we non-dimensionalize different parameters by constant water depth h. We consider $(d-c)/h$ as the length of the plate and the distance of the plate from upper surface of water is fixed $(c/h = 0.1)$. The effect of the length of elastic plate on reflection and transmission coefficients for fixed values of the parameters $\theta = \frac{\pi}{4}$, $D/h^4 = 0.5$, $D'/h^4 = 0.1$ and $\epsilon/\epsilon' = 0.01$ is shown in Figs. 2 and 3, respectively. Here, we consider different values of $(d-c)/h = 0.1, 0.5$ and 0.8. This figure reveals the fact that as the length of the thin elastic plate increases the amount of the reflection increases, whereas that of the transmission decreases. This happens because the surface waves find less space for transmission with the increase in the length of the plate. Also, increasing length of the barrier decreases the amplitude of transmission coefficient which is also quite obvious physically.

Effect of variation of angle of incidence on reflection and transmission coefficients

In Figs. 4 and 5, magnitudes of the reflection coefficient $|R|$ and the transmission coefficient $|T|$ are plotted against the dimensionless wave number Kh for three different values of the parameter $\theta(= \pi/4, \pi/6, \pi/10)$. Here, we choose $(d-c)/h = 0.4$, $D/h^4 = 0.5$, $D'/h^4 = 0.1$ and $\epsilon/\epsilon' = 0.01$, where $\epsilon = 0.001, \epsilon' = 0.1$. These figures reveal the fact that as the angle of incidence increases the amount of the reflection increases, whereas that of the transmission decreases. For small wave number, more reflection occurs and it gradually decreases for large values of the wave number. The vice versa phenomenon is occurred in transmission curve.

Effect of variation of elasticity of ice cover and elastic coefficient of the barrier on reflection coefficients

In Fig. 6, magnitude of the reflection coefficient $|R|$ is plotted against the dimensionless wave number Kh for different values of the parameter $D/h^4(= 0.01, 0.50, 2.00, 5.00)$. Here, we take the fixed values of $(d-c)/h = 0.4$, $D'/h^4 = 0.1$, $\epsilon/\epsilon' = 0.01$ and $\theta = \pi/4$. In this figure, we see that for increasing values of the parameter

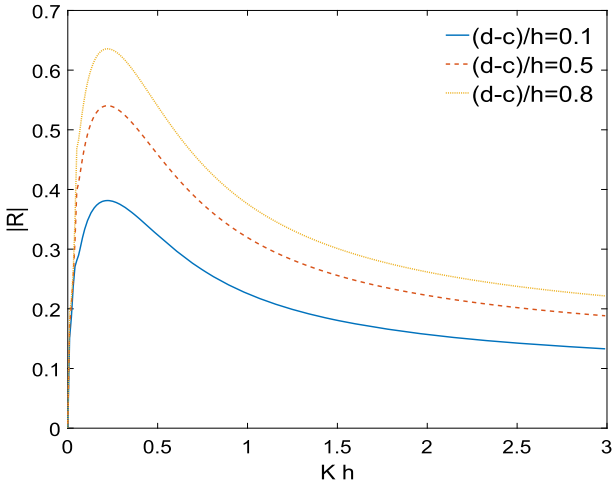

Fig. 2 Reflection coefficient against Kh for different values of $(d-c)/h$ with $\theta = \pi/4$, $\epsilon/\epsilon' = 0.01$, $D'/h^4 = 0.1$, $D/h^4 = 0.5$

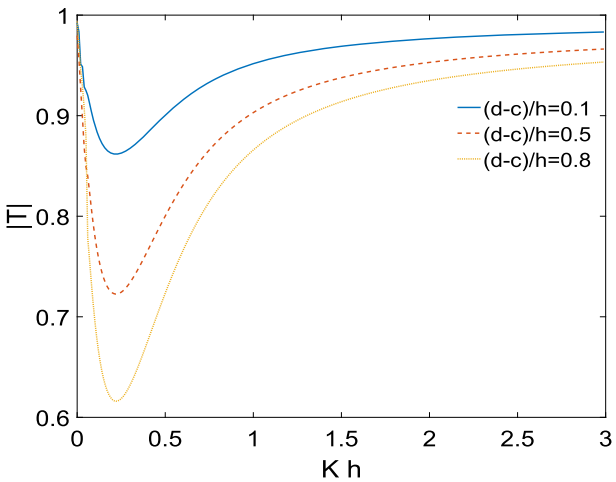

Fig. 3 Transmission coefficient against Kh for different values of $(d-c)/h$ with $\theta = \pi/4$, $\epsilon/\epsilon' = 0.01$, $D'/h^4 = 0.1$, $D/h^4 = 0.5$

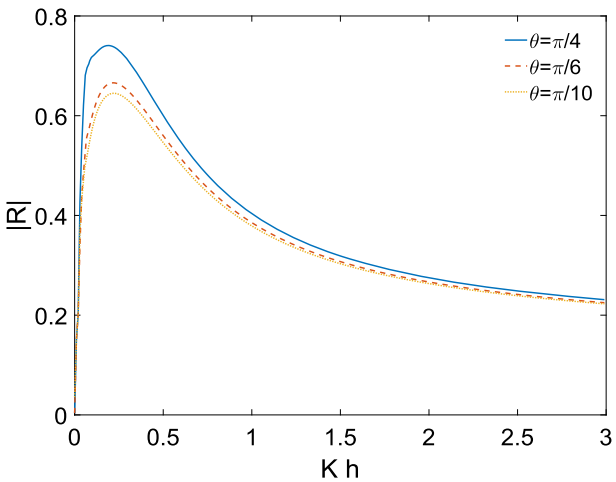

Fig. 4 Reflection coefficient against Kh for different values of θ with $(d-c)/h = 0.4$, $\epsilon/\epsilon' = 0.01$, $D'/h^4 = 0.1$, $D/h^4 = 0.5$

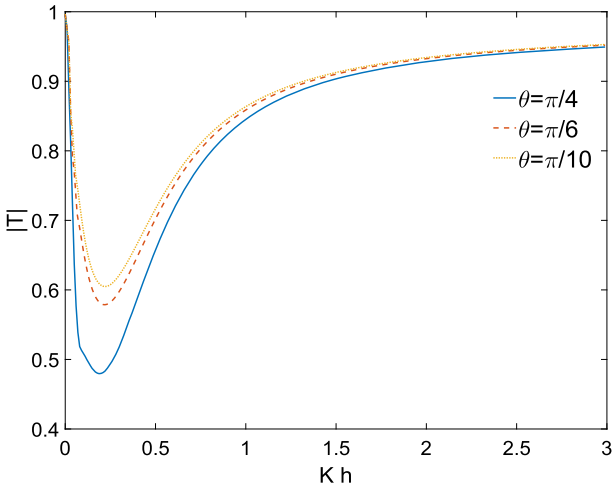

Fig. 5 Transmission coefficient against Kh for different values of θ with $(d-c)/h = 0.4$, $\epsilon/\epsilon' = 0.01$, $D'/h^4 = 0.1$, $D/h^4 = 0.5$

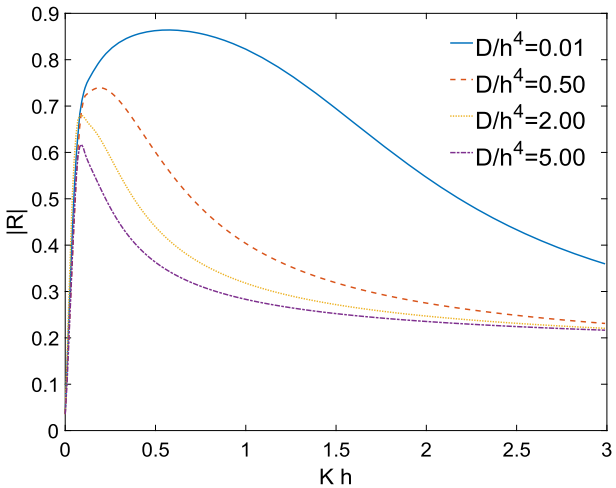

Fig. 6 Reflection coefficient against Kh for different values of D/h^4 with $(d-c)/h = 0.4$, $\epsilon/\epsilon' = 0.01$, $D'/h^4 = 0.1$, $\theta = \pi/4$

D/h^4 the magnitude of reflection coefficient decreases. Thus, the elasticity of the ice cover decreases the amount of reflection.

In Fig. 7, the magnitude of the reflection coefficient $|R|$ is plotted against the dimensionless wave number Kh for different values of the parameter $D'/h^4 (= 0.01, 0.50, 1.00)$. Here, we take the fixed values of $(d-c)/h = 0.4$, $D/h^4 = 0.5$, $\epsilon/\epsilon' = 0.01$ and $\theta = \pi/4$. Here, also we see that for increasing values of the elastic coefficient of the barrier the amount of reflection decreases.

4.1 Normal wave

The following figures are drawn for normal incidence wave

Effect of variation of elasticity of ice cover on reflection and transmission coefficients

In Figs. 8 and 9, magnitudes of the reflection and transmission coefficients are plotted against the dimensionless wave number Kh for four different values of the parameter $D/h^4 (= 0.01, 0.5, 2.0, 5.0)$, respectively. Here, we choose $(d-c)/h = 0.2$, $\theta = 0$, $D'/h^4 = 0.1$ and $\epsilon/\epsilon' = 0.01$, where $\epsilon = 0.001$, $\epsilon' = 0.1$, $c/h = 0.2$.

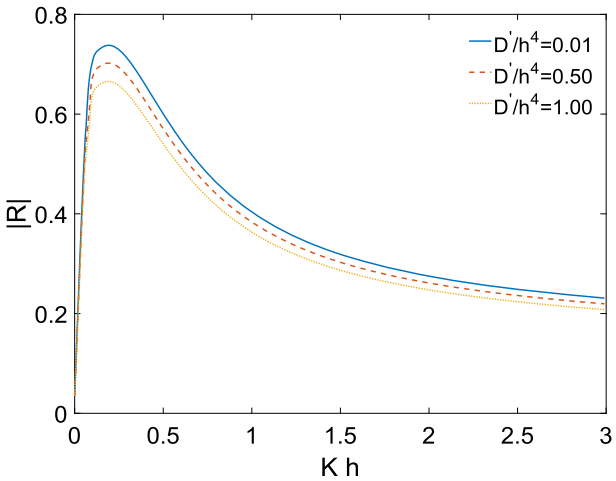

Fig. 7 Reflection coefficient against Kh for different values of D'/h^4 with $(d-c)/h = 0.4$, $D/h^4 = 0.5$, $\epsilon/\epsilon' = 0.01$, $\theta = \pi/4$

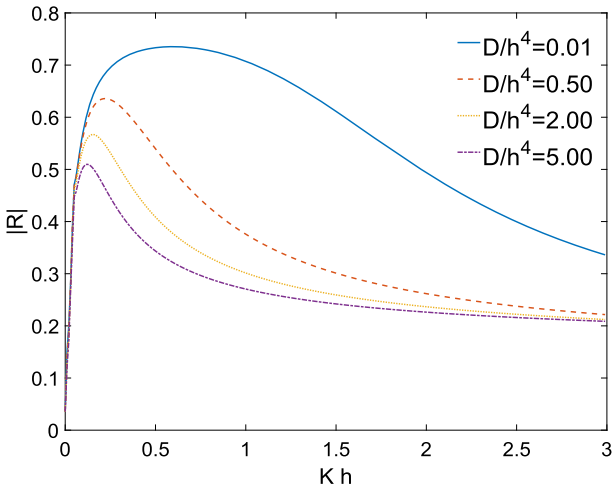

Fig. 8 Reflection coefficient against Kh for different values of D/h^4 with $(d-c)/h = 0.2, \epsilon/\epsilon' = 0.01$, $D'/h^4 = 0.1, \theta = 0$

In all the following figures, we consider the same values of c/h. Figure 8 reveals the fact that $|R|$ decreases as D/h^4 increases, and Fig. 9 shows $|T|$ increases with increasing values of D/h^4. Thus, the effect of elasticity of the ice cover is to reduce the reflection and amplify the transmission of the incident wave energy.

Effect of variation of elastic coefficient of the barrier on reflection coefficients

Figure 10 shows the behavior of $|R|$ for different values of $D'/h^4 = 0.01, 0.50$ and 1 and fixed values of $(d-c)/h = 0.3, \theta = 0$, $D/h^4 = 0.1$ and $\epsilon/\epsilon' = 0.01$, where $\epsilon = 0.001, \epsilon' = 0.1$. It is clearly visible from the figure that increasing elasticity of the barrier reflects less energy which is also true physically. For small values of wave number, this phenomenon is more clear than the large wave numbers.

Effect of change of density ratio between elastic plate and ice cover on reflection coefficient

In Fig. 11, magnitudes of the reflection coefficient $|R|$ are plotted against the dimensionless wave number Kh for three different values of the parameter $\epsilon/\epsilon'(= 0.01, 0.50, 1.00)$, where ϵ' is taken as 0.1. Here we choose $(d-c)/h = 0.2, \theta = 0$, $D/h^4 = 0.5$ and $D'/h^4 = 0.1$. This figure reveals the fact that $|R|$ decreases as ϵ/ϵ' increases.

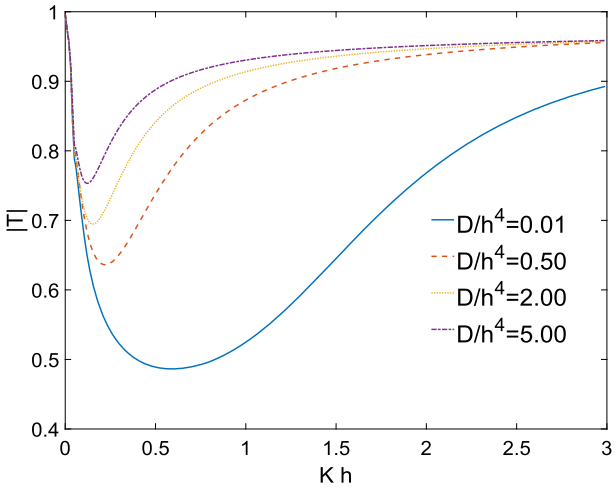

Fig. 9 Transmission coefficient against Kh for different values of D/h^4 with $(d-c)/h = 0.2$, $\epsilon/\epsilon' = 0.01$, $D'/h^4 = 0.1$, $\theta = 0$

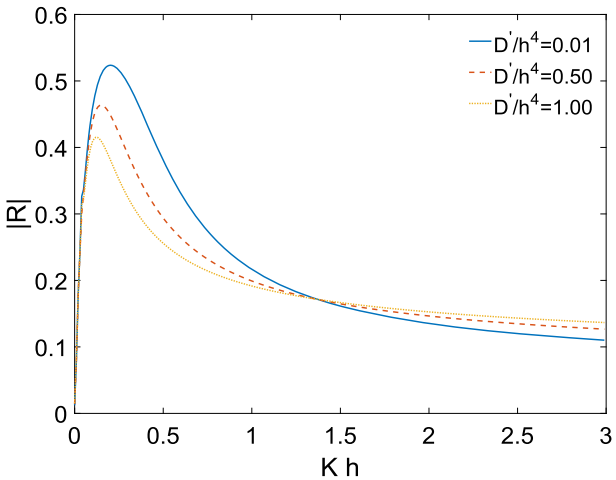

Fig. 10 Reflection coefficient against Kh for different values of D'/h^4 with $(d-c)/h = 0.3$, $D/h^4 = 0.1$, $\epsilon/\epsilon' = 0.01$, $\theta = 0$

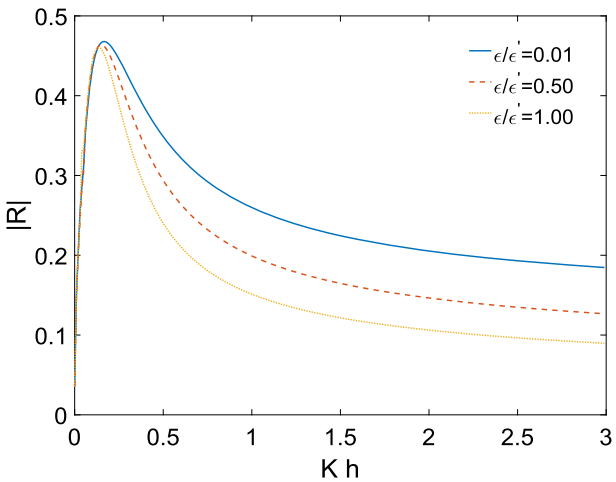

Fig. 11 Reflection coefficient against Kh for different values of ϵ/ϵ' with $(d-c)/h = 0.2$, $D/h^4 = 0.5$, $D'/h^4 = 0.1$, $\theta = 0$

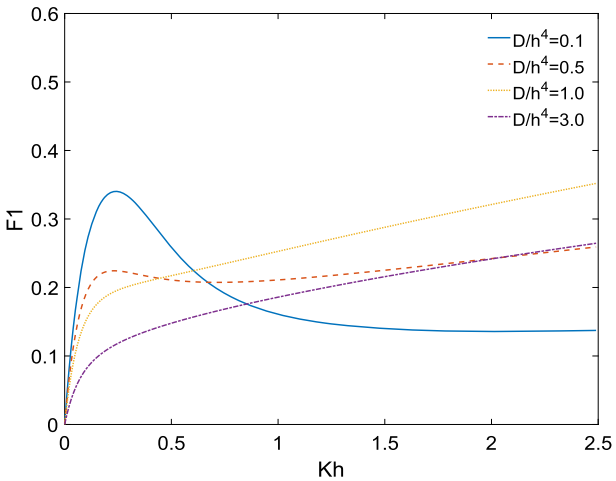

Fig. 12 Hydrodynamic force against wave number for different values of D/h^4 and $D'/h^4 = 0.05$, $(d-c)/h = 0.1$, $\epsilon/h = 0.01$, $\theta = 0$

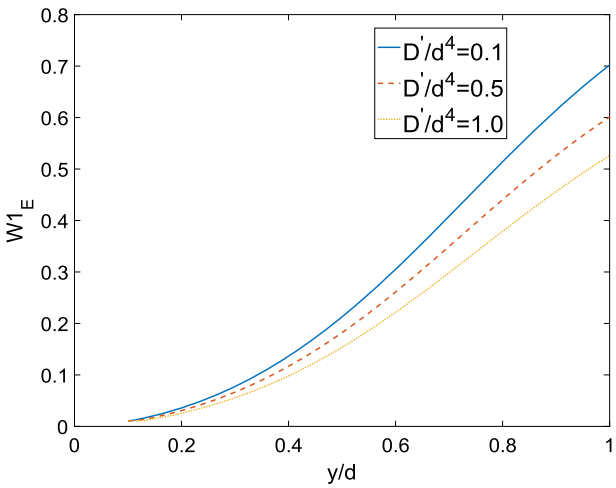

Fig. 13 Magnitude of plate deflection of the elastic plate against y/d for different values of D'/d^4 and fixed values of $c/d = 0.5$, $h/d = 1.5$, $D/d^4 = 2.5$, $Kh = 0.5$, $\frac{\epsilon}{d} = 0.15$, $\frac{\epsilon'}{d} = 0.015$, $\theta = 0$

Effect of change of flexural rigidity of elastic barrier on horizontal force

The magnitude of the horizontal component of the hydrodynamic force acting on the elastic plate is evaluated from the relation (30) and is represented graphically in Fig. 12. In this figure, the graphs are plotted for four different values of $D/h^4 (= 0.1, 0.5, 1.0, 3.0)$. The hydrodynamic force considerably reduces with the increase in D/h^4. For this reason, the elastic barriers are effective in reducing the disturbances caused by the waves in the sea.

Deflection of the elastic plate

The effect of flexural rigidity parameter of the elastic plate on the plate deflection is presented against y/d in Fig. 13. Here, we non-dimensionalize all the parameters with respect to d. In this figure, the graphs are plotted for three different values of $D'/d^4 (= 0.1, 0.5, 1.0)$ and for fixed values of the parameters $c/d = 0.5$, $h/d = 1.5$, $D/d^4 = 2.5$, $Kh = 0.5$, $\frac{\epsilon}{d} = 0.15$, $\frac{\epsilon'}{d} = 0.015$, $\theta = 0$. If D'/d^4 increases, the displacement of the plate from its mean position decreases. With increasing D', the plate prefers to less deflect and more energy transmitted.

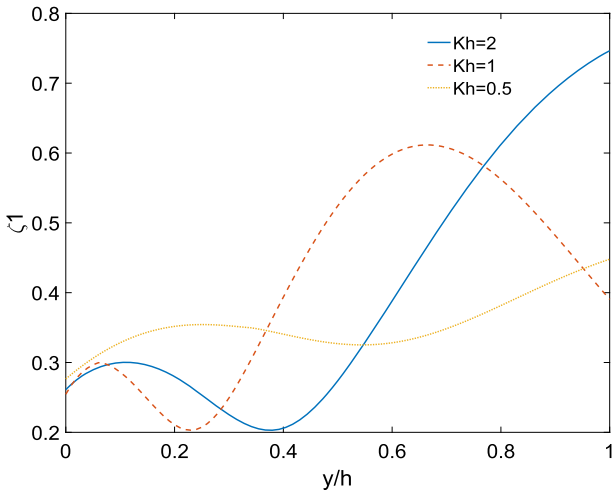

Fig. 14 Magnitude of shear force for elastic plate $\frac{\epsilon}{h} = 0.1$, $\frac{\epsilon'}{h} = 0.01$, $D/h^4 = 0.5$, $D'/h^4 = 0.1$, $(d-c)/h = 0.4$, $\theta = 0$

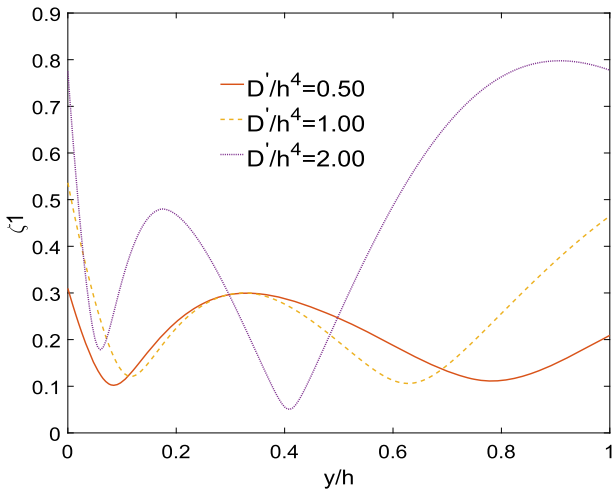

Fig. 15 Magnitude of shear force for elastic plate $\frac{\epsilon}{h} = 0.1$, $\frac{\epsilon'}{h} = 0.01$, $D/h^4 = 0.5$, $Kh = 0.01$, $(d-c)/h = 0.4$, $\theta = 0$

Variation of shear force

The magnitude of the shear force of the plate as a function of y/h is presented in Fig. 14. The graphs are for the different values of the wave number $Kh(= 0.50, 1.00, 2.00)$, $\frac{\epsilon}{h} = 0.1$, $\frac{\epsilon'}{h} = 0.01$, $D/h^4 = 0.5$, $D'/h^4 = 0.1$, $(d-c)/h = 0.4$, $\theta = 0$. The shear force is observed to be an increasing function of Kh. Large values of Kh show more oscillating behavior in reflection curve.

In Fig. 15, the shear force graphs taken against y/h for different values of elastic parameter, $\frac{D'}{h^4}(= 0.50, 1.00, 2.00)$ of the barrier and fixed values of $\frac{\epsilon}{h} = 0.1$, $\frac{\epsilon'}{h} = 0.01$, $D/h^4 = 0.5$, $Kh = 0.01$, $(d-c)/h = 0.4$, $\theta = 0$. It is clearly visible in the figure that the magnitude of shear force increases with increasing values of elastic coefficient of the barrier.

Shear strain of the elastic plate

Figure 16 shows the variation of magnitude of the shear strain against y/h for an elastic plate submerged in finite depth water with $Kh = 0.05, 0.1, 1$ and 2, $\frac{\epsilon}{h} = 0.1$, $\frac{\epsilon'}{h} = 0.01$, $D/h^4 = 0.5$, $D'/h^4 = 0.1$, $(d-c)/h = 0.4$, $\theta = 0$. From the figure, it is seen that in the presence of ice cover increasing non-dimensional wave number increases the shear strain on the plate.

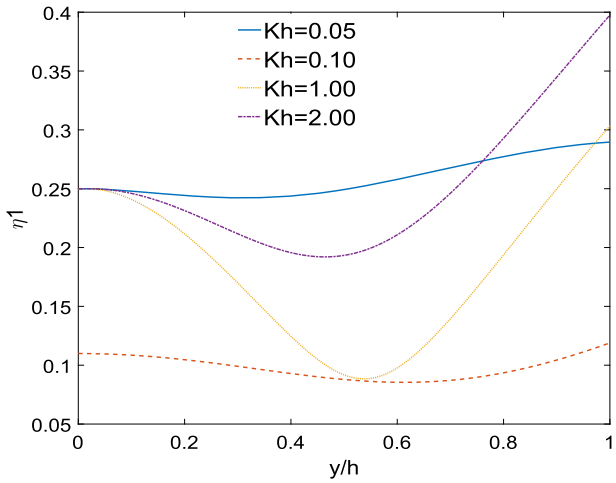

Fig. 16 Magnitude of shear strain for elastic plate $\frac{\epsilon}{h} = 0.1$, $\frac{\epsilon'}{h} = 0.01$, $D/h^4 = 0.5$, $D'/h^4 = 0.1$, $(d-c)/h = 0.4$, $\theta = 0$

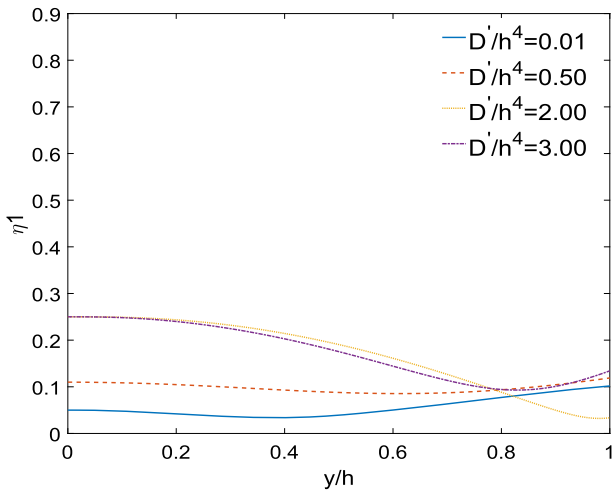

Fig. 17 Magnitude of shear strain for elastic plate. $\frac{\epsilon}{h} = 0.1$, $\frac{\epsilon'}{h} = 0.01$, $D/h^4 = 0.5$, $Kh = 0.1$, $(d-c)/h = 0.4$, $\theta = 0$

Figure 17 depicts the variation of shear strain against y/h for an elastic plate submerged in finite depth water with $\frac{D'}{h^4} = 0.01, 0.5, 2$ and 3, $\frac{\epsilon}{h} = 0.1$, $\frac{\epsilon'}{h} = 0.01$, $D/h^4 = 0.5$, $Kh = 0.1$, $(d-c)/h = 0.4$, $\theta = 0$. The figure shows that increasing flexural rigidity of the elastic plate increases the shear strain on the plate.

In most of the graphical results, it is clear that the variation of different parameters affects the nature of reflection and transmission curves more for small wave numbers. Increasing values of wave number reduce the differences between the reflection curves drawn for different parametric values in the same figure.

5 Conclusions

In this paper, the interaction between linear oblique waves with a elastic thin barrier submerged in ice-covered ocean is investigated. The boundary conditions on the elastic plate and upper surface of water are derived from the Bernoulli–Euler's beam equation. The Green's function technique is used to solve the problem.

Some outcomes are summarized below:

Physical quantities such as reflection, transmission coefficients, horizontal hydrodynamic force, deflection of elastic plate, shear force, and shear strain on the elastic plate are evaluated and plotted graphically against suitable parameters. The effect of elasticity of the barrier reduces the amplitude of reflection coefficient and hydrodynamic force . Long-length barrier reflects more energy than the short one. The effect is more visible for small values of wave numbers. The elastic plate deflection in the water becomes higher for large wave

numbers. These phenomena have been shown clearly by numerical graphs. In the presence of ice cover, it is found that shear force and shear strain curves are seen to be significantly uniform along the ice sheet.

In the present study, we have considered both the ends of the barrier to be free. However, one can consider one end or both ends clamped in infinitely deep water. For these problems, the same procedure can be allied to evaluate numerical results of different physical quantities.

Declarations

Conflict of interest The authors declare that they have no conflict of interest.

References

1. Bhattacharjee, J., Soares, C.G.: Flexural gravity wave over a floating ice sheet near a vertical wall. J. Eng. Math. **75**, 29–48 (2012)
2. Chakraborty, R., Mandal, B.N.: Water waves scattering by an elastic thin vertical plate submerged in finite depth water. J. Mar. Sci. Appl. **12**, 393–399 (2013)
3. Chakraborty, R., Mandal, B.N.: Scattering of water waves by a submerged thin vertical elastic plate. Arch. Appl. Mech. **84**, 207–217 (2014)
4. Chakraborty, R., Mondal, A., Gayen, R.: Interaction of surface water waves with a vertical elastic plate: a hypersingular integral equation approach. Z. Angew. Math. Phys. **67**, 115 (2016)
5. Evans, D.V.: Diffraction of water waves by a submerged vertical plate. J. Fluid Mech. **40**, 433–451 (1970)
6. Evans, D.V., Porter, R.: Wave Scattering by Narrow Cracks in the Ice-Sheets on Water of Finite Depth. J. Fluid Mech. **404**, 143–165 (2003)
7. Fox, C., Squire, V.A.: On the oblique reflection and transmission of ocean waves from shore fast sea ice. Philos. Trans. R. Soc. Lond. A. **347**, 185–218 (1994)
8. Fox, C., Squire, V.A.: Reflection and transmission characteristics at the edge of shore fast sea ice. J Geophys Res **95**, 11629–11639 (1990)
9. Gayen, R., Mandal, B.N.: Scattering of surface water waves by a floating elastic plate in two dimensions. SIAM J. Appl. Math. **69**(6), 1520–1541 (2009)
10. Goswami, S.K.: Scattering of surface waves by a submerged fixed vertical plate in water of finite depth. J. Indian Inst. Sci. **64B**, 79–88 (1983)
11. Hassan, M., Meylan, M.H., Peter, M.A.Q.: Water-wave scattering by submerged elastic plates. J. Mech. Appl. Math. **62**(321), (2009)
12. Kaligatla, R.B., Manam, S.R.: Flexural gravity wave scattering by a nearly vertical porous wall. J. Eng. Math. **88**, 49–66 (2014)
13. Kashiwagi, M.: Transient responses of a VLFS during landing and take-off of an airplane. J. Mar. Sci. Technol. **9**, 14–23 (2004)
14. Maiti, P., Rakshit, P., Banerjea, S.: Wave motion in an ice covered ocean due to small oscillations of a submerged thin vertical plate. J. Mar. Sci. Appl. **14**, 355–365 (2015)
15. Mandal, B.N., Dolai, D.P.: Oblique water wave diffraction by thin vertical barriers in water of uniform finite depth. Appl. Ocean Res. **16**(4), 195–203 (1994)
16. Meylan, M.: A flexible vertical sheet in waves. Int. J. Offshore Polar Eng. **5**, 105–110 (1995)
17. Meylan, M., Squire, V.A.: The response of ice floes to ocean waves. J. Geophys. Res. **99**, 891–900 (1994)
18. Mondal, D., Banerjea, S.: Scattering of water waves by an inclined porous plate submerged in ocean with ice cover. Q. J. Mech. Appl. Math. **69**, 195–213 (2016)
19. Peter, M.A., Meylan, M.H.: A general spectral approach to the time-domain evolution of linear water waves impacting on a vertical elastic plate. SIAM J. Appl. Math. **70**, 2308–2328 (2010)
20. Porter, R., Evans, D.V.: Complementary approximation to wave scattering by vertical barriers. J. Fluid Mech. **249**, 155–180 (1995)
21. Squire, V.A.: Of Ocean Waves and Sea-Ice Revisited. Cold Regions Sci. Technol. **49**, 110–133 (2007)
22. Stoker, J.J.: Water waves. Intersicence Publishers, New York, pp. 430-449 (1957)
23. Sturova, I.V.: The action of an unsteady load on a circular elastic plate floating on shallow water. J. Appl Math. Mech. **67**, 407–416 (2003)
24. Sturova, I.V.: Hydrodynamic Loads Acting on an Oscillating Cylinder Submerged in a Stratified Fluid with Ice Cover. J. Appl. Mech. Tech. Phys. **52**(3), 415–426 (2011)
25. Thorne, R.C.: Multipole expansions in the theory of surface waves. Math. Proc. Cambridge Philos. Soc. **49**(4), 707–716 (1953)
26. Vaughan, G.L., Squire, V.A.: Scattering of Ice-Coupled Wave by Variable Sea-Ice Terrain. Ann. Glaciology **44**, 88–94 (2006)

Journal of Marine Science and Application (2024) 23: 85-100
https://doi.org/10.1007/s11804-024-00396-4

RESEARCH ARTICLE

Effect of Porosity on Wave Scattering by a Vertical Porous Barrier over a Rectangular Trench

Gour Das[1] and Rumpa Chakraborty[2]

Received: 15 March 2023 / Accepted: 25 June 2023

Abstract
The effect of porosity on surface wave scattering by a vertical porous barrier over a rectangular trench is studied here under the assumption of linearized theory of water waves. The fluid region is divided into four subregions depending on the position of the barrier and the trench. Using the Havelock's expansion of water wave potential in different regions along with suitable matching conditions at the interface of different regions, the problem is formulated in terms of three integral equations. Considering the edge conditions at the submerged end of the barrier and at the edges of the trench, these integral equations are solved using multi-term Galerkin approximation technique taking orthogonal Chebyshev's polynomials and ultra-spherical Gegenbauer polynomial as its basis function and also simple polynomial as basis function. Using the solutions of the integral equations, the reflection coefficient, transmission coefficient, energy dissipation coefficient and horizontal wave force are determined and depicted graphically. It was observed that the rate of convergence of the Galerkin method in computing the reflection coefficient, considering special functions as basis function is more than the simple polynomial as basis function. The change of porous parameter of the barrier and variation of trench width and height significantly contribute to the change in the scattering coefficients and the hydrodynamic force. The present results are likely to play a crucial role in the analysis of surface wave propagation in oceans involving porous barrier over submarine trench.

Keywords Water wave scattering; Rectangular trench; Vertical porous barriers; Havelock's inversion formula; Multi-term galerkin approximation; Reflection and transmission coefficients; Energy dissipation; Hydrodynamic force

1 Introduction

During the last few decades, the study of propagation of surface water waves over a rectangular trench was being considered by many researchers because of their possible applications in coastal and ocean engineering. It has a significant role in understanding the characteristics of wave in harbour and offshore regions. The scattering of normally incident monochromatic plane progressive wave by rectangular submarine trench of constant depth containing two fluids of constant but different densities was studied by Lassiter (1972). Lee and Ayer (1981) investigated the effect of a symmetric rectangular trench by dividing the fluid domain into subregions. Miles (1982) used a conformal mapping to solve the trench problem for normal incidence of wave train. The diffraction of obliquely incident surface waves by an asymmetric trench was investigated using linearized potential theory by Kirby and Dalrymple (1983). They solved a set of integral equations derived by matching eigen function expansions of the velocity potentials. Later, Kirby and Dalrymple (1987) developed the theory of wave diffraction over a rectangular trench where currents flowing parallel to the trench boundary. The normal and oblique incidence by the two-dimensional wave scattering by a rectangular submarine trench was considered by Chakraborty and Mandal (2014; 2015) reducing the problem to solving appropriate integral equation which is solved by multi-term Galerkin approximation involving ultraspherical Gegenbauer polynomials. Later, Roy et al. (2017) considered the problem of water wave scattering by an asymmetric rectangular trench using an approach similar to Chakraborty and Mandal (2014; 2015).

Article Highlights

- Considering linear theory, problem of water wave scattering by porous thin submerged plate over rectangular trench is studied.
- Two different positions of the barrier are considered.
- A multi term Galerkin approximation technique together with taking orthogonal polynomials as well as simple polynomial as basis function. To test the rate of convergence compares the both results numerically.
- The reflection coefficient, transmission coefficient, energy dissipation coefficient and horizontal wave force are determined and depicted graphically.
- Porous parameter of the barrier, variation of trench width and height affect the energy coefficients significantly.

✉ Rumpa Chakraborty
chak.rumpa@gmail.com

[1] Department of Mathematics, Jadavpur University, Kolkata-700032, India

[2] Department of Mathematics, Diamond Harbour Women's University, South 24 Parganas-743368, India

Interaction of water waves with thin plate assuming the linear theory has been a subject of considerable interest as this phenomenon serves as a model for a wide range of physical situations which include wave interaction with breakwaters, very large floating structures. Breakwaters are coastal structures which are widely constructed to reduce the wave action in inshore water and thereby reduce the coastal erosion and protect a port or harbour from the effect of rough sea. Usually the breakwaters are mathematically modeled as rigid impermeable thin vertical plate either partially immersed or submerged in ocean. A number of researchers were engaged in the study to handle the boundary value problem associated with the study of water wave scattering by a thin rigid vertical plate present in ocean with free surface and consequently many sophisticated mathematical concepts have evolved. Dean (1945), Ursell (1947) and Evans (1970) worked with such types of problems. It may be noted here that exact solution of the aforesaid boundary value problem exists when the barrier is in the form of a rigid vertical plate present in the deep ocean and for normal incidence of the incoming wave train. In all other cases only approximate analytical or numerical methods are used to obtain approximate solution. The scattering problem involving a partially immersed and submerged rigid plate using first kind of hypersingular integral equation was studied by Parson and Martin (1992; 1994). Based on application of Green's integral theorem they have reduced the boundary value problem to a solution of first kind hypersingular integral equation where the unknown function is the difference of velocity potential across the plate. The hypersingular integral equation was then solved by using collocation method based on approximating the unknown function satisfying the integral equation Chebyshev's polynomial. The problem of wave diffraction by rigid vertical barrier in finite depth water was considered by Goswami (1983). Goswami (1983) employed Green's function technique to reduce the scattering problem involving a fixed vertical rigid plate submerged in uniform finite depth water to an integral equation. The integral equation was then solved approximately by using a perturbation method and reflection and transmission coefficients are thereby obtained. Losada et al. (1992) obtained the reflection and transmission coefficients of the above mentioned problem by using an eigenfunction expansion method. Later on, Porter and Evans (1995) considered oblique wave scattering by a thin vertical rigid barrier in uniform finite depth water having four basic configurations namely, a surface piercing barrier, a bottom standing barrier, a barrier with a gap and a totally submerged barrier. For each case, they have used an approximate method based on the Galerkin approximation. Also, Mandal and Dolai (1994) considered oblique water wave scattering by thin vertical barrier in uniform finite depth water. They employed one-term Galerkin approximation to evaluate the upper and lower bounds for the transmission and reflection coefficients.

During the later half of twentieth century, study of wave interaction with porous coastal structures like rubble mound breakwaters became important in coastal engineering as the structural voids in the porous breakwaters can dissipate wave energy efficiently. Also in coastal engineering, porous breakwaters drawn special attention to the scientist and researchers because of the rigid breakwaters were collapsed due to huge load, which were mainly constructed to protect harbours and coastal villages. Porous structures in the form of thin permeable barriers have been used to dissipate and reflect incoming wave energy from sea. Also, a porous breakwaters are moved eco-friendly as water can pass through the holes which helps to protect marine environment. For low engineering cost, porous breakwaters are more useful with respect rigid one. Mathematical modeling of porous structure as thin porous vertical wave maker was pioneered by Chwang (1983). Based on the model of Solitt and Cross (1972), Yu (1995) examined the wave diffraction by a semi-infinite porous barriers. The rapid convergence of the solution to the problem of water wave scattering by thin vertical porous barriers utilizing multi-term Galerkin approximation was examined by Li et al. (2015). Roy et al. (2016a; 2016b) analyzed water wave scattering by two unequal vertical barriers and two submerged plates by using Galerkin's approximation technique. More recently, Ray et al. (2021) considered the wave scattering problem by thin rigid plate above the rectangular trench and Sarkar et al. (2022) analyzed oblique wave scattering by two thin rigid plate over an asymmetrical trench. The above mentioned problems were solved by considering multiterm Galerkin approximation technique using simple polynomial as basis functions. But as per authors knowledge, no research work is done when porosity is present in vertical plate. Present of porosity is actually more effective in dissipating wave energy and it helps to reduce wave force on the barrier [cf. Manam and Sivanesan (2016)].

In the present paper, water wave scattering by a rectangular submarine trench in presence of a thin vertical porous barrier are investigated. Here we consider that the porous barrier positioned in the right side, at a distance '*l*' from the middle of the trench. We divide the whole fluid region into four subregions and using Havelock's inversion formula in four subregions and matching conditions at the interfaces of these subregions we construct three Fredholm type integral equations. To solve these integral equations we use multi-term Galerkin approximation technique taking orthogonal Chebyshev's polynomials and ultra-spherical Gegenbauer polynomial as its basis function due to the edge conditions at the submerged end of the barrier and at the edge of the trench respectively. We have also consider simple polynomial as basis function to solve the integral equation as done in Ray et al. (2021). Then the reflection coefficient and the transmission coefficient are determined

in terms of the solutions of the integral equations. Due to porosity, how the proposed system affects the reflection coefficient, transmission coefficient, energy dissipation, wave force acting on the structure are discussed in numerical section. In the absence of porosity, known result evaluated by Ray et al. (2021) is recovered. We may mention here that the use of special function as basis function in multi term Galerkin approximation gives better rate of convergence of the method than using simple polynomial as basis function as in the work of Ray et al. (2021).

2 Problem construction

We consider two dimensional, time harmonic, irrotational motion in water due to interaction of a wave train incident normally on a thin vertical porous barrier partially immersed in water region with a submarine trench at the bottom. We choose rectangular cartesian coordinate system where x-axis is along the mean free surface and y-axis is taken vertically downwards into the fluid region. A rectangular submarine trench symmetrical about y-axis, of width '$2b$' and depth 'c' below the mean free surface is situated at the bottom of water region so that water occupies the region $(-\infty < x < b, 0 < y < h) + (-b < x < b, 0 < y < c) + (b < x < \infty, 0 < y < h)$. A porous thin vertical barrier is situated along a vertical line $x = l$, which is partially immersed upto a depth 'a' below the mean free surface so that configuration of the barrier is given by $x = l,\ 0 < y < a\,;\ l < b$. A train of time harmonic waves from negative infinity with angular frequency σ represented by the velocity potential function $\mathrm{Re}\,[\varphi^{\mathrm{inc}}(x,y)\mathrm{e}^{-\mathrm{i}\sigma t}]$, is incident normally on the barrier and is partially reflected and partially transmitted below the barrier so that R and T are the amplitudes of the reflected and transmitted waves respectively. A schematic diagram of the problem is shown in Figure 1.

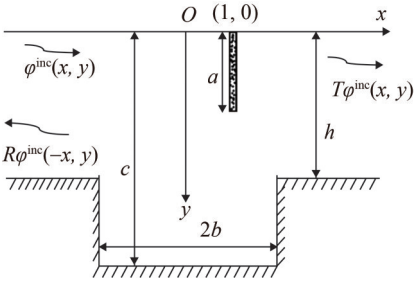

Figure 1 Schematic diagram

Here

$$\varphi^{\mathrm{inc}}(x,y) = \frac{2\cosh\alpha_0(h-y)\,\mathrm{e}^{-\mathrm{i}\alpha_0(x-b)}}{\cosh\alpha_0 h} \tag{1}$$

where α_0 is the unique real positive root of dispersion relation

$$\alpha\tanh\alpha h = K \tag{2}$$

where $K = \sigma^2/g$, g is the acceleration due to gravity.

To study the problem under consideration we divide the fluid region into four subregions, viz, R_1, R_2, R_3, R_4 (see Figure 2), where

$$R_1 \equiv (-\infty < x < -b, 0 < y < h)$$
$$R_2 \equiv (-b < x < l, 0 < y < c)$$
$$R_3 \equiv (l < x < b, 0 < y < c)$$
$$R_4 \equiv (b < x < \infty, 0 < y < h)$$

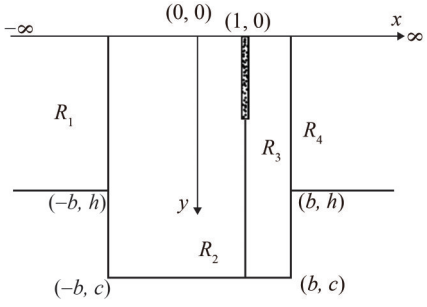

Figure 2 Subregions of the fluid domain

Let the resulting motion in the fluid be described by the velocity potential $\mathrm{Re}\,[\varphi_j(x,y)\mathrm{e}^{-\mathrm{i}\sigma t}]$, then $\varphi_j(x,y)$ satisfies

$$\nabla^2\varphi_j = 0, \quad \text{in the fluid domain} \tag{3}$$

the linearized free surface condition

$$\left(\frac{\partial}{\partial y} + K\right)\varphi_j = 0 \text{ on } y = 0,\ -\infty < x < \infty \tag{4}$$

the bottom boundary condition

$$\varphi_{jy} = 0 \text{ on } \begin{cases} y = c,\ j = 2,3 \\ y = h,\ j = 1,4 \end{cases} \tag{5}$$

the conditions on the two sides of the trench

$$\varphi_{jx} = 0 \text{ on } x = \pm b,\ j = 2,3,\ h < y < c \tag{6}$$

the edge conditions

$$r_1^{\frac{1}{3}}\nabla\varphi_1, r_2^{\frac{1}{2}}\nabla\varphi_2, r_3^{\frac{1}{3}}\nabla\varphi_3 \text{ are bounded as } r_1, r_2, r_3 \to 0 \tag{7}$$

where r_1, r_2, r_3 are the distances from the submerged left edge of the trench, the submerged edge of the barrier and the submerged right edge of the trench respectively so that

$$r_1^2 = (x+b)^2 + (y-h)^2$$
$$r_2^2 = (x-l)^2 + (y-a)^2$$
$$r_3^2 = (x-b)^2 + (y-h)^2$$

The condition on the porous barrier surface is given by

$$\frac{\partial\varphi_2}{\partial x} = \frac{\partial\varphi_3}{\partial x} = -\mathrm{i}\alpha_0 G(\varphi_3 - \varphi_2) \text{ on } x = l,\ 0 < y < a \tag{8}$$

Here $G = G^r + \mathrm{i}G^i$ is the dimensionless porous parameter given by $G = \dfrac{\delta(f + \mathrm{i}S)}{K\tau(f^2 + S^2)}$, where δ is the porosity, f is

the resistance force coefficient, S is the inertial force coefficient and τ is the thickness of the porous medium. The real part G^r represents the resistance force coefficient and the imaginary part G^i represents the inertial force coefficient of the porous material. The quantity G^r resists passage of fluid through the pores while G^i allows the fluid through the pores of the porous material. When $G^i \ll G^r$, i.e., when the inertial force coefficient is much less than the resistance force coefficient then G is considered as real.

The continuity of normal velocity and pressure across the free-flowing interfaces yields

$$\begin{aligned} \frac{\partial \varphi_1}{\partial x} = \frac{\partial \varphi_2}{\partial x} \text{ and } \varphi_1 = \varphi_2, \text{ for } x = -b,\ y \in (0,h) \\ \frac{\partial \varphi_2}{\partial x} = \frac{\partial \varphi_3}{\partial x}, \text{ for } x = l,\ y \in (0,c) \\ \varphi_2 = \varphi_3, \text{ for } x = l,\ y \in (a,c) \\ \frac{\partial \varphi_3}{\partial x} = \frac{\partial \varphi_4}{\partial x} \text{ and } \varphi_3 = \varphi_4, \text{ for } x = b,\ y \in (0,h) \end{aligned} \tag{9}$$

The far field behavior of the potential functions are described by

$$\begin{aligned} \varphi_1(x,y) \sim \varphi^{\text{inc}}(x,y) + R\varphi^{\text{inc}}(-x,y) \text{ as } x \to -\infty \\ \varphi_4(x,y) \sim T\varphi^{\text{inc}}(x,y) \text{ as } x \to \infty \end{aligned} \tag{10}$$

where R and T are the unknown complex reflection and transmission coefficients respectively to be determined.

3 Method of solution

By Havelock's expansion of water wave potential, the eigen function expansions of $\varphi_j(x,y)$ satisfying (3) to (9) in the different regions R_j, $j = 1, 2, 3, 4$ are given below.

$$\begin{aligned} \varphi_1(x,y) &= \left\{e^{i\alpha_0(x+b)} + Re^{-i\alpha_0(x-b)}\right\}\psi_0(y) \\ &\quad + \sum_{n=1}^{\infty} A_n e^{\alpha_n(x+b)}\psi_n(y) \\ \varphi_2(x,y) &= \left\{B_0 \cos\lambda_0 x + C_0 \sin\lambda_0 x\right\}\chi_0(y) \\ &\quad + \sum_{n=1}^{\infty} \{B_n \cosh\lambda_n x + C_n \sinh\lambda_n x\}\chi_n(y) \\ \varphi_3(x,y) &= \left\{D_0 \cos\lambda_0 x + E_0 \sin\lambda_0 x\right\}\chi_0(y) \\ &\quad + \sum_{n=1}^{\infty} \{D_n \cosh\lambda_n x + E_n \sinh\lambda_n x\}\chi_n(y) \\ \varphi_4(x,y) &= Te^{i\alpha_0(x-b)}\psi_0(y) + \sum_{n=1}^{\infty} F_n e^{-\alpha_n(x-b)}\psi_n(y) \end{aligned} \tag{11}$$

where $\{A_n\}_{n=1}^{\infty}$, $\{B_n\}_{n=0}^{\infty}$, $\{C_n\}_{n=0}^{\infty}$, $\{D_n\}_{n=0}^{\infty}$, $\{E_n\}_{n=0}^{\infty}$, $\{F_n\}_{n=1}^{\infty}$, R, T are unknowns to be determined. Here

$$\begin{aligned} \psi_0(y) = \frac{\cosh\alpha_0(h-y)}{\cosh\alpha_0 h}, \psi_n(y) = \frac{\cos\alpha_n(h-y)}{\cos\alpha_n h}, n = 1,2,\cdots \\ \chi_0(y) = \frac{\cosh\alpha_0(c-y)}{\cosh\alpha_0 c}, \chi_n(y) = \frac{\cos\alpha_n(c-y)}{\cos\alpha_n c}, n = 1,2,\cdots \end{aligned} \tag{12}$$

and $\alpha_0, \pm i\alpha_n$ are the roots of the Equation (2) and $\lambda_0, \pm i\lambda_n$ are the roots of the equation

$$\lambda \tanh \lambda c = K \tag{13}$$

For determination of the unknowns $A_n's$, $B_n's$, $C_n's$, $D_n's$, $E_n's$, $F_n's$, R and T we proceed as follows. Let us define

$$\begin{aligned} f_j(y) &= \left[\frac{\partial \varphi_j}{\partial x}\right]_{x=-b,l,b} = \left[\frac{\partial \varphi_{j+1}}{\partial x}\right]_{x=-b,l,b} \quad j = 1,2,3 \\ g_j(y) &= \left[\varphi_{j+1} - \varphi_j\right]_{x=-b,l,b} \qquad\qquad j = 1,2,3 \end{aligned} \tag{14}$$

where $y \in (0,h)$ for $j = 1, 3$ and $y \in (0,c)$ for j=2. Using the representation (11) in the Equation (14), we obtain

$$\begin{aligned} f_1(y) &= i\alpha_0\{1-R\}\psi_0(y) + \sum_{n=1}^{\infty} \alpha_n A_n \psi_n(y) \\ &= \lambda_0\{B_0 \sin\lambda_0 b + C_0 \cos\lambda_0 b\}\chi_0(y) \\ &\quad + \sum_{n=1}^{\infty} \lambda_n \{-B_n \sinh\lambda_n b + C_n \cosh\lambda_n b\}\chi_n(y) \\ g_1(y) &= \{B_0 \cos\lambda_0 b - C_0 \sin\lambda_0 b\}\chi_0(y) \\ &\quad + \sum_{n=1}^{\infty} \{B_n \cosh\lambda_n b - C_n \sinh\lambda_n b\}\chi_n(y) \\ &\quad - \{1+R\}\psi_0(y) - \sum_{n=1}^{\infty} A_n \psi_n(y) \\ f_2(y) &= \lambda_0\{-B_0 \sin\lambda_0 l + C_0 \cos\lambda_0 l\}\chi_0(y) \\ &\quad + \sum_{n=1}^{\infty} \lambda_n \{B_n \sinh\lambda_n l + C_n \cosh\lambda_n l\}\chi_n(y) \\ &= \lambda_0\{-D_0 \sin\lambda_0 l + E_0 \cos\lambda_0 l\}\chi_0(y) \\ &\quad + \sum_{n=1}^{\infty} \lambda_n \{D_n \sinh\lambda_n l + E_n \cosh\lambda_n l\}\chi_n(y) \\ g_2(y) &= \{D_0 \cos\lambda_0 l + E_0 \sin\lambda_0 l\}\chi_0(y) \\ &\quad + \sum_{n=1}^{\infty} \{D_n \cosh\lambda_n l + E_n \sinh\lambda_n l\}\chi_n(y) \\ &\quad - \{B_0 \cos\lambda_0 l + C_0 \sin\lambda_0 l\}\chi_0(y) \\ &\quad - \sum_{n=1}^{\infty} \{B_n \cosh\lambda_n l + C_n \sinh\lambda_n l\}\chi_n(y) \\ f_3(y) &= \lambda_0\{-D_0 \sin\lambda_0 b + E_0 \cos\lambda_0 b\}\chi_0(y) \\ &\quad + \sum_{n=1}^{\infty} \lambda_n \{D_n \sinh\lambda_n b + E_n \cosh\lambda_n b\}\chi_n(y) \\ &= i\alpha_0 T\psi_0(y) - \sum_{n=1}^{\infty} \alpha_n F_n \psi_n(y) \\ g_3(y) &= T\psi_0(y) + \sum_{n=1}^{\infty} F_n \psi_n(y) \\ &\quad - \{D_0 \cos\lambda_0 b + E_0 \sin\lambda_0 b\}\chi_0(y) \\ &\quad - \sum_{n=1}^{\infty} \{D_n \cosh\lambda_n b + E_n \sinh\lambda_n b\}\chi_n \end{aligned} \tag{15}$$

Now applying the Havelock's inversion formula to Equation (15) we obtain the unknown constants as,

$$1 - R = \frac{-4\mathrm{i}\cosh\alpha_0 h}{\delta_0}\int_0^h f_1(u)\cosh\alpha_0(h-u)\,\mathrm{d}u \quad (16)$$

$$A_n = \frac{4\cos\alpha_n h}{\delta_n}\int_0^h f_1(u)\cos\alpha_n(h-u)\,\mathrm{d}u \quad (17)$$

$$B_0 = \frac{4\cosh\lambda_0 c}{\gamma_0\sin\lambda_0(b+l)}\left[\cos\lambda_0 l\int_0^h f_1(u)\cosh\lambda_0(c-u)\,\mathrm{d}u - \cos\lambda_0 b\int_0^c f_2(u)\cosh\lambda_0(c-u)\,\mathrm{d}u\right] \quad (18)$$

$$B_n = \frac{4\cos\lambda_n c}{\gamma_n\sinh\lambda_n(b+l)}\left[\cosh\lambda_n b\int_0^c f_2(u)\cos\lambda_n(c-u)\,\mathrm{d}u - \cosh\lambda_n l\int_0^h f_1(u)\cos\lambda_n(c-u)\,\mathrm{d}u\right] \quad (19)$$

$$C_0 = \frac{4\cosh\lambda_0 c}{\gamma_0\sin\lambda_0(b+l)}\left[\sin\lambda_0 l\int_0^h f_1(u)\cosh\lambda_0(c-u)\,\mathrm{d}u + \sin\lambda_0 b\int_0^c f_2(u)\cosh\lambda_0(c-u)\,\mathrm{d}u\right] \quad (20)$$

$$C_n = \frac{4\cos\lambda_n c}{\gamma_n\sinh\lambda_n(b+l)}\left[\sinh\lambda_n l\int_0^h f_1(u)\cos\lambda_n(c-u)\,\mathrm{d}u + \sinh\lambda_n b\int_0^c f_2(u)\cos\lambda_n(c-u)\,\mathrm{d}u\right] \quad (21)$$

$$D_0 = \frac{4\cosh\lambda_0 c}{\gamma_0\sin\lambda_0(b-l)}\left[\cos\lambda_0 b\int_0^c f_2(u)\cosh\lambda_0(c-u)\,\mathrm{d}u - \cos\lambda_0 l\int_0^h f_3(u)\cosh\lambda_0(c-u)\,\mathrm{d}u\right] \quad (22)$$

$$D_n = \frac{-4\cos\lambda_n c}{\gamma_n\sinh\lambda_n(b-l)}\left[\cosh\lambda_n b\int_0^c f_2(u)\cos\lambda_n(c-u)\,\mathrm{d}u - \cosh\lambda_n l\int_0^h f_3(u)\cos\lambda_n(c-u)\,\mathrm{d}u\right] \quad (23)$$

$$E_0 = \frac{4\cosh\lambda_0 c}{\gamma_0\sin\lambda_0(b-l)}\left[\sin\lambda_0 b\int_0^c f_2(u)\cosh\lambda_0(c-u)\,\mathrm{d}u - \sin\lambda_0 l\int_0^h f_3(u)\cosh\lambda_0(c-u)\,\mathrm{d}u\right] \quad (24)$$

$$E_n = \frac{4\cos\lambda_n c}{\gamma_n\sinh\lambda_n(b-l)}\left[\sinh\lambda_n b\int_0^c f_2(u)\cos\lambda_n(c-u)\,\mathrm{d}u - \sinh\lambda_n l\int_0^h f_3(u)\cos\lambda_n(c-u)\,\mathrm{d}u\right] \quad (25)$$

$$T = \frac{-4\mathrm{i}\cosh\alpha_0 h}{\delta_0}\int_0^h f_3(u)\cosh\alpha_0(h-u)\,\mathrm{d}u \quad (26)$$

$$F_n = \frac{-4\cos\alpha_n h}{\delta_n}\int_0^h f_3(u)\cos\alpha_n(h-u)\,\mathrm{d}u \quad (27)$$

where $\delta_0 = 2\alpha_0 h + \sinh 2\alpha_0 h$; $\delta_n = 2\alpha_n h + \sin 2\alpha_n h$; $\gamma_0 = 2\lambda_0 c + \sinh 2\lambda_0 c$; $\gamma_n = 2\lambda_n c + \sin 2\lambda_n c\,(n = 1, 2, \cdots)$.

Thus all the unknown constants are expressed in terms of the function $f_j(y)$ and $g_j(y)$. $j = 1, 2, 3$ so that once $f_j(y)$ and $g_j(y)$, $j = 1, 2, 3$ are known then the problem is solved. In the next section we proceed to determine $f_j(y)$, j=1, 2, 3 through integral equation formulation.

3.1 Formation of integral equation

In this section we will derive integral equations for $f_j(y)$, j=1, 2, 3. For this we first consider the continuity of $\varphi_j(x,y)$ across the gaps in the boundaries of different regions as given in relation (9). This gives

$$\begin{aligned}
&\varphi_1(-b-0,y) = \varphi_2(-b+0,y),\ 0<y<h\\
&\varphi_2(l-0,y) - \varphi_3(l+0,y) = -\frac{\mathrm{i}}{\alpha_0 G}f_2(y),\ 0<y<a\\
&\varphi_2(l-0,y) - \varphi_3(l+0,y) = 0,\ a<y<c\\
&\varphi_3(b-0,y) = \varphi_4(b+0,y),\ 0<y<h
\end{aligned} \quad (28)$$

These provides the three integral equations given by

$$\begin{aligned}
&\int_0^h p_1(u)\,L_j(y,u)\,\mathrm{d}u + \int_0^c p_2(u)\,M_j(y,u)\,\mathrm{d}u\\
&+\int_0^h p_3(u)\,N_j(y,u)\,\mathrm{d}u = X_j,\ j = 1,2,3
\end{aligned} \quad (29)$$

where $X_1 = \psi_0(y)$, $X_2 = q_2(y)$, $X_3 = 0$; $p_i(u) = \dfrac{g_i(u)}{1+R}$, i = 1, 2, 3.

$$q_2(u) = \frac{f_2(u)}{1+R} \quad (30)$$

$$\begin{aligned}
L_1(y,u) = &-\sum_{n=1}^{\infty}\frac{4\cos\alpha_n(h-y)\cos\alpha_n(h-u)}{\delta_n}\\
&+\frac{4\cosh\lambda_0(c-y)\cosh\lambda_0(c-u)}{\gamma_0\tan\lambda_0(b+l)}\\
&-\sum_{n=1}^{\infty}\frac{4\cos\lambda_n(c-y)\cos\lambda_n(c-u)}{\gamma_n\tanh\lambda_n(b+l)}
\end{aligned} \quad (31)$$

$$\begin{aligned}
M_1(y,u) = &-\frac{4\cosh\lambda_0(c-y)\cosh\lambda_0(c-u)}{\gamma_0\sin\lambda_0(b+l)}\\
&+\sum_{n=1}^{\infty}\frac{4\cos\lambda_n(c-y)\cos\lambda_n(c-u)}{\gamma_n\sinh\lambda_n(b+l)}
\end{aligned} \quad (32)$$

$$N_1(y,u)=0 \tag{33}$$

$$L_2(y,u)=-\frac{4\cosh\lambda_0(c-y)\cosh\lambda_0(c-u)}{\gamma_0\sin\lambda_0(b+l)}+\sum_{n=1}^{\infty}\frac{4\cos\lambda_n(c-y)\cos\lambda_n(c-u)}{\gamma_n\sinh\lambda_n(b+l)} \tag{34}$$

$$M_2(y,u)=\frac{4\cosh\lambda_0(c-y)\cosh\lambda_0(c-u)}{\gamma_0\tan\lambda_0(b-l)}+\frac{4\cosh\lambda_0(c-y)\cosh\lambda_0(c-u)}{\gamma_0\tan\lambda_0(b+l)}-\sum_{n=1}^{\infty}\frac{4\cos\lambda_n(c-y)\cos\lambda_n(c-u)}{\gamma_n\tanh\lambda_n(b-l)}-\sum_{n=1}^{\infty}\frac{4\cos\lambda_n(c-y)\cos\lambda_n(c-u)}{\gamma_n\tanh\lambda_n(b+l)} \tag{35}$$

$$N_2(y,u)=-\frac{4\cosh\lambda_0(c-y)\cosh\lambda_0(c-u)}{\gamma_0\sin\lambda_0(b-l)}+\sum_{n=1}^{\infty}\frac{4\cos\lambda_n(c-y)\cos\lambda_n(c-u)}{\gamma_n\sinh\lambda_n(b-l)} \tag{36}$$

$$L_3(y,u)=0 \tag{37}$$

$$M_3(y,u)=-\frac{4\cosh\lambda_0(c-y)\cosh\lambda_0(c-u)}{\gamma_0\sin\lambda_0(b-l)}+\sum_{n=1}^{\infty}\frac{4\cos\lambda_n(c-y)\cos\lambda_n(c-u)}{\gamma_n\sinh\lambda_n(b-l)} \tag{38}$$

$$N_3(y,u)=\frac{4\cosh\lambda_0(c-y)\cosh\lambda_0(c-u)}{\gamma_0\tan\lambda_0(b-l)}-\sum_{n=1}^{\infty}\frac{4\cos\lambda_n(c-y)\cos\lambda_n(c-u)}{\gamma_n\tanh\lambda_n(b-l)}-\frac{4\mathrm{i}\cosh\alpha_0(h-y)\cosh\alpha_0(h-u)}{\delta_0}-\sum_{n=1}^{\infty}\frac{4\cos\alpha_n(h-y)\cos\alpha_n(h-u)}{\delta_n} \tag{39}$$

3.2 Solution of integral equation

We solve the integral Equations (29) using the multi-term Galerkin approximation method. For this we write the unknown functions $p_i(y)$, $i=1,2,3$ as

$$p_1(y)=\sum_{n=0}^{N}a_n u_n(y),\ 0<y<h \tag{40}$$

$$p_2(y)=\sum_{n=0}^{N}b_n z_n(y),\ 0<y<c \tag{41}$$

where $z_n(y)=v_n(y)$ for $0<y<a$ and $z_n(y)=x_n(y)$ for $a<y<c$.

$$p_3(y)=\sum_{n=0}^{N}c_n w_n(y),\ 0<y<h \tag{42}$$

$$q_2(y)=\sum_{n=0}^{N}b_n v_n(y),\ 0<y<a$$

where the basis functions $u_n(y)$ for $0<y<h$ and $w_n(y)$ for $0<y<h$ are chosen in terms of ultraspherical Gegenbauer polynomials of order 1/6 and $z_n(y)$ for $0<y<a$ are chosen in terms of orthogonal Chebyshev polynomial of order $2n$ with suitable weights respectively. The choice of basis functions depends on the types of singularities at the corners of the trench and at the submerged sharp edge of the barrier as given by the edge condition (7). Here we also consider simple polynomial as basis function to solve the integral equation. The basis function in various intervals are given below.

3.3 Basis functions

3.3.1 Approximation of basis functions in terms of orthogonal polynomials

In each integral Equation of (29) there are three integrals where the unknown functions are $p_1(y), p_2(y), p_3(y)$ in first, second and third integral respectively. As given in Equations (40) to (42), these unknown function are expanded in terms of suitable basis functions. The choice of basis functions are explained in section 3.2 and are given below.

For the first integral in (29) we write,

$$u_n(y)=-\frac{\mathrm{d}}{\mathrm{d}y}\left[\mathrm{e}^{-Ky}\int_y^h \mathrm{e}^{-Kt}\tilde{u}_n(t)\,\mathrm{d}t\right],\ 0<y<h \tag{43}$$

We choose the basis functions in terms of $\tilde{u}_n(y)$ as follows

$$\tilde{u}_n(y)=\frac{2^{\frac{7}{6}}\Gamma\left(\frac{1}{6}\right)(2n)!}{\pi\Gamma\left(2n+\frac{1}{3}\right)(h)^{\frac{1}{3}}\left(h^2-y^2\right)^{\frac{1}{3}}}C_{2n}^{\frac{1}{6}}\left(\frac{y}{h}\right),\ 0<y<h \tag{44}$$

where $C_{2n}^{\frac{1}{6}}\left(\frac{y}{h}\right)$ are Gegenbauer polynomials of order 1/6.

For the second integral in (29) we write,

$$v_n(y)=-\frac{\mathrm{d}}{\mathrm{d}y}\left[\mathrm{e}^{-Ky}\int_0^a \mathrm{e}^{-Kt}\tilde{v}_n(t)\,\mathrm{d}t\right],\ 0<y<a$$
$$x_n(y)=-\frac{\mathrm{d}}{\mathrm{d}y}\left[\mathrm{e}^{-Ky}\int_a^c \mathrm{e}^{-Kt}\tilde{x}_n(t)\,\mathrm{d}t\right],\ a<y<c \tag{45}$$

We choose the basis functions in terms of $\tilde{v}_n(y)$ as follows

$$\tilde{v}_n(y) = \frac{2(-1)^n}{\pi(2n+1)ah}\left(a^2 - y^2\right)^{\frac{1}{2}} U_{2n}\left(\frac{y}{a}\right), 0 < y < a$$
$$\tilde{x}_n(y) = \frac{2(-1)^n}{\pi\left\{(h-y)^2 - (h-a)^2\right\}^{\frac{1}{2}}} T_{2n}\left(\frac{h-y}{h-a}\right), a < y < c \tag{46}$$

where $T_{2n}(y)$ and $U_{2n}(y)$ are Chebychev's polynomial of first and second kind of order $2n$.

For the third integral in (29) we write,

$$w(y) = -\frac{\mathrm{d}}{\mathrm{d}y}\left[\mathrm{e}^{-Ky}\int_y^h \mathrm{e}^{-Kt}\tilde{w}_n(t)\,\mathrm{d}t\right], 0 < y < h \tag{47}$$

Here also we choose the $\tilde{w}_n(y)$ in terms of Gegenbauer polynomials of order 1/6 as given below.

$$\tilde{w}_n(y) = \frac{2^{\frac{7}{6}}\Gamma\left(\frac{1}{6}\right)(2n)!}{\pi\Gamma\left(2n+\frac{1}{3}\right)(h)^{\frac{1}{3}}\left(h^2-y^2\right)^{\frac{1}{3}}} C_{2n}^{\frac{1}{6}}\left(\frac{y}{h}\right), 0 < y < h \tag{48}$$

Thus the unknown functions satisfying the integral Equation (29) are expanded in terms of suitable orthogonal polynomials as shown in Equations (43) to (48). However the unknown functions satisfying the integral Equation (29) can also be expanded in terms of simple polynomials as shown below.

3.3.2 Approximation of basis functions in terms of simple polynomials

For the first integral in (29) we write,

$$u_n(y) = \left(\frac{h}{h-y}\right)^{\frac{1}{3}}\left(\frac{y}{h}\right)^n, 0 < y < h \tag{49}$$

For the second integral in (29) we write,

$$v_n(y) = \left(\frac{a}{a-y}\right)^{\frac{1}{2}}\left(\frac{y}{a}\right)^n, 0 < y < a \tag{50}$$

and

$$x_n(y) = \left(\frac{a}{y-a}\right)^{\frac{1}{2}}\left(\frac{y}{a}\right)^n, a < y < c \tag{51}$$

For the third integral in (29) we write,

$$w_n(y) = \left(\frac{h}{h-y}\right)^{\frac{1}{3}}\left(\frac{y}{h}\right)^n, 0 < y < h \tag{52}$$

3.4 Formation of linear system of equations

As the three integral equations given by (29) are in different ranges, they can be extended to the range $(0, c)$ as in (Morris, 1975) by multiplying with appropriate Heaviside unit functions. This gives the linear system of equations as follows

$$\sum_{n=0}^{N} a_n \mathcal{K}_{mn} + \sum_{n=0}^{N} b_n \mathcal{L}_{mn} = d_m, m = 0, 1, \cdots, N \tag{53}$$

$$\sum_{n=0}^{N} a_n \mathcal{M}_{mn} + \sum_{n=0}^{N} b_n \mathcal{N}_{mn} + \sum_{n=0}^{N} c_n \mathcal{P}_{mn} = 0,\ m = 0, 1, \cdots, N \tag{54}$$

$$\sum_{n=0}^{N} b_n \mathcal{Q}_{mn} + \sum_{n=0}^{N} c_n \mathcal{R}_{mn} = 0, m = 0, 1, \cdots, N \tag{55}$$

where

$$\mathcal{K}_{mn} = \int_0^h\left(\int_0^h L_1(y,u)\,u_n(u)\,\mathrm{d}u\right)u_m(y)\,\mathrm{d}y$$
$$\mathcal{L}_{mn} = -\mathrm{i}\alpha_0 G\int_0^a\left(\int_0^a M_1(y,u)\,v_n(u)\,\mathrm{d}u\right)v_m(y)\,\mathrm{d}y + \int_a^c\left(\int_a^c M_1(y,u)\,x_n(u)\,\mathrm{d}u\right)x_m(y)\,\mathrm{d}y$$
$$\mathcal{M}_{mn} = \int_0^h\left(\int_0^h L_2(y,u)\,u_n(u)\,\mathrm{d}u\right)u_m(y)\,\mathrm{d}y$$
$$\mathcal{N}_{mn} = -\mathrm{i}\alpha_0 G\int_0^a\left(\int_0^a M_2(y,u)\,v_n(u)\,\mathrm{d}u\right)v_m(y)\,\mathrm{d}y + \int_a^c\left(\int_a^c M_2(y,u)\,x_n(u)\,\mathrm{d}u\right)x_m(y)\,\mathrm{d}y - \int_0^a v_n(y)\,v_m(y)\,\mathrm{d}y$$
$$\mathcal{P}_{mn} = \int_0^h\left(\int_0^h N_2(y,u)\,w_n(u)\,\mathrm{d}u\right)w_m(y)\,\mathrm{d}y$$
$$\mathcal{Q}_{mn} = -\mathrm{i}\alpha_0 G\int_0^a\left(\int_0^a M_3(y,u)\,v_n(u)\,\mathrm{d}u\right)v_m(y)\,\mathrm{d}y + \int_a^c\left(\int_a^c M_3(y,u)\,x_n(u)\,\mathrm{d}u\right)x_m(y)\,\mathrm{d}y$$
$$\mathcal{R}_{mn} = -\int_0^h\left(\int_0^h N_3(y,u)\,w_n(u)\,\mathrm{d}u\right)w_m(y)\,\mathrm{d}y$$

and

$$d_m = \int_0^h \frac{\cosh\alpha_0(h-u)}{\cosh\alpha_0 h}\,u_m(y)\,\mathrm{d}y$$

with $m, n = 0, 1, 2, \cdots, N$.

Substituting the expression of $f_1(y)$ in terms of $p_1(y)$

in (16), we obtain the reflection coefficient as follows

$$R = \frac{1 + C_s}{1 - C_s} \tag{56}$$

where

$$C_s = \frac{4\mathrm{i}\cosh\alpha_0 h}{\delta_0}\sum_{n=0}^{N} a_n \int_0^h \cosh\alpha_0(h-y)u_n(y)\,\mathrm{d}y \tag{57}$$

and substituting the expression of $f_3(y)$ in terms of $p_3(y)$ in (26), we obtain transmission coefficient as follows

$$T = -\frac{4\mathrm{i}(1+R)\cosh\alpha_0 h}{\delta_0}\sum_{n=0}^{N} c_n \int_0^h \cosh\alpha_0(h-y)w_n(y)\,\mathrm{d}y \tag{58}$$

3.5 Evaluation of coefficients of linear system of equations

The various coefficients $\mathcal{K}_{mn}$, $\mathcal{L}_{mn}$, $\mathcal{M}_{mn}$, $\mathcal{N}_{mn}$, $\mathcal{P}_{mn}$, $\mathcal{Q}_{mn}$, $\mathcal{R}_{mn}$, occurring in the linear system of algebraic Equations (53) to (55), can be evaluated by choosing the basis functions in terms of simple polynomial as given by equations (49) to (52) and orthogonal polynomials as given by Equations (44) to (48). The choice of basis functions in terms of orthogonal polynomial simplifies the coefficients of the linear system of Equations (53) to (55) considerably using the properties of the orthogonal polynomials. The simplified form of various coefficients using the properties of orthogonal polynomials are given below.

$$\begin{aligned}\mathcal{K}_{mn} = \int_0^h\left(\int_0^h L_1(y,u)u_n(u)\,\mathrm{d}u\right)u_m(y)\,\mathrm{d}y &= -\sum_{r=1}^{\infty}\frac{4}{\delta_r}\left(\int_0^h \cos\alpha_r(h-y)u_m(y)\,\mathrm{d}y\right)\left(\int_0^h \cos\alpha_r(h-u)u_n(u)\,\mathrm{d}u\right)\\ &+\frac{4}{\gamma_0\tan\lambda_0(b+l)}\left(\int_0^h \cosh\lambda_0(c-y)u_m(y)\,\mathrm{d}y\right)\left(\int_0^h \cosh\lambda_0(c-u)u_n(u)\,\mathrm{d}u\right)\\ &-\sum_{r=1}^{\infty}\frac{4}{\gamma_r\tanh\lambda_r(b+l)}\left(\int_0^h \cos\lambda_r(c-y)u_m(y)\,\mathrm{d}y\right)\left(\int_0^h \cos\lambda_r(c-u)u_n(u)\,\mathrm{d}u\right)\end{aligned}$$

Now,

$$\int_0^h \cos\alpha_r(h-y)u_m(y)\,\mathrm{d}y = \frac{2^{\frac{7}{6}}\Gamma\left(\frac{1}{6}\right)(2m)!}{\pi\Gamma\left(2m+\frac{1}{3}\right)(h)^{\frac{1}{3}}}\int_0^h \cos\alpha_r(h-y)\frac{1}{\left(h^2-y^2\right)^{\frac{1}{3}}}C_{2m}^{\frac{1}{6}}\left(\frac{y}{h}\right)\mathrm{d}y = \frac{2(-1)^m}{(\alpha_r h)^{\frac{1}{6}}}\cos(\alpha_r h)J_{2m+\frac{1}{6}}(\alpha_r h)$$

where J_n's are Bessel functions of first kind.

Similarly other integrals in the expression for $\mathcal{K}_{mn}$ can be evaluated. Using this result in the expression for $\mathcal{K}_{mn}$, we get

$$\begin{aligned}\mathcal{K}_{mn} = &-\sum_{r=1}^{\infty}\frac{16(-1)^{m+n}\cos^2(\alpha_r h)}{\delta_r(\alpha_r h)^{\frac{1}{3}}}J_{2m+\frac{1}{6}}(\alpha_r h)J_{2n+\frac{1}{6}}(\alpha_r h) + \frac{16\cosh^2(\lambda_0 c)}{\gamma_0(\lambda_0 h)^{\frac{1}{3}}\tan\lambda_0(b+l)}I_{2m+\frac{1}{6}}(\lambda_0 h)I_{2n+\frac{1}{6}}(\lambda_0 h)\\ &-\sum_{r=1}^{\infty}\frac{16(-1)^{m+n}\cos^2(\lambda_r c)}{\gamma_r(\lambda_r h)^{\frac{1}{3}}\tanh\lambda_r(b+l)}J_{2m+\frac{1}{6}}(\lambda_r h)J_{2n+\frac{1}{6}}(\lambda_r h)\end{aligned}$$

where I_n's are modified Bessel function of first kind.

$$\begin{aligned}\mathcal{L}_{mn} = &\mathrm{i}\alpha_0 G\left[\frac{16\cosh^2(\lambda_0 c)}{\gamma_0(\lambda_0 c)\sin\lambda_0(b+l)}I_{2m+1}(\lambda_0 a)I_{2n+1}(\lambda_0 a) - \sum_{r=1}^{\infty}\frac{16(-1)^{m+n}\cos^2(\lambda_r c)}{\gamma_r(\lambda_r c)\sinh\lambda_r(b+l)}J_{2m+1}(\lambda_r a)J_{2n+1}(\lambda_r a)\right]\\ &-\frac{16}{\gamma_0(\lambda_0 c)\sin\lambda_0(b+l)}I_{2m}(\lambda_0(c-a))I_{2n}(\lambda_0(c-a)) + \sum_{r=1}^{\infty}\frac{16(-1)^{m+n}}{\gamma_r(\lambda_r c)\sinh\lambda_r(b+l)}J_{2m}(\lambda_r(c-a))J_{2n}(\lambda_r(c-a))\end{aligned}$$

$$\mathcal{M}_{mn} = -\frac{16\cosh^2(\lambda_0 c)}{\gamma_0(\lambda_0 h)^{\frac{1}{3}}\sin\lambda_0(b+l)}I_{2m+\frac{1}{6}}(\lambda_0 h)I_{2n+\frac{1}{6}}(\lambda_0 h) + \sum_{r=1}^{\infty}\frac{16(-1)^{m+n}\cos^2(\lambda_r c)}{\gamma_r(\lambda_r h)^{\frac{1}{3}}\sinh\lambda_r(b+l)}J_{2m+\frac{1}{6}}(\lambda_r h)J_{2n+\frac{1}{6}}(\lambda_r h)$$

$$\mathcal{N}_{mn} = \mathrm{i}\alpha_0 G\Bigg[-\frac{16\cosh^2(\lambda_0 c)}{\gamma_0(\lambda_0 c)\tan\lambda_0(b-l)} I_{2m+1}(\lambda_0 a) I_{2n+1}(\lambda_0 a) - \frac{16\cosh^2(\lambda_0 c)}{\gamma_0(\lambda_0 c)\tan\lambda_0(b+l)} I_{2m+1}(\lambda_0 a) I_{2n+1}(\lambda_0 a)$$
$$+\sum_{r=1}^{\infty}\frac{16(-1)^{m+n}\cos^2(\lambda_r c)}{\gamma_r(\lambda_r c)\tanh\lambda_r(b-l)} J_{2m+1}(\lambda_r a) J_{2n+1}(\lambda_r a) + \sum_{r=1}^{\infty}\frac{16(-1)^{m+n}\cos^2(\lambda_r c)}{\gamma_r(\lambda_r c)\tanh\lambda_r(b+l)} J_{2m+1}(\lambda_r a) J_{2n+1}(\lambda_r a)\Bigg]$$
$$+\frac{16}{\gamma_0(\lambda_0 c)\tan\lambda_0(b+l)} I_{2m}(\lambda_0(c-a)) I_{2n}(\lambda_0(c-a)) - \sum_{r=1}^{\infty}\frac{16(-1)^{m+n}}{\gamma_r(\lambda_r c)\tanh\lambda_r(b+l)} J_{2m}(\lambda_r(c-a)) J_{2n}(\lambda_r(c-a))$$
$$+\frac{16}{\gamma_0(\lambda_0 c)\tan\lambda_0(b-l)} I_{2m}(\lambda_0(c-a)) I_{2n}(\lambda_0(c-a)) - \sum_{r=1}^{\infty}\frac{16(-1)^{m+n}}{\gamma_r(\lambda_r c)\tanh\lambda_r(b-l)} J_{2m}(\lambda_r(c-a)) J_{2n}(\lambda_r(c-a))$$
$$-\frac{4(-1)^{m+n}}{\pi^2 a^2 h^2 (2m+1)(2n+1)}\int_0^a (a^2-y^2) U_{2m}\left(\frac{y}{a}\right) U_{2n}\left(\frac{y}{a}\right)\mathrm{d}y$$

$$\mathcal{P}_{mn} = = -\frac{16\cosh^2(\lambda_0 c)}{\gamma_0(\lambda_0 h)^{\frac{1}{3}}\sin\lambda_0(b-l)} I_{2m+\frac{1}{6}}(\lambda_0 h) I_{2n+\frac{1}{6}}(\lambda_0 h) + \sum_{r=1}^{\infty}\frac{16(-1)^{m+n}\cos^2(\lambda_r c)}{\gamma_r(\lambda_r h)^{\frac{1}{3}}\sinh\lambda_r(b-l)} J_{2m+\frac{1}{6}}(\lambda_r h) J_{2n+\frac{1}{6}}(\lambda_r h)$$

$$\mathcal{Q}_{mn} = \mathrm{i}\alpha_0 G\Bigg[\frac{16\cosh^2(\lambda_0 c)}{\gamma_0(\lambda_0 c)\sin\lambda_0(b-l)} I_{2m+1}(\lambda_0 a) I_{2n+1}(\lambda_0 a) - \sum_{r=1}^{\infty}\frac{16(-1)^{m+n}\cos^2(\lambda_r c)}{\gamma_r(\lambda_r c)\sinh\lambda_r(b-l)} J_{2m+1}(\lambda_r a) J_{2n+1}(\lambda_r a)\Bigg]$$
$$-\frac{16}{\gamma_0(\lambda_0 c)\sin\lambda_0(b-l)} I_{2m}(\lambda_0(c-a)) I_{2n}(\lambda_0(c-a)) + \sum_{r=1}^{\infty}\frac{16(-1)^{m+n}}{\gamma_r(\lambda_r c)\sinh\lambda_r(b-l)} J_{2m}(\lambda_r(c-a)) J_{2n}(\lambda_r(c-a))$$

$$\mathcal{R}_{mn} = -\frac{16\,\mathrm{i}\cosh^2(\alpha_0 h)}{\delta_0(\alpha_0 h)^{\frac{1}{3}}} I_{2m+\frac{1}{6}}(\alpha_0 h) I_{2n+\frac{1}{6}}(\alpha_0 h)$$
$$-\sum_{r=1}^{\infty}\frac{16(-1)^{m+n}\cos^2(\alpha_r h)}{\delta_r(\alpha_r h)^{\frac{1}{3}}} J_{2m+\frac{1}{6}}(\alpha_r h) J_{2n+\frac{1}{6}}(\alpha_r h)$$
$$+\frac{16\cosh^2(\lambda_0 c)}{\gamma_0(\lambda_0 h)^{\frac{1}{3}}\tan\lambda_0(b-l)} I_{2m+\frac{1}{6}}(\lambda_0 h) I_{2n+\frac{1}{6}}(\lambda_0 h)$$
$$-\sum_{r=1}^{\infty}\frac{16(-1)^{m+n}\cos^2(\lambda_r c)}{\gamma_r(\lambda_r h)^{\frac{1}{3}}\tanh\lambda_r(b-l)} J_{2m+\frac{1}{6}}(\lambda_r h) J_{2n+\frac{1}{6}}(\lambda_r h)$$

$$d_m = \frac{2 I_{2m+\frac{1}{6}}(\alpha_0 h)}{(\alpha_0 h)^{\frac{1}{6}}}$$

3.6 Dynamic wave force

The dynamic pressure $P(x,y)$ can be obtained according to the Bernoulli equation (Li et al., 2015)

$$P(x,y) = -\mathrm{i}\rho\sigma g_2(y) \tag{59}$$

where ρ is the fluid density. The magnitude of horizontal wave force acting on barriers can be obtained by integrating the dynamic pressure along the porous barriers as follows

$$C_f = -\mathrm{i}\rho\sigma\int_0^a g_2(y)\,\mathrm{d}y \tag{60}$$

The non-dimensional form of the horizontal force coefficient on the vertical porous barriers is given by

$$K_f = \frac{K|C_f|}{\rho g} \tag{61}$$

3.7 Energy identity relation

The energy identity plays an important role in the theoretical study of water waves scattering by barriers. A part of incident wave energy can be dissipated by the porous barriers. The absolute values of the reflection and transmission coefficients are connected by the relation

$$|R|^2 + |T|^2 = 1 - J \tag{62}$$

Here J signifies the amount of dissipated energy due to the permeability of barriers and its expression in terms of the potential differences across the barriers is found to be

$$J = 2K\mathrm{Re}(G)\int_0^a \left|g_2(y)\right|^2\mathrm{d}y \tag{63}$$

where $\mathrm{Re}(G)$ is the real part of the porous effect parameters. It is clearly noticed from the expression of J that the integrand in the right-hand side of (63) is always positive

for a non-zero $\mathrm{Re}(G)$ so that $|R|^2 + |T|^2 < 1$ for the case of permeable barriers, whereas for impermeable barriers the energy identity relation satisfies $|R|^2 + |T|^2 = 1$, which provides the convergence of result in the present study.

4 Numerical results

In this section the numerical results of hydrodynamic quantities viz. reflection coefficient, transmission coefficient, energy dissipation coefficient and hydrodynamic force are depicted graphically. Here this quantities are non dimensionalized by the water depth h.

In Table 1, we display the numerical results for $|R|$ showing its convergence with the truncation number N in Equations (53) to (55), taking $N = 2, 3, 4, 5$ for different values of Kh and fixed values of $a/h = 0.5$, $b/h = 1.5$, $c/h = 1.5$, $l/h = 0.5$, $G = 0.5$. In this case we see that, for $N = 3, 4, 5$, the numerical values computed here coincide up to 5 decimal places. We have also checked that the present method converges for all other values of the parameters and the wave number when N is 3. So, for all the calculations we have chosen N=3.

Table 1 Convergence of $|R|$ with N

Kh	N=2	N=3	N=4	N=5
0.000 01	0.001 271	0.001 351	0.001 372	0.001 377
0.500 01	0.090 594	0.090 595	0.090 596	0.090 596
1.000 01	0.249 584	0.251 970	0.252 254	0.252 259
1.500 01	0.570 622	0.575 437	0.577 160	0.577 165
2.000 01	0.179 136	0.187 224	0.187 403	0.187 405
2.500 01	0.263 810	0.251 276	0.254 864	0.254 867

Then the accuracy of the numerical results are established in Table 2, by comparing our present result with Ray et al. (2021). In Table 2, the numerical values of $|R|$ computed by present method are compared with those given in Table 1 of Ray et al. (2021) for a rigid barrier placed along the y-axis, by considering $a/h = 0.5$, $b/h = 1.5$, $c/h = 1.5$, $l/h = 0$, $G = 0$. Ray et al. (2021) used Galerkin technique with simple polynomial as a basis function, whereas in the present work, suitable orthogonal polynomials (Gegenbauer polynomial for 1/3 rd singularity and Chebyshev polynomial for half singularity) are chosen as a basis function. From Table 2, it is clearly noticed that the linear system of Equations (53) to (55), converges for $N = 5$ in Ray et al. (2021), where as in the present study the same converges for $N = 3$. Thus the rate of convergence of the linear system taking algebraic polynomials as basis function is slower than the orthogonal polynomials as basis function.

In Table 3, the values of reflection coefficient are presented for different wave numbers Kh and fixed values of

Table 2 Comparision of our results with the results of Ray et al. (2021)

Kh	$\|R\|$ (N=5) (Ray et al., 2021)	$\|R\|$ (N=5) (Present study)	$\|T\|$ (N=5) (Ray et al., 2021)	$\|T\|$ (N=3) (Present study)
0.001	0.013 015	0.013 019	0.999 915	0.999 915
0.491	0.132 204	0.132 209	0.991 213	0.991 221
0.981	0.047 433	0.047 441	0.998 867	0.998 874
1.471	0.315 932	0.315 937	0.947 309	0.948 780
1.961	0.636 024	0.636 030	0.783 752	0.771 664
2.451	0.873 816	0.873 824	0.474 271	0.486 242
2.941	0.966 781	0.966 789	0.262 009	0.255 576

$a/h = 0.6$, $b/h = 1.5$, $c/h = 1.3$, $l/h = 0.5$, $G = 0.5$, and compared by choosing simple polynomials and orthogonal polynomial as basis functions in Galerkin method. It is observed that rate of convergence of the method choosing basis function as orthogonal polynomial (N=3) is faster than taking basis function as simple polynomial (N=5). Also the Table 2 shows that the values of $|R|$ choosing orthogonal polynomial as basis function matches with values of $|R|$ choosing simple polynomial as basis function upto five places of decimal. Hence we may infer that the orthogonal polynomials as basis function is definitely a better choice.

Table 3 $|R|$ for orthogonal and simple polynomial

Kh	Orthogonal polynomials (N=3)	Simple polynomials (N=5)
0.000 01	0.000 948	0.000 945
0.500 01	0.024 745	0.024 751
1.000 01	0.344 937	0.344 935
1.500 01	0.379 658	0.379 654
2.000 01	0.956 727	0.956 721
2.500 01	0.265 245	0.265 241

The numerical values of the reflection coefficient, transmission coefficient, energy dissipation coefficients and the energy identity are presented in Table 4 for different values of Kh and fixed values of $a/h = 0.5$, $b/h = 1.5$, $c/h = 1.5$, $l/h = 0.5$, $G = 1.0$. In this table for all the values of Kh we observe that the energy identity relation $|R|^2 + |T|^2 + J = 1$ is satisfied. This tables provide a partial check on the correctness of the results obtained by the present method.

Table 4 Energy identity

Kh	$\|R\|$	$\|T\|$	J	$\|R\|^2 + \|T\|^2 + J$
0.100 01	0.113 531 0	0.994 401	0.001 723 29	1.003
1.200 01	0.361 891 0	0.904 478	0.050 953 60	1.000
2.000 01	0.077 184 6	0.715 724	0.481 782 00	1.000
2.500 01	0.270 846 0	0.745 861	0.370 333 00	1.000
2.830 01	0.976 509 0	0.136 927	0.027 680 90	1.000

4.1 Validation of the results

To show the validity of the analytical solutions obtained in the present work, it is compared with the results of Lee and Chwang (2000) considering limiting values of certain parameters in our results. By taking $c/h = 1$, $b/h = 0.001$, i.e., in absence of trench, in the present configuration, the reflection coefficient $|R|$ is compared with the results of Lee and Chwang (2000) by taking $a/h = 0.5$ and $G(= 0.25, 0.5, 1)$ in Figure 3. A good matching of $|R|$ is observed in the figure.

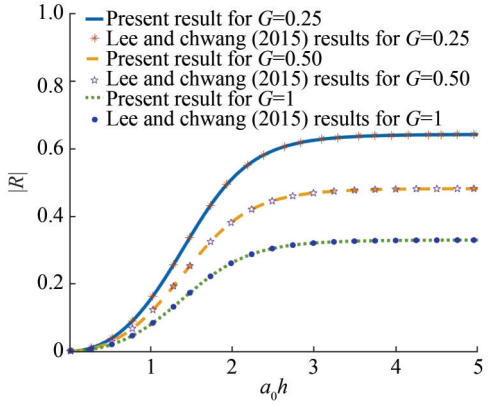

Figure 3 Comparison of our results to the Figure 6 of Lee and Chwang (2000) taking $\frac{a}{h} = 0.5$. $\frac{b}{h} = 0.001$, $\frac{c}{h} = 1$ and different values of G

In absence of barrier (i.e., making $a/h \rightarrow 0$, $G = 0$ in the present analysis), the problem reduces to study of wave propagation over a ractangular trench which was studied earlier by Lee and Ayer (1981). Choosing $a/h = 0.000\,1$, $b/h = 2.5$, $c/h = 2$ and G=0 in Figure 4 of the present analysis, if we plot reflection coefficient $|R|$ against $\alpha_0 h/2\pi$ we see that our result almost match with the Figure 2 of Lee and Ayer (1981).

In Figure 5, $|R|$ for rigid barrier, obtained in the present analysis by making $a/h = 0.9$, $b/h = 1.5$, $c/h = 1.5$, $G = 0$, is compared with the results given by Ray et al. (2021) (Figure 4a there). A good matching of the results are observed from Figure 5.

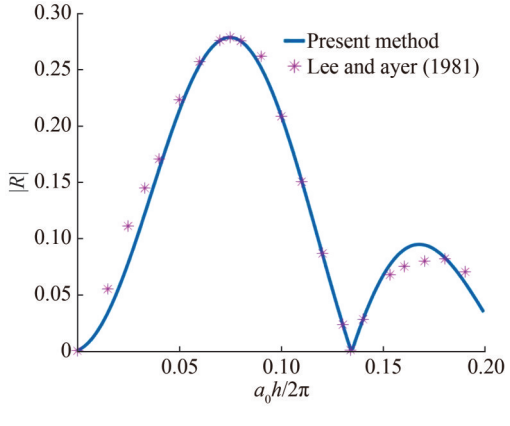

Figure 4 Comparison of our results to the Figure 2 of Lee and Ayer (1981) taking $\frac{a}{h} = 0.000\,1$, $\frac{b}{h} = 2.5$, $\frac{c}{h} = 2$ and G=0

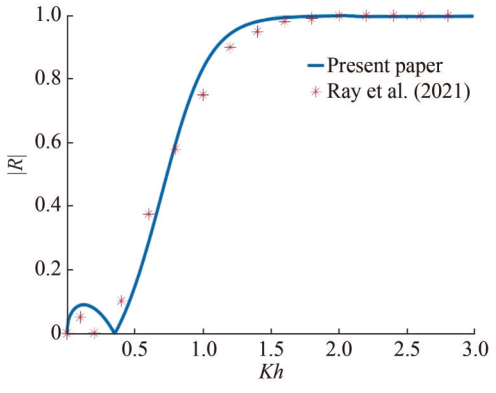

Figure 5 Comparison of our results to the Figure 4 a of Ray et al. (2021) taking $\frac{a}{h} = 0.9$, $\frac{b}{h} = 1.5$, $\frac{c}{h} = 1.5$ and G=0

4.2 Effect of various parameters on scattering coefficients ($|R|$ and $|T|$)

Figure 6 illustrates the effect of width of the trench on the reflection coefficients in presence of porous barrier. Here $|R|$ is plotted against the non-dimensional wave number Kh for three different width of the trench $b/h = 1.3$, 1.4, 1.5 and fixed values of $a/h = 0.7$, $c/h = 1.3$, $l/h = 0.5$ and G=0.5. We observe oscillatory behaviour of $|R|$ and the frequency of oscillation increases as the width of the trench b/h increases. Also we observe that for Kh>2, larger width of the trench increases the amount of reflection and the same behavior have shown in Chakraborty and Mandal (2014).

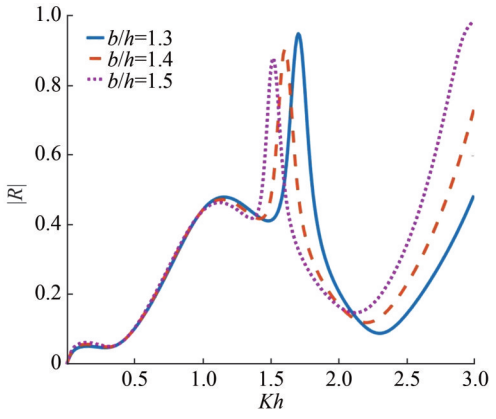

Figure 6 Reflection coefficient for different $\frac{b}{h}$ and fixed $\frac{a}{h} = 0.7$, $\frac{c}{h} = 1.3$, $\frac{l}{h} = 0.5$, $G = 0.5$

The effect of the length of the partially immersed porous barrier on the reflection coefficient $|R|$ is studied in Figure 7 where $|R|$ is plotted against the non-dimensional wave number Kh for various values of the length of the barrier

($a/h = 0.3, 0.6, 0.9$) and fixed values of $b/h = 1.5$, $c/h = 1.3$, $l/h = 0.5$ and G=0.5. Figure 7 shows that $|R|$ exhibits oscillatory behaviour and the amplitude of oscillation increases with increasing length of the porous barrier. For Kh near about 1.5 there occurs a sharp increase in amplitude of oscillation in $|R|$ showing resonating behaviour of the reflection coefficient.

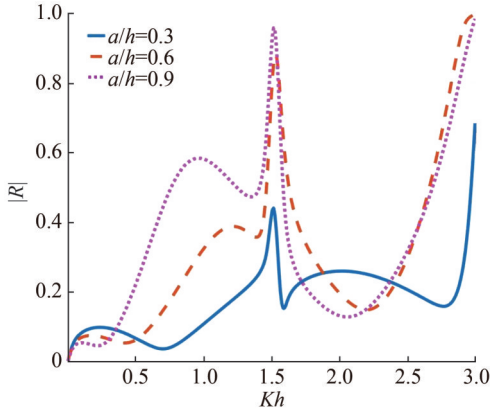

Figure 7 Reflection coefficient for different $\frac{a}{h}$ and fixed $\frac{b}{h} = 1.5$, $\frac{c}{h} = 1.3$, $\frac{l}{h} = 0.5$, $G = 0.5$

Figure 8 illustrate the effect of depth of the trench on the reflection coefficient. Here $|R|$ is plotted against the non-dimensional wave number Kh, for $a/h = 0.7$, $b/h = 1.4$, $l/h = 0.5$ and G=0.5 and for various depth of the trench viz, $c/h = 1.1, 1.2, 1.3$. It is observed that $|R|$ shows oscillatory behaviour and amplitude of oscillation increases with the increasing values of the trench depth c/h. Also for Kh~1.5, there occur resonance in $|R|$.

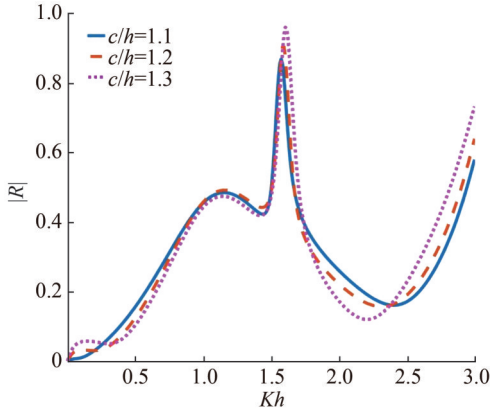

Figure 8 Reflection coefficient for different $\frac{c}{h}$ and fixed $\frac{a}{h} = 0.7$, $\frac{b}{h} = 1.4$, $\frac{l}{h} = 0.5$, $G = 0.5$

In Figure 9, reflection coefficient $|R|$ is plotted against the non-dimensional wave number Kh for different values of the porosity parameter G (= 0.5, 1, 2) and for $a/h = 0.7$, $b/h = 1.4$, $l/h = 0.5$, $c/h = 1.3$. It is seen that $|R|$ shows oscillatory behaviour with multiple peaks and for Kh~1.75 a resonance occurs in the reflection coefficient $|R|$ for all values of porosity parameter G. This occurs as a consequence of the interaction between porous barrier, trench and the waves. It is seen that with increasing porosity parameter reflection decreases. This is due to the porous effect of the barrier.

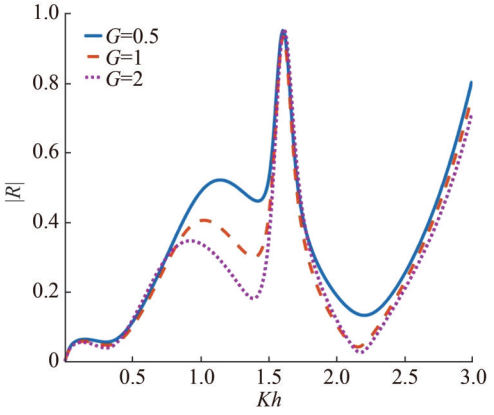

Figure 9 Reflection coefficient for different G and fixed $\frac{a}{h} = 0.7$, $\frac{b}{h} = 1.4$, $\frac{c}{h} = 1.3$, $\frac{l}{h} = 0.5$

In Figure 10, reflection coefficient $|R|$ is plotted against the non-dimensional wave number Kh for different values of l/h (= 0.4, 0.5, 0.6) and keeping $a/h = 0.7$, $b/h = 1.4$, $l/h = 0.5$, $c/h = 1.3$, fixed. Here $|R|$ shows oscilltory behaviour. For $Kh < 1.5$, $|R|$ almost coincide for all values of l/h. For $1.5 < Kh < 1.7$, a sharp peak is observed in $|R|$ for each value of l/h and the peaks shift towards left as l/h decreases. Thus as the barrier is placed away from the central line of the trench, there is a phase shift in the peak of $|R|$. Also $|R|$ increases with decreasing values of l/h. It means that the reflection coefficient increases when the porous barrier is shifted towards the centre of the trench from the right side of the trench. In all curves, $|R|$ starts from zero near Kh=0 and for large values of Kh, $|R|$ becomes unity.

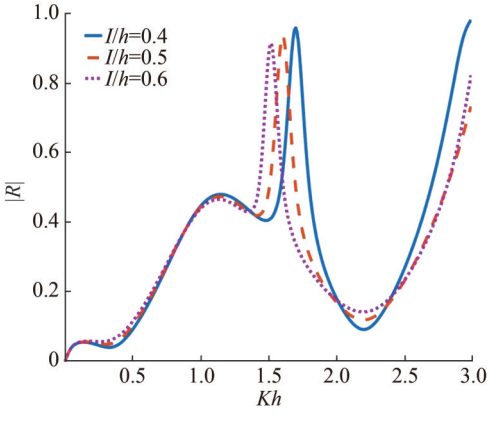

Figure 10 Reflection coefficient for different $\frac{l}{h}$ and fixed $\frac{a}{h} = 0.7$, $\frac{c}{h} = 1.3$, $\frac{b}{h} = 1.4$, $G = 0.5$

In Figure 11, amplitude of the energy dissipation coefficient J is plotted against the non-dimensional wave number Kh for different values of the porosity parameter $G\,(=1,2,3)$ and keeping $a/h = 0.7$, $b/h = 2.0$, $l/h = 0.5$, $c/h = 1.3$ fixed. From this figure it is seen that J exhibits oscillatory behaviour and J increases as Kh increases. Initially for small wave number $Kh < 1.2$, the energy dissipation increases with increasing porosity, then for $1.2 < Kh < 2$ energy dissipation decreases with increasing porosity. But for large wave number $Kh > 2$, energy dissipation again increases with increasing porosity parameter of the barrier. This may be due to the interaction of waves with the barrier and the trench.

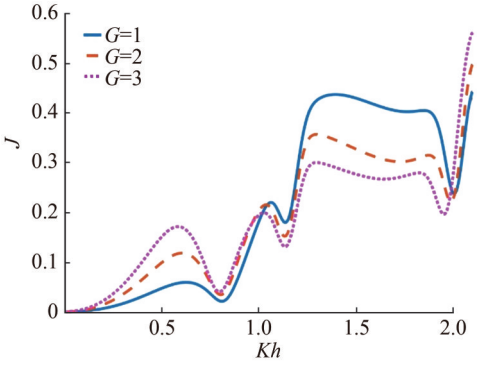

Figure 11 Energy dissipation for different G and fixed $\frac{a}{h} = 0.7$, $\frac{c}{h} = 1.3$, $\frac{b}{h} = 2.0$, $\frac{l}{h} = 0.5$

In Figure 12, non-dimensional horizontal wave force K_f is plotted against the non-dimensional wave number Kh for different values of the porosity parameter $G\,(=1,2,3)$ and keeping $a/h = 0.7$, $b/h = 1.5$, $l/h = 0.5$, $c/h = 1.3$ fixed. It is observed that the horizontal wave force increases with decreasing porosity G showing that with the decrease in G, the resistance force coefficient of the porous barrier decreases, allowing water to pass through the pores of the barrier and so the horizontal wave force increases.

4.3 Partially immersed porous barrier at middle of the trench

The porous barrier is along the y-axis, i. e., along the centre of the trench, when l/h=0. The Figures 13–18 depicts the behaviour of $|R|, J, K_f$ for various values of the parameters a/h, b/h, c/h, G.

Figure 13 exhibits the effect of width of the trench on the reflection coefficients for three different widths of the trench $(b/h = 0.5, 1.5, 2.5)$ and fixed values of $a/h = 0.6$, $c/h = 1.5$, $G = 0.5 + \mathrm{i}$. In this figure we see that $|R|$ exhibits oscillatory behaviour and the number of oscillation increases as the width of the trench b/h increases. Also there occurs resonance in $|R|$ for a particular value of Kh and multiple resonance occurs as the width of the trench increases when the barrier is along the central vertical line of the trench. This phenomena is not observed when the barrier is shifted to the right of the central line.

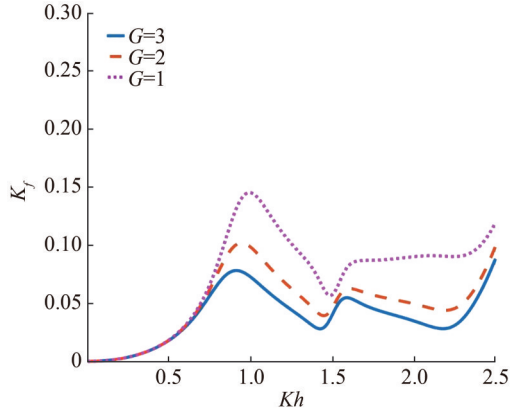

Figure 12 Hydrodynamic wave force for different G and fixed $\frac{a}{h} = 0.7$, $\frac{c}{h} = 1.3$, $\frac{b}{h} = 1.5$, $\frac{l}{h} = 0.5$

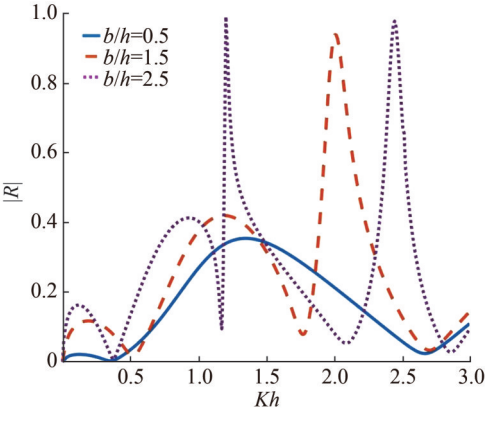

Figure 13 Reflection coefficient for different $\frac{b}{h}$ and fixed $\frac{a}{h} = 0.6$, $\frac{c}{h} = 1.5$, $G = 0.5 + \mathrm{i}$

The effect of the length of the partially immersed porous barrier a/h on the reflection coefficient $|R|$ is studied in Figure14. Here $|R|$ is plotted against the non-dimensional wave number Kh for various values of the length of the barrier $(a/h = 0.5, 0.8, 1.2)$ and fixed values of $b/h = 1.5$, $c/h = 1.5$, $G = 0.5 + \mathrm{i}$. Figure 14 shows oscillatory behaviour in $|R|$ exhibits and the amplitude of oscillation increases with increasing length of the porous barrier.

In Figure 15, $|R|$ is depicted against the non-dimensional wave number Kh, keeping $a/h = 0.6$, $b/h = 1.5$, $G = 0.5 + \mathrm{i}$ fixed and taking $c/h = 1.1, 1.3, 1.5$ to visualize the effect of the trench depth on the reflection coefficient. Here also $|R|$ exhibits oscillatory behaviour It is observed that the amplitude of the reflection coefficients increases as the depth of the trench increases. Also we observe that waves with large wave numbers, i.e., the short waves which are near the free surface do not feel much the presence of trench in bottom of the ocean.

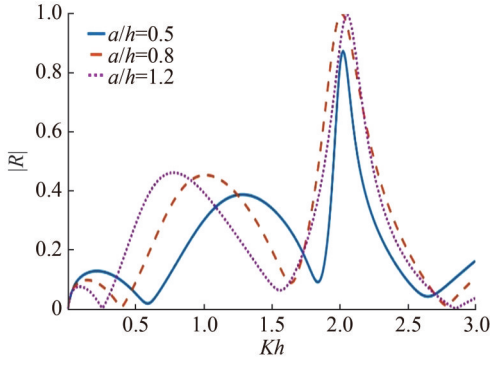

Figure 14 Reflection coefficient for different $\frac{a}{h}$ and fixed $\frac{b}{h} = 1.5$, $\frac{c}{h} = 1.5$, $G = 0.5 + \mathrm{i}$

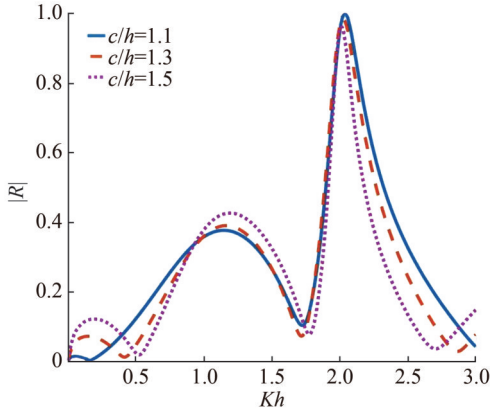

Figure 15 Reflection coefficient for different $\frac{c}{h}$ and fixed $\frac{a}{h} = 0.6$, $\frac{b}{h} = 1.5$, $G = 0.5 + \mathrm{i}$

In Figure 16, reflection coefficient $|R|$ is plotted against the non-dimensional wave number Kh for different values of the porosity parameter $G\,(= 0.5, 1, 2 + \mathrm{i})$ and keeping $a/h = 0.6$, $b/h = 1.5$, $c/h = 1.3$ fixed. It is seen that multiple peaks occur in the reflection coefficient. This phenomena occurs due to the interaction of wave with the porous barrier. It is seen that with as G increases from 0.5 to 1, the reflection coefficient decreases. Also it is seen that $|R|$ is least when G=2+i. This is due to the fact that presence of inertial force coefficient G_i in G allows the passage of water through the pores which diminishes reflection.

In Figure 17, coefficient of energy dissipation J is plotted against the non-dimensional wave number Kh for different values of the porosity parameter $G\,(= 1, 2, 3)$ and keeping $a/h = 0.5$, $b/h = 1.5$, $c/h = 1.5$ fixed. From the figure it is visible that, for small wave numbers $Kh < 1$, energy dissipation increases as porosity parameter increases while for $Kh > 1$ energy dissipation decreases with increasing porosity parameter G. The occurrence of this phenomena is due to the fact that as Kh increases, the wavelength decreases and the short waves which are near the free surface interact

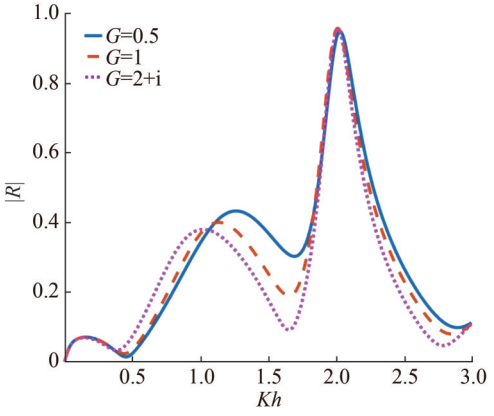

Figure 16 Reflection coefficient for different G and fixed $\frac{a}{h} = 0.6$, $\frac{b}{h} = 1.5$, $\frac{c}{h} = 1.3$

with the porous barrier. Here G is real $G = G^r$ which means that the inertial force coefficient G^i is much less than the resistance force coefficient G^r of the porous barrier and so as $G = G^r$ increases, the resistance force coefficient of the porous barrier resists the passage of water through the pores and reflects back the short waves thereby reducing the energy dissipation.

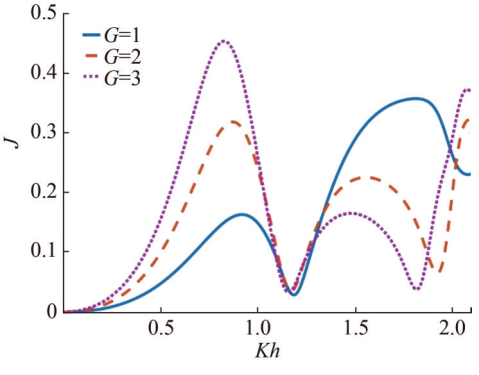

Figure 17 Energy dissipation for different G and fixed $\frac{a}{h} = 0.5$, $\frac{b}{h} = 1.5$, $\frac{c}{h} = 1.5$

In Figure 18, non-dimensional horizontal wave force K_f is plotted against the non-dimensional wave number Kh for different values of the porosity parameter $G\,(= 1, 2, 3)$ and keeping $a/h = 0.7$, $b/h = 1.5$, $c/h = 1.3$ fixed. The coefficient of wave force increases with decreasing porosity parameters.

From all these oscillatory behavior of the curves, one can find the values of wave number in which maximum reflection and transmission occurs. Also full reflection of waves occurs for some wave numbers. This behavior may be due to the interaction of waves with the depression of the bottom and the porous barrier. These outcomes are very useful for marine engineers to construct breakwaters to protect sea shore areas.

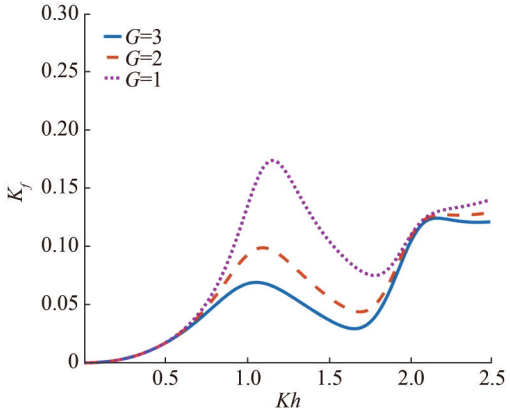

Figure 18 Hydrodynamic wave force for different G and fixed $\frac{a}{h} = 0.7$, $\frac{b}{h} = 1.5$, $\frac{c}{h} = 1.3$

5 Conclusions

The problem of water waves scattering by thin porous plate over a rectangular trench is discussed here considering linearized theory of water waves. The physical problem is mathematically modeled in terms of a boundary value problem for two different positions of the porous plate. Havelock's expansion of potential function together with its inversion formulae have been employed to the problem which then modified into a system of linear integral equations in terms of horizontal component of velocity function above the trench and below the edge of the vertical barrier. There are two types of integrable singularities occurred in the integral equations. One is square root singularity at the sharp edge of the thin barrier and the other type is 1/3 rd singularity at the edges of the rectangular trench. To manage both types of singularities a multi term Galerkin approximation technique with appropriate basis functions is considered. For 1/3 rd singularity Gegenbauer polynomial of order 1/6 and Chebyshev polynomial for 1/2 singularity are utilized here. Also we consider simple polynomials as basis function in mathematical computations and compare the rate of convergence of the method taking two types of basis functions in Table 3. It is observed that use of special function as basis function produces better rate of convergence of the method than simple polynomial as basis function. The numerical appraise of reflection and transmission coefficients, energy dissipation and horizontal wave force are determined for different parameter values. These results are illustrated in a number of figures that some of them are quite well matched with earlier works. For both positions of the barrier, effect of porosity decreases the reflection coefficient but increasing length of the barrier reflect more energy and less transmit. Larger width of the trench transmit more energy. Hence form present study, it is clear that scattering nature of surface waves in presence of bottom obstacle in form a rectangular trench is really influenced by thin porous barrier. These changes of surface waves play a crucial role in marine structures in coastal regions.

Nomenclature

a	Length of the partially immersed barrier
$2b$	Width of the trench
c	Depth of the trench from the free surface
h	Depth of the fluid region
l	Distance of the barrier from the middle of the trench on the free surface
σ	Angular frequency of incoming wave train
K	Wavenumber
φ^{inc}	Velocity potential of the incident wave
φ_1, φ_2, φ_3, φ_4	Velocity potential of resultant motion in the fluid subregions
r_1	Distance from the submerged left edge of the trench
r_2	Distance from the submerged edge of the barrier
r_3	Distance from the submerged right edge of the trench
G	Dimensionless porous parameter
G^r,G^i	Resistance force coefficient and inertial force coefficient of the porous material
R, T	Reflection and Transmission coefficient

Acknowledgement The authors thank Prof. Sudeshna Banerjea, Department of Mathematics, Jadavpur University, India, for providing helpful suggestions to improve the work. They also thank the referees for their valuable suggestions and comments that improved the presentation of the paper.

Competing interest The authors have no competing interests to declare that are relevant to the content of this article.

References

Chakraborty R, Mandal BN (2014) Water wave scattering by a rectangular trench. J. Eng. Math. 89: 101-112. DOI: 10.1007/s10665-014-9705-6

Chakraborty R, Mandal BN (2015) Oblique wave scattering by a rectangular submarine trench. ANZIAM J. 56: 286-298. DOI: 10.1017/S1446181115000024

Chwang AT (1983) A porous wave maker theory. Journal of Fluid Mechanics 132: 395-406. DOI:10.1017/S0022112083001676

Dean W (1945) On the reflexion of surface waves by a submerged plane barrier. Mathematical Proceedings of the Cambridge Philosophical Society, Cambridge University Press, 41, 231-238. DOI:10.1017/S030500410002260X

Evans D (1970) Diffraction of water waves by a submerged vertical plate. Journal of Fluid Mechanics 40(3): 433-451. DOI: 10.1017/S0022112070000253

Goswami SK (1983) Scattering of surface waves by a submerged

fixed vertical plate in water of finite depth. J. Indian Inst. Sci. 64B: 79-88.

Kirby JT, Dalrymple RA (1983) Propagation of obliquely incident water waves over a trench. Journal of Fluid Mechanics 113: 47-63. DOI: 10.1017/S0022112083001780

Kirby JT, Dalrymple RA (1987) Propagation of obliquely incident water waves over a trench. Part 2. Currents flowing along the trench. Journal of Fluid Mechanics 176: 95-116. DOI: 10.1017/S0022112087000582

Lassiter JB (1972) The propagation of water waves over sediment pockets. PhD thesis, Massachusetts Institutes of Technology, Cambridge, 1-51

Lee JJ, Ayer RM (1981) Wave propagation over a rectangular trench. Journal of Fluid Mechanics 110: 335-347. DOI: 10.1017/S0022112081000773

Lee MM, Chwang AT (2000) Scattering and radiation of water waves by permeable barriers. Physics of Fluids 12: 54-65. DOI: 10.1063/1.870284

Li AJ, Liu Y, Li HJ (2015) Accurate solutions to water wave scattering by vertical thin porous barriers. Math Probl Eng. 2015: 985731. DOI: 10.1155/2015/985731

Losada I, Miguel J, Losada A, Roldan AJ (1992) Propagation of oblique incident waves past rigid vertical thin barriers. Applied Ocean Research 14(3): 191-199. DOI: 10.1016/0141-1187(92)90014-B

Manam SR, Sivanesan M (2016) Scattering of water waves by vertical porous barriers: An analytical approach. Wave Motion 67: 89-101. DOI:10.1016/j.wavemoti.2016.07.008

Mandal BN, Dolai DP (1994) Oblique water wave diffraction by thin vertical barriers in water of uniform finite depth. Applied Ocean Research 16: 195-203. DOI: 10.1016/0141-1187(94)90020-5

Miles JW (1982) On surface-wave diffraction by a trench. Journal of Fluid Mechanics 115: 315-325. DOI:10.1017/S0022112082000779

Morris CAN (1975) A variational approach to an unsymmetric water wave scattering problem. J. Eng. Math. 9: 291-300. DOI:10.1007/BF01540666

Parsons NF, Martin PA (1992) Scattering of water waves by submerged plates using hypersingular integral equations. Applied Ocean Research 14: 313-321. DOI:10.1016/0141-1187(92)90035-I

Parsons NF, Martin PA (1994) Scattering of water waves by submerged curved platesand by surface-piercing flat plates. Applied Ocean Research 16: 129-139. DOI: 10.1016/0141-1187(94)90024-8

Porter R, Evans DV (1995) Complementary approximations to wave scattering by vertical barriers. Journal of Fluid Mechanics 294: 155-180. DOI:10.1017/S0022112095002849

Ray S, De S, Mandal BN (2021) Wave propagation over a rectangular trench in the presence of a partially immersed barrier. Fluid Dyn. Res. 53: 035509. DOI:10.1088/1873-7005/ac0a93

Roy R, Basu U, Mandal BN (2016a) Oblique water scattering by two unequal vertical barriers. J Eng Math. 97: 119-133. DOI:10.1007/s10665-015-9800-3

Roy R, Basu U, Mandal BN (2016b) Water wave scattering by two submerged thin vertical unequal plates. Arch. Appl. Mech. 86: 1681-1692. DOI:10.1007/s00419-016-1143-7

Roy R, Chakraborty R, Mandal BN (2017) Propagation of water waves over an asymmetrical rectangular trench. Q. J. Mech. Appl. Math 70: 49-64. DOI:10.1093/qjmam/hbw015

Sarkar B, Roy R, De S (2022) Oblique wave interaction by two thin vertical barriers over an asymmetric trench. Mathematical Methods in the Applied Sciences 45(17): 11667-11682. DOI: 10.1002/mma.8473

Sollitt CK, Cross RH (1972) Wave transmission through permeable breakwaters. Coast Eng Proc. 1: 1827-1846. DOI:10.1061/9780872620490.106

Ursell F (1947) The effect of a fixed vertical barrier on surface waves in deep water. Mathematical Proceedings of the Cambridge Philosophical Society, Cambridge University Press, 43, 374-382. DOI:10.1017/S0305004100023604

Yu X (1995) Diffraction of water waves by porous breakwaters. J Waterw Port Coast Ocean Eng 121: 275-282. DOI: 10.1017/S0305004100023604

Scattering of water waves by rectangular thick barriers in presence of surface tension

Gour Das [a], Rumpa Chakraborty [b] [1]

[a.] Department of Mathematics, Jadavpur University, Kolkata-700032, India.

[b.] Department of Mathematics, Diamond Harbour Women's University, South 24 Parganas-743368, India

Abstract

The influence of surface tension over an oblique incident waves in presence of thick rectangular barriers present in water of uniform finite depth is discussed here. Three different structures of a bottom-standing submerged barrier, submerged rectangular block not extending down to the bottom and fully submerged block extending down to the bottom with a finite gap are considered. An appropriate multi-term Galekin approximation technique involving ultraspherical Gegenbauer polynomial is employed for solving the integral equations arising in the mathematical analysis. The reflection and transmission coefficients of the progressive waves for two-dimensional time harmonic motion are evaluated by utilizing linearized potential theory. The theoretical result is validated numerically and explained graphically in a number of figures. The present result will almost match analytically and graphically with those results already available in the literature without considering the effect of surface tension. From the graphical representation, it is clearly visible that the amplitude of reflection coefficient decreases with increasing values of surface tension. It is also seen that the presence of surface tension, the change of width, and the height of the thick barriers affect the nature of the reflection coefficients significantly.

Keywords: Oblique wave scattering, Surface tension, Thick rectangular barrier, Multi-term Galerkin approximation, Transmission and Reflection coefficients.

1 Introduction

Problems of water wave scattering by thin vertical barriers submerged in finite depth water are well studied in the literature using the linearized theory of water waves. For normal incident wave trains in finite depth water, the problems are solved explicitly employing various mathematical techniques by a number of researchers(cf. Packman and Williams [1], Losada *et al.* [2], Porter and Evans [3], Mandal and Dolai [4], Kanoria and Mandal [5], Banerjea *et al.* [6], Das *et al.* [7], Das, De and Mandal[8]). When the obstacle is in the form of a thick vertical barrier with a rectangular cross-section present in the water of uniform finite depth, the corresponding water wave scattering problems for normal incidence wave train have been investigated earlier by Mei and Black [9], Kanoria *et al.* [10]. Mei and Black [9] considered surface piercing and bottom standing thick vertical barriers and used variational formulations as the basis for numerical computations of the reflection and the transmission coefficients. Kanoria *et al.*[10] and Mandal and Kanoria [11] considered the problems of

[1]Corresponding author(e-mail: chak.rumpa@gmail.com tel: 9432852418)

normal and oblique wave scattering by thick barriers respectively, wherein the barriers have four types of configurations such as surface-piercing or bottom standing thick barrier or a submerged block, or a thick wall with a gap. They used the multi-term Galerkin approximation method involving ultraspherical Gegenbauer polynomials for solving first kind integral equations arising in the mathematical analysis to obtain very accurate numerical estimates for the reflection coefficient. However, for oblique incidence of the wave trains in finite depth water, these problems cannot be solved explicitly.

None of the above research considered the effect of surface tension. Due to presence of cohesive forces in between water molecule in the upper surface of water, sometimes it's become necessary to consider the effect of surface tension on water wave scattering problems. A few of them such as Evans [12], [13], Rhodes-Robinson [14], [15], [16], Chakrabarti and Sahoo [17] included the effect of surface tension in water wave scattering problems. However, the scattering problem due to the thick rectangular barrier in presence of surface tension does not investigated yet. The amplitude and the frequency of the wave depend on both the surface tension and gravity. For this reason, it may not be possible to neglect the effect of surface tension while doing experimental study. As mentioned by Hocking and Mahdmina [18], another important reason for including surface tension is that in the absence of surface tension the transient motion initiated by an impulsive start is singular, but when the effect of surface tension is taken into account this singularity is removed. The uniqueness of the solution of the problem depends on the behavior of a special combination of the derivatives of the velocity potential at the edge because of the effect of surface tension as mentioned by Chakrabarti and Sahoo [17]. This is also an important reason for including the surface tension.

In our present study, we analyze the effect of surface tension on wave scattering problem by oblique incidence waves due to thick rectangular barrier. Three types of barrier, submerged bottom standing, submerged plate of finite height and fully submerged block with a gap are considered here. Due to geometrical symmetry about its central line, the scattering problems for all the cases are split into two separate boundary value problems in terms of symmetric and antisymmetric potential functions. Analytically the boundary value problems involving potential functions are reduced in to first kind integral equations using inverse Havelock inversion formulae. The integral equations are solved analytically by using multi term Galerkin approximation technique and there is used the ultra spherical Gegenbauer polynomial as a basis function as was done by Chakraborty and Mandal [19],[20], Newman [21] Sasmal and De [24], Paul and De[25]. The analytical result is explained numerically in terms of reflection coefficients of wave energy by a number of figures. The numerical results of the reflection coefficient for both types of thick barriers are obtained with almost six figure accuracies by taking only 6 terms in the multi-term Galerkin approximations and all of these results are depicted graphically against the non dimensional wave numbers. Some figures are compared with Kanoria *et al.*'s [10] result for normal incidence wave (incidence angle $\theta = 0^0$) without taking the surface tension and a good agreement is achieved here. For large horizontal length of type I, II and III barriers, the numbers of zeros of the reflection coefficient as a function of wave number increases, which is also consistent with the observation of Kanoria *et al.*[10] for thick vertical barriers with free surface and Newman [21] for

long bottom obstacles. In the present study, the energy balance relation involving reflection and transmission coefficients is also satisfied numerically. These all results provide the checks of the correctness of the present numerical method utilized here. The new outcome of this article is that the surface tension together with the change of width of the barrier affects the amplitude of reflection coefficients significantly.

2 Problem Construction

We consider a time harmonic wave motion of angular frequency σ under the action of both gravity with acceleration g and surface tension T in region of finite water depth h in which a thick rectangular barrier of uniform width $2b$ is immersed. Here water is taken as an inviscid, homogeneous fluid with irrotational motion.

A rectangular cartesian coordinate system is chosen, where y axis is taken vertically downwards and the (x, z) plane corresponds to the undisturbed surface. Here we study three different cases of barrier placement(as shown in fig 1), the barrier may occupy the region $-b \leq x \leq b$ with (I) $y \in L = L_1(= (c, h))$, (II) $y \in L = L_2(= (a, c))$, with $0 \leq a \leq c \leq h$ and (III) $y \in L = L_3(= (a, c) + (d, h))$, with $0 \leq a \leq c \leq d \leq h$. In the present computation L_1, L_2 and L_3, corresponding type-I, type II and type-III barrier configuration respectively.

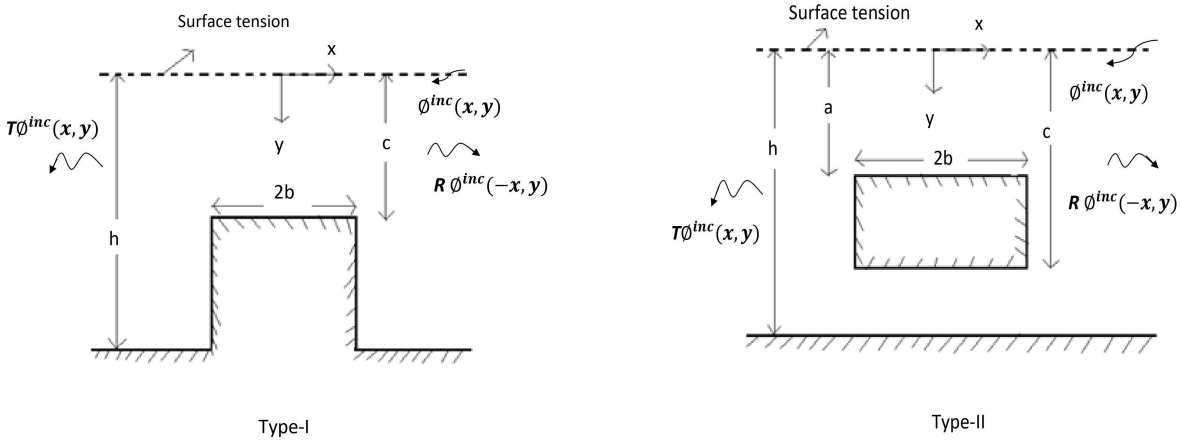

Here we consider a harmonically time dependent progressive wave, obliquely incident from negative infinity and its direction makes an angle θ with the horizontal $x-$ axis. We denote the wave number by γ_0, where $\gamma_0 = \frac{2\pi}{\lambda}$, λ is the wave length of incident wave. The incident wave number γ_0 satisfy the transcendental equation

$$\gamma(1 + M\gamma^2) \tanh \gamma h = K, \; K = \frac{\sigma^2}{g}, \tag{1}$$

$M = \frac{\tau}{\rho g}$, τ is the coefficient of surface tension at the free surface of the ocean, ρ is the density of the fluid.

The position of roots of the transcendental equation (1) is shown numerically in Fig. 2 using a contour plot. To draw the contour, we consider some fixed values of $\frac{M}{h^2}(= 2)$ and

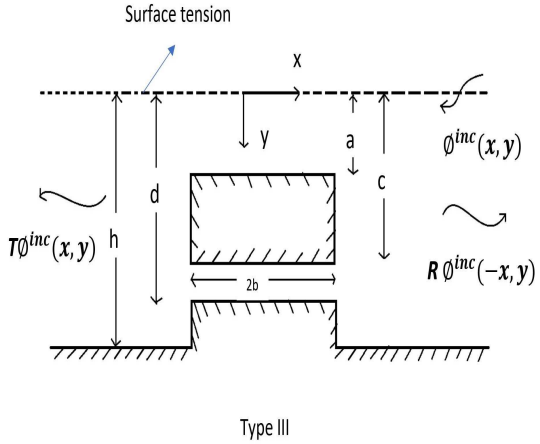

Figure 1: Diagram of thick barriers

$Kh = 0.8$. In the figure, the black dots signify the position of the roots and it is very clear that, in presence of surface tension, the dispersion equation has two real roots $\pm\gamma_0$ and infinitely many purely imaginary roots $\pm i\gamma_n, n = 1, 2, ...(\gamma_n > 0)$. [cf. Chakrabarti and Sahoo[17], Sasmal, Paul and De[22], Paul *et. al.*,[23]]. Assuming linear theory, a train of incident wave is represented by $\Re\{\phi^{inc}(x, y)e^{i(\nu z-\sigma t)}\}$ where

$$\phi^{inc}(x, y) = \frac{2\cosh\gamma_0(h - y)e^{-i\mu(x-b)}}{\cosh\gamma_0 h}, \tag{2}$$

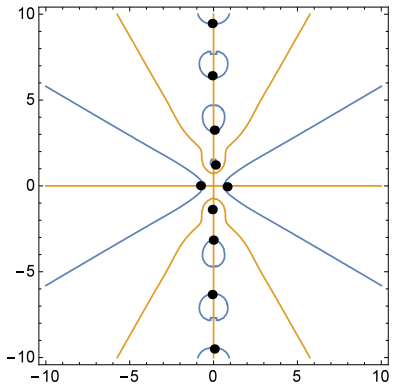

Figure 2: Contour plot Γ of the roots of the dispersion equation for $\frac{M}{h^2} = 2, Kh = 0.8$.

Here $\mu = \gamma_0\cos\theta$ and $\nu = \gamma_0\sin\theta$ where $0 < \theta < \pi/2$ and $e^{i(\nu z)}$ is the z dependence term of the fluid. Due to geometrical symmetry of the problem, the z dependent term can be eliminated by assuming the velocity potential to be of the form $\Re\{\phi^{inc}(x, y)e^{i(\nu z-\sigma t)}\}$. Henceforth, the factor $e^{i(\nu z-\sigma t)}$ will be omitted.

Then velocity potential function $\phi(x, y)$ satisfies the boundary value problem

$$(\nabla^2 - \nu^2)\phi = 0 \quad \text{in the fluid region} \tag{3}$$

$$K\phi + \frac{\partial \phi}{\partial y} + M\frac{\partial^3 \phi}{\partial y^3} = 0 \quad \text{on} \quad y = 0, \quad |x| < \infty \tag{4}$$

$$\phi_x = 0 \quad \text{on} \quad x = \pm b, \quad y \in L_j, j = 1, 2, 3 \tag{5}$$

$$r^{\frac{1}{3}}\nabla\phi \quad \text{is bounded as} \quad r \to 0, \tag{6}$$

r is the distance from a submerged edge of the thick barrier,

$$\phi_y = 0 \quad \text{on} \quad y = l_j, \quad |x| < b, \quad \text{for j-th type of barrier, } j = 1, 2, 3 \tag{7}$$

$$\phi_y = 0 \quad \text{on} \quad y = h, \quad \begin{cases} |x| > b & \text{for type I and III barrier} \\ |x| < \infty & \text{for type II barrier} \end{cases} \tag{8}$$

and finally

$$\phi(x, y) \sim \begin{cases} \phi^{inc}(x, y) + R\phi^{inc}(-x, y) & \text{as} \quad x \to \infty, \\ T\phi^{inc}(x, y) & \text{as} \quad x \to -\infty \end{cases} \tag{9}$$

where R and T is the unknown reflection and transmission coefficients respectively and is to be determined for each barrier configuration. In (7), $l_1 = c; l_2 = a, c; l_3 = a, c, d$; corresponding to type I, II, III barriers configurations respectively depicted in Figure 1.

3 Method of solution

Presence of the uniform geometrical structure of the rectangular barrier about $x = 0$; $\phi(x, y)$ can be divided into symmetric and antisymmetric parts, $\phi^{SMM}(x, y)$ and $\phi^{ANSMM}(x, y)$, respectively, so that

$$\phi(x, y) = \phi^{SMM}(x, y) + \phi^{ANSMM}(x, y) \tag{10}$$

where

$$\phi^{SMM}(-x, y) = \phi^{SMM}(x, y), \phi^{ANSMM}(-x, y) = -\phi^{ANSMM}(x, y) \tag{11}$$

Therefore, we consider only the region $x \geq 0$. Now $\phi^{SMM,ANSMM}(x, y)$ satisfy (3) to (8) together with

$$\phi_x^{SMM}(0, y) = 0 \quad \text{and} \quad \phi^{ANSMM}(0, y) = 0, \quad 0 < y < h. \tag{12}$$

Let the behavior of $\phi^{SMM,ANSMM}(x, y)$ for large x be represented by

$$\phi^{SMM,ANSMM}(x, y) \sim \frac{\cosh \gamma_0(h - y)}{\cosh \gamma_0 h}\{e^{-i\mu(x-b)} + R^{SMM,ANSMM}e^{i\mu(x-b)}\} \quad \text{as} \quad x \to \infty \tag{13}$$

where R^{SMM} and R^{ANSMM} are unknown constants. These constants are related to R and T by

$$R, T = \frac{1}{2}(R^{SMM} \pm R^{ANSMM})e^{-2i\mu b}. \tag{14}$$

Now the eigen function expansions of $\phi^{SMM,ANSMM}(x, y)$ satisfying (3) to (8) and (12) for $x > 0$ in the different regions for each barrier configuration are below.

Region I $(x > b,\ 0 < y < h)$**:**

$$\phi^{SMM,ANSMM}(x,y) = \frac{\cosh\gamma_0(h-y)}{\cosh\gamma_0 h}\{e^{-i\mu(x-b)} + R^{SMM,ANSMM}e^{i\mu(x-b)}\}$$

$$+\sum_{n=1}^{\infty}\mathcal{A}_n^{SMM,ANSMM}\cos\gamma_n(h-y)e^{-s_n(x-b)} \tag{15}$$

where γ_n $(n = 1, 2, ...)$ are the real positive roots of the equation

$$x(1 - Mx^2)\tan xh + K = 0. \tag{16}$$

and $s_n = (\gamma_n^2 + \nu^2)^{\frac{1}{2}}$.

Region II $(0 < x < b,\quad y \in (0,h) - L_j,\quad j = 1,2,3)$**:**

Type I:
For $y \in (0,c)$, $\phi^{SMM}(x,y)$ and $\phi^{ANSMM}(x,y)$ are given by

$$\begin{pmatrix} \phi^{SMM}(x,y) \\ \phi^{ANSMM}(x,y) \end{pmatrix} = \frac{\cosh\alpha_0(c-y)}{\cosh\alpha_0 c}\begin{pmatrix} \mathcal{B}_0^{SMM}\cos(\alpha_0^2-\nu^2)^{\frac{1}{2}}x \\ \mathcal{B}_0^{ANSMM}\sin(\alpha_0^2-\nu^2)^{\frac{1}{2}}x \end{pmatrix}$$

$$+\sum_{n=1}^{\infty}\begin{pmatrix} \mathcal{B}_n^{SMM}\cosh t_n x \\ \mathcal{B}_n^{ANSMM}\sinh t_n x \end{pmatrix}\cos\alpha_n(c-y) \tag{17}$$

where $\pm\alpha_0, \pm i\alpha_n (n = 1, 2, ...)$ are the roots of the equation

$$\alpha(1 + M\alpha^2)\tanh\alpha c = K. \tag{18}$$

and

$$t_n = (\alpha_n^2 + \nu^2)^{\frac{1}{2}}, (n = 1, 2, ..). \tag{19}$$

Type II:
For $y \in (0,a) + (c,h)$, $\phi^{SMM,ANSMM}(x,y)$ will have two types of expressions depending on whether $0 < y < a$ *or* $c < y < h$. For $0 < y < a$ the expressions of $\phi^{SMM,ANSMM}(x,y)$ are similar to equation (17) with $\mathcal{B}_n^{SMM,ANSMM}$ replaced by $D_n^{SMM,ANSMM}$, α_n replaced by β_n, t_n replaced by u_n and c replaced by a, where $\pm\beta_0$, $\pm i\beta_n (n = 1, 2, ...)$ are the roots of the equation

$$\beta(1 + M\beta^2)\tanh\beta a = K \tag{20}$$

$$\text{and} \quad u_n = (\beta_n^2 + \nu^2)^{\frac{1}{2}}, (n = 1, 2, ..). \tag{21}$$

For $c < y < h$ the expressions of $\phi^{SMM,ANSMM}(x,y)$ are given by

$$\begin{pmatrix} \phi^{SMM}(x,y) \\ \phi^{ANSMM}(x,y) \end{pmatrix} = \begin{pmatrix} 0 \\ E_0^{ANSMM}x \end{pmatrix} + \sum_{n=1}^{\infty}\begin{pmatrix} E_n^{SMM}\cosh\frac{n\pi x}{h-c} \\ E_n^{ANSMM}\sinh\frac{n\pi x}{h-c} \end{pmatrix}\cos\frac{n\pi(y-c)}{h-c} \tag{22}$$

Type III:

For $y \in (0,a)+(c,d)$, $\phi^{SMM,ANSMM}(x,y)$ will have two types of expressions depending on whether $0<y<a$ *or* $c<y<d$. For $0<y<a$ the expressions of $\phi^{SMM,ANSMM}(x,y)$ are similar to equation (17) with $\mathcal{B}_n^{SMM,ANSMM}$ replaced by $D_n^{SMM,ANSMM}$, α_n replaced by β_n, t_n replaced by u_n and c replaced by a, where $\pm\beta_0$, $\pm i\beta_n (n=1,2,...)$ are the roots of the equation (20) and u_n are given by (21).

For $c<y<d$ the expressions of $\phi^{SMM,ANSMM}(x,y)$ are given by

$$\begin{pmatrix} \phi^{SMM}(x,y) \\ \phi^{ANSMM}(x,y) \end{pmatrix} = \begin{pmatrix} U_0^{SMM}\cosh\nu x \\ U_0^{ANSMM}\sinh\nu x \end{pmatrix} + \sum_{n=1}^{\infty} \begin{pmatrix} U_n^{SMM}\cosh\zeta_n x \\ U_n^{ANSMM}\sinh\zeta_n x \end{pmatrix} \cos\frac{n\pi(d-y)}{d-c} \tag{23}$$

where

$$\zeta_n = \sqrt{\left(\frac{n\pi}{d-c}\right)^2 + \nu^2} \tag{24}$$

Now let us define

$$\phi_x^{SMM,ANSMM}(b+0,y) = f^{SMM,ANSMM}(y), 0<y<h, \tag{25}$$

Then

$$f^{SMM,ANSMM}(y) = 0, \quad for\ y \in L_j \tag{26}$$

and $\quad \phi_x^{SMM,ANSMM}(b-0,y) = f^{SMM,ANSMM}(y),$ for $y \in (0,h)-L_j, j=1,2,3.$ (27)

Also, due to the edge condition described in equation (6), we must have the requirement that

$$f^{SMM,ANSMM}(y) = O(|y-l_j|^{-\frac{1}{3}}) \quad \text{as} \quad y \to l_j, j=1,2,3. \tag{28}$$

Using the expression of equation (15) for $\phi^{SMM,ANSMM}(y)$ in (25) and followed by Havelock inversion formula gives

$$1 - R^{SMM,ANSMM} = \frac{4i\gamma_0}{\delta_0\mu}\cosh\gamma_0 h \int_a^h f^{SMM,ANSMM}(y)\cosh\gamma_0(h-y)dy \tag{29}$$

and

$$\mathcal{A}_n^{SMM,ANSMM} = -\frac{4\gamma_n}{\delta_n s_n}\int_a^h f^{SMM,ANSMM}(y)\cos\gamma_n(h-y)dy \tag{30}$$

with $\delta_0 = 2\gamma_0 h + \sinh 2\gamma_0 h$; $\delta_n = 2\gamma_n h + \sin 2\gamma_n h \quad (n=1,2,...)$.

3.1 Evaluate the values of constants for region II

For Type I

Substituting the equation (17) in condition (27) and using Fourier cosine inversion, we get

$$\mathcal{B}_0^{SMM,ANSMM} = \frac{4\alpha_0\cosh\alpha_0 c}{\lambda_0(\alpha_0^2-\nu^2)^{\frac{1}{2}}}\left(\frac{1}{-\sin(\alpha_0^2-\nu^2)^{\frac{1}{2}}b}, \frac{1}{\cos(\alpha_0^2-\nu^2)^{\frac{1}{2}}b}\right)$$

$$\times \int_0^c f^{SMM,ANSMM}(y)\cosh\alpha_0(c-y)dy \tag{31}$$

$$\mathcal{B}_n^{SMM,ANSMM} = \frac{4\alpha_n}{\lambda_n t_n}\left(\frac{1}{\sinh t_n b}, \frac{1}{\cosh t_n b}\right)\int_0^c f^{SMM,ANSMM}(y)\cos\alpha_n(c-y)dy \tag{32}$$

with $\lambda_0 = 2\alpha_0 c + \sinh\alpha_0 c$; $\lambda_n = 2\alpha_n c + \sin 2\alpha_n c \quad (n = 1, 2, ...)$.

For Type II

Here we can derive the constants $D_n^{SMM,ANSMM}$ from $\mathcal{B}_n^{SMM,ANSMM}$ by replacing α_n by β_n, t_n by u_n, λ_n by ϵ_n and c by a with $\epsilon_0 = 2\beta_0 a + \sinh\beta_0 a$; $\epsilon_n = 2\beta_n a + \sin 2\beta_n a \quad (n = 1, 2, ...)$.

$$\text{and} \quad E_0^{ANSMM} = \frac{1}{h-c}\int_c^h f^{ANSMM}(y)dy \tag{33}$$

$$E_n^{SMM,ANSMM} = \frac{2}{n\pi}\left(\frac{1}{\sinh\frac{n\pi b}{h-c}}, \frac{1}{\cosh\frac{n\pi b}{h-c}}\right)\int_c^h f^{SMM,ANSMM}(y)\cos\frac{n\pi(y-c)}{h-c}dy \tag{34}$$

and $f^{SMM}(y)$ for type II barrier must satisfy the condition

$$\int_c^h f^{SMM}(y)dy = 0 \tag{35}$$

For Type III

Here the constants $D_n^{SMM,ANSMM}$ are obtained from $\mathcal{B}_n^{SMM,ANSMM}$ by changing α_n by β_n, t_n by u_n, λ_n by ϵ_n and c by a with $\epsilon_0 = 2\beta_0 a + \sinh\beta_0 a$; $\epsilon_n = 2\beta_n a + \sin 2\beta_n a \quad (n = 1, 2, ...)$.
and

$$U_0^{SMM,ANSMM} = \frac{1}{\nu(d-c)}\left(\frac{1}{\sinh\nu b}, \frac{1}{\cosh\nu b}\right)\int_c^d f^{SMM,ANSMM}(y)dy \tag{36}$$

$$U_n^{SMM,ANSMM} = \frac{2}{\zeta_n(d-c)}\left(\frac{1}{\sinh\zeta_n b}, \frac{1}{\cosh\zeta_n b}\right)\int_c^d f^{SMM,ANSMM}(y)\cos\frac{n\pi(d-y)}{d-c}dy \tag{37}$$

3.2 Formation of integral equation:

Now equating $\phi^{SMM,ANSMM}(x,y)$ through $x = b$, we get

$$\phi_x^{SMM,ANSMM}(b+0,y) = \phi_x^{SMM,ANSMM}(b-0,y), \tag{38}$$

$for \quad y \in (0,h) - L_j$, and it ultimately constructs the integral equation

$$\int_{(0,h)-L_j} F^{SMM,ANSMM}(u)N^{SMM,ANSMM}(y,u)du = \frac{\cosh\gamma_0(h-y)}{\cosh\gamma_0 h}, \ for\ y \in (0,h) - L_j, \tag{39}$$

$$\text{where} \quad F^{SMM,ANSMM}(y) = \frac{4\gamma_0 \cosh^2 \gamma_0 h}{\delta_0 \mu (1 + R^{SMM,ANSMM})} f^{SMM,ANSMM}(y), \tag{40}$$

and $N^{SMM,ANSMM}(y,u)(y,u \in (0,h) - L_j)$ $(j = 1,2,3)$ are real symmetric in y and u and their constructions are given below

Type I

$$N^{SMM}(y,u) = \frac{\delta_0 \mu}{\gamma_0 \cosh^2 \gamma_0 h} \left[\sum_{n=1}^{\infty} \left\{ \frac{\gamma_n \cos \gamma_n (h-y) \cos \gamma_n (h-u)}{\delta_n s_n} + \frac{\alpha_n \coth t_n b \cos \alpha_n (c-y) \cos \alpha_n (c-u)}{\lambda_n t_n} \right\} + (-\cot(\alpha_0^2 - \nu^2)^{\frac{1}{2}} b) \frac{\alpha_0 \cosh \alpha_0 (c-y) \cosh \alpha_0 (c-u)}{\lambda_0 (\alpha_0^2 - \nu^2)^{\frac{1}{2}}} \right], 0 < y, u < h. \tag{41}$$

$$N^{ANSMM}(y,u) = \frac{\delta_0 \mu}{\gamma_0 \cosh^2 \gamma_0 h} \left[\sum_{n=1}^{\infty} \left\{ \frac{\gamma_n \cos \gamma_n (h-y) \cos \gamma_n (h-u)}{\delta_n s_n} + \frac{\alpha_n \tanh t_n b \cos \alpha_n (c-y) \cos \alpha_n (c-u)}{\lambda_n t_n} \right\} + (\tan(\alpha_0^2 - \nu^2)^{\frac{1}{2}} b) \frac{\alpha_0 \cosh \alpha_0 (c-y) \cosh \alpha_0 (c-u)}{\lambda_0 (\alpha_0^2 - \nu^2)^{\frac{1}{2}}} \right], 0 < y, u < h. \tag{42}$$

Type II

For $y, u \in (0,a) + (c,h)$, we get three different cases for $N^{SMM,ANSMM}(y,u)$

Case I:

$y, u \in (0,a)$

$$N^{SMM}(y,u) = \frac{\delta_0 \mu}{\gamma_0 \cosh^2 \gamma_0 h} \left[\sum_{n=1}^{\infty} \left\{ \frac{\gamma_n \cos \gamma_n (h-y) \cos \gamma_n (h-u)}{\delta_n s_n} + \frac{\beta_n \coth u_n b \cos \beta_n (a-y) \cos \beta_n (a-u)}{\epsilon_n u_n} \right\} + (-\cot(\beta_0^2 - \nu^2)^{\frac{1}{2}} b) \frac{\beta_0 \cosh \beta_0 (a-y) \cosh \beta_0 (a-u)}{\epsilon_0 (\beta_0^2 - \nu^2)^{\frac{1}{2}}} \right], 0 < y, u < h. \tag{43}$$

$$N^{ANSMM}(y,u) = \frac{\delta_0 \mu}{\gamma_0 \cosh^2 \gamma_0 h} \left[\sum_{n=1}^{\infty} \left\{ \frac{\gamma_n \cos \gamma_n (h-y) \cos \gamma_n (h-u)}{\delta_n s_n} + \frac{\beta_n \tanh u_n b \cos \beta_n (a-y) \cos \beta_n (a-u)}{\epsilon_n u_n} \right\} \right.$$

$$+(\tan(\beta_0^2-\nu^2)^{\frac{1}{2}}b)\frac{\beta_0\cosh\beta_0(a-y)\cosh\beta_0(a-u)}{\epsilon_0(\beta_0^2-\nu^2)^{\frac{1}{2}}}\Bigg],0<y,u<h. \tag{44}$$

Case II

$y,u\in(c,h)$

$$N^{SMM}(y,u)=\frac{\delta_0\mu}{\gamma_0\cosh^2\gamma_0 h}\Bigg[\sum_{n=1}^{\infty}(\frac{\gamma_n\cos\gamma_n(h-y)\cos\gamma_n(h-u)}{\delta_n s_n}+ \frac{1}{2n\pi}\coth\frac{n\pi b}{h-c}\cos\frac{n\pi(y-c)}{h-c}\cos\frac{n\pi(u-c)}{h-c})\Bigg] \tag{45}$$

$$N^{ANSMM}(y,u)=\frac{\delta_0\mu}{\gamma_0\cosh^2\gamma_0 h}\Bigg[\frac{b}{4(h-c)}+\sum_{n=1}^{\infty}(\frac{\gamma_n\cos\gamma_n(h-y)\cos\gamma_n(h-u)}{\delta_n s_n}+ \frac{1}{2n\pi}\tanh\frac{n\pi b}{h-c}\cos\frac{n\pi(y-c)}{h-c}\cos\frac{n\pi(u-c)}{h-c})\Bigg] \tag{46}$$

Case III

$y\in(0,a),u\in(c,h)\quad or\quad y\in(c,h),u\in(0,a)$

$$N^{SMM,ANSMM}(y,u)=\frac{\delta_0\mu}{\gamma_0\cosh^2\gamma_0 h}\Bigg[\sum_{n=1}^{\infty}\frac{\gamma_n\cos\gamma_n(h-y)\cos\gamma_n(h-u)}{\delta_n s_n}\Bigg] \tag{47}$$

Type III

For $y,u\in(0,a)+(c,d)$, we have three different cases for $N^{SMM,ANSMM}(y,u)$

Case I:

$y,u\in(0,a)$

$$N^{SMM}(y,u)=\frac{\delta_0\mu}{\gamma_0\cosh^2\gamma_0 h}\Bigg[\sum_{n=1}^{\infty}\Bigg\{\frac{\gamma_n\cos\gamma_n(h-y)\cos\gamma_n(h-u)}{\delta_n s_n} + \frac{\beta_n\coth u_n b\cos\beta_n(a-y)\cos\beta_n(a-u)}{\epsilon_n u_n}\Bigg\}$$

$$+(-\cot(\beta_0^2-\nu^2)^{\frac{1}{2}}b)\frac{\beta_0\cosh\beta_0(a-y)\cosh\beta_0(a-u)}{\epsilon_0(\beta_0^2-\nu^2)^{\frac{1}{2}}}\Bigg],0<y,u<h. \tag{48}$$

$$N^{ANSMM}(y,u)=\frac{\delta_0\mu}{\gamma_0\cosh^2\gamma_0 h}\Bigg[\sum_{n=1}^{\infty}\Bigg\{\frac{\gamma_n\cos\gamma_n(h-y)\cos\gamma_n(h-u)}{\delta_n s_n} + \frac{\beta_n\tanh u_n b\cos\beta_n(a-y)\cos\beta_n(a-u)}{\epsilon_n u_n}\Bigg\}$$

$$+(\tan(\beta_0^2-\nu^2)^{\frac{1}{2}}b)\frac{\beta_0\cosh\beta_0(a-y)\cosh\beta_0(a-u)}{\epsilon_0(\beta_0^2-\nu^2)^{\frac{1}{2}}}\Bigg],0<y,u<h. \tag{49}$$

Case II

$y, u \in (c, d)$

$$N^{SMM}(y,u) = \frac{\delta_0\mu}{\gamma_0 \cosh^2 \gamma_0 h}\left[\sum_{n=1}^{\infty}\left(\frac{\gamma_n \cos\gamma_n(h-y)\cos\gamma_n(h-u)}{\delta_n s_n} + \frac{\coth\zeta_n b}{2(d-c)\zeta_n}\cos\frac{n\pi(d-y)}{d-c}\cos\frac{n\pi(d-u)}{d-c}\right) + \frac{\coth\nu b}{4(d-c)\nu}\right]. \tag{50}$$

$$N^{ANSMM}(y,u) = \frac{\delta_0\mu}{\gamma_0 \cosh^2 \gamma_0 h}\left[\sum_{n=1}^{\infty}\left(\frac{\gamma_n \cos\gamma_n(h-y)\cos\gamma_n(h-u)}{\delta_n s_n} + \frac{\tanh\zeta_n b}{2(d-c)\zeta_n}\cos\frac{n\pi(d-y)}{d-c}\cos\frac{n\pi(d-u)}{d-c}\right) + \frac{\tanh\nu b}{4(d-c)\nu}\right]. \tag{51}$$

Case III

$y \in (0, a), u \in (c, d)$ *or* $y \in (c, d), u \in (0, a)$

$$N^{SMM,ANSMM}(y,u) = \frac{\delta_0\mu}{\gamma_0 \cosh^2 \gamma_0 h}\left[\sum_{n=1}^{\infty}\frac{\gamma_n \cos\gamma_n(h-y)\cos\gamma_n(h-u)}{\delta_n s_n}\right] \tag{52}$$

Now if we define

$$C^{SMM,ANSMM} = -i\frac{1-R^{SMM,ANSMM}}{1+R^{SMM,ANSMM}}, \tag{53}$$

then by using (29) and (39), we obtain

$$C^{SMM,ANSMM} = \int_{(0,h)-L_j} F^{SMM,ANSMM}(y)\frac{\cosh\gamma_0(h-y)}{\cosh\gamma_0 h}dy \tag{54}$$

and $F^{SMM,ANSMM}(y)$ and $C^{SMM,ANSMM}$ are real quantities. Thus if the integral equations (39) can be solved, then these solutions can be used to evaluate $C^{SMM,ANSMM}$ from the relations (54), and these produce the actual reflection and transmission coefficients $|R|$ and $|T|$ by using

$$|R| = \frac{|1 + C^{SMM}C^{ANSMM}|}{\triangle} \quad \text{and} \quad |T| = \frac{|C^{SMM} - C^{ANSMM}|}{\triangle} \tag{55}$$

with

$$\triangle = \{1 + (C^{SMM})^2 + (C^{ANSMM})^2 + (C^{SMM}C^{ANSMM})^2\}^{\frac{1}{2}}, \tag{56}$$

which are obtained from equations (14) and (53).

3.3 Solution of integral equation

Utilizing Galerkin technique, we approximate $F^{SMM,ANSMM}(y)$ as

$$F^{SMM,ANSMM}(y) \approx \mathcal{F}^{SMM,ANSMM}(y), y \in (0,h) - L_j, j = 1, 2, 3 \tag{57}$$

$\mathcal{F}^{SMM,ANSMM}(y)$ is expanded in terms of multi-term Galerkin expansions with a suitable choice of basis function. In case of type-I barrier, there is a single interval but for type-II

and type-III barriers there are two disjoint intervals.

For type-I,

$$\mathcal{F}^{SMM,ANSMM}(y) = \sum_{n=0}^{N} a_n^{SMM,ANSMM} f_n^{SMM,ANSMM}(y), y \in (0,h) - L_1 \tag{58}$$

and for type-II

$$\mathcal{F}^{SMM,ANSMM}(y) = \begin{cases} \sum_{n=0}^{N} a_n^{SMM,ANSMM} p_n^{SMM,ANSMM}(y), 0 < y < h \\ \sum_{n=0}^{N} b_n^{SMM,ANSMM} q_n^{SMM,ANSMM}(y), c < y < h \end{cases} \tag{59}$$

and for type-III

$$\mathcal{F}^{SMM,ANSMM}(y) = \begin{cases} \sum_{n=0}^{N} a_n^{SMM,ANSMM} p1_n^{SMM,ANSMM}(y), 0 < y < h \\ \sum_{n=0}^{N} b_n^{SMM,ANSMM} q1_n^{SMM,ANSMM}(y), c < y < d \end{cases} \tag{60}$$

where the basis functions $f_n^{SMM,ANSMM}(y) \quad for \quad a < y < h$ and $p_n^{SMM,ANSMM}(y)$ for $0 < y < a$, $q_n^{SMM,ANSMM}(y) \quad for \quad c < y < h$ and $p1_n^{SMM,ANSMM}(y)$ for $0 < y < a$, $q1_n^{SMM,ANSMM}(y) \quad for \quad c < y < d$ are taken in terms of ultraspherical Gegenbauer polynomials of order 1/6 with suitable weights [cf. Porter[3]]. The basis functions in different intervals are given below.

3.4 Basis functions

Type-I :

For this type of fully submerged barrier, we have to take the surface tension condition and the behavior becomes

$$F_m^{SMM,ANSMM} \sim (c-y)^{\frac{-1}{3}}$$

as $y \to c^{-0}$ derived by considering the flow field near the corner point (b,c). Thus here

$$f_m^{SMM}(y) = f_m^{ANSMM}(y) = f_m(y) = -\frac{d}{dy}[e^{\frac{-Ky}{\gamma+M\gamma^3}} \int_y^c e^{\frac{-Kt}{\gamma+M\gamma^3}} \tilde{f}_m(t)dt], 0 < y < c \tag{61}$$

We choose the basis functions in terms of $\tilde{f}_m(y)$ as follows

$$\tilde{f}_m(y) = \frac{2^{\frac{7}{6}}\Gamma(\frac{1}{6})(2m)!}{\pi\Gamma(2m+\frac{1}{3})(c)^{\frac{1}{3}}(c^2-y^2)^{\frac{1}{3}}} C_{2m}^{\frac{1}{6}}(\frac{y}{c}), 0 < y < c \tag{62}$$

Type II:

Here we choose two different basis functions for two disjoint intervals.

$$p_m^{SMM}(y) = p_m^{ANSMM}(y) = p_m(y) = -\frac{d}{dy}[e^{\frac{-Ky}{\gamma+M\gamma^3}} \int_y^a e^{\frac{-Kt}{\gamma+M\gamma^3}} \tilde{p}_m(t)dt], \ 0 < y < a \tag{63}$$

where

$$\tilde{p}_m(y) = \frac{2^{\frac{7}{6}}\Gamma(\frac{1}{6})(2m)!}{\pi\Gamma(2m+\frac{1}{3})(a)^{\frac{1}{3}}(a^2-y^2)^{\frac{1}{3}}} C_{2m}^{\frac{1}{6}}(\frac{y}{a}), 0 < y < a \tag{64}$$

and

$$q_m^{SMM}(y) = g1_{m+1}^{(1)}(y), m = 0, 1, 2, ...$$

$$q_m^{ANSMM}(y) = g1_m^{(1)}(y), m = 0, 1, 2, ... \tag{65}$$

where

$$g1_m^{(1)}(y) = \frac{2^{\frac{7}{6}}\Gamma(\frac{1}{6})(2m)!}{\pi\Gamma(2m+\frac{1}{3})(h-c)^{\frac{1}{3}}((h-c)^2-(h-y)^2)^{\frac{1}{3}}} C_{2m}^{\frac{1}{6}}(\frac{h-y}{h-c}),\ c < y < h \tag{66}$$

Type III:

Here we choose two different basis functions for two disjoint intervals.

$$p1_m^{SMM}(y) = p1_m^{ANSMM}(y) = p1_m(y) = -\frac{d}{dy}[e^{\frac{-Ky}{\gamma+M\gamma^3}} \int_y^a e^{\frac{-Kt}{\gamma+M\gamma^3}} \tilde{x}_m(t)dt],\ 0 < y < a \tag{67}$$

where

$$\tilde{p}1_m(y) = \frac{2^{\frac{7}{6}}\Gamma(\frac{1}{6})(2m)!}{\pi\Gamma(2m+\frac{1}{3})(a)^{\frac{1}{3}}(a^2-y^2)^{\frac{1}{3}}} C_{2m}^{\frac{1}{6}}(\frac{y}{a}), 0 < y < a \tag{68}$$

and

$$q1_m^{SMM,ANSMM}(y) = \frac{2^{\frac{7}{6}}\Gamma(\frac{1}{6})(m)!}{\pi\Gamma(m+\frac{1}{3})(\frac{d-c}{2})^{\frac{1}{3}}((y-c)(d-y))^{\frac{1}{3}}} C_m^{\frac{1}{6}}(\frac{2y-c-d}{d-c}),\ c < y < d \tag{69}$$

As the horizontal velocity component near the corner points of the thick barriers of all the three types, have a cube root singularity, then allowing similar arguments as given in Kanoria *et al.* [10], here also the basis functions are chosen in terms of Gegenbauer polynomials of order 1/6.

3.5 Formation of linear system of equations

For type I, we substitute the approximation (58) in equation (39), and then multiplying both side by appropriate $f^{SMM,ANSMM}(y)$ and integrate over (a, h) to obtain the linear system of equations

$$\sum_{n=0}^{N} a_n^{SMM,ANSMM} \chi_{mn}^{SMM,ANSMM} = \omega_m^{SMM,ANSMM}, \quad m = 0, 1, ..., N \tag{70}$$

where

$$\chi_{mn}^{SMM,ANSMM} = \int_a^h \int_a^h N^{SMM,ANSMM}(y,u) f_n^{SMM,ANSMM}(u) f_m^{SMM,ANSMM}(y) du\ dy,$$

$$m, n = 0, 1, 2, ..., N, \tag{71}$$

and

$$\omega_m^{SMM,ANSMM} = \int_a^h \frac{\cosh \gamma_0 (h-y)}{\cosh \gamma_0 h} f_m^{SMM,ANSMM}(y) dy, m = 0, 1, ..., N. \tag{72}$$

The integrals (71) and (72) can be evaluated explicitly, as in Kanoria *et al.* [10] by using the different properties and standard results on Gegenbaur polynomials. Thus the constants $a_n^{SMM,ANSMM}(n = 0, 1, ...N)$ are obtained by solving the linear equations (70). The relation (54) produce

$$C^{SMM,ANSMM} = \sum_{n=0}^{N} a_n^{SMM,ANSMM} \omega_n^{SMM,ANSMM} \tag{73}$$

so that $C^{SMM,ANSMM}$ are now found and $|R|$ and $|T|$ are evaluated from the relations (55).

For type II, we replace the equation (59) by (39) and multiplying both sides first by $p_m^{SMM,ANSMM}(y)$ $(0 < y < a)$ and then by $q_m^{SMM,ANSMM}(y)$ $(c < y < h)$ and then integrate over $(0, a)$ and (c, h) respectively, we get the linear system of equations as follows:

$$\sum_{n=0}^{N} a_n^{SMM,ANSMM} \begin{pmatrix} \mathcal{G}_{mn}^{SMM,ANSMM} \\ \mathcal{P}_{mn}^{SMM,ANSMM} \end{pmatrix} + \sum_{n=0}^{N} b_n^{SMM,ANSMM} \begin{pmatrix} \mathcal{H}_{mn}^{SMM,ANSMM} \\ \mathcal{Q}_{mn}^{SMM,ANSMM} \end{pmatrix}$$

$$= \begin{pmatrix} \omega_m^{(1)SMM,ANSMM} \\ \omega_m^{(2)SMM,ANSMM} \end{pmatrix}, \quad m = 0, 1, ..., N \tag{74}$$

where

$$\mathcal{G}_{mn}^{SMM,ANSMM} = \int_0^a \left(\int_0^a N^{SMM,ANSMM}(y,u) p_n^{SMM,ANSMM}(u) du \right) p_m^{SMM,ANSMM}(y) dy,$$

$$\mathcal{H}_{mn}^{SMM,ANSMM} = \int_0^a \left(\int_c^h N^{SMM,ANSMM}(y,u) q_n^{SMM,ANSMM}(u) du \right) p_m^{SMM,ANSMM}(y) dy,$$

$$\mathcal{P}_{mn}^{SMM,ANSMM} = \int_c^h \left(\int_0^a N^{SMM,ANSMM}(y,u) p_n^{SMM,ANSMM}(u) du \right) q_m^{SMM,ANSMM}(y) dy,$$

$$\mathcal{Q}_{mn}^{SMM,ANSMM} = \int_c^h \left(\int_c^h N^{SMM,ANSMM}(y,u) q_n^{SMM,ANSMM}(u) du \right) q_m^{SMM,ANSMM}(y) dy,$$

$$m, n = 0, 1, 2, ..., N, \tag{75}$$

so that $\mathcal{P}_{mn}^{SMM,ANSMM} = \mathcal{H}_{mn}^{SMM,ANSMM}$, and

$$\omega_m^{(1)SMM,ANSMM} = \int_0^a \frac{\cosh\gamma_0(h-y)}{\cosh\gamma_0 h} p_m^{SMM,ANSMM}(y)dy,$$

$$\omega_m^{(2)SMM,ANSMM} = \int_c^h \frac{\cosh\gamma_0(h-y)}{\cosh\gamma_0 h} q_m^{SMM,ANSMM}(y)dy,$$

$$m = 0, 1, ..., N. \tag{76}$$

The integrals in the relations (75) and (76) can be evaluated explicitly and thus the constants for type II barrier $a_n^{SMM,ANSMM}$ *and* $b_n^{SMM,ANSMM}$ $(n = 0, 1, 2, ..N)$ from linear equations (59) are obtained. We approximate $C^{SMM,ANSMM}$ as

$$C^{SMM,ANSMM} = \sum_{n=0}^{N} a_n^{SMM,ANSMM}\omega_n^{(1)SMM,ANSMM} + \sum_{n=0}^{N} b_n^{SMM,ANSMM}\omega_n^{(2)SMM,ANSMM} \tag{77}$$

For type III, we substitute the equation (60) in (39) and multiplying both sides first by $p1_m^{SMM,ANSMM}(y)$ $(0 < y < a)$ and then by $q1_m^{SMM,ANSMM}(y)$ $(c < y < d)$ and then integrate over $(0, a)$ and (c, d) respectively, we get the linear system of equations as follows:

$$\sum_{n=0}^{N} a_n^{SMM,ANSMM} \begin{pmatrix} R_{mn}^{SMM,ANSMM} \\ X_{mn}^{SMM,ANSMM} \end{pmatrix} + \sum_{n=0}^{N} b_n^{SMM,ANSMM} \begin{pmatrix} S_{mn}^{SMM,ANSMM} \\ Y_{mn}^{SMM,ANSMM} \end{pmatrix}$$

$$= \begin{pmatrix} \omega 1_m^{(1)SMM,ANSMM} \\ \omega 1_m^{(2)SMM,ANSMM} \end{pmatrix}, \quad m = 0, 1, ..., N \tag{78}$$

where

$$R_{mn}^{SMM,ANSMM} = \int_0^a \left(\int_0^a N^{SMM,ANSMM}(y,u) p1_n^{SMM,ANSMM}(u)du \right) p1_m^{SMM,ANSMM}(y)dy,$$

$$S_{mn}^{SMM,ANSMM} = \int_0^a \left(\int_c^d N^{SMM,ANSMM}(y,u) q1_n^{SMM,ANSMM}(u)du \right) p1_m^{SMM,ANSMM}(y)dy,$$

$$X_{mn}^{SMM,ANSMM} = \int_c^d \left(\int_0^a N^{SMM,ANSMM}(y,u) p1_n^{SMM,ANSMM}(u)du \right) q1_m^{SMM,ANSMM}(y)dy,$$

$$Y_{mn}^{SMM,ANSMM} = \int_c^d \left(\int_d^h N^{SMM,ANSMM}(y,u) q1_n^{SMM,ANSMM}(u)du \right) q1_m^{SMM,ANSMM}(y)dy,$$

$$m, n = 0, 1, 2, ..., N, \tag{79}$$

so that $X_{mn}^{SMM,ANSMM} = S_{mn}^{SMM,ANSMM}$, and

$$\omega 1_m^{(1)SMM,ANSMM} = \int_0^a \frac{\cosh\gamma_0(h-y)}{\cosh\gamma_0 h} p1_m^{SMM,ANSMM}(y)dy,$$

$$\omega 1_m^{(2)SMM,ANSMM} = \int_c^d \frac{\cosh\gamma_0(h-y)}{\cosh\gamma_0 h} q1_m^{SMM,ANSMM}(y)dy,$$

$$m = 0, 1, ..., N. \tag{80}$$

Solving the integrals present in (79) and (80) explicitly, the constants for type III barrier $a_n^{SMM,ANSMM}$ *and* $b_n^{SMM,ANSMM}$ $(n = 0, 1, 2, ..N)$ from linear equations (60) are obtained. We evaluate $C^{SMM,ANSMM}$ as

$$C^{SMM,ANSMM} = \sum_{n=0}^{N} a_n^{SMM,ANSMM}\omega 1_n^{(1)SMM,ANSMM} + \sum_{n=0}^{N} b_n^{SMM,ANSMM}\omega 1_n^{(2)SMM,ANSMM} \tag{81}$$

3.6 Coefficients of linear system of equations

Type I

$$\chi_{mn}^{SMM} = \frac{\delta_0\mu}{\gamma_0\cosh^2\gamma_0 h}\left[4(-1)^{m+n}\sum_{r=1}^{\infty}\left\{\frac{\gamma_r\cos^2\gamma_r h}{\delta_r s_r(\gamma_r c)^{\frac{1}{3}}}J_{2m+\frac{1}{6}}(\gamma_r c)J_{2n+\frac{1}{6}}(\gamma_r c)\right.\right.$$

$$\left.\left. + \coth t_r b\frac{\alpha_r\cos^2\alpha_r c}{\lambda_r t_r(\alpha_r c)^{\frac{1}{3}}}J_{2m+\frac{1}{6}}(\alpha_r c)J_{2n+\frac{1}{6}}(\alpha_r c)\right\}\right.$$

$$\left. +(-\cot(\alpha_0^2-\nu^2)^{\frac{1}{2}}b)\frac{\cosh^2\alpha_0 c}{\lambda_0(\alpha_0^2-\nu^2)^{\frac{1}{6}}c^{\frac{1}{3}}}I_{2m+\frac{1}{6}}(\alpha_0 c)I_{2n+\frac{1}{6}}(\alpha_0 c)\right] \tag{82}$$

$$\chi_{mn}^{ANSMM} = \frac{\delta_0\mu}{\gamma_0\cosh^2\gamma_0 h}\left[4(-1)^{m+n}\sum_{r=1}^{\infty}\left\{\frac{\gamma_r\cos^2\gamma_r h}{\delta_r s_r(\gamma_r c)^{\frac{1}{3}}}J_{2m+\frac{1}{6}}(\gamma_r c)J_{2n+\frac{1}{6}}(\gamma_r c)\right.\right.$$

$$\left.\left. + \tanh t_r b\frac{\alpha_r\cos^2\alpha_r c}{\lambda_r t_r(\alpha_r c)^{\frac{1}{3}}}J_{2m+\frac{1}{6}}(\alpha_r c)J_{2n+\frac{1}{6}}(\alpha_r c)\right\}\right.$$

$$\left. +(\tan(\alpha_0^2-\nu^2)^{\frac{1}{2}}b)\frac{\cosh^2\alpha_0 c}{\lambda_0(\alpha_0^2-\nu^2)^{\frac{1}{6}}c^{\frac{1}{3}}}I_{2m+\frac{1}{6}}(\alpha_0 c)I_{2n+\frac{1}{6}}(\alpha_0 c)\right] \tag{83}$$

$$\omega_m^{SMM,ANSMM} = \frac{I_{2m+\frac{1}{6}}(\gamma_0 c)}{(\gamma_0 c)^{\frac{1}{6}}}, \quad m = 0, 1, ..., N. \tag{84}$$

Type II

$$\mathcal{G}_{mn}^{SMM} = \frac{\delta_0\mu}{\gamma_0\cosh^2\gamma_0 h}\left[4(-1)^{m+n}\sum_{r=1}^{\infty}\left\{\frac{\gamma_r\cos^2\gamma_r h}{\delta_r s_r(\gamma_r a)^{\frac{1}{3}}}J_{2m+\frac{1}{6}}(\gamma_r a)J_{2n+\frac{1}{6}}(\gamma_r a)\right.\right.$$
$$\left.\left. + \coth u_r b\frac{\beta_r\cos^2\beta_r a}{\epsilon_r u_r(\beta_r a)^{\frac{1}{3}}}J_{2m+\frac{1}{6}}(\beta_r a)J_{2n+\frac{1}{6}}(\beta_r a)\right\}\right.$$
$$\left. +(-\cot(\beta_0^2-\nu^2)^{\frac{1}{2}}b)\frac{\cosh^2\beta_0 a}{\epsilon_0(\beta_0^2-\nu^2)^{\frac{1}{6}}a^{\frac{1}{3}}}I_{2m+\frac{1}{6}}(\beta_0 a)I_{2n+\frac{1}{6}}(\beta_0 a)\right] \tag{85}$$

$$\mathcal{G}_{mn}^{ANSMM} = \frac{\delta_0\mu}{\gamma_0\cosh^2\gamma_0 h}\left[4(-1)^{m+n}\sum_{r=1}^{\infty}\left\{\frac{\gamma_r\cos^2\gamma_r h}{\delta_r s_r(\gamma_r a)^{\frac{1}{3}}}J_{2m+\frac{1}{6}}(\gamma_r a)J_{2n+\frac{1}{6}}(\gamma_r a)\right.\right.$$
$$\left.\left. + \tanh u_r b\frac{\beta_r\cos^2\beta_r a}{\epsilon_r u_r(\beta_r a)^{\frac{1}{3}}}J_{2m+\frac{1}{6}}(\beta_r a)J_{2n+\frac{1}{6}}(\beta_r a)\right\}\right.$$
$$\left. +(\tan(\beta_0^2-\nu^2)^{\frac{1}{2}}b)\frac{\cosh^2\beta_0 a}{\epsilon_0(\beta_0^2-\nu^2)^{\frac{1}{6}}a^{\frac{1}{3}}}I_{2m+\frac{1}{6}}(\beta_0 a)I_{2n+\frac{1}{6}}(\beta_0 a)\right] \tag{86}$$

$$\mathcal{H}_{mn}^{SMM} = 4(-1)^{m+n+1}\frac{\delta_0\mu}{\gamma_0\cosh^2\gamma_0 h}\sum_{r=1}^{\infty}\frac{\gamma_r\cos\gamma_r h}{\delta_r s_r(\gamma_r a)^{\frac{1}{6}}}$$
$$\frac{1}{(\gamma_r(h-c))^{\frac{1}{6}}}J_{2m+\frac{1}{6}}(\gamma_r a)J_{2n+\frac{13}{6}}(\gamma_r(h-c)) \tag{87}$$

$$\mathcal{H}_{mn}^{ANSMM} = \mathcal{H}_{m,n-1}^{SMM} \tag{88}$$

$$\mathcal{P}_{mn}^{SMM} = \mathcal{H}_{mn}^{SMM} \tag{89}$$

$$\mathcal{P}_{mn}^{ANSMM} = \mathcal{P}_{m-1,n}^{SMM} \tag{90}$$

$$\mathcal{Q}_{mn}^{SMM} = \frac{\delta_0\mu}{\gamma_0\cosh^2\gamma_0 h}\left[(-1)^{m+n}\sum_{r=1}^{\infty}\left\{\frac{4\gamma_r}{\delta_r s_r(\gamma_r(h-c))^{\frac{1}{3}}}\right.\right.$$
$$J_{2m+\frac{13}{6}}(\gamma_r(h-c))J_{2n+\frac{13}{6}}(\gamma_r(h-c))$$
$$\left.\left. + \frac{2}{r\pi}\coth\frac{r\pi b}{h-c}\frac{J_{2m+\frac{13}{6}}(r\pi)J_{2n+\frac{13}{6}}(r\pi)}{(r\pi)^{\frac{1}{3}}}\right\}\right] \tag{91}$$

$$\mathcal{Q}_{mn}^{ANSMM} = \frac{\delta_0\mu}{\gamma_0\cosh^2\gamma_0 h}\left[\frac{12\pi b}{h-c}\frac{2^{\frac{1}{3}}}{\Gamma(\frac{1}{3})^4}\delta_{0n}\delta_{0m}\right.$$
$$\left.+(-1)^{m+n}\sum_{r=1}^{\infty}\left\{\frac{4\gamma_r}{\delta_r s_r(\gamma_r(h-c))^{\frac{1}{3}}}\right.\right. J_{2m+\frac{1}{6}}(\gamma_r(h-c))J_{2n+\frac{1}{6}}(\gamma_r(h-c))$$

$$+\frac{2}{r\pi}\tanh\frac{r\pi b}{h-c}\frac{J_{2m+\frac{1}{6}}(r\pi)J_{2n+\frac{1}{6}}(r\pi)}{(r\pi)^{\frac{1}{3}}}\Bigg\}\Bigg] \tag{92}$$

where $\delta_{0n}=1$ for $n=0$, and $\delta_{0n}=0$ for $n\geq 1$ and $J's$ are Bessel functions of first kind and

$$\omega_m^{(1)SMM}=\frac{I_{2m+\frac{1}{6}}(\gamma_0 a)}{(\gamma_0 a)^{\frac{1}{6}}},\quad m=0,1,...,N. \tag{93}$$

$$\omega_m^{(1)ANSMM}=\omega_m^{(1)SMM} \tag{94}$$

$$\omega_m^{(2)SMM}=\frac{1}{\cosh\gamma_0 h}\frac{I_{2m+\frac{7}{6}}(\gamma_0(h-c))}{(\gamma_0(h-c))^{\frac{1}{6}}},m=0,1,...,N. \tag{95}$$

$$\omega_m^{(2)ANSMM}=\omega_{m-1}^{(2)SMM} \tag{96}$$

Type III

$$R_{mn}^{SMM}=\frac{\delta_0\mu}{\gamma_0\cosh^2\gamma_0 h}\Bigg[4(-1)^{m+n}\sum_{r=1}^{\infty}\Bigg\{\frac{\gamma_r\cos^2\gamma_r h}{\delta_r s_r(\gamma_r a)^{\frac{1}{3}}}J_{2m+\frac{1}{6}}(\gamma_r a)J_{2n+\frac{1}{6}}(\gamma_r a)$$
$$+\coth u_r b\frac{\beta_r\cos^2\beta_r a}{\epsilon_r u_r(\beta_r a)^{\frac{1}{3}}}J_{2m+\frac{1}{6}}(\beta_r a)J_{2n+\frac{1}{6}}(\beta_r a)\Bigg\}$$
$$+(-\cot(\beta_0^2-\nu^2)^{\frac{1}{2}}b)\frac{\cosh^2\beta_0 a}{\epsilon_0(\beta_0^2-\nu^2)^{\frac{1}{6}}a^{\frac{1}{3}}}I_{2m+\frac{1}{6}}(\beta_0 a)I_{2n+\frac{1}{6}}(\beta_0 a)\Bigg] \tag{97}$$

$$R_{mn}^{ANSMM}=\frac{\delta_0\mu}{\gamma_0\cosh^2\gamma_0 h}\Bigg[4(-1)^{m+n}\sum_{r=1}^{\infty}\Bigg\{\frac{\gamma_r\cos^2\gamma_r h}{\delta_r s_r(\gamma_r a)^{\frac{1}{3}}}J_{2m+\frac{1}{6}}(\gamma_r a)J_{2n+\frac{1}{6}}(\gamma_r a)$$
$$+\tanh u_r b\frac{\beta_r\cos^2\beta_r a}{\epsilon_r u_r(\beta_r a)^{\frac{1}{3}}}J_{2m+\frac{1}{6}}(\beta_r a)J_{2n+\frac{1}{6}}(\beta_r a)\Bigg\}$$
$$+(\tan(\beta_0^2-\nu^2)^{\frac{1}{2}}b)\frac{\cosh^2\beta_0 a}{\epsilon_0(\beta_0^2-\nu^2)^{\frac{1}{6}}a^{\frac{1}{3}}}I_{2m+\frac{1}{6}}(\beta_0 a)I_{2n+\frac{1}{6}}(\beta_0 a)\Bigg] \tag{98}$$

$$S_{mn}^{SMM,ANSMM}=\frac{4\delta_0\mu}{\gamma_0\cosh^2\gamma_0 h}\sum_{r=1}^{\infty}\frac{\gamma_r\cos\gamma_r h}{\delta_r s_r(\gamma_r a)^{\frac{1}{6}}}$$
$$\frac{\cos(\frac{n\pi}{2}-\gamma_r(h-\frac{c+d}{2}))}{(\gamma_r\frac{d-c}{2})^{\frac{1}{6}}}J_{2m+\frac{1}{6}}(\gamma_r a)J_{n+\frac{1}{6}}(\gamma_r\frac{d-c}{2}) \tag{99}$$

$$S_{mn}^{SMM,ANSMM}=X_{mn}^{SMM,ANSMM} \tag{100}$$

$$Y_{mn}^{SMM}=\frac{\delta_0\mu}{\gamma_0\cosh^2\gamma_0 h}\Bigg[2\sum_{r=1}^{\infty}\Bigg\{\frac{2\gamma_r}{s_r\delta_r}\cos(\frac{n\pi}{2}-\gamma_r(h-\frac{c+d}{2}))$$

$$\cos(\frac{m\pi}{2}-\gamma_r(h-\frac{c+d}{2}))\frac{J_{m+\frac{1}{6}}(\gamma_r\frac{d-c}{2})J_{n+\frac{1}{6}}(\gamma_r\frac{d-c}{2})}{(\gamma_r\frac{d-c}{2})^{\frac{1}{3}}}$$

$$+\frac{coth\zeta_r b}{(d-c)\zeta_r}\cos\left\{\frac{m\pi}{2}-\frac{r\pi}{2}\right\}\cos\left\{\frac{n\pi}{2}-\frac{r\pi}{2}\right\}\frac{J_{m+1/6}(\frac{r\pi}{2})J_{n+1/6}(\frac{r\pi}{2})}{(\frac{r\pi}{2})^{1/3}}\Bigg\}$$

$$+\frac{12\pi}{(d-c)}\frac{2^{1/3}}{(\Gamma(1/3))^4}\frac{\coth\nu b}{\nu}\delta_{0m}\delta_{0n}\Bigg] \tag{101}$$

where $\delta_{0n}=1$ for $n=0$, and $\delta_{0n}=0$ for $n\geq 1$.
After replacing 'coth' by 'tanh', we obtain Y_{mn}^{ANSMM} from (101).

$$\omega 1_m^{(1)SMM,ANSMM}=\frac{I_{2m+1/6}(\gamma_0 a)}{(\gamma_0 a)^{\frac{1}{6}}} \tag{102}$$

$$\omega 1_m^{(2)SMM,ANSMM}=\frac{(-1)^m e^{\gamma_0(h-\frac{c+d}{2})}e^{-\gamma_0(h-\frac{c+d}{2})}}{2\cosh\gamma_0 h}\frac{I_{m+1/6}(\gamma_0\frac{d-c}{2})}{(\gamma_0\frac{d-c}{2})^{\frac{1}{6}}} \tag{103}$$

where $I's$ are modified Bessel function of first kind.

4 Numerical results and discussions

The present numerical results describe the nature of reflection coefficient $|R|$ against the non dimensional wave numbers Kh for different values of the parameters $b/h, a/h$ and different values of incident angle θ. For numerical computation of three type of barriers, we consider $N=10$ in equation (70), (74) and (78) respectively. The coefficients are obtained by employing $(N+1)$ Galerkin approximation technique. These are seen to satisfy the energy balance relations numerically. This gives a partial check on the correctness of the numerical result obtained here. We consider 200 terms in each series of $\chi_{m,n}^{SMM,ANSMM}$ and almost a six figure accuracy is obtained is obtained in the result. In the Table 1, we study the convergence of the analytical solution by showing the numerical values of $|R|$ for different values of kh with the truncation size $N=2,5,7,10$ of the finite series (70) for type I barrier. From this table it is seen that the results for $|R|$ converge very rapidly with N. For $N=7$, an accuracy of almost five decimal places is achieved.

Table 1: Convergence of $|R|$ with N for Type I Barrier with $b/h=0.5, c/h=0.5, \theta=25^0, M/h^2=0.5$

Kh	**N**=2	**N**=5	**N**=7	**N**=10
0.2	0.35462	0.38562	0.395131	0.395133
1.0	0.29652	0.31236	0.327913	0.327916
1.8	0.13256	0.16235	0.175689	0.175692

Table 2 shows the convergence of the numerical values of $|R|$ for different values of kh with the truncation size $N=2,5,7,10$ of the finite series (74) for type II barrier. Here also a five figure accuracy is achieved for $N=7$. Thus, from these two tables, we can say

the present method is quite efficient for the numerical calculation of $|R|$ (and $|T|$). In a similar manner one can show the convergence analysis for Type III barrier. Here we avoid the similar calculations.

Table 2: Convergence of $|R|$ with N for Type II Barrier with $a/h = 0.4, b/h = 1.0, c/h = 0.8, \theta = 25^0, M/h^2 = 0.5$

Kh	**N**=2	**N**=5	**N**=7	**N**=10
0.2	0.31562	0.35841	0.361959	0.361966
1.0	0.221024	0.261021	0.272900	0.272902
1.8	0.361120	0.405543	0.417920	0.417921

4.1.1 *Discussion of energy identity relation*

In Table 3, the numerical values of the components present in the energy identity relation are provided for different values of the dimensionless wavenumber kh for Type I barrier with fixed values of $a/h = 0.4, b/h = 1.0, c/h = 0.8, \theta = 25^0, M/h^2 = 0.5$. It is observed from the table that the energy balance relation $|R|^2 + |T|^2 = 1$ satisfied numerically. It shows a partial check of our present method. Thus numerically we can show that reflection and transmission coefficients are satisfied the energy balance relation, which is $|R|^2 + |T|^2 = 1$. Thus in present numerical analysis, it is quite enough to show the behavior change of $|R|$ considering different parametric values.

Table 3: Energy identity, Type I barrier for $b/h = 0.5, c/h = 0.5, \theta = 25^0, M/h^2 = 0.5$

Kh	$\|R\|$	$\|T\|$	$\|R\|^2 + \|T\|^2$
0.1	0.127612	0.991824	1.0000
0.5	0.412045	0.911164	1.0000
1.0	0.327916	0.944707	1.0000
1.5	0.229463	0.969256	1.0000
2.0	0.143046	0.989716	1.0000
2.5	0.0729557	0.997335	1.0000
2.9	0.0278562	0.999612	1.0000

4.1.2 *Comparison with existing results*

In Fig. 3, the reflection coefficient verses non dimensional wave number for type I and type II barriers have been plotted without the effect of surface tension. For comparison with my present result with the figures given in Kanoria et. al's [10], we consider very small values of non dimension surface tension factor, $\frac{M}{h^2} = 0.0001$, $\theta = 0^0$ and other non dimensional parameters are taken same as Kanoria et. al's [10] data for their Figures 4 and 5. In Fig. 3, dashed line and thick line corresponds our present data line and star and thick dot points represent the data of Kanoria's Figure 4 and 5 respectively. We can say that our present figure 3 almost matched with those figures of Kanoria et al's[10] paper. This shows the partial check of the correctness of our present numerical data.

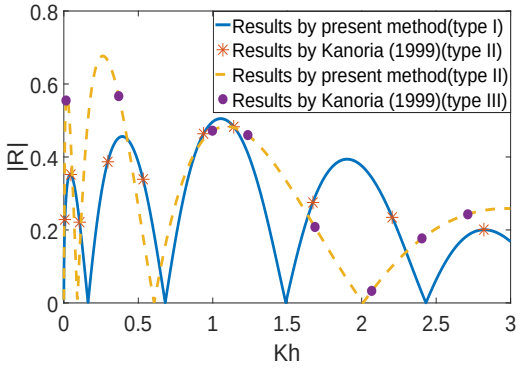

Figure 3: Reflection coefficients for two types of barriers without surface tension

4.2 *Effect of various parameters on reflection coefficients*

We now discuss the results associated with type I and type II barriers in separate figures. The variation of reflection coefficients ($|R|$) as a function of wave numbers (Kh)are explained considering different parametric values.

4.2.1 *Type I barrier*

Figs. 4A, 4B and 5A, 5B show the plots of reflection coefficient ($|R|$) of bottom standing thick barrier (Type I barrier) against non-dimensional wave number (Kh). Fig 4A is drawn with fixed values of $\frac{c}{h} = 0.5, \frac{M}{h^2} = 1$ and $\theta = 45^0$ for different values of width of the barrier $\frac{b}{h} = 0.5, 1.5$ and 2. It is seen that increasing values of the width reflect less energy and also oscillation in the curve increases with increasing width of the barrier.

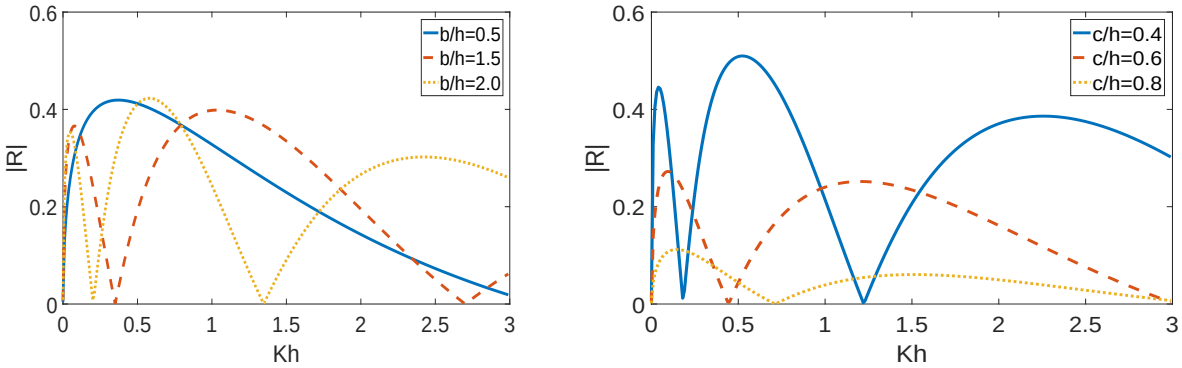

(A) $\frac{c}{h} = 0.5, \frac{M}{h^2} = 0.5, \theta = 25^0$ (B) $\frac{b}{h} = 1.5, \frac{M}{h^2} = 0.5, \theta = 25^0$

Figure 4: Reflection coefficient for type I barrier (A)for different $\frac{b}{h}$; (B)for different $\frac{c}{h}$

In Fig. 4B, $|R|$ is depicted against Kh for different $\frac{c}{h}(= 0.4, 0.6, 0.8)$ and consider fixed values of $\frac{b}{h} = 2, \frac{M}{h^2} = 0.5, \theta = 25^0$. When depth from the free surface of the bottom standing thick barrier gradually increases less energy reflected and more energy transmitted. Zero reflection also decreases with increasing $\frac{c}{h}$.

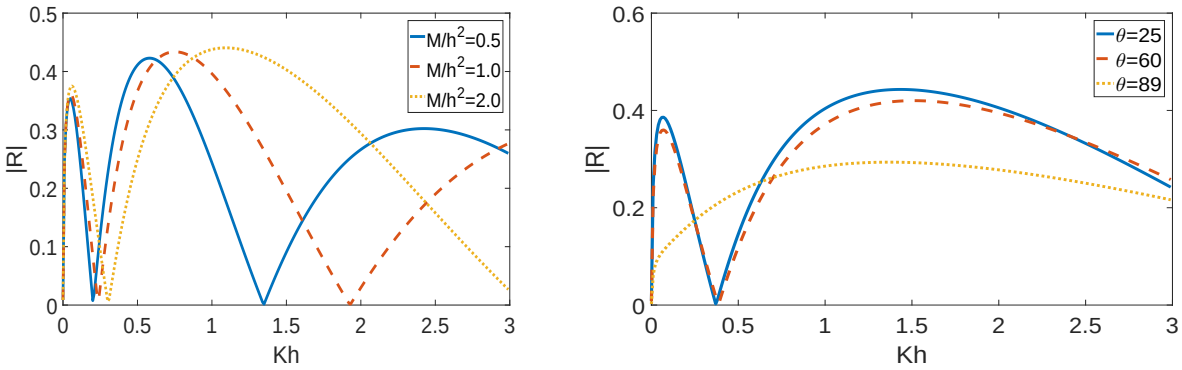

(A) $\frac{b}{h} = 2, \frac{c}{h} = 0.5, \theta = 25^0$ (B) $\frac{b}{h} = 2, \frac{c}{h} = 0.5, \frac{M}{h^2} = 3$

Figure 5: Reflection coefficient for type I barrier (A)for different $\frac{M}{h^2}$; (B)for different θ

The effect of surface tension on reflection coefficient is described in Fig. 5A which is drawn for three different values of surface tension factor $\frac{M}{h^2} = 0.5, 1.5$ and 2 with fixed values of $\frac{b}{h} = 2, \frac{c}{h} = 0.5, \theta = 25^0$. It is clear that the amplitude of reflection coefficient decreases with increase of surface tension which agrees the presence of cohesive force in between the water molecule due to the surface tension. The graphs depicted in Fig. 5B are the reflection coefficients against wave numbers with fixed values of $\frac{b}{h} = 2, \frac{c}{h} = 0.5$ and $\frac{M}{h^2} = 3$ and different values of incidence angle $\theta = 25^0, 60^0, 89^0$. The peak values of $|R|$ gradually decreases with the increasing values of incidence wave angle. It is also noticed that when θ is almost 90^0 the amplitude of $|R|$ is very small compared to the small incident angles.

4.2.2 *Type II barrier*

In Figs. 6A, 6B, 7A, 7B and 8, the variation of reflection energy coefficient is plotted against non dimensional wave number for type II barrier (submerged rectangular block). The graphs depicted in Fig. 6A are drawn with fixed values of $\frac{b}{h} = 1, \frac{c}{h} = 0.8, \frac{M}{h^2} = 0.5$ and $\theta = 25^0$ and for different depth of the barrier from the upper surface of water, $\frac{a}{h} = 0.4, 0.5, 0.6$. It is seen that increasing values of $\frac{a}{h}$ decreases the amplitude of reflection coefficient. Fig. 6B shows the effect of change of width of the barrier on reflection coefficients by considering $\frac{b}{h} = 1.0, 0.7$ and 0.4 and fixed values of $\frac{a}{h} = 0.5, \frac{c}{h} = 0.8, \frac{M}{h^2} = 0.5$ and $\theta = 25^0$. Barrier with large width reflects more energy than the thinner one.

Fig. 7A is drawn for different values of $\frac{c}{h} (= 0.5, 0.7, 0.9)$ and fixed values of $\frac{a}{h} = 0.4, \frac{b}{h} = 1, \frac{M}{h^2} = 0.5$ and $\theta = 45^0$. From the figure it can be say that with increasing $\frac{c}{h}$, $|R|$ gradually increases. It is physically quite obvious because large height of the barrier reflects more energy than the smaller one. Fig. 7B is drawn for $|R|$ with different values of $\frac{M}{h^2} = 0.5, 1.0,$ and1.5 and fixed values of $\frac{a}{h} = 0.5, \frac{b}{h} = 1, \frac{c}{h} = 0.8$ and $\theta = 25^0$. The effect of surface tension increases the amplitude of $|R|$ for type II barrier. Fig. 8 is plotted the variation of reflection coefficient $|R|$ against wave number Kh for different angles of incidence $\theta (= 25^0, 50^0, 75^0$ and $89^0)$ and fixed values of $\frac{a}{h} = 0.5, \frac{b}{h} = 1, \frac{c}{h} = 0.8$ and $\frac{M}{h^2} = 0.5$. Figure shows that for presence of surface tension in the upper surface and submerged block

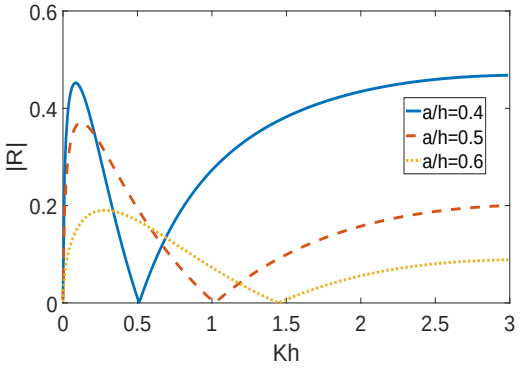

(A) $\frac{b}{h} = 1, \frac{c}{h} = 0.8, \frac{M}{h^2} = 0.5, \theta = 25^0$

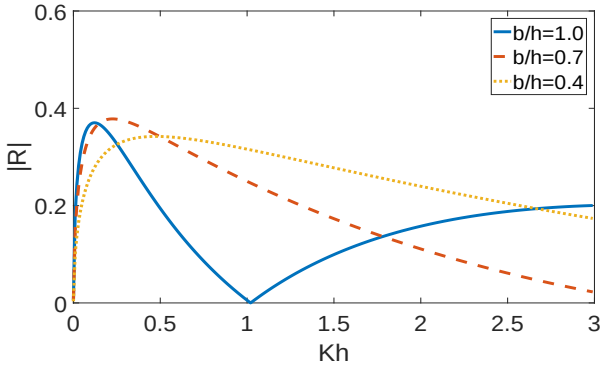

(B) $\frac{a}{h} = 0.5, \frac{c}{h} = 0.8, \frac{M}{h^2} = 0.5, \theta = 25^0$

Figure 6: Reflection coefficient for type II barrier (A)for different $\frac{a}{h}$; (B)for different $\frac{b}{h}$

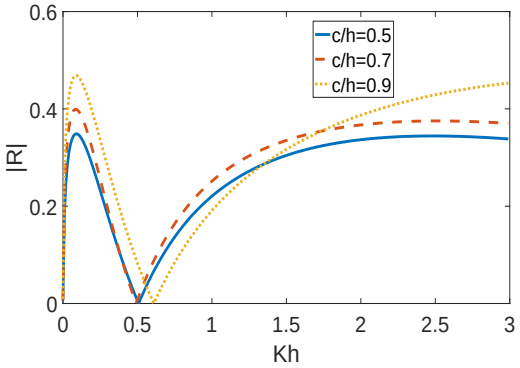

(A) $\frac{a}{h} = 0.4, \frac{b}{h} = 1, \frac{M}{h^2} = 0.5, \theta = 25^0$

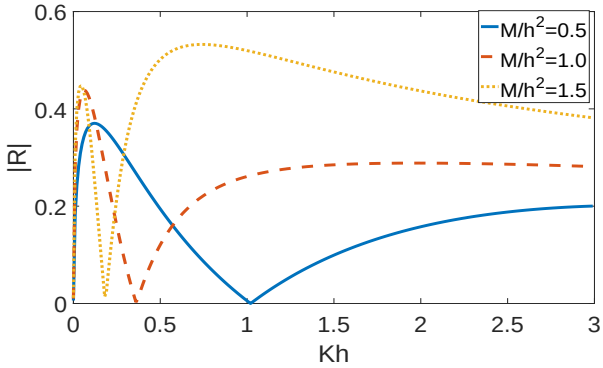

(B) $\frac{a}{h} = 0.5, \frac{b}{h} = 1, \frac{c}{h} = 0.8, \theta = 25^0$

Figure 7: Reflection coefficient for type II barrier (A)for different $\frac{c}{h}$; (B)for different $\frac{M}{h^2}$

in water, the amplitude of $|R|$ gradually increases with decreasing values of θ.

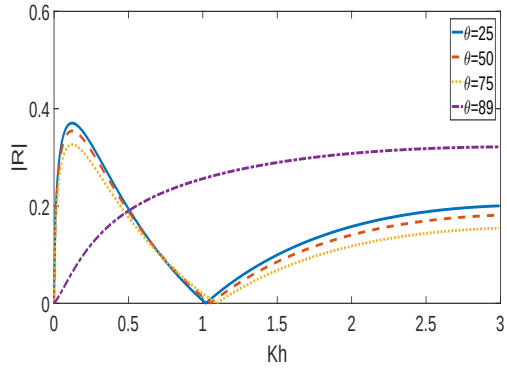

Figure 8: Reflection coefficient for type II barrier for different θ with $\frac{a}{h} = 0.5, \frac{b}{h} = 1, \frac{c}{h} = 0.8, \frac{M}{h^2} = 0.5$

4.2.3 *Type III barrier*

Figs. 9A, 9B, 10 depict the behavior of $|R|$ against non dimensional wave numbers, for type III barrier. Fig. 9A is drawn for different values of width ($\frac{b}{h} = 0.4, 0.7$ and 1.0) of the thick barrier and fixed values of $\frac{a}{h} = 0.2, \frac{M}{h^2} = 0.5, \frac{(d-c)}{h} = 0.3, \theta = 25^0$. The figure have shown that increasing width of the barrier gradually increases the reflection coefficient and oscillating behavior in reflection curve also seen for large values of $\frac{b}{h}$.

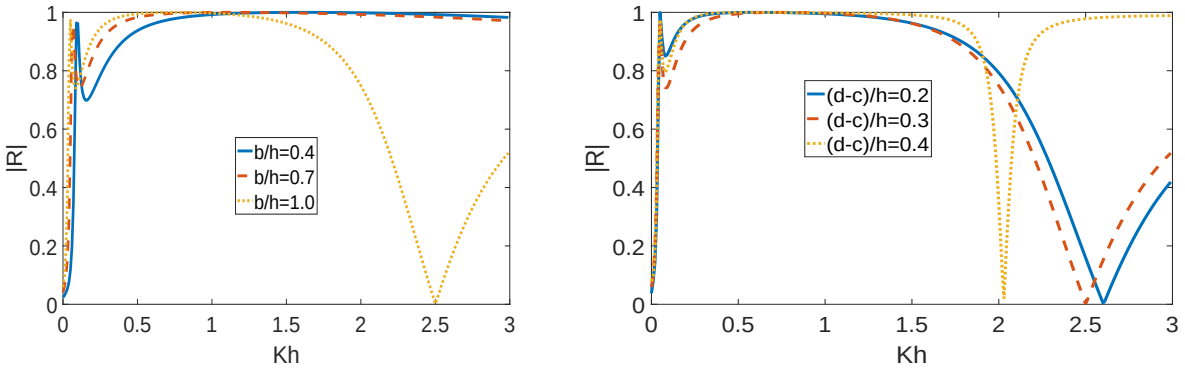

(A) $\frac{a}{h} = 0.2, \frac{M}{h^2} = 0.5, \frac{(d-c)}{h} = 0.3, \theta = 25^0$ (B) $\frac{a}{h} = 0.2, \frac{b}{h} = 1, \frac{M}{h^2} = 0.5, \theta = 25^0$

Figure 9: Reflection coefficient for type III barrier (A)for different $\frac{b}{h}$; (B)for different $\frac{d-c}{h}$

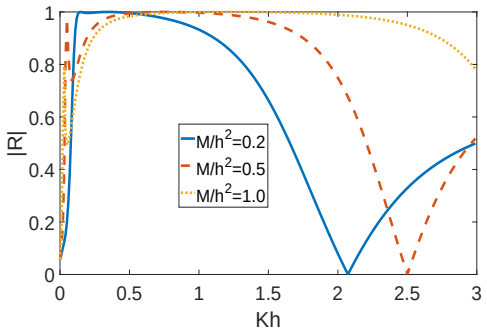

Figure 10: Reflection coefficient for type III barrier for different $\frac{M}{h}$ with $\frac{a}{h} = 0.2, \frac{b}{h} = 1, \frac{(d-c)}{h} = 0.3, \theta = 25^0$.

In Fig. 9B, $|R|$ is depicted for various values of the gap of the barrier ($\frac{d-c}{h} = 0.2, 0.3$ and 0.4) and fixed values of $\frac{a}{h} = 0.2, \frac{b}{h} = 1, \frac{M}{h^2} = 0.5, \theta = 25^0$. The figure has clearly shown that amplitude and oscillation the reflection curve increases with large values of the gap in the barrier. Fig. 10 shows the behavior of $|R|$ for different values of $\frac{M}{h} = 0.2, 0.5$ and 1.0 with fixed values of $\frac{a}{h} = 0.2, \frac{b}{h} = 1, \frac{(d-c)}{h} = 0.3, \theta = 25^0$. Same as the type I and type II barriers, also in case of type III barrier, the effect of surface tension increases the amplitude of reflection coefficient of wave energy and it is more clear for large values of wave numbers. It can be noted that, all the reflection curves for each type of barriers with different parametric values show the zero reflection behavior. This phenomenon is true due to geometrical symmetry in the barrier's configuration. Also, number of zeros in reflection curve increases with increasing width of the barrier. For each type of barriers, the reflection curves for long waves confine near the origin.

5 Conclusion

Oblique wave scattering by thick rectangular barrier in presence of surface tension at the upper surface have been studied here by employing multi-term Galerkin approximation technique. Three different geometrical positions of the barrier are considered here. The numerical estimate of reflection coefficient for different values of wave numbers and other parameters involved in the physical problem have been obtained and exemplify graphically. The numerical results also satisfy the energy balance relation. The results without surface tension have been recovered from present result by considering very small values of M. From the present study, it is clear that the amplitude of reflection coefficient decreases when the value of surface tension increases. The width and height of the thick barriers play a crucial role to the nature of scattering waves. The zero reflection and oscillation behavior of reflection coefficient are also observed here.

Acknowledgment

The authors would like to gratefully acknowledge the Editor and Reviewers for their valuable comments and suggestions to improve the quality of the manuscript.

References

[1] B.A. Packham, W.E. Williams, J. Inst. Maths Applics. 10 (1972) 176-184.

[2] I.J. Losada, M.A. Losada, A.J. Roldhn, Applied Ocean Research 14 (1992) 191-199.

[3] R. Porter, D,V. Evans, J Fluid Mech. 294 (1995) 155-180.

[4] B.N. Mandal, D.P. Dolai, Appl. Ocean Res. 16 (1994) 195-203.

[5] B.N. Mandal, M. Kanoria, J Offshore Mech Arctic Eng. 122 (2) (2000) 100-108.

[6] S. Banerjea, M. Kanoria, D. P. Dolai, B. N. Mandal, Appl Ocean Res. 18 (1996) 319-327.

[7] P. Das, D.P. Dolai, B.N. Mandal, J. Wtry. Port, Coastal and Ocean Engng. 123 (1997) 163-171.

[8] B.C. Das, S. De, B.N. Mandal, Journal of Engineering Mathematics 122 (2020) 81-99.

[9] C. Mei, J. Black, Journal of Fluid Mechanics 38 (3) (1969) 499-511.

[10] M. Kanoria, D. Dolai, B. Mandal, Journal of Engineering Mathematics 35 (1999) 361-384.

[11] B.N. Mandal, M. Kanoria, Proceedings of 17th International Conference on Offshore Mechanics and Arctic Engineering, ASME, Lisbon, Portugal, July(1998).

[12] D. Evans, In Proceedings of Cambridge Philosophical Society 64 (1968a) 833-847.

[13] D. Evans, In Proceedings of Cambridge Philosophical Society 64 (1968b) 795-810.

[14] P. Rhodes-Robinson, Bulletin of the Australian Mathematical Society 2 (1970) 317-333.

[15] P. Rhodes-Robinson, In Proceedings of Cambridge Philosophical Society 70 (1971) 323-337.

[16] P. Rhodes-Robinson, In Proceedings of Cam-bridge Philosophical Society 92 (1982) 369-373.

[17] A. Chakrabarti, T. Sahoo, Journal of the Australian Mathematical Society B 39 (1998) 539-556.

[18] L. Hocking, D. Mahdmina, Journal of Fluid Mechanics 224 (1991) 217-226.

[19] R. Chakraborty, B.N. Mandal, J Eng Math. 89 (2014) 101-112.

[20] R. Chakraborty, B.N. Mandal, ANZIAM J. 56 (2015) 286-298.

[21] J.N. Newman, J. Fluid Mech. 23 (1965) 23-29.

[22] A. Sasmal, S. Paul,S. Dey, J. Appl Fluid Mech. 12 (2019) 233-241.

[23] S. Paul, A. Sasmal, S. Dey, Ocean Engineering 193 (2019) 106613 (1-8).

[24] A. Sasmal, S. De, Journal of Ocean Engineering and Science 6 (2) (2021) 206-214.

[25] S. Paul, S. De, Ocean Engineering 220 (2021) 108449.

[26] D. Porter, Proc. Camb. Phil. Soc. 71 (1972) 411-421.

[27] D.V. Evans, M. Fernyhough, J. Fluid Mech. 297 (1995) 307-325.